Application of Amorphous Silicon for Photovoltaic silicon surface passivation

Jonathon Mitchell

A thesis submitted for the degree of Doctor of Philosophy of

The Australian National University

November 2011

Department of Engineering

College of Engineering and Computer Science

The Australian National University

Canberra, Australia 0200

Declaration

I certify that this thesis does not incorporate without acknowledgement any material previously submitted for a degree or diploma in any university, and that, to the best of my knowledge, it does not contain any material previously published or written by another person except where due references was made in the text. The work in this thesis is my own, except for the contributions made by others as described in the Acknowledgements.

Jonathon Mitchell

ACKNOWLEDGMENTS

I would like to express my appreciation to Prof. Andres Cuevas for his encouragement and enthusiasm which have been invaluable throughout this PhD. The skills and knowledge he has imparted to me are something that can be considered irreplaceable and I thank him for the opportunity to perform the research in this thesis. In particular, the latitude in the topic and support in the work performed at other institutions cannot be understated.

To Dr. Daniel Macdonald, for his time, discussions and assistance towards getting much of the early work in this thesis off the ground. His insightful viewpoint has helped greatly in narrowing down a seemingly endless topic.

To Murdoch University, namely Prof. Phillip Jennings and Dr. John Cornish for the generous use of the PECVD system there, which was vital for the depositions of all a-Si:H layers as part of this work. Without this access, this thesis would never have come about.

Many thanks to all the staff at the Centre for Sustainable Energy Systems for providing the resources and a safe environment in which to prepare most samples. In particular, to Kathryn Hanton, who got me up to speed on the techniques of wafer preparation; and most importantly, who was able to lend me a hand at the 11th hour with the tremendous number of wafers required for the unique nature of the experimental work had to be accomplished in.

To the Research School of Chemistry (ANU) for access to their FTIR equipment and the staff who patiently waited through the countless measurements. My thanks also to the Research School of Physical Sciences (ANU), for finding time to include some samples as part of their measurements early on. I am very appreciative of Dr. Jan Schmidt at the Institut für Solarenergieforschung Hameln (ISFH) for his generous gift of additional wafers when my supplies were running low. These wafers were very useful in completing some of the experiments in this thesis in time and I could not have done without them. I would also like to recognise Alana Treasure at the University of Canberra for her assistance with Raman spectroscopy and single-handedly maintaining the equipment there.

Finally, to many friends in Perth who gave me a place to stay over the years when I wasn't hard at work in the laboratory.

ABSTRACT

In recent years, the application of hydrogenated amorphous silicon (a-Si:H) to crystalline silicon (c-Si) solar cells for the purpose of surface passivation has begun to move rapidly forward following early innovations by Sanyo. The bulk of the research conducted throughout this thesis has been performed prior to this new drive in the development of a-Si:H/c-Si devices. Understanding the underlying principles and the essential physics concerning the interaction of these two materials has been often overlooked, making further improvements difficult, and limiting new technological developments therein. In this light, the strategies towards merging a-Si:H with c-Si to achieve high-efficiency, low-cost photovoltaics are studied in this thesis, with a focus on the interface and lowering interface states.

Plasma-Enhanced chemical vapour deposition (PECVD) of a-Si:H has commonly been an effective method for achieving uniform coverage of the c-Si surface. However, many deposition parameters have been reported as optimal, stemming from the limited range of experimental conditions examined. In this study, a more complete range of deposition conditions are tested, with the nature of the a-Si:H across a broad array of parameters being investigated. Ideally, a-Si:H layers which are most likely to result in high quality surface passivation should be deposited using temperatures of 225°C, applied *rf*-power at 4W (51mW/cm^2), and partial pressure of 650mT. Notably, the ranges for deposition that can be ideally utilised, are with temperatures between 200°C and 250°C, *rf*-power up to 8W (100mW/cm^2), and partial pressures between 400mT and 750mT. Although the ideal values are somewhat system specific, these broader ranges are common to many PECVD systems.

Previously overlooked in many studies on a-Si:H and indeed most hydrogenated materials is the influence of hydrides on the surface passivation. A widespread belief is that layers hydrogen-rich in their bulk are best for passivation, due to a plentiful source of hydrogen. Analysis of hydride density by IR-spectroscopy has revealed several interesting results which identify some misconceptions concerning surface passivation and the influence of hydrides. In particular, this thesis clarifies the function of the composition and distribution of hydrides throughout the layer and their influence on the quality of the surface passivation; the existence of bulk and interface regions within the a-Si:H layer; and the influence of deposition conditions on the composition and density of hydrides. Ideally, a hydride-rich interface region is shown to yield the most reliable results.

The diffusion of hydrogen from within the a-Si:H bulk towards the interface with c-Si at an energy of 1.5eV has been a widely accepted mechanism governing surface passivation. However, experimental evidence to support this preferential diffusion through a high-defect material such as a-Si:H has been somewhat absent. In this work, an Arrhenius relationship between temperature and surface passivation is revealed, providing evidence that disputes the a-Si:H bulk-diffusion hypothesis in favour of a surface-diffusion mechanism at the a-Si:H/c-Si interface. The thermally activated surface passivation is shown to have energy of 0.7 ± 0.1eV, below that required for bulk diffusion or spontaneous release of hydrogen. From this experimental study, new insight into a surface-related transport model governing the passivation of the c-Si surface by hydrogen already present at or near the interface is presented in this thesis. Determined in this physical model, is the relationship between the likelihood of hydrogen diffusion across a c-Si surface and temperature.

Following from early experimentation using post-deposition thermal annealing to improve surface passivation by a-Si:H, a new plasma-enhanced chemical vapour deposition (PECVD) technique was developed as part of this work. Multi-Layer-PECVD involves the deposition of sub-layers of a-Si:H with thermal cycling, to build up a total layer thickness. This technique of sub-layer deposition is shown to improve the control of hydride density, composition, surface coverage and reduce the inherent thin-film stresses for very thin a-Si:H layers. Comparison of layers deposited by ML-PECVD in-place of standard PECVD showed improved reliability and stability thanks to this new approach to deposition of a-Si:H.

With a greater understanding for the properties of a-Si:H in passivating c-Si and improvements in deposition technique, stacked a-Si:H structures which combine n-type or p-type a-Si:H with a thin intrinsic a-Si:H layer in a HiT-like design are investigated from the perspective of passivating c-Si. Results here show that high-quality surface passivation can be maintained, with recombination velocities and saturation current densities at the c-Si surface as low as $3cms^{-1}$ and averaged below $30fA/cm^2$, respectively, which are equivalent to those achieved with SiO_x and SiN layers.

In a world first application, the a-Si:H(i) and stacked a-Si:H layer structure have been applied in this thesis to the mc-Si surface; whereby, excellent surface passivation results are achieved using both n- and p-type mc-Si. Recombination velocities below $100cms^{-1}$ using only a-Si:H(i) were reduced further to approximately $40cms^{-1}$ with stacked a-Si:H(i/n) or a-Si:H(i/n) layers, without a diffused emitter. In addition, low current saturation densities of $4.5 \times 10^{-14}Acm^{-2}$ and implied open-circuit voltages of 670mV were achieved. In the case of 100μm mc-Si, further reductions are shown

to be possible, opening the doorway for simple, high-efficiency mc-Si based photovoltaic designs at low-cost.

The work in this thesis has yielded an improved understanding relating to a-Si:H/c-Si devices. Fundamental misconceptions concerning the hydrogen passivation mechanism, hydride content and configuration have been identified and a more accurate understanding has been proposed. Although many of the principles in the Sanyo HIT design have recently been reproduced by other groups, the implications of this research remain applicable. Importantly, the research regarding the optimisation of a-Si:H, development of ML-PECVD and many of the preliminary findings of this research are focused on high-efficiency, low-cost next generation photovoltaic designs yet to be developed.

Table of Contents

Glossary of terms and Symbols

Abbreviation	Definition
a-Si:H	Hydrogenated amorphous silicon, annotated, (i) for intrinsic, (n) for p-type, or (p) for n-type.
a-SiC_x:H	Hydrogenated amorphous silicon carbide.
Adsorption	Process involving only a surface reaction, not the entire volume (i.e. absorption).
Alnealed	Sintering of Aluminium on Si/SiO_2 at 400°C in forming gas, then Al layer removed by phosphoric acid.
ARC	Anti-reflection coating
AFM	Atomic force microscopy
Bifacial	Layers deposited onto either side of material
Bond angle deviation	The mean shift in the Si-H bond angle.
BSF	Back-surface field
Cz	Czochralski-method crystalline silicon
DI	Deionised water
B_2H_6	Diborane dopant gas
Float-zone (FZ)	Single crystal silicon, typically of high purity.
[Fe_i]	Interstitial Iron
FGA	Forming gas anneal, usually in N_2 ambient.
FTIR	Fourier Transform Infra-red spectroscopy
Gettering	Surface region which acts as a 'sink' to metallic impurities
Hydrogenation	Passivation by hydrogen of silicon dangling bonds located at the c-Si surface.
H%-content	Measure of hydride content with a-Si:H and at interface with c-Si.
Heterogeneity	Ratio of hydride concentration between interface and bulk regions within a-Si:H.
Heterostructure	Being of two different semiconductors in junction.
HiT	Heterojunction with Intrinsic Thin layer
HNO_3/HF	Nitric acid/Hydrofluoric acid
HWCVD	Hot-wire Chemical Vapour Deposition.
Inter-conversion	Process by which hydrogen is weakly bonded to a 5-fold coordinated silicon atom.

Glossary of Terms and Symbols continued

Abbreviation	Definition
Interstitial trap	Hydrogen made immobile by surrounding network (not by dangling bond).
ITO	Indium Tin Oxide, a transparent conducting material.
RAMAN	Infra-red spectroscopy technique
SRO	Short-range order (<3nm)
microvoids	Vacancies within the a-Si:H layer by which hydrogen clusters around.
ML-PECVD	Multi-layer Plasma-Enhanced Chemical Vapour Deposition
MRO	Medium-range order (<10nm)
Mixed-phase	Involving two phases, (i.e. amorphous and microcrystalline)
n^+	Phosphorus doped emitter region at the surface of c-Si
PECVD	Plasma-Enhanced Chemical Vapour Deposition
PH_3	Phosphine dopant gas
$POCl_3$	Phophorus dopant gas Phosphorus Oxide Chloride.
Pachen limit	Minimum power that can be used to ionise gas given a certain pressure.
Shallow trap	Hydrogen undergoing inter-conversion between silicon atoms.
SiH	Monohydride consisting of a silicon atom bonded with one hydrogen atom.
SiH_2	Dihydride consisting of a silicon atom bonded with two hydrogen atoms.
SiH_x	Polysilyl configuration involving one or more silicon atoms bonded with multiple hydrogens.
SiH_4	Silane feed-gas
SiH_3	Silyl radical
SiO_x	silicon oxide, thin film or alnealed
SiN_x	Silicon nitride
SRO	Short-range order (<3nm)
sub-layer	Individual layer ≤ 1nm, which is deposited at the intial stages of deposition.
TCO	Transparent Conducting Oxide
TEM	Transmission electron microscopy

Mathematical symbols

Symbol	Definition	Si units
α	Absorption coefficient	cm^{-1}
α	Hopping distance between surface silicon trapping sites (2 x 10^{-8}cm)	cm
$A_{0,1,2}$	Pre-exponential factors determined during fitting	cm^{-3}
D_H	Hydrogen diffusion coefficient	-
D_o	Diffusion coefficient for mobile hydrogen	cm^2s^{-1}
E_g	Optical band gap	eV
E_A	Thermal activation energy	eV
J_{oE}	Emitter saturation current density for single c-Si/mc-Si side	fA/cm^2
J_o	Saturation current density	fA/cm^2
k_b	Boltzmann constant	eVK^{-1}
k_a/ k_d	Rate of adsorption/desorption	s^{-1}
k	Extinction coefficient	mol^{-1}
k_{des}	Desorption rate of hydrogen	s^{-1}
λ_{rt}	Mean distance mobile-H travels between emission site & deep-trap site	Nm
λ	Wavelength	M
m	Reaction order of adsorption/desorption	-
n	Refractive index	-
n_i	Intrinsic carrier density	cm^{-3}
N_A	Acceptor doping density	(cm^{-3})
N_{db}	Density of dangling bonds at c-Si surface	cm^{-3}
N_H	Immobile hydrogen density	cm^{-3}
q	Electron charge (1.6×10^{-19} C)	C
ρ	Density of a-Si:H layer	g/cm^3
rf	Radio excitation frequency	Hz
R_{db}	Trapping rate of mobile hydrogen by silicon dangling bond	s^{-1}

Mathematical symbols continued

Symbol	Definition	Si units
R_{th}	Thermal emission rate of hydrogen	s^{-1}
r'	Heterogeneity	-
rms	Root mean square	nm
Γ	Linear relationship between mean bong angle and FWHM	cm^{-1}
S_{eff}	Surface recombination velocity	cms^{-1}
τ_{eff}	Effective minority carrier lifetime at the surface	μs, ms
τ_b	Effective bulk minority carrier lifetime	μs, ms
ω	Wavenumber	cm^{-1}
$\Delta\Theta$	Mean bond angle deviation	degrees
Φ	Flux of mobile hydrogen	cm^{-2}
θ	Hydrogen coverage of the c-Si surface(i.e. passivation of dangling bonds)	cm^{-2}
θ_{max}	Maximum expected hydrogen coverage of the silicon surface (i.e. dangling bond passivation).	cm^{-2}
TA/ω_A	Transverse acoustic Raman mode	cm^{-1}
TO/ω_o	Transverse optical Raman mode	cm^{-1}
LO/ω_{Lo}	Longitudinal optical Raman mode	cm^{-1}
LA/ω_{LA}	Longitudinal acoustic Raman mode	cm^{-1}
Δn	Excess carrier density (cm^{-3})	cm^{-3}
W	c-Si or mc-Si wafer thickness	μm
s/s_o	Trapping probability/coefficient	s^{-1}
ν_d	Desorption pre-factor or desorption attempt frequency.	s^{-1}
ν_H	Emission rate for one mobile hydrogen per Si-H site.	s^{-1}
ν_{th}°	Thermal emission rate	s^{-1}
V_{oc}-limit	Estimated limit in open-circuit voltage	V

1.

General Introduction

As of March 2010, carbon dioxide in the Earth's atmosphere reached 387ppm [1], and based upon a 2ppm/year rate of increase is expected to reach a minimum of 450ppm by 2030. This would correspond to a 2°C rise in global temperatures. To limit the concentration of CO_2 in the atmosphere to 450ppm level, significant mitigation of emissions from power and transport sectors would be required by 2050. This projection does not account for emerging industrial and transitioning economies which, without improved global efficiency can be expected to double or even triple global energy consumption within 10 years. Financially, $4.1 trillion (0.24% of world GDP) of investment has been estimated between 2010 and 2030 to maintain the emission level below 550ppm [2].

> "Humanity already possesses the fundamental scientific, technical and industrial know-how to solve the carbon and climate problems..."
>
> Pacala & Socolow (Science, August 13, 2004) [3]

Indeed, one solution to the growing energy demand, the photovoltaic (PV) effect, a conversion of light to electricity, was first observed in an electrolyte solution more than 170 years ago [4], and in 1954 the first silicon solar cell with a conversion efficiency of 6% was reported [5]. Over the past 30 years, the worldwide photovoltaic market has grown rapidly. Since 2000, production capacity has increased from 288MW/year to 4.28GW/year in 2007, 7.91GW/year in 2008, and in 2010, 18.2GW/year generating an estimated US$82billion of income [6].

1.1 Photovoltaic technologies

Silicon based devices represent 96% of the photovoltaic market and can be divided into four main types: single crystalline (c-Si), multi-crystalline (mc-Si), ribbon and thin-film. An industrially mature technology requiring high purity silicon and strict processing, c-Si accounts for 33.8% of worldwide solar cell production. Although high efficiencies up to 25% ($1cm^2$) [7] have been reported in the laboratory, where, ultra-clean environments and complex processes are available, cell conversion efficiencies below 20% for industry are common [8]. This stems from the difficulty in replicating high-technology processing at industrial scales.

In 1976, conversion efficiencies above 9% ($+4cm^2$) were reported when the c-Si was replaced with mc-Si [9], demonstrating that the purity requirements for silicon PV could be relaxed. In the past decade, mc-Si has become increasingly popular due to lower material cost while achieving laboratory efficiencies of 20.4% ($1cm^2$) in 2004 [10]. Despite industrial efficiencies of mc-Si cells remaining below those for c-Si, their use has grown to almost 48% of the PV market [11]. Currently, most research focuses on achieving laboratory efficiencies in industrial PV production, and reducing overall material costs by reducing the thickness of the base wafers.

For silicon-based solar cells, illumination generates an electron-hole pair which undergoes recombination, either by radiative (inverse of electron-hole generation), band-to-band Auger processes, or via defect levels in the forbidden bandgap. Coulomb-enhanced Auger [12] recombination and Shockley-Read-Hall bulk [13] recombination can be reduced with improvements in the quality and processing of bulk c-Si during growth; however, considerable disruptions to the silicon lattice continue to represent significant recombination sinks. The largest dislocation in the crystalline silicon lattice symmetry occurs at the surface of the material, resulting in unsaturated dangling bonds. Consequently, a high density of surface-state defect within the bandgap occurs which increase the rate of recombination, via these defect states. Importantly, the diffusion length of photogenerated minority carriers from within the bulk of high-quality silicon is in many cases

greater than the dimensions of the solar cell itself, and for thinner wafers, recombination at the surface begins to dominate over that of the bulk. Therefore, the importance of reducing the concentration of these surface defect states is important in improving solar cell performance. Fundamentally, two distinct approaches are employed to reduce recombination losses at the surface:

- Reduction of surface state density,
- Reduction of free electron or hole concentration at the silicon surface

The density of surface states can be significantly reduced by the deposition of a suitable dielectric material onto the c-Si surface. Currently, two leading technologies have found popularity for the past two decades in reducing surface recombination:

- State-of-the-art thermal oxidation of the c-Si surface (SiO_x) at temperatures between 900°C and 1000°C [14], and
- Amorphous Silicon Nitride (SiN_x:H) thin-film by deposition

The transition towards a thin-film passivating layer has led SiN_x to find wide-spread market acceptance for both c-Si and mc-Si surfaces [15, 16], owing to lower deposition temperatures (400°C), improved ultra-violet stability, compatibility with metallised contact formation and use as an anti-reflection coating. Despite the advantages of SiN_x, there are still some inherent impediments, including the dependence on a rear-surface field by metallisation and thermal dopant diffusion. At the research level, SiN_x is deposited onto the metal layer yielding better performance; however, industry uses fire-through metallisation which adds complexity to achieve similar results. By comparison SiO_x requires expensive electronic grade gases, very clean environments, long processing times at high temperatures making the process unsuitable for mc-Si [15, 17, 18]. These aspects are further discussed in chapter 4.

1.2 Hydrogenated Amorphous Silicon

Hydrogenated amorphous silicon (a-Si:H) is an emerging technology, first deposited by Spear and LeComber using Plasma-Enhanced Chemical Vapour Deposition (PECVD) in 1965 [19] and more extensively in studies by Chittick, Alexander and Sterling [20]. The material is unique compared to other passivation layer materials as it can be doped during deposition, transforming the material

into p- or n-type material, which allows the formation of a n/p heterojunction [21]. Although preliminary research into a-Si:H solar cells has been reported since 1981 [22-24] One of the first successful commercial applications of this technology was in the development of a functional imaging device in 1987 [25]. In photovoltaic applications however, using a-Si:H as a bulk photogenerating layer, the material is plagued by degradation following exposure to sunlight, a process known as the Staebler-Wronski effect [26]. However, in the past decade the use of thinner a-Si:H layers and in double or triple-junction device structures [27, 28] in PV applications have made this material more competitive.

In 1985, Yoshiro Hamakawa fabricated the first heterojunction of a-Si:H to c-Si following its proposal by Walther Fuhs in 1974. Then in 1991, Sanyo announced the development of the HIT (Heterojunction with Intrinsic Thin-layer) solar cell, reporting a world record for power conversion of 20% (1cm^2) on CZ-grown n-type c-Si [29, 30]. Several years later, conversion efficiencies of 21% for HIT and HIT-like solar cells on n-type c-Si and 16.2% on p-type c-Si were reported [31, 32]. In 2009, a conversion efficiency of 23% for Sanyo HIT over 100cm^2 was achieved [33-35]. The a-Si:H/c-Si heterojunction design and band-gap structure for c-Si(p) based HIT solar cells is shown in Figure 1.

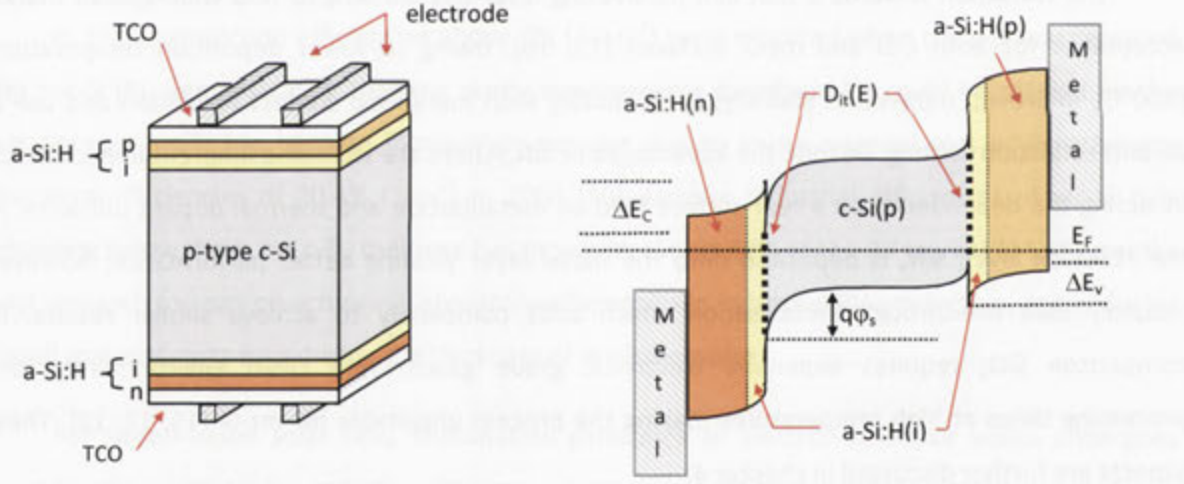

Figure 1: HIT-like a-Si:H heterostructure on p-type c-Si, including electrodes and TCO layer. Band structure is given. Electrons are repelled by the a-Si:H(p) layer, holes are repelled by the a-Si:H(n) layer. For n-type c-Si layers the reverse structure is deposited.

Here, interface recombination is suppressed due to the passivation provided by the intrinsic a-Si:H layer, and secondly by the doped a-Si:H layers which act as a barrier to minority carriers injected from the c-Si wafer bulk. In contrast, a-Si:H deposited onto c-Si exhibit only small, if any, fixed charge densities and are not likely to cause parasitic shunting [36]. In order to achieve a good electronic

interface, suitable wafer pre-treatment prior to deposition is necessary to reduce the density of states at the c-Si surface, which have resulted from structural damage and lattice mismatch, to a minimum. The HIT-like device can be completed entirely at temperatures below 300°C using low-damage plasma deposition, sputtering and evaporation processes.

In Figure 2, the conversion efficiencies achieved by HIT and HIT-like solar cell designs are compared to other photovoltaic device, which are currently record leaders in their classes, according to open-circuit voltage and area. Although, some more traditional designs achieved higher efficiencies, these involved complicated device structures, processing and are generally over much smaller areas. In terms of fabrication to final result, the Hit device presents a significant advantage over both small and large surface areas.

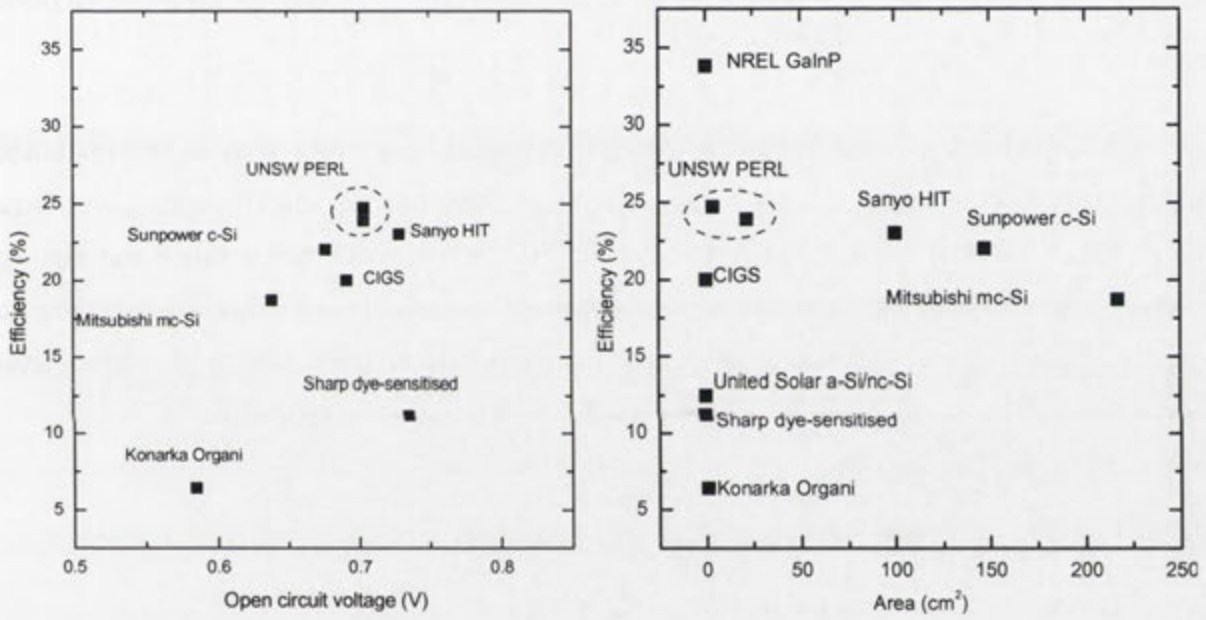

Figure 2: Record conversion efficiencies of HIT and HIT-like solar cells compared to other leading photovoltaic structures/materials [37] in terms of open-circuit voltage and area in which these efficiencies were achieved for.

As for many device types, records do not reflect the standard, and the same is true for HIT-like devices where a diverse range of reported conversion efficiencies are found in the literature (Figure 3). For most HIT-like devices, photovoltaic performance depends heavily on additional anti-reflection coating (ARC) and transparent conductive oxide (TCO) layers. In many devices, the difficulty in balancing the requirements of the a-Si:H layer(s), namely the optimisation of the interface with c-Si, and the requirement for current collection, results in notable losses in performance. For Sanyo n-series HiT, commercial production efficiencies are near 19% (100cm^2) [37].

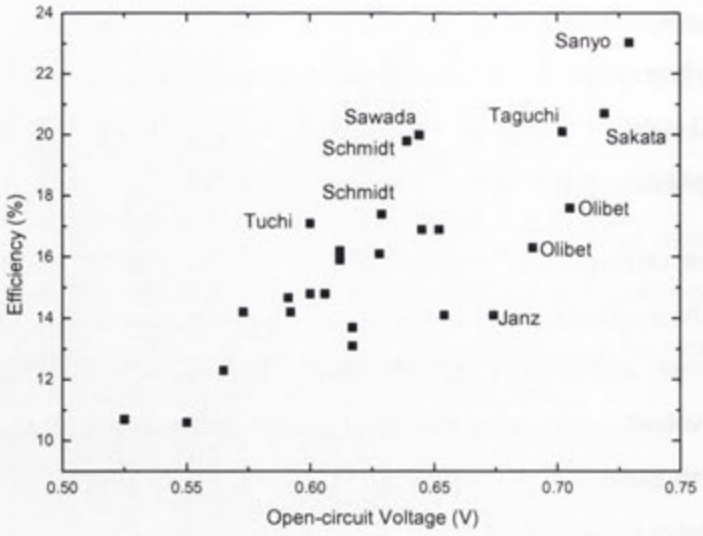

Figure 3: Conversion efficiencies of HIT and HIT-like devices as of 2010. Full details, including area, fill factor and references are given in Table 7 of Appendix C.

In the past few years, interest in a-Si:H and HIT devices has grown rapidly as new materials, processes and technology are being sought to increase overall conversion efficiencies over large areas while simultaneously reducing cost and manufacturing time. With the relaxation and expiring of key patents held by Sanyo on the technology, many in research and industry are rushing to produce similar HiT-like, high quality devices and panels. For clarity, the full listing of research level HiT-like devices is not given here, instead they are provided in Table 7 of Appendix C.

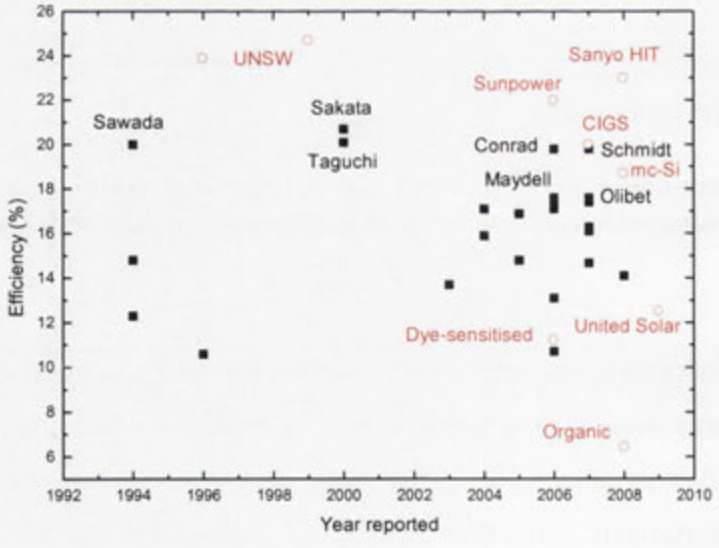

Figure 4: Chronology of HIT and HIT-like device conversion efficiencies. Red (hollow) markers indicate current world leaders by photovoltaic device category [37].

Although alternatives to Sanyo's HiT design are in development, many of the fundamental processes governing a-Si:H and the interactions with the c-Si surface are the same. While deposition and processing conditions are somewhat system specific, our understanding of the interaction of the a-Si:H layers with the c-Si surface and contact formation is frequently inadequate.

In the last 30 years, many techniques and conditions have been reported for the deposition of hydrogenated amorphous silicon layers leading to a range of reported efficiencies (Figure 4). For most cases, PECVD has been demonstrated to produce a-Si:H easily [38-40], although the effectiveness of these layers in passivating c-Si surfaces has been varied. The reasoning for the deviations reported between groups has been largely overlooked, as have the fundamental influences of deposition and processing which govern the a-Si:H layer. Illustrated in Figure 5, are the various processes likely to occur at the growing a-Si:H surface during plasma deposition which may either add directly to the growing surface or subtract from it via sub-surface ion-displacement [41, 42]. The prevalence of each of these processes is dependent upon the deposition conditions and determines the quality of the deposited layer.

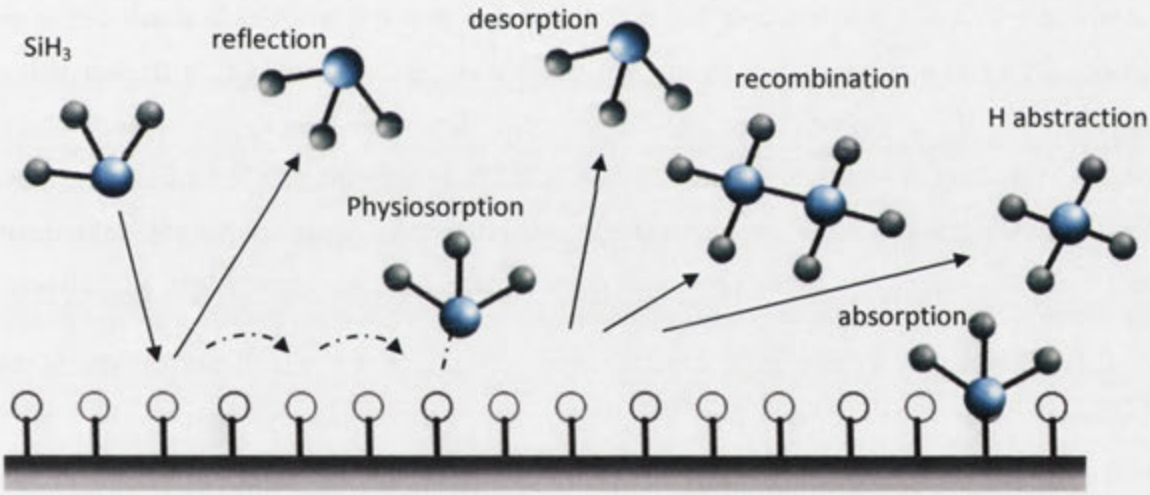

Figure 5: Schematic of SiH_3 processes occurring at the a-Si:H surface during growth [41].

Depending on the deposition conditions and system geometry these mechanisms may be detrimental like ion-damage at high *rf*-power or can be beneficial, as is the case for sub-surface ion displacement [41-43]. Radio frequency powers in excess of 10W [44-46] are often reported as ideal, although surfaces which do not incur plasma-damage from low *rf*-power systems (i.e. ≤ 4W) have also shown improved results [47]. Deposition temperatures between 100°C and 300°C are often reported as optimal, yet contradictory, with performance being linked to differences in the a-Si:H quality and the hydrogen content [20, 29, 44, 45, 48-53]. To this extent, the literature has generally

accepted that surface passivation appeared most effective in occurrence with uniform hydrogen content throughout the a-Si:H(i) layer. To provide sufficient hydrogen for any bulk diffusion towards the interface which may occur, high *rf*-power was presumed necessary due to the direct association with higher hydrogen contents within the a-Si:H bulk [42, 54-58]. The third parameter, partial pressure or the ratio of flow rates of feed-gas and exhaust gasses during deposition is largely system specific and often associated with plasma composition [44, 49, 59]. The uncertainty has been compounded further by debate over optimal layer thicknesses required for passivation of the c-Si surface [45, 60-62]. The premise for many of these assumption overlooks the actual distribution of hydrides within the a-Si:H layer itself.

Although, HIT-like devices are simpler in design, they still must undergo post-deposition thermal treatments for completion in addition to obtaining high quality layers during deposition. Indeed, Gleason *et. al.* [63] reported that the deposition temperature and anneal temperature both influenced the total hydrogen content of the a-Si:H layer. Given that the density and microstructure are controlled by the deposition temperature the optimal range is important. Similarly, thermal annealing of deposited a-Si:H at high temperatures commonly resulted in degradation of the material [59]. At lower temperatures, thermally induced improvements in surface passivation were possible, although until recently, only thought suitable above 200°C [54, 64]. It is clear that our understanding of the hydrogenation process from thin film passivating layers remains obscure. Studies of hydrogen in SiN_x at temperatures above 400°C had suggested that bulk hydrogen diffusion from within the thin-film layer is responsible for passivating the c-Si surface [65-69]. Subsequently this process was assumed to be the case for all lower temperatures and applicable to a-Si:H layers.

However, a number of questions remain unanswered with this hypothesis, like why is there preferential diffusion of hydrogen through a highly defective bulk material towards the interface with c-Si? What is the cause of hydrogenation of the c-Si surface at temperatures below 200°C? As previously mentioned, it was thought that surface diffusion of SiH at temperatures below 200°C did not occur as thermally induced improvements in surface passivation had only been observed above this temperature. However, improvements have been reported at temperatures below 200°C [29, 30, 70-72].

In 1975, Pandey, Sakurai and Hagstrum introduced the concept of a trihydride (SiH_3) which could aid hydrogenation [73], a concept supported by Takakuwa *et. al.* [74], despite the degrading effects that the presence of SiH_3 has on passivation quality. Appelbaum, Hamann and Tasso [75] argued on the possibility for H-atoms to bond to a subsurface (2nd layer) of silicon atoms at the

<100> surface with a lower binding energy. In both cases, these and other alternative explanations were dismissed in favour of the bulk hydrogen model.

The confusion surrounding deposition, thermal processing, thickness, structure, and hydride composition necessary for producing the ideal a-Si:H layer, as well as a higher level of light absorption for thick layers (i.e. above 200nm) has until recently, resulted in this material largely being dismissed as an alternative to SiO_x and SiN_x for photovoltaics, except as a thin rear-side layer in some cases [76] (excluding the work of Panasonic Solar). It becomes clear that the potential of this material has not been fully utilised due to our lack of understanding.

1.3 Objectives and Thesis Outline

In this thesis, the deposition conditions, post-processing thermal characteristics of a-Si:H and this material's application to HiT-like structures are investigated on single and, for the first time, on multicrystalline silicon to both clarify processing conditions and to improve our understanding of a-Si:H for solar cell passivation. The large array of different thicknesses, deposition conditions, system geometry, and other processing parameters has meant no clear profile of a-Si:H layers suitable for photovoltaic applications has been forthcoming. These results and conclusions reported by previous studies are provided, where relevant, at the beginning of each chapter.

In the literature, the goal has often been to reproduce the results of Panasonic's (Sanyo) HIT, overlooking much of the underlying processes. Therefore, in this work a key objective is to identify the deposition and processing conditions required for utilising thin a-Si:H layers on the front and rear surface of photovoltaic devices, with the focus being on lowering interface states. Various techniques are employed to identify not just the ideal conditions required but also to contribute to clarifying the ambiguity causing those earlier results. In particular, the mechanism of surface passivation is re-considered for low deposition temperatures of a-Si:H. Finally, the optimal a-Si:H layers from this work are applied to *float-zone* c-Si and mc-Si aiming, solely at improving surface passivation.

This work focuses on surface passivation and on the properties of a-Si:H. Although some consideration is given to the solar cell, functional devices are not reported here. Nevertheless, solar cell precursors based on a-Si:H stacked layers are investigated for their fundamental properties concerning surface passivation. In addition, the first use of a HiT-like, a-Si:H stacked layers on the multicrystalline silicon surface as a method of passivation is also investigated in this thesis. Once the

understanding of the characteristics for a-Si:H layers themselves and the role they play is more extensive, thinner layers, less processing and more reliable efficiencies are likely possible.

Chapter 2 examines the importance of deposition processing conditions on the passivation of a-Si:H onto *float-zone* c-Si. The suitability for passivation of these surfaces by a-Si:H is presented in respect to thickness, deposition rf-power, temperature, and partial pressure by introducing the concepts of hydride classification and density in addition to standard characterisation techniques.

Chapter 3 examines the influence which post-deposition thermal annealing has on the optical, electronic and structural properties of the a-Si:H(i) layers relevant to solar cells, including the stability of these layers. Hydrogen from the a-Si:H layer and its interaction with the c-Si surface is studied, to determine the activation energy for thermal surface passivation at low temperature. An alternative mechanism for surface passivation which is governed through a series of surface states and the origins of the hydrogen involved in this passivation is presented in this chapter.

Chapter 4 addresses the use of a-Si:H stacked heterostructures on non-diffused *float-zone* c-Si wafer surfaces after looking firstly at surface recombination for n+ diffused emitters passivated by optimised a-Si:H. The ability of doped-intrinsic heterostructures to replace thermally diffused emitters and the Aluminium Back-Surface-Field is assessed only so far as demonstrating surface passivation.

Chapter 5 reports on the first application of a-Si:H(i) and stacked heterostructures onto both non-diffused n- and p-type multicrystalline surfaces at low temperature. A further extension of a new deposition technique is applied to optimise the surface passivation achieved for wafer thicknesses as thin as 100μm.

Chapter 6 gives a summary of the main contributions of this thesis, outlining future progress and the technical applicability of this work.

In **Appendix A**, the electrical and optical characterisation techniques used in this thesis are presented, including reference to values discussed. **Appendix B**, provides some supplementary information concerning the annealing of a-Si:H layers in relation to dopant concentration of c-Si base wafers. **Appendix C**, provides a list of current research level devices which are discussed in the introduction.

2.

Optimisation of Deposition

The unique structure of hydrogenated amorphous silicon and the mechanisms therein have led to widespread discrepancies over the past 20 years regarding the optimal thickness of both intrinsic and doped layers [45], and processing conditions [59, 77-79]. A consequence of this is that many deposition and process conditions are often recommended to achieve high-quality a-Si:H layers with little emphasis placed on the characteristics or application of the material.

- Deposition temperatures ranging from 100°C to 300°C [20, 29, 44, 45, 48-53, 80]
- Deposition radio frequency power in excess of 10W [44-46]
- Deposition gas flow rates from 2sccm to 200sccm with variable feed-gas ratios [44, 49, 59]

Additional post-deposition processing, including thermal annealing and light soaking, have further extended the range in results. In this chapter, work is presented concerning the effect of different deposition parameters.

2.1 Deposition technique and experimental procedure

2.1.1 Plasma Enhanced Chemical Vapour Deposition (PECVD) of a-Si:H

Deposition by PECVD consists of the excitation of molecules in a precursor gas to a charged, plasma state whereby they deposit as a film onto a substrate under the influence of a bias electric potential. A 13.56MHz radio-frequency (*rf*) excitation field is used as standard in most capacitively-coupled systems due to the reduced radiation damage of the silicon surface at this frequency [81]. The primary growth species of a-Si:H during PECVD originates in the ionisation and decomposition of Silane (SiH_4) into the Silyl (SiH_3) radical [82, 83]. During deposition, SiH_3 incident onto the silicon substrate surface decomposes further into monohydride (SiH). In some cases, dihydride (SiH_2) can also occur, although according to Oura *et.al.* [84], due to the slower formation of this hydride, it is expected to have a lower concentration during deposition.

Deposition of a-Si:H layers in this work was performed by direct *rf*-PECVD using a low-power *rf*-excitation parallel plate system custom-manufactured at Murdoch University, which places the deposition growth surface above the plasma (see Figure 6) as opposed to most commercial systems which deposit downwards, onto the lower electrode.

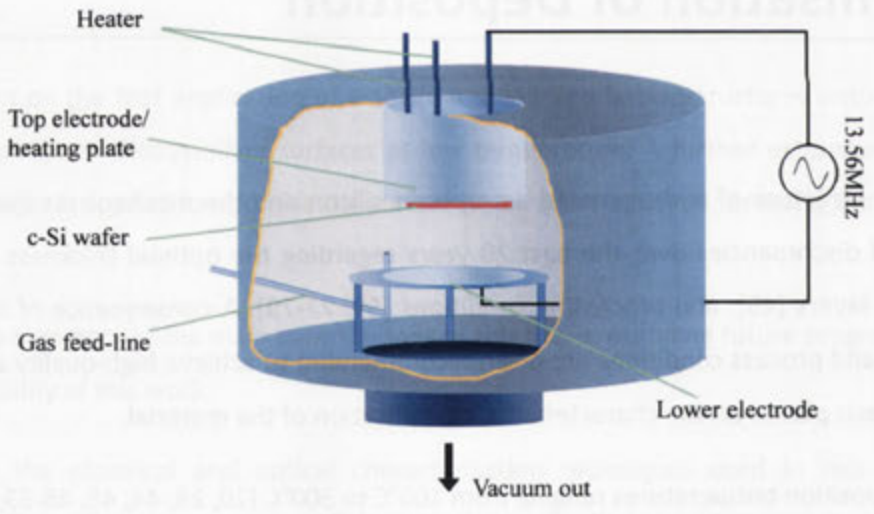

Figure 6: Schematic diagram of PECVD system used in this work. Samples are placed inverted onto the top heating electrode.

All silicon wafers, following silicon damage etch, RCA clean and dilute HF immersion (see section 2.1.2), are loaded into the PECVD system. Each sample wafer is fitted within a substrate holder which is then fitted to the upper heating electrode approximately 25mm from the lower

electrode. The chamber is then sealed and evacuated to below 10^{-7} mT. Argon flushing is done to remove any residual contaminates before the process gases are mixed in-line at the desired flow rates, before entering the chamber. Partial pressure and suitable atmosphere were maintained by the continuous supply of process gases, while heavier ionised gases were extracted away from the substrate, beneath the lower electrode. Silane (SiH_4), diborane (B_2H_6) and phosphine (PH_3) process gases are used to deposit intrinsic (i), p-type (p) and n-type (n) a-Si:H layers, respectively. For doping a-Si:H layers, the diborane or phosphine are pre-mixed with silane before entering the chamber.

Standard process variables of this investigation included:

- Deposition temperature – varied from between 100°C and 280°C
- Gas flow rates – Silane (45-100sccm), Diborane (35sccm), Phosphine (35sccm)
- Deposition partial pressure – varied from between 0.2T and 1.4T
- Deposition *rf*-power – varied from minimum of 1W to a maximum of 20W

It should be noted that the deposited region for this system represents a fraction of the total plasma deposition area to avoid the effects of the plasma 'sheath' at the edges. Consequently the actual power density for the deposition area is approximately 0.012 Wcm^{-2}. The role of plasma dynamics was not investigated during this optimisation study, although some consideration of the relationship between plasma-based and surface-based deposition parameters is discussed.

All c-Si wafers substrates were bifacially deposited with a-Si:H layer(s). As illustrated in Figure 6, it is only possible to deposit one surface at a time; therefore, the wafer must be removed from the system, and turned over before being placed back into the system and returned to vacuum. The total time the samples were removed from the system and exposed to ambient air was less than one minute, which would limit any native oxide growth.

2.1.2 Preparation of crystalline silicon surface

The nanometre dimensions of the a-Si:H layers deposited onto the c-Si substrate require the careful preparation of the silicon surface to ensure its suitability both chemically and physically. All c-Si wafers underwent a Nitric/Fluoric acid (HNO_3/HF) silicon etch (4:1) to remove surface damage. Following this, wafer surfaces were cleaned. The preparation procedure is outlined below.

- Larger 125cm x 125cm wafers were etched for, on average, 7 minutes until a uniform 'shiny' surface was achieved, then rinsed in deionised (DI) water.
- Each wafer was then diced into 12 smaller segments by a dicing saw
- Samples first being immersed into H_2O:NH_4:H_2O_2 (4:1:1) solution for 10 minutes, followed by rinsing in DI water
- A second immersion in H_2O:HCl: H_2O_2 (4:1:1) solution for 10 minutes to remove metallic contaminates, followed by a rinse in DI water.
- Immersion in diluted HF(10% in DI water) to remove native oxide [85, 86], DI water rinse and N_2-dry is performed

The importance of Shockley-Read-Hall recombination within the silicon bulk is reduced for high-quality *float-zone* silicon improving the sensitivity of the surface recombination measurement [87, 88]. Unless otherwise stated, two types of *float-zone* c-Si have been used throughout this thesis.

- 1.4Ωcm phosphorus doped n-type
- 0.9Ωcm boron doped p-type

Throughout this chapter c-Si(n) wafers are primarily discussed, although similar experiments were performed on c-Si(p). The latter results have been omitted for clarity. Thin a-Si:H layers were also deposited onto glass substrates to assist in ellipsometry measurements. Glass sides (Corning 7059) were prepared by cleaning in iso-2-propanol, acetone and DI water rinsed under ultrasonic agitation, and N_2-dry.

2.2 Deposition rate and a-Si:H thickness

In deposition of a-Si:H by PECVD there often exists a direct relationship between the deposition time and the thickness of the deposited layer, allowing the rate of deposition to be easily calculated. In many cases this overlooks the dynamic nature of ionisation at ignition and also the growth properties of the a-Si:H. Consequently, thin layers are often variable in quality, uniformity and likely stoichiometry. In situ ellipsometry is useful for thin layers during deposition, although difficult to implement on many systems, as was the case here. To determine the deposition rate, thickness and quality of the deposited a-Si:H layers, a series of c-Si and glass substrates are used with a-Si:H(i) deposition times between a few seconds, up to 10 minutes. For this, the deposition

conditions of 225°C, nominal 4W (50mWcm^{2}), and 650mT are adopted, although others were tested. Multispectral ellipsometry, first developed for in-situ studies in 1987 [89, 90] and since expanded upon this work is used to measure a-Si:H layers simultaneously deposited onto both c-Si and glass substrates due to the difficulty in discerning α and k for very thin layers on c-Si at the commonly used single wavelength of 632nm.

In Figure 7, a strong linear correlation between the deposition time and the thickness of the a-Si:H(i) layer is shown to exist. For the thickness range examined, a high degree of control over the layer thickness is achievable with the PECVD system in this work. A high growth rate of 4Ås^{-1} is determined.

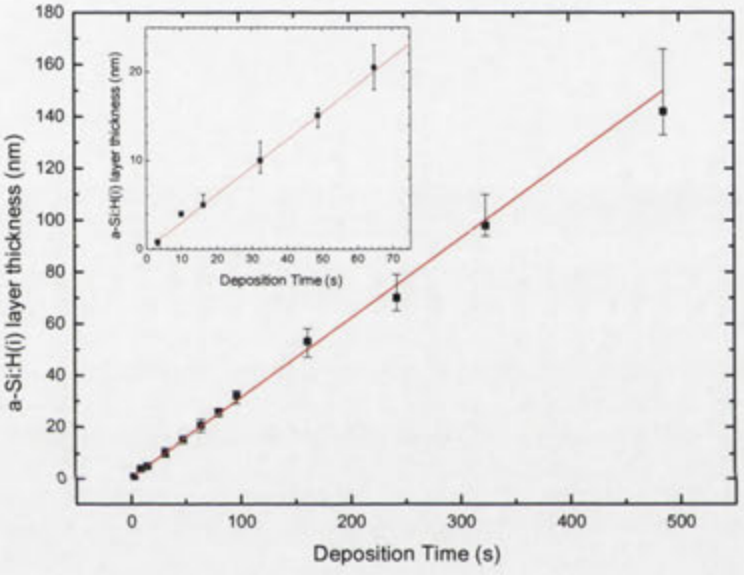

Figure 7: The mean, upper and lower layer thicknesses of a-Si:H(i) determined by deposition time. Deposition conditions: temperature = 225°C, *rf*-power = 4W applied, partial pressure = 650mT. Insert: shows non-linear region for very short deposition times.

A slight divergence in the linear relationship occurs at either extreme of the tested range of thicknesses. Variation of thicker layers can be expected as growth kinetics and their rates change. During the initial stages of growth, different growth surface kinetic mechanisms occur, beginning with 'islands'[1] [47]. The first few monolayers of coverage are formed during the coalescence of these islands [91], which may lead to initially differing, but temporary thickness variations. It is the continuation of columnar growth from these islands into the aggregation phase that can introduce

[1] 'Islands' form from the initial seed points of SiH_3 bonding to the c-Si surface. Ideally the density of these islands per cm^{2} would yield improved surface coverage prior to aggregation.

regions of unpassivated c-Si surface and the formation of voids [92, 93] when using non-ideal deposition conditions.

The evolution of a-Si:H(i) is examined over this range of thicknesses, between 5nm and 100nm in Figure 8, for the first time, by measuring the Raman scattering spectra according to the method described in Appendix A. No correction for the spectra to remove the c-Si substrate is necessary as silicon in crystalline form has only one active Raman mode located at 520cm^{-1} [94-96]. Typically, increases in the thermal acoustic (TA) band suggest that medium range order is improved [97-99], although this also occurs as the dihedral angle of Si-H bonds shift for thicker layers under stress due to the presence of hydrogen [100]. The unchanged broad thermal optical (TO) band implies that short-range order (SRO) [101-103]. That is the layers remain amorphous despite increases in thickness.

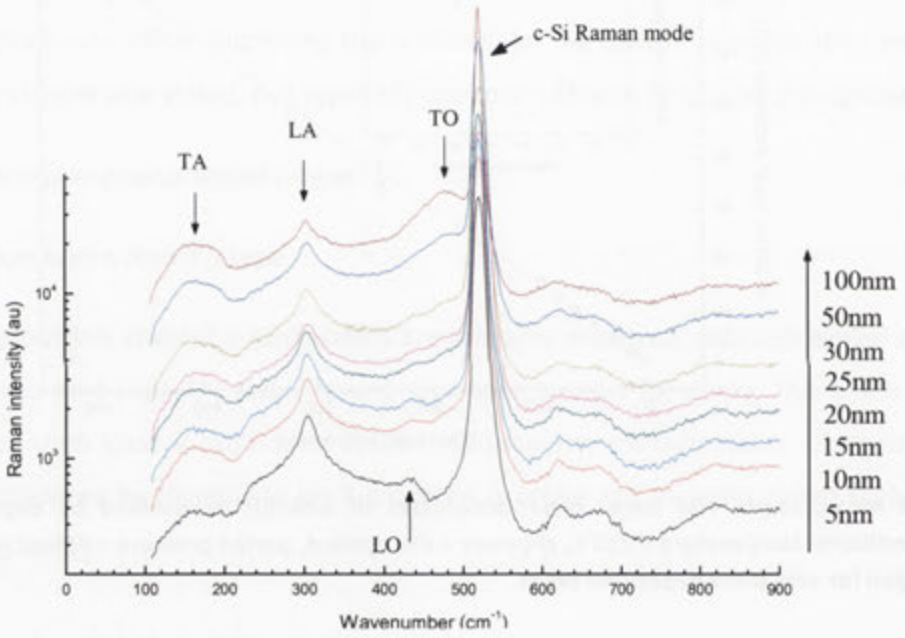

Figure 8: Evolution of a-Si:H(i) Raman scattering spectra for layer thicknesses between 5nm and 100nm on 1.4Ωcm c-Si(n) *FZ*. The curves on the graph have been shifted vertically to show the effect of different temperatures more clearly.

The peak position of the TO, LO, and TA-bands for a-Si:H(i) layers between 5nm and 100nm in thickness are given in Figure 9. The TO-band (ω_{TO}) can be seen to have shifted to higher wavenumbers as layer thickness increased up to 50nm as would be likely for thicker layers but remains approximately 480cm^{-1}; the shift may simply be an artefact related to thicker layers absorption. Typically, blue-shift in ω_{TO} has normally been associated with some crystallisation

around the surface of micro-voids forming hydrogen clusters [45, 104-107]. However, consistent with Tanino *et. al.* [47], no decrease in the full-width half-maximum (FWHM) is observed, indicating that no improvement in SRO, characteristic with crystallisation around micro-voids by hydrogen clusters has occurred.

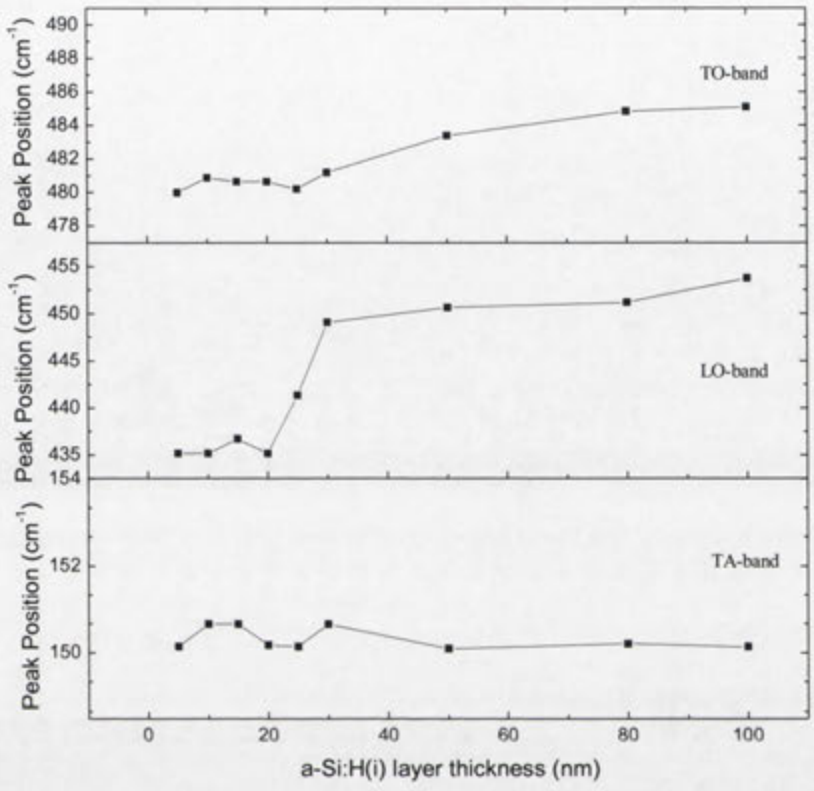

Figure 9: Peak position (ω) of TO, LO, and TA-bands for a-Si:H(i) layers of different thicknesses. The LA-band is omitted as no change was observed.

Increases in the intensity of the TA-band but not the position of ω_{TA} confirm that the blue-shift in ω_{TO} is related to variations in the Si-H bond-angle concerning a hydrogen-rich layer at the interface which has been previously reported [108, 109]. Lastly, the relaxation of Si-H bonds and an increase in the hydrogen content of the a-Si:H(i) is described by the shift in ω_{LO} without an increase in the intensity of the LO-band. From Raman studies, it is concluded from this, that no crystallisation or increase in SRO was observable either at the interface with the c-Si surface or within the bulk of the a-Si:H layer, and the layers deposited in work are indeed amorphous. The silicon-hydrogen bonding relationship is discussed in later sections of this thesis.

Studying the surface of amorphous materials by atomic force microscopy (AFM) and transmission electron microscopy (TEM) reveals the macroscopic structure of layers deposited.

Operating in non-contact mode, the AFM of a 15nm a-Si:H(i) layer deposited onto 1.4Ωcm c-Si(n) *FZ* reveals a relatively smooth layer is deposited (Figure 10) as indicated by the calculated r.m.s. ≤ 1nm, suggesting that the aggregation smoothing mechanism is uniform.

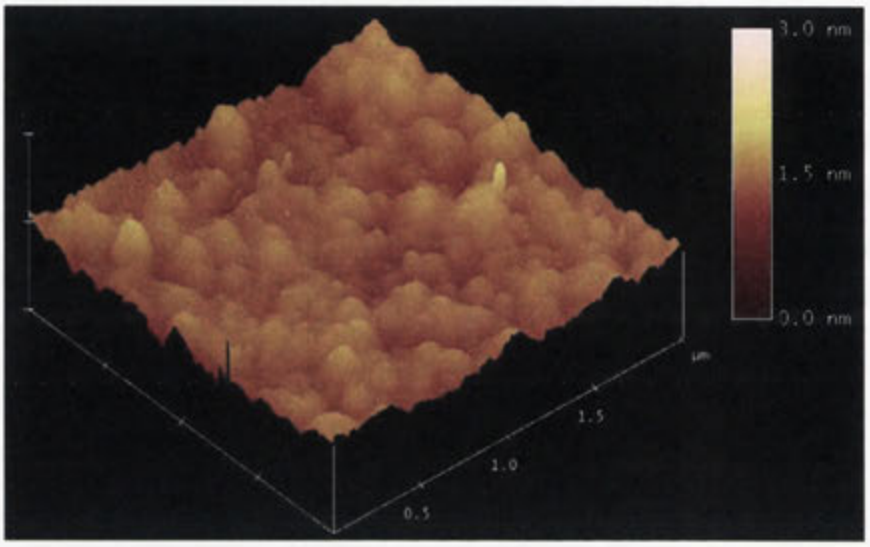

Figure 10: Atomic force microscopy of 15nm a-Si:H(i) layer deposited onto c-Si(n) *FZ* surface at 225°C, 4W applied, 650mT. Surface roughness is on average ~*1nm*.

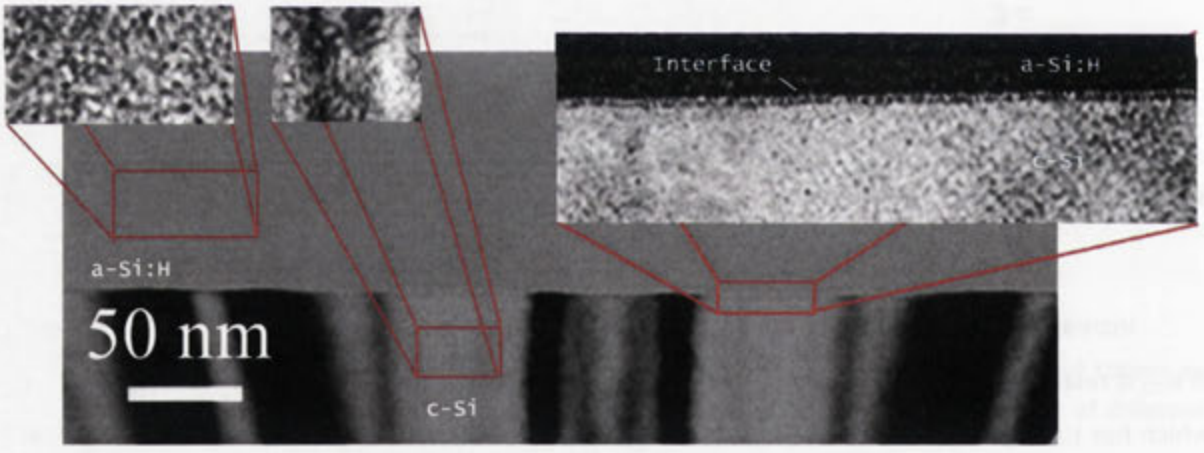

Figure 11: Micrograph taken using TEM of 100nm a-Si:H(i) layer deposited onto c-Si(n) *FZ* at 225°C, 4W applied, 650mT. The contrast has been enhanced to show more clearly the a-Si:H/c-Si interface and the a-Si:H bulk.

The roughness of the interface can be visualised in the micrographs taken using TEM of 100nm a-Si:H(i), shown in Figure 11. A smooth interface region is apparent here, demonstrating that suitable fine-control of the initial a-Si:H(i) layer growth at low *rf*-power is achieved. Furthermore, the deposition of thicker a-Si:H(i) layers does not impact on the smoothness of the interface region as

has been commonly reported [64, 110]. The TEM micrograph also confirms Raman and FTIR spectroscopy results concerning the lack of microcrystalline Si formation in the a-Si:H(i) bulk or epitaxial growth at the interface.

2.3 Influence of *rf*-power on a-Si:H

In direct PECVD, the applied power of the radio frequency which excites gases to their ionised state needs to be sufficiently high to maintain plasma stability. Many systems will operate at 70 W (130mW/cm^2) and above [45], referred to as a 'high' *rf*-power regime in this work. Characteristic of high *rf*-power PECVD, is the ion-damage of the c-Si surface and to the growing a-Si:H layer, which has led to mixed results in the quality of the a-Si:H layer and passivation of the c-Si surface [65, 111, 112]. It is known that the defect density at the c-Si surface and within the a-Si:H layer increases as a result of the ion-damage during deposition [113]. Ion-damage causes an alteration of the material, including epitaxial growth and void formation. Kim *et. al* [111] reported high epitaxial growth for a-Si:H films deposited at *rf*-powers between 50W and 400W at a temperature of 150°C.

Therefore, deposition using lower *rf*-powers, limiting ion-damage, appears a likely solution. However, the poorer quality of the a-Si:H layers when deposited at the minimum operating *rf*-power levels of many systems remains somewhat problematic [87]. Indeed a high density of voids within the a-Si:H layer have been reported by Danesh *et. al.* [45]; reducible only when using both higher temperatures and a *rf*-power of 133mW/cm^2. These results were confirmed by Fujiwara and Kondo [40], who reported mixed phase a-Si:H/μc-Si:H occurring when using low *rf*-power and deposited at 150°C. The adherence for depositions to occur using either high *rf*-power with high temperatures (>280°C) or low *rf*-power with very low temperatures (<180°C) are localised solutions which overlook the direct impact ionisation has on the a-Si:H layer quality.

The PECVD system in this work operates easily within a low *rf*-power regime below 5W (~60mW/cm^2), although intermediate to high regimes are possible. Intrinsic a-Si:H layers are deposited for a range of rf-powers onto 180μm-210μm thick 1.4Ωcm *FZ* c-Si(n), with the effective carrier lifetime[2] measured according to the method described in Appendix A and the surface recombination velocity calculated using equation (A 5). The results are shown in Figure 12. For simplicity, *rf*-powers are given in terms of applied power; although, as a guide intermediate rf-

[2] A measure of the time delay before a photogenerated charge recombines at the interface (i.e. electron with hole)

powers are considered to be above 10W (~120mW/cm^2) and high *rf*-power considered as above 20W (~240mW/cm^2). A deposition temperature of 225°C and partial pressure of 650mT are used. Evident is the passivation performance of the a-Si:H(i) layers deposited within the low *rf*-power regime compared to higher *rf*-powers. The results here show a clear improvement over passivation results for similar layers deposited at higher *rf*-powers [45, 112, 114]. The significant decrease in passivation when a-Si:H layers are deposited with increasing *rf*-power, particularly above 10W, highlights the effects of ion-damage and the negative impact on passivation. From this, it can be concluded that deposition of a-Si:H(i) is best performed at low *rf*-power, below 8W (~100mW/cm^2), ideally at 4W (~50mW/cm^2). This is not to say that suitable passivation quality cannot be achieved at higher *rf*-power as indicated by some results, although variable for layers deposited at 12W. This is the case if the ion-damage during deposition remains limited to the a-Si:H bulk and does not impact the c-Si surface and interface region.

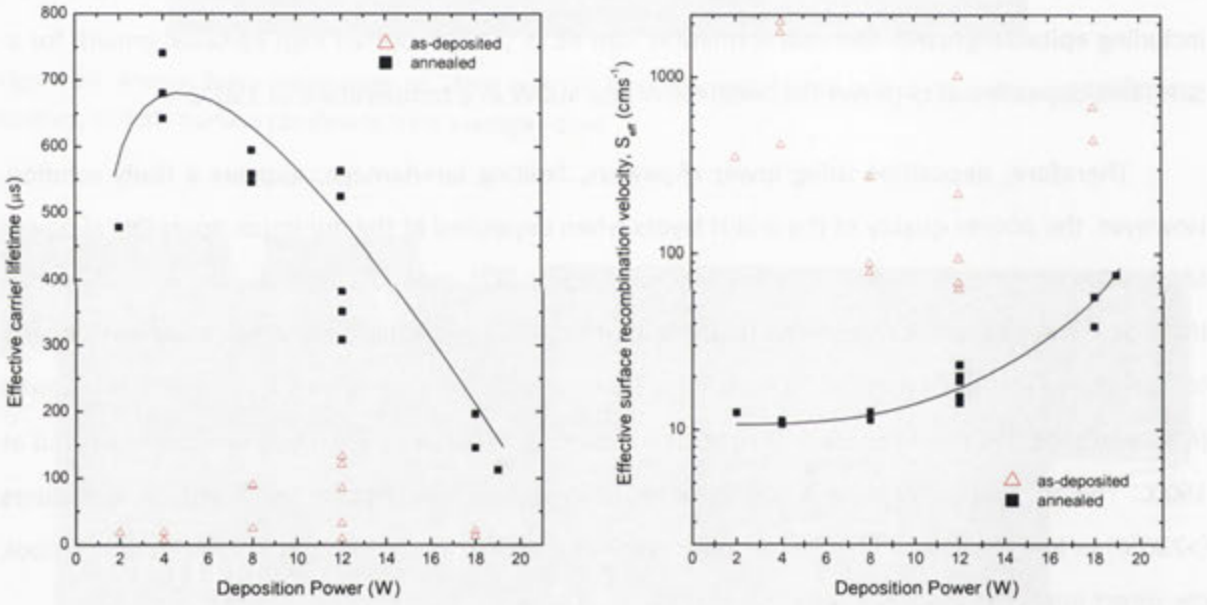

Figure 12: The influence deposition *rf*-power has on the measured τ_{eff} and S_{eff} for 1.4Ωcm *FZ* c-Si(n) at 225°C and 650mT. As-deposited (hollow) and post-deposition annealed (solid) states are shown. Post-deposition thermal anneal performed at 230°C. Line is a guide only.

To better understand how the *rf*-power impacts the a-Si:H(i) layers and influences the ability for this layer to reduce recombination at the c-Si surface, FTIR spectroscopy of as-deposited and annealed layers of different thicknesses are evaluated focusing on bulk and interface monohydride (SiH) density and composition. All results were background corrected to c-Si only. The most relevant results from analysis of the FTIR spectroscopy, that being thinner a-Si:H layers, is given in Figure 13.

As the deposition *rf*-power is increased, the extent of the ion-damage is most clearly observed for 5nm, which shows a significant decrease in hydride bond density (Figure 13a). This agrees with similar experiments using higher rf-powers performed by Danesh *et. al.* [113]. For 10nm and 25nm a-Si:H(i) layers, the effect is seen to be less pronounced (Figure 13b/c).

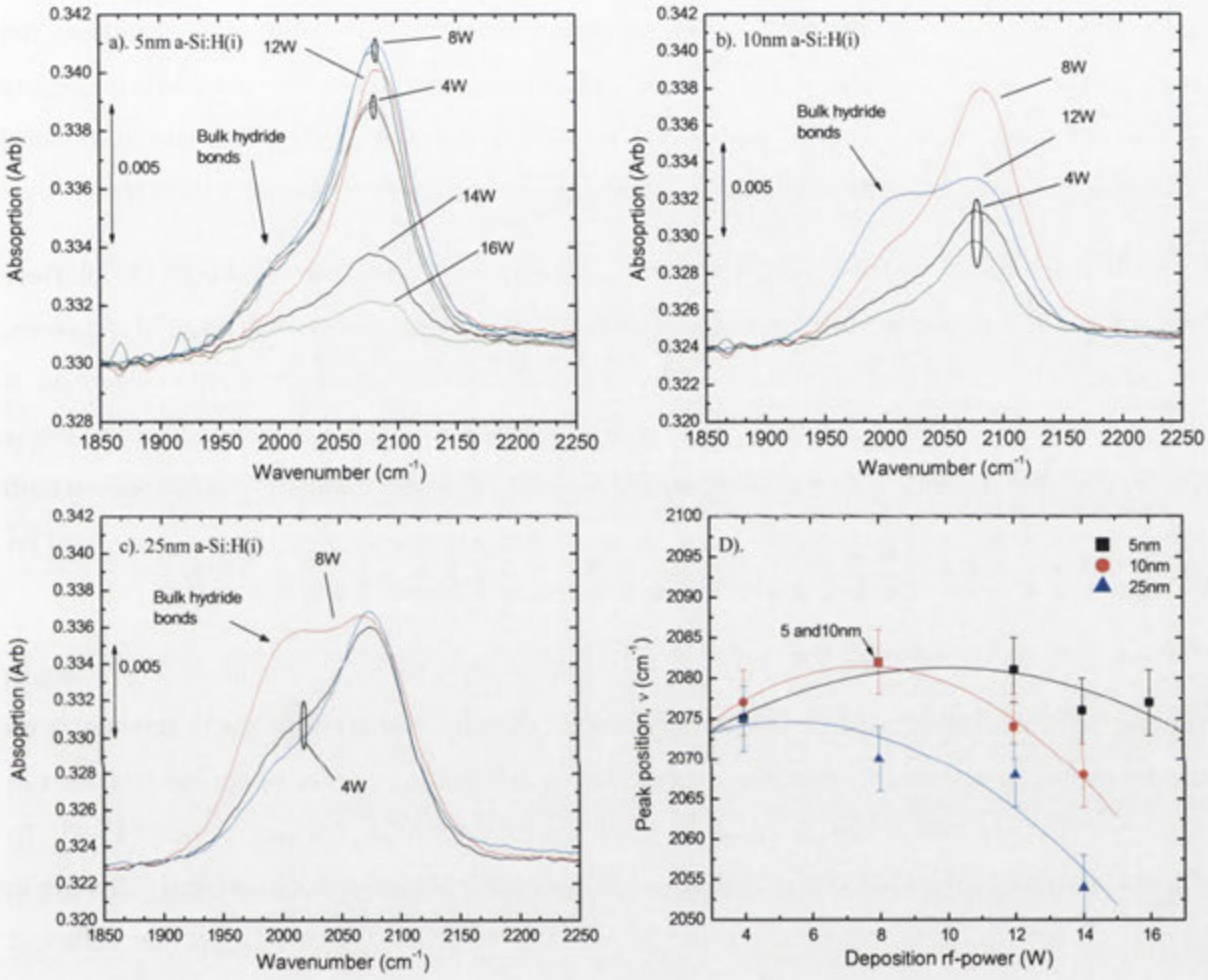

Figure 13: IR absorption spectra for annealed a). 5nm, b). 10nm, c). 25nm a-Si:H(i) layers deposited onto 1.4Ωcm c-Si(n) *FZ* with increasing *rf*-power. (d). Shows the shift in high-frequency hydride stretching mode.

A shift in peak position shown in Figure 13d suggests that the passivation of the c-Si surface and the effect that *rf*-power has on the a-Si:H is more complex than simple ion-damage when using high *rf*-power.

During growth, incident ions continually extract hydrogen in certain hydride configurations from the a-Si:H surface [38, 115-118] (see Figure 5), which can deteriorate the quality of the a-Si:H layer, however, may also allow for optimal repacking. At higher *rf*-powers, ion-damage is less discriminating and can deplete the hydrogen surface states essential to passivation of the c-Si

surface itself. The shift to lower wavenumbers for higher *rf*-powers observed in Figure 13d, representing increases in the concentration of the bulk hydride mode, characterises the higher hydrogen content of bulk a-Si:H region. Generally speaking, this would be thought to be beneficial for the purposes of passivation, on the basis that hydrogen diffuses from the bulk of this layer towards the interface with c-Si. However, the results in Figure 12 showed that improvements in the passivation of c-Si were not forthcoming by simply increasing hydrogen content. Alternatively, the shift towards lower wavenumbers has been associated with variations in the local electronegativity of the Si-H bond, influencing Si-H inter-atomic distances and would signify a decrease in the local hydrogen concentration for films containing a fractional percentage of hydrogen [119-121].

To resolve the confusion in this, calculation of the hydride bond densities at both the interface and within the bulk of the a-Si:H layer are performed for the first time over this range of *rf*-powers, according to the method in Appendix A-3. The results of this analysis are displayed in Figure 14. It can be seen that the bulk and interface hydride densities are similar for *rf*-powers of 10W and below, consistent with the levels of passivation given in Figure 12. However, the density of hydrides in both the bulk and interface regions exhibit the same rapid decrease when higher *rf*-powers are used for deposition, coinciding with the fall in passivation also observed in this work.

It is known that during PECVD several mechanisms can occur to assist in improving hydrogen content and thin film quality of a-Si:H through reconstruction or repacking [41, 42]. Depending on the deposition conditions and system geometry these may mechanisms may be detrimental like ion-damage at high *rf*-power or can beneficial, as is the case for sub-surface ion displacement [41-43]. To this extent, the literature has generally accepted that surface passivation appeared most effective in occurrence with uniform hydrogen content throughout the a-Si:H(i) layer. To provide sufficient hydrogen for any bulk diffusion towards the interface which may occur, high *rf*-power was presumed necessary due to the direct association with higher hydrogen contents within the a-Si:H bulk [42, 54-58]. However, the premise for this assumption overlooks the actual distribution of hydrides within the a-Si:H layer itself.

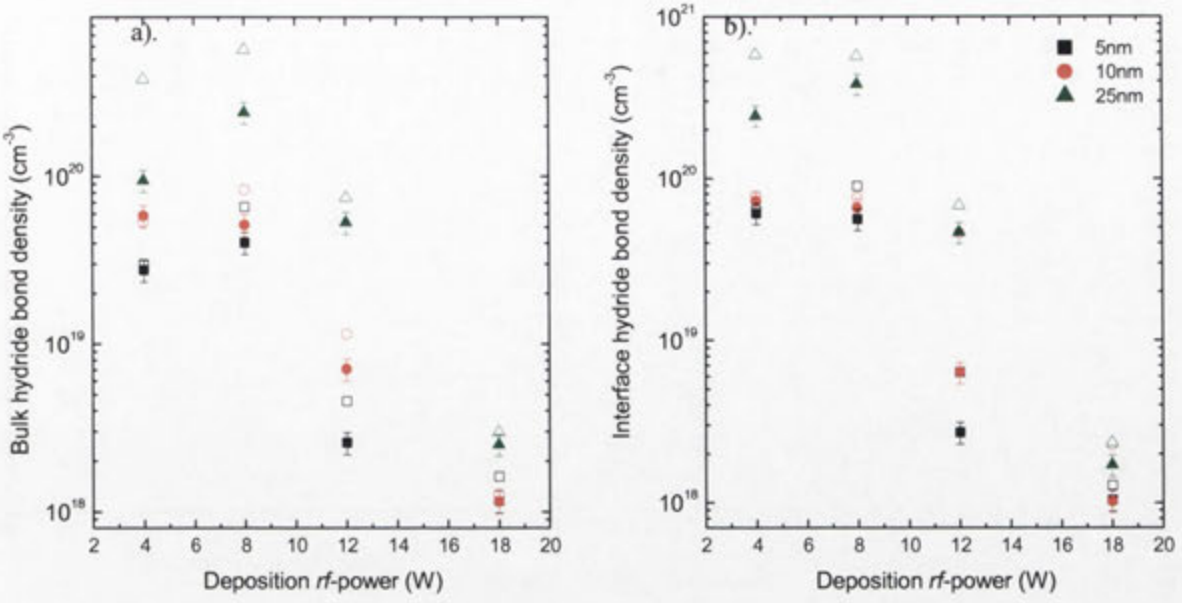

Figure 14: Hydride bond densities calculated from IR absorbance spectra 5nm, 10nm and 25nm a-Si:H(i) layers deposited onto 1.4Ωcm *FZ* c-Si(n) according to method in Appendix A, a). Bulk monohydride (SiH) and b). interface hydride (SiH and SiH_2). Hollow markers indicate as-deposited measurement. A conservative 15% error has been shown.

In Figure 15, the total monohydride bonded hydrogen content at the interface and the heterogeneity, a measure of the proportion between interface and bulk hydrides, is given. The total bonded hydrogen content is seen to decrease rapidly when higher *rf*-powers, above 10W, are used; indicating that ion-damage to the growing a-Si:H layer is significant. The calculation of H-content according to equation (A 7) in Appendix A excludes the presence of SiH_2 which is not expected to contribute to passivating the c-Si surface, however, may be representative of the decrease in H-content. Of importance, is the clear maintaining of hydrogen content at approximately 15% when deposition is performed using *rf*-powers below 10W. The hydrogen content % in this work is similar to that reported by Foncuberta i Moral *et.al.* [42], however, it was achieved at a much lower *rf*-powers compared to 30W.

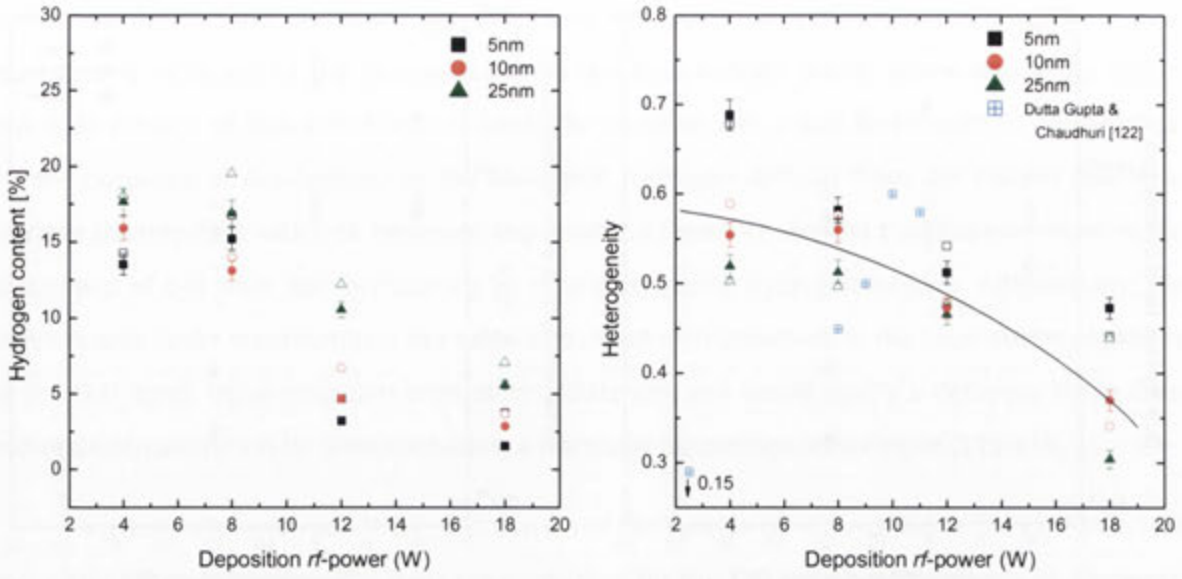

Figure 15: Dependence of a). hydrogen content and b). heterogeneity on the deposition *rf*-power for 5nm, 10nm and 25nm a-Si:H(i) layers onto *FZ* 1.4Ωcm. Hollow markers represent the as-deposited measurement. Heterogeneity of a-Si:H deposited under similar conditions by Dutta Gupta and Chaudhuri [122].

From these observations, two conditions may be thought to occur:

- Ion-damage of the bulk and interface regions takes place when using high *rf*-powers during deposition.
- The evolution of bulk hydrides when using intermediate *rf*-powers observed in 10nm and 25nm thickness of a-Si:H(i) may be an indication of H-clusters surrounding nano-voids, which have a greater resilience to ion-damage during deposition, or the presence of a different hydride type (i.e. Dihydride, SiH_2).

The FTIR results in Figure 15b, reveal a higher concentration of hydrogen occurs within the interface region for depositions undertaken with low *rf*-power and likely, explains partly the higher surface passivation quality achieved in this range (see Figure 12). In terms of heterogeneity, a distinct shift towards the bulk region for hydride occurs, observed as the value decreasing below 0.5, for bulk layers deposited at higher *rf*-powers (above 10W). By comparison to the results reported by Dutta Gupta and Chaudhuri [122] exhibit the reverse trend, however, it is noted that no distinction between monohydride and dihydride at the interface appears to have been made to the analysis in reported in this reference.

Ion-damage occurring for depositions undertaken at high *rf*-powers are likely to cause a defect rich bulk region which extracts hydrogen away from the interface region, subsequently, depleting the hydrogen available for passivation of the c-Si surface; or alternatively, a SiH_2 rich region which will reduce passivation quality. Either of these causes would occur when heterogeneity approaches 0.3, and are observed with high *rf*-powers. The phenomenon is most prominent for 5nm a-Si:H(i) layers as the absence of any significant bulk region will likely prevent repair during thermal annealing. Previously, it has been thought that as the distribution of the hydrogen within the a-Si:H was not homogeneous (i.e. bulk dominant), the influence of the bulk in thicker layers are more significant in aiding hydrogen diffusion, hence the choice for the high *rf*-power. However, it appears that increasing the concentration of monohydrides at the interface instead of the bulk is possible when using low *rf*-power.

From these results it can be concluded that an inverse relationship exists between interface-hydride density and *rf*-power. Ideally, hydride bond density at the interface is determined by the proclivity of suitable bonds, which in turn governs surface passivation quality. Maintaining the interface-rich hydride concentration requires sufficient control of the plasma during deposition. It is concluded from this work that *rf*-power levels suitable for depositing high-quality a-Si:H(i) layers should be optimally kept well-below 10W (100mW/cm^2), yet maintained above the Paschen-limit where plasma ignition and stability are affected. In this work, 4W (51mW/cm^2) appears to be optimal.

2.4 Influence of deposition temperature on a-Si:H

According to the kinetic growth models discussed in Chapter 1, incident SiH_3 during plasma deposition of a-Si:H is strongly influenced by the temperature of deposition and the equilibrium between the SiH_3 and the surface [20, 44, 45, 123-127]. Ideally, passivation of the c-Si surface is best accomplished by a single hydrogen atom per silicon atom (i.e. monohydride). The early work of von Roedern *et. al.* [48], indicated that singly bonded hydrogen occurs at temperatures near 300°C. Since then, most research has reported excellent passivation of the c-Si surface by a-Si:H(i) for deposition temperatures well below 300°C. More often, lower deposition temperatures have been reported as optimal, some of which are listed below:

- Martin *et.al.* [87], has reported excellent passivation of the c-Si surface by a-Si:H when deposited at temperatures as low as 100°C.

- Sanyo has demonstrated that temperatures below 200°C are capable of producing high quality a-Si:H layers utilised in the HIT solar cell [34].
- Maydell *et. al.* [49], also reported temperatures below 220°C as optimal for achieving good passivation of the c-Si surface.

In considering the role of hydrogen in passivating the c-Si surface, Rinnert and Vergnat [53] reported on the effusion of hydrogen and stability of a-Si:H with increasing temperature, suggesting that temperatures near to 200°C were ideal. However, contrary results by Danesh *et. al.* [45] reported an increase in void density within the a-Si:H layer and an increase in network stress as temperatures decreased below 250°C. Indeed a 12% crystallisation of the a-Si:H(i) when deposited at temperatures of approximately 250°C has been reported by Ray *et. al.*[44]; and also shown by Burrows *et. al.* [128] to provide suitable passivation of the c-Si surface. The most significant result is by Fujiwara and Kondo [40] for layers deposited at 150°C (*rf*-power~ 6 to 50mW/cm^2, partial pressure = 50mTorr) who have shown a mixed-phase a-Si:H(i) which undergoes complete epitaxial growth for temperatures above 180°C. In terms of hydride bonding, Lim *et. al.*[129] reported that the concentration of Si-H did not change for temperatures up to 350°C, although increases in SiH_2 were recorded with increases in temperature.

The difficulty in discerning an optimal deposition temperature is a result of the differing conditions by which it is defined. Variations in thickness, rf-power, silane gas dilution by hydrogen, and a small range of investigated temperatures have led to different conclusions for the ideal deposition temperature. Not surprisingly, a wide range of deposition temperatures have since been previously proposed for achieving high quality a-Si:H(i) layers, most between 150°C and 300°C.

The influence that deposition temperature has upon the quality of the a-Si:H(i) layer is investigated here for a broad range of temperatures between 100°C and 280°C by this layers effectiveness in passivating the c-Si surface. The results for τ_{eff} and S_{eff} (according to the method described in Appendix A) are given in Figure 16. As low *rf*-power has been shown in the previous section to limit plasma-damage, the optimal 4W applied *rf*-power; and a partial pressure of 650mT is used. All a-Si:H(i)/c-Si samples underwent a post-deposition thermal anneal, discussed in detail in Chapter 3, which is shown there to have a negligible impact on the overall trend resulting from different deposition temperatures.

Observed in Figure 16, concerning the surface passivation profile relating to the deposition temperature of a-Si:H, the highest and most consistent results are obtained when temperatures between 220°C and 240°C are used. It can be argued that a deposition temperature in this range, ideally 225°C at low *rf*-power, would appear optimal for high quality surface passivation.

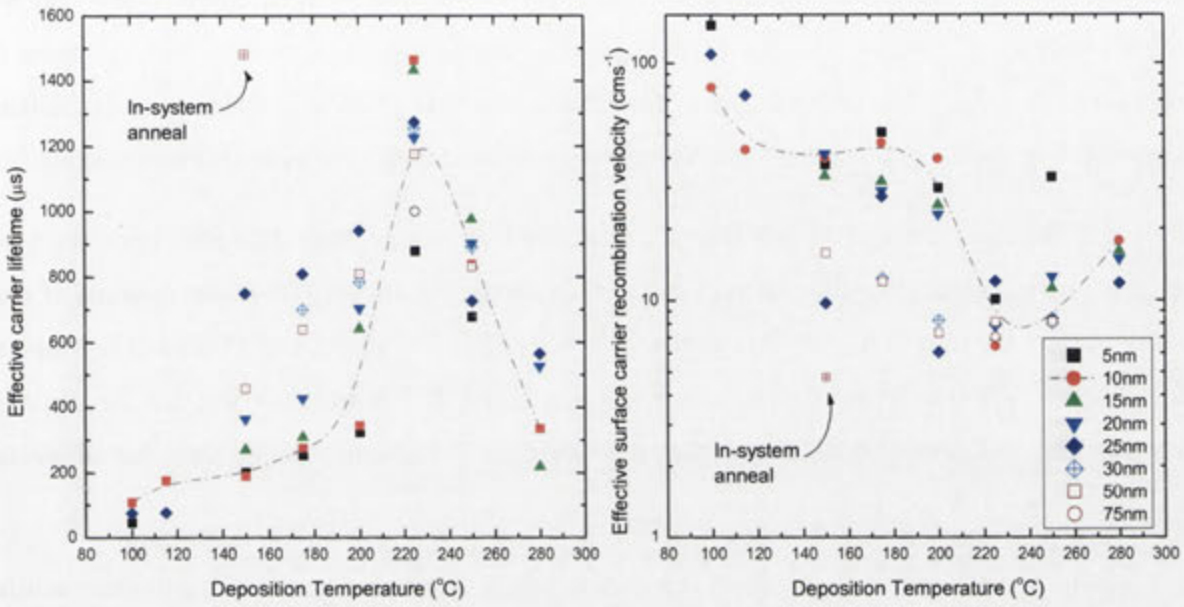

Figure 16: Passivation profile of a-Si:H(i) deposited onto 1.4Ωcm *FZ* c-Si(n) prepared using different deposition temperatures with constant *rf*-power and partial pressure. For clarity, only post-deposition annealed results are given.

The outcome here, agrees with observations accounted for earlier depositions under similar deposition conditions of a-Si:H(i) at low *rf*-power. In response to the reported optimal deposition temperatures found in the literature which suggest values well above or below the ideal range shown here in this work, a careful comparison of their surface passivation and stability would suggest that the literature values for deposition temperature are more likely local minima, which may also be system and/or process specific [40, 130], or which overlook other key aspects in terms of a-Si:H passivation of the c-Si surface.

Of some interest is the higher quality of surface passivation achieved for both 25nm and 50nm a-Si:H(i) layers deposited at temperatures even as low as 150°C (thermally annealed at 230°C). As initial carrier lifetime measurements were low, it is likely that the significant improvement is a result of the thermal annealing process. This may offer an explanation as to the high quality results reported for deposition temperatures below 200°C, in that a healing of the a-Si:H(i) layer occurs

during thermal processing. Freeman and Paul have reported that annealing of samples 'in-system'[3] following deposition of the a-Si:H layer has led to improved optical and electronic properties. This phenomenon was confirmed in this study, by depositing three a-Si:H(i) layers (25nm, 50nm and 75nm) at 150°C and annealing 'in-system', each showing comparable responses to those achieved with similar thicknesses deposited at 225°C (following thermal annealing). It may be surmised that for some lower deposition temperatures, in conjunction with other system parameters, Si-H may be trapped within the stressed network, becoming mobile during thermal anneal. A likely outcome if the formation of SiH_2 is minimal during deposition. In either case, it is clear that deposition temperature is likely to influence the bonding arrangement and density of hydrogen with silicon.

In order to understand the influence thermal properties during deposition have upon the Si-H bonding and the correlation this has with the surface passivation result, FTIR measurements of the a-Si:H(i) layers are examined. The IR absorbance spectra for 5nm, 10nm, and 25nm a-Si:H(i) layers deposited at different temperatures and are given in Figure 17. Clearly observed are the distinct interface and bulk regions consisting of SiH at 2080cm^{-1} and 2000cm^{-1}, respectively, for all layers deposited above 175°C.

Analysis of the hydride peak position for each thickness reveals a consistent shift downwards to bulk SiH for higher deposition temperatures. Also shown in this analysis between wavenumbers associated with dihydride (≥2090cm^{-1}) and those common to monohydride (≤2085cm^{-1}), is an indication that the dominant hydride configuration is dihydride not monohydride at the lower end of the investigated temperature range.

[3] 'in-system' thermal annealing is undertaken immediately following deposition, under vacuum with no plasma, prior to removal from the system,.

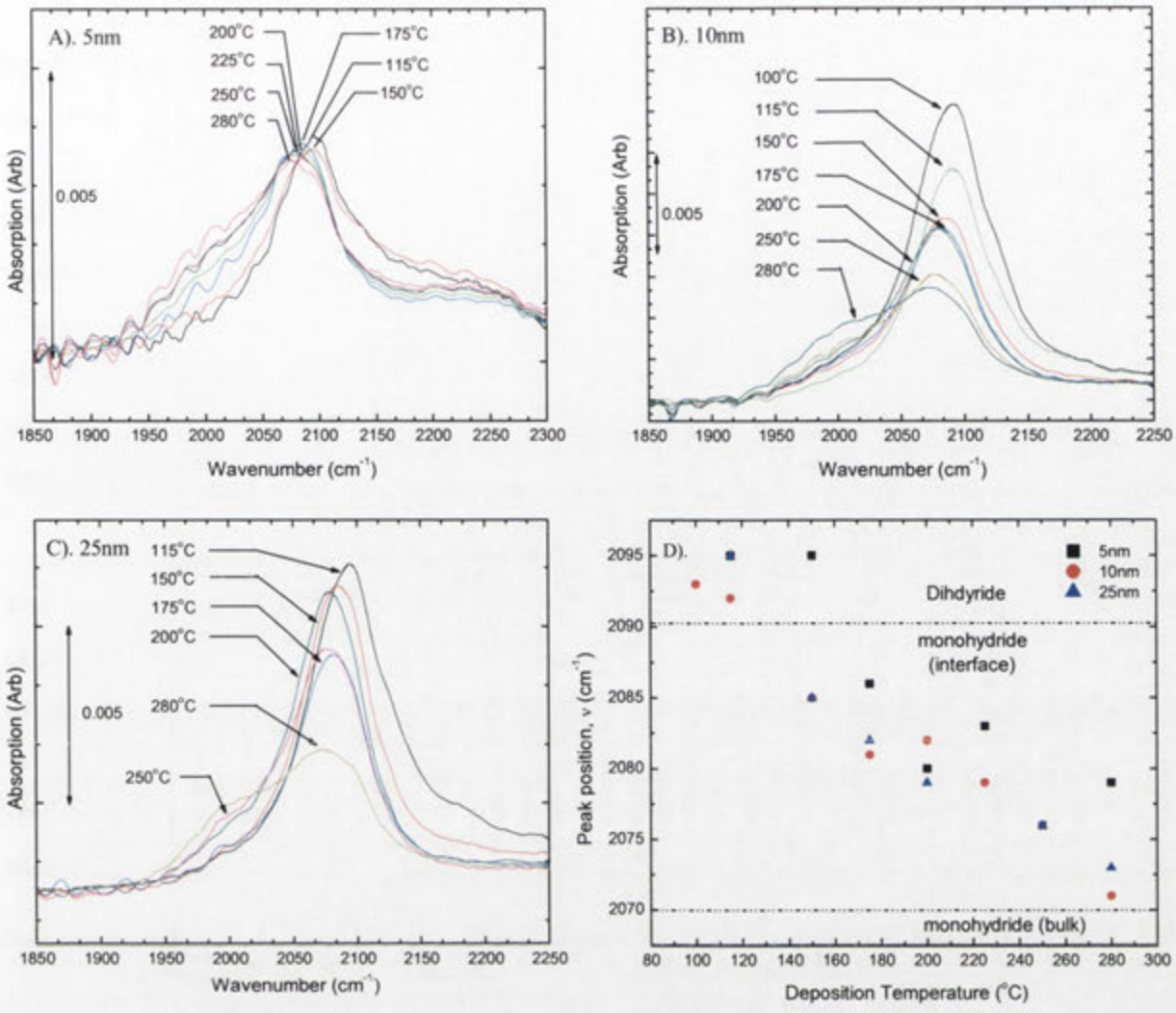

Figure 17: IR absorption spectra for annealed a). 5nm, b). 10nm, and c). 25nm a-Si:H(i) deposited at different temperatures from 150°C to 280°C onto 1.4Ωcm c-Si(n) *FZ* surface. The shift in the high-frequency hydride stretching mode with increasing temperature is shown in (d).

The measured monohydride and dihydride density at the interface and within the a-Si:H(i) layer, (as calculated according to the method in Appendix A), both for as-deposited and thermally annealed cases, are given in Figure 18. The influence that post-deposition thermal annealing has upon the profile of the hydride configuration compared to their as-deposited states is considered negligible in terms of the effect on passivation which the hydride configuration (e.g. monohydride or dihydride) near the interface is likely to have.

The dominance of the dihydride in a-Si:H(i) layers deposited below 160°C is clearly observed, and is more pronounced for the interface region (see Figure 18c). For layers deposited above this temperature, the density of the SiH_2 decreases rapidly, coinciding with an increase in monohydride (SiH) density.

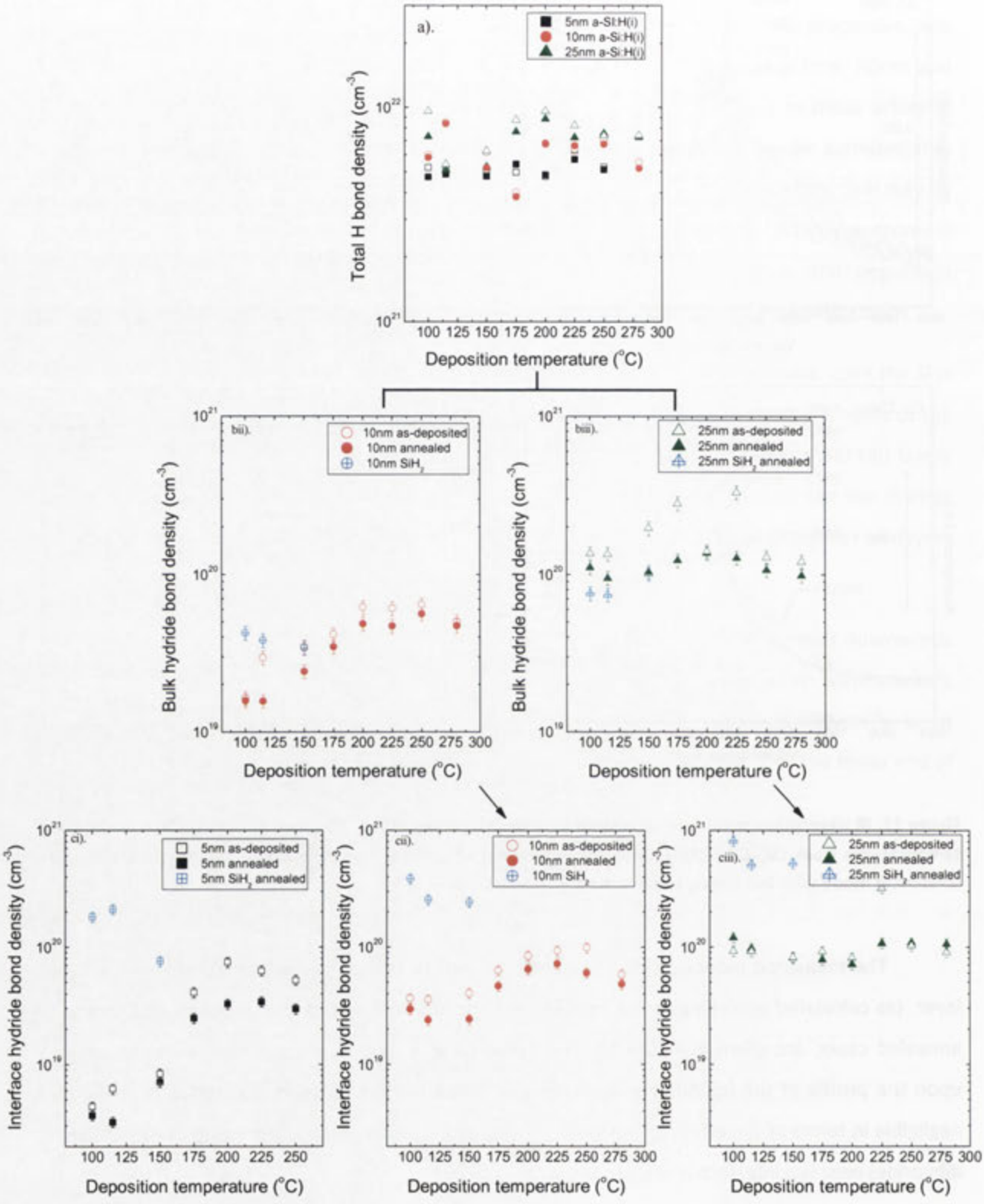

Figure 18: Hydride bonding configuration and densities for a-Si:H(i) deposited at different temperatures, a). Total bonded hydrogen, b). Bulk monohydride (SiH), and c). Interface hydride (SiH and some SiH_2) bond densities for i). 5nm, ii). 10nm, and iii). 25nm a-Si:H(i) layers deposited onto 1.4Ωcm c-Si(n) *FZ* at different deposition temperature.

Also observed, is the relatively constant bulk hydride densities for higher deposition temperatures (See Figure 18a/b) signifying that the influence of thermal conditions during deposition do not yield significantly higher or lower hydrogen concentrations, but merely reduce the concentration of SiH_2 in favour of SiH at low temperatures. Indeed Lim *et. al.* [129] reported on the lack of change in SiH below 350°C, in what has now identified to be a bulk a-Si:H measurement. The rapid increase in SiH_2 at the interface, seen for 5nm a-Si:H(i) layers (see Figure 18ci), demonstrates that a minimum or threshold deposition temperature of 175°C is necessary for monohydride a-Si:H(i) layer. For thicker layers, preferential diffusion of any SiH_2 into the bulk, leaving SiH primarily at the interface, lowers this threshold temperature. The concentration of any SiH_2 in a-Si:H(i) layers deposited above 200°C is negligible at the interface.

At temperatures above 240°C, a slight decrease in the density of hydrides within the bulk and interface regions is seen to occur. These results agree with similar decreases reported for deposition of a-Si:H(i) at temperatures approaching 300°C [53]. A point of interest is the significance of the SiH density with deposition temperature between a-Si:H(i) layers of different thicknesses; specifically, the densities for 25nm do not vary as much as for thinner layers. This would indicate that the relationship between the bulk and the interface region during deposition is more complex than previously thought.

The H-content profiles, according to the straight-forward interpretation of hydride bond density, are shown in Figure 19 (hollow-crossed symbols). Here, it can be seen that when SiH_2 is not accounted for in the calculation for H-content, the percentage of hydrogen is likely to be overestimated at much lower temperatures and an inverse trend with temperature may be interpreted. However, the more accurate response to deposition temperature for different thickness of a-Si:H(i) is clearly observed in the hydrogen content when the presence of SiH_2 is accounted and corrected for in calculation of H-content (see Figure 19). For 5nm layers, H-content increases from 3% to above 10% with increases in deposition temperature; similarly 10nm and 25nm layers also show increases in hydrogen content with temperature. At much higher temperatures and for thicker layers a higher proportion of suitable Si-bonds may be capable of dissociating SiH_2 in favour of the SiH which remains at the interface. Comparable values are reported by Danesh *et. al.* [45] and Naito *et. al.* [131] using analogous layers for some of these temperatures between 100°C and 270°C, although no information on the exact thickness of these layers is given (likely between 100nm and 600nm)

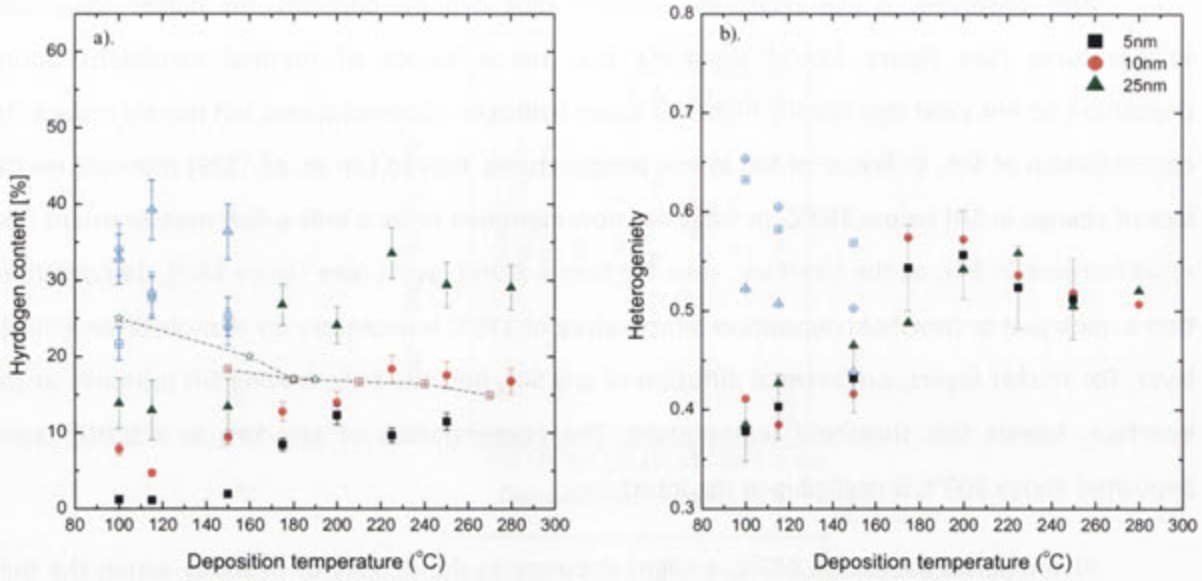

Figure 19: Dependence of a). hydrogen content and b). heterogeneity on the deposition temperature for 5nm, 10nm and 25nm a-Si:H(i) layers onto *FZ* 1.4Ωcm. Error is shown only for 5nm layer. Similar a-Si:H layers by Danesh *et. al.* [45] (crossed squares) and Naito *et. al.* [131] are shown for comparison. Dashed line is a guide for these references.

Similarly, the heterogeneity or ratio between hydride at the interface and within the bulk shows a similar discrepancy when SiH_2 is not accounted for. The higher proportion of SiH_2 at lower temperatures can influence the heterogeneity of the layer; as such, a correction is applied. For a-Si:H(i) layers, values between 0.35 and 0.60 are obtained, and a distinct shift in monohydride concentration and distribution towards the interface region at higher deposition temperatures (i.e. above 180°C) can be observed (see Figure 19b). Fujiwara *et. al.* [132] has reported a similar non-homogenous nature in PECVD a-Si:H layers when using a deuterium indicator layer and measurements by 'real-time' spectroscopic ellipsometry and IR spectroscopy.

The cause of the decrease in heterogeneity for 25nm a-Si:H(i) layers deposited between 100°C and 200°C is likely linked firstly to the repacking of hydride near the interface, and secondly, to high SiH_2 within the a-Si:H(i) bulk. The sharp increases in heterogeneity for temperatures above 200°C points to this being the case. This trend may also account for the negative interpretation regarding hydrogen concentration at deposition temperatures above 200°C as is reported for thicker layers [97].

To better understand the significance which hydride concentration has on surface passivation, the interaction between the bulk and interface region hydrides needs to be considered. Low hydride concentration in the bulk has been reported to improve defect mobility across the interface-bulk

transition [133]. In this hydrogen is drawn away from the interface during post-deposition thermal anneal. When the hydride distribution is applied to deposition growth models for a-Si:H, by accounting for parallel abstraction and addition reactions [134], the non-homogenous layer describes an ideal layer for passivation of the c-Si surface. In this work, it has been shown that the ideal hydride concentration within the bulk is at minimum 10%, with a lower limit of 50% hydride concentration at the interface/near-interface region for high quality passivation of the c-Si surface.

This result confirms that SiH_2 molecules mostly dominate in a-Si:H(i) deposited at lower temperatures (<160°C) and low *rf*-power, correlating well with the low passivation quality observed for the c-Si surface by these layers. The presence of SiH_2 is undesirable for two reasons: the surface passivation is less effective for c-Si, and the necessity of a Si-dimer to eliminate SiH_2 and make available SiH for passivation. Certainly, SiH_2 assists in the formation of μc-Si:H when annealed at high temperatures and similarly it has been reported that for thinner a-Si:H layers (<150nm), microcrystallite formation does occur when deposition is performed at higher temperatures [40, 135].

To assess the role of deposition temperature on the micro-structure for each of the a-Si:H(i) layers, Raman scattering for TO, LA and TA-bands of the above layers are shown in Figure 20. Here, the width of the TO-band remains above $70cm^{-1}$, indicating no significant improvement in SRO is observed occurs within this temperature range, hence, no crystallite formation occurs. In fact, only slight increases in bandwidth and in ω_{TO} are measured for 25nm a-Si:H layers. It can be quickly concluded that no epitaxial growth of template microcrystallite formation occurs for thin a-Si:H(i) layers for deposition temperatures up to 280°C, in agreement with FTIR results of this work.

For a-Si:H(i) layers less than 20nm in thickness, shifts in ω_{TO} are less apparent, as optimal reconfiguration to improve relaxation is increasingly critical given the higher levels of stress for hydrides at the interface with c-Si. This stress occurs during the initial stages of deposition (i.e. during islanding) even after aggregation occurs. Smoothing, observed by the broadening of the TO-band for increases in deposition temperature, can lead to a relaxation of this stress. This is first suggested by the slight blue- shift in ω_{LA} seen in Figure 20 and later confirmed by Γ_{TO}.

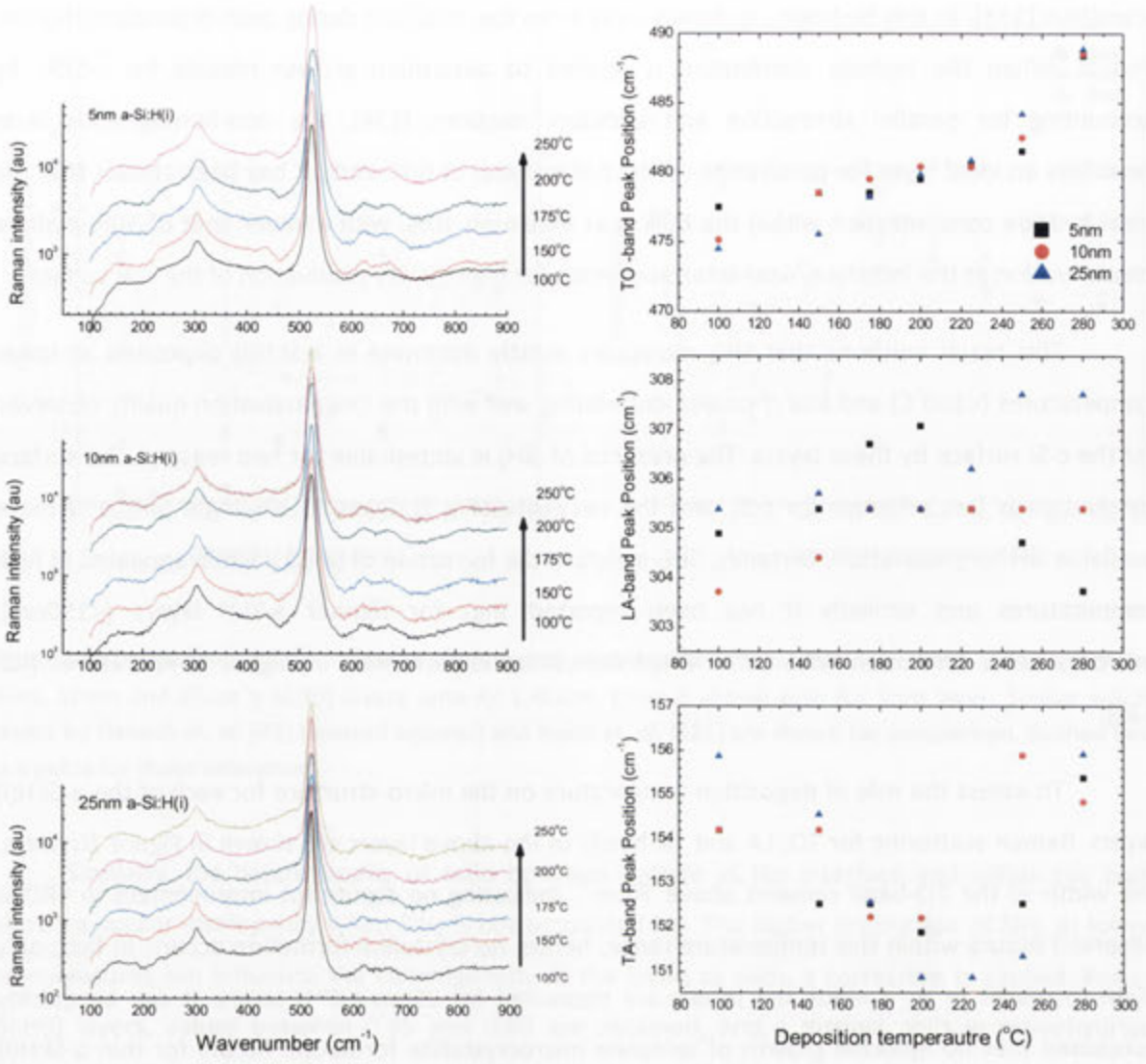

Figure 20: Evolution of Raman scattering spectra and peak position of TO, LA and TA-bands for 5nm, 10nm and 25nm a-Si:H layers deposited at temperatures between 100°C and 280°C. The LO-band has been omitted as no change in ω_{LO} could be observed. The curves on the left graphs have been shifted vertically to show the effect of different temperatures more clearly.

Maley and Lannin [97] have shown the effect of hydrogen on number of fluctuation for the bond-bending mode is stronger than for the fluctuation in the bond-angle mode. It has also been argued that the presence of SiH_2 (<200°C) eventually leads to improvements in SRO and MRO. Indeed the shift in both the ω_{TO} and ω_{LA} bands at lower deposition temperatures is attributed to the presence of the SiH_2 measured in FTIR. The higher than expected position of ω_{TO} for a-Si:H(i) layers deposited below 200°C, initially suggested an improvement in short and mid-range ordering which can occur with relaxation of strained bonds in a dihydride-rich layer. However, significant narrowing of the band width, to near 60cm^{-1}, is not observed. In this work, comparisons between hydride

distribution and the measured surface passivation for a-Si:H(i) layers deposited at higher temperatures indicate that beyond a critical loss of bulk-hydrogen, a consequential loss of hydrogen from the interface is likely to occur. Also, that for lower deposition temperatures (<180°C), the surface passivation is influenced mainly by the presence of SiH_2, rather than hydride distribution.

In Figure 21, the raw and corrected hydride bonds, calculated according to equations (A 9) and (A 13) in Appendix A, respectively, shows no relaxation occurring for temperatures below 180°C; in fact the opposite is apparent, where bonds are further stressed between 100°C and 180°C. From the corrected bond angle shift, the optimum mean bond angle for achieving maximum surface passivation occurs between 9.3° to 11.6° corresponding a relaxed a-Si:H network and to the previously identified ideal deposition temperature [102].

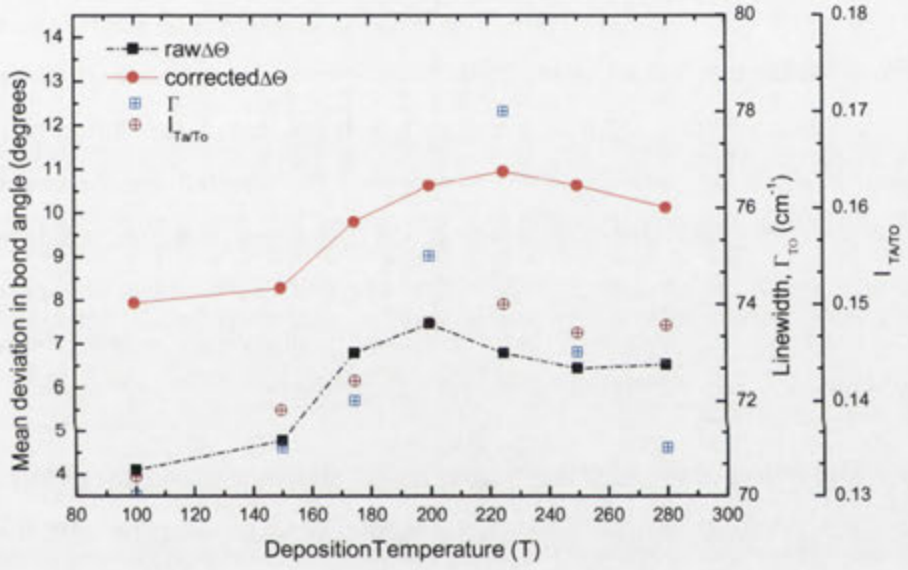

Figure 21: Raw and corrected mean bond angles for SiH calculated from ω_{TO} according to Eq. 1.10.

From the analysis in this section, it can be concluded that surface passivation is ideally achieved when monohydride is dominant at the a-Si:H/c-Si interface and throughout the bulk of the a-Si:H layer. That is when the deposition temperature is above 200°C, ideally 225°C in this work. The corrected deviation in mean bond angle of 11° does show that a relaxed a-Si:H network indeed does occur for the this range. Shifts in hydride formation over the deposition temperature range reported here highlight the importance of the thermal properties during deposition on the quality of the a-Si:H layer and the passivation of the c-Si surface. Dihydride formation occurring for temperatures below 170°C should be avoided. Conversely, it has been reported that temperatures above 310°C will result in significant improvements in MRO (~1nm), [63, 136], which was also observed in this

work (not shown). Although, no crystallite formation was observed in this work across the temperature range examined (including 320°C), it can be suggested that this phenomenon is not directly related to the temperature during deposition itself but to other causes.

2.5 Influence of partial pressure on a-Si:H

The final deposition parameter investigated in this study, partial pressure, concerns the balance between the feed-in gas entering the system at a constant rate with the removal of exhaust gases and plasma by-products from the system. Wide ranging values for ideal partial pressure have been proposed over the years based upon certain assumptions and it may be appropriate to consider in many cases that these are system dependent. Deposition of a-Si:H(i) layers at partial pressures anywhere between 500mT and 2200mT have been reported by others to yield improved carrier lifetimes and stabilities, despite the significantly increased concentration of poly-silyl hydrides above 1000mT [137, 138]. This is in contrast to reported improvements in optical properties and lower poly-silyl hydride concentrations as being ideal for a-Si:H when partial pressures during deposition are 500mT [139]. The ambiguity surrounding the partial pressure parameter and the influence it has upon the a-Si:H layer quality would appear somewhat system dependent in nature

This work examines partial pressures over a broader range than previously considered, between 200mT and 2400T and seeks to highlight the importance of this parameter on the efficacy of passivation by the a-Si:H(i) layer on the c-Si surface. Partial pressures below this range could not be initiated in this system, and similarly, above this range could not be maintained without significant increases in *rf*-power. Deposition temperature and *rf*-power are maintained at 225°C and 4W. The profile for the effect that partial pressure has upon the passivation quality is shown in Figure 22. In this, it is apparent that the highest levels of passivation occur for partial pressures of 500mT, in agreement with the results reported Ray *et. al.*[139]. However, the S_{eff} reveals the existence of a broad minimum for deposition partial pressures between 400mT and 750mT.

It is thought that below 400mT, a 'starving-plasma' condition occurs, where layer growth is compromised by insufficient feed gas within the chamber during deposition. This may lead to several phenomena occurring, including, prolonged exposure of the c-Si surface to ion-damage when using higher rf-powers, limited hydrogenation of the c-Si surface during the initial stages of growth, and deposition of a hydrogen deficit bulk layer which can deplete the interface. A similar effect has been

observed for a-SiC_x:H deposited between 200mT and 300mT, improving for higher partial pressures [51]. For partial pressures above 750mT, surface passivation decreases rapidly and it is suspected the presence of poly-silyl hydrides may be a factor in this decline.

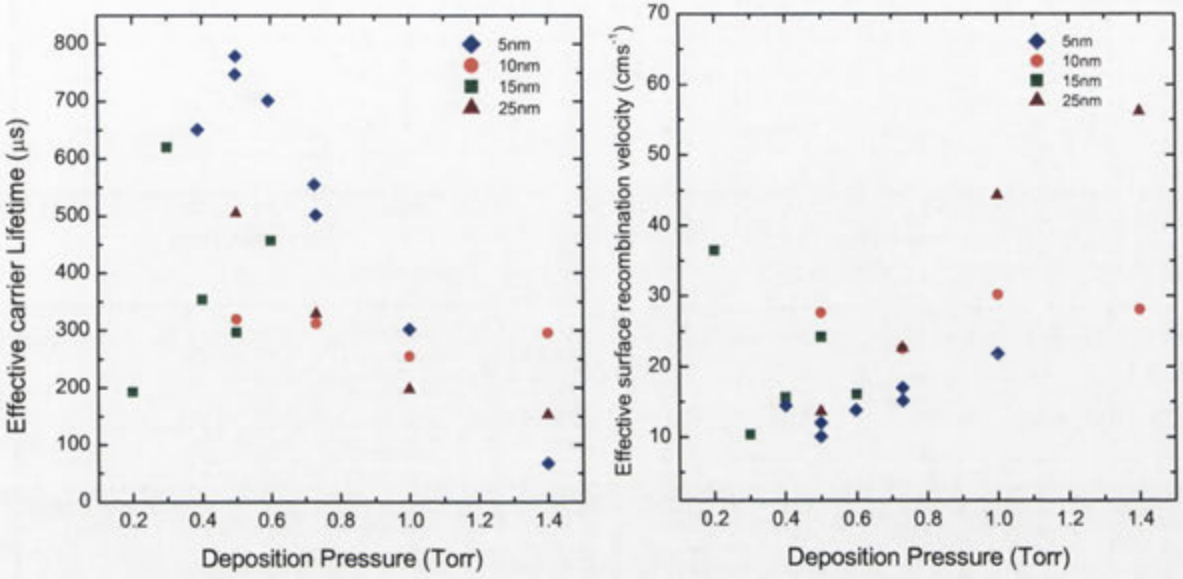

Figure 22: Passivation profile of a-Si:H(i) deposited onto 1.4Ωcm *FZ* c-Si(n) prepared using different partial pressures with constant temperature and *rf*-power. For clarity, only post-deposition annealed results are given.

The results of the FTIR analysis into hydride composition with the bulk and the interface region for the range of deposition partial pressures are given in Figure 23. Evident is the increase in total hydride bond density for all a-Si:H(i) layers when deposited above 'starving' plasma conditions, but below 800mT. Indeed, no further increase in the total hydride density can be seen above 750mT, corresponding to the negligible increases in bulk and interface monohydride densities (see Figure 23b/c).

Importantly, despite hydride density for layers deposited at partial pressures above 800mT being higher than those deposited at 500mT, it is the lower of these pressures that coincided with the highest quality passivation of the c-Si surface. Certainly for higher partial pressures, significant 'dusting' could be observed following a singular deposition on both the surface of the c-Si wafer and within the chamber itself. At these pressures, 'dusting' at the edges of deposition surface occurs, inferring that polymerised hydrides are likely to have been incorporated into the growing layer.

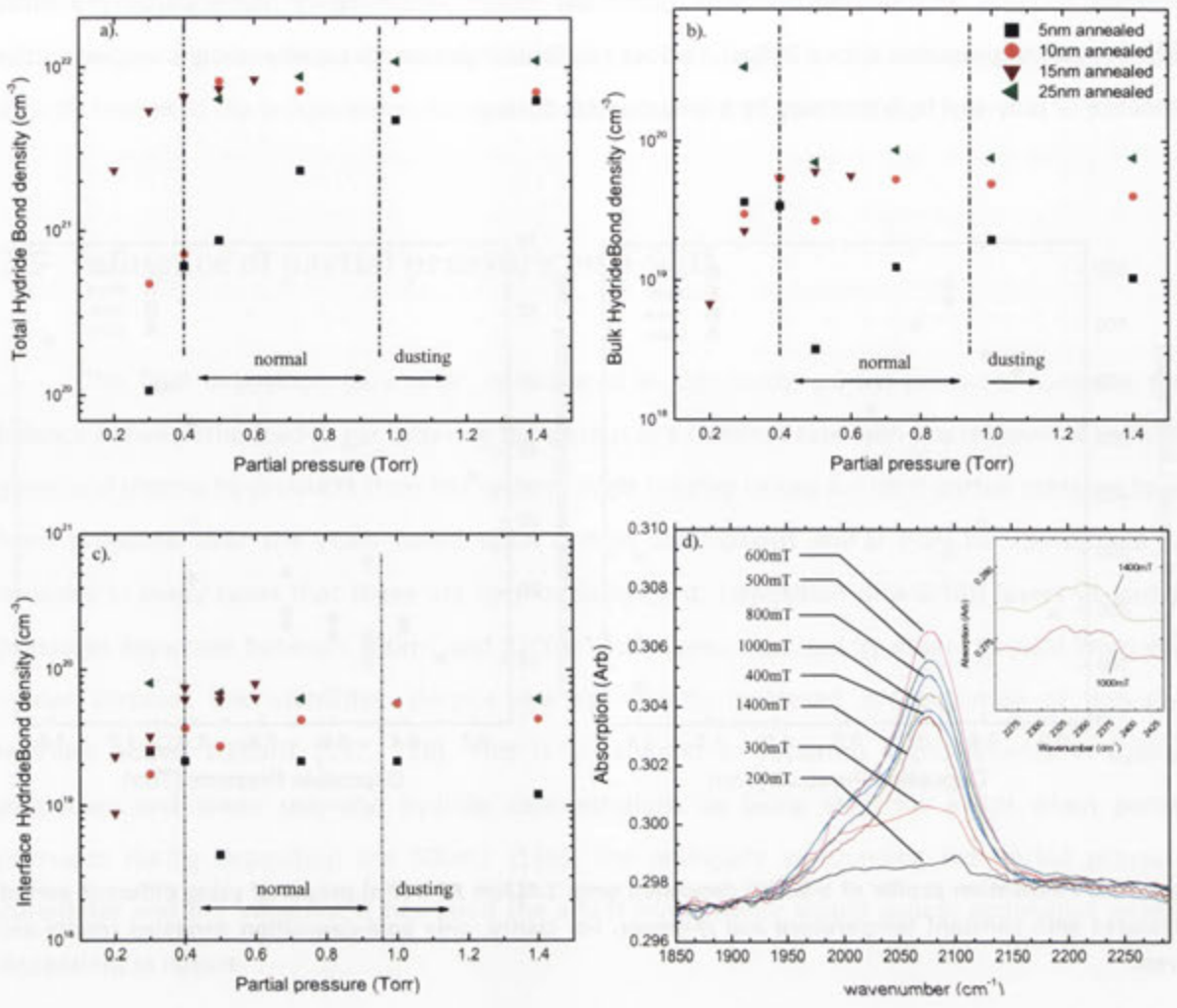

Figure 23: IR hydride bond and absorbance spectra results a). Total bonded hydride, b). Bulk monohydride, c). Interface monohydride densities for 5nm, 10nm, 15nm and 25nm a-Si:H(i) deposited onto 1.4Ωcm *FZ* c-Si(n) for differing partial pressures. The change in the hydride stretching mode is shown in (d) (INSERT: shows evolution of poly-silyl trihydride peaks when using higher pressures) .

Dusting indicated the formation of higher-order and poly-silyl hydrides, including trihydride (SiH_3) and $(SiH)_2$, respectively, occurs when using higher partial pressures. These reduce the overall SiH density without contributing towards passivation of the c-Si surface. Although improved stability was reported for poly-silyl rich a-Si:H deposited at much higher partial pressures by Middya *et. al.* [138] it is plausible that suitable monohydride coverage occurred in the presence of limited poly-silyl hydrides. This is confirmed by the polymerisation of hydride species when low *rf*-powers and high partial pressures were used. However, it should be noted that higher *rf*-powers do not prevent 'dusting' from occurring, which still have a detrimental effect on the quality of the a-Si:H layer.

A distinct SiH_3 peak is observed to occur for a-Si:H(i) layers deposited at partial pressures above 800T (*rf*-power at 8W), increasing further for higher partial pressures (see Figure 23d). The presence of SiH_3 is known to negatively affect the surface passivation by increasing the density of stress-induced unpassivated defects (i.e. micro-voids) within the a-Si:H(i) layer [140]. Apparent, is the necessity to distinguish hydride bonds is not simply limited to whether monohydride (SiH) or dihydride (SiH_2), but also to whether these are occurring at the interface with c-Si, within the a-Si:H bulk, and even on the surface of any microvoids which may occur within the a-Si:H layer. If this discrimination is not made, errors in bond density calculations can occur, particularly for a-Si:H layers deposited above 1000mT

In Figure 24a, the bonded hydrogen content of the a-Si:H(i) deposited with different partial pressures is given. Here, the H-content has been determined by SiH and SiH_2, and we account for the presence of SiH_2 in the bulk only. It can be seen that when bulk SiH_2 is not removed calculation, an overestimation of the H-content occurs. For the calibrated H-content, depositions within the starving plasma region (below 400mT) show hydrogen content falls sharply from an average of 15% to as little as 5%. Similarly, depositions at partial pressures above 750mT exhibited a similar decline in hydrogen content. However, when the SiH_3 and poly-silyl hydrides are included in this calculation, hydrogen content displayed a similar profile to that indicated in the results by advocates of higher partial pressures [137, 138, 141].

SiH_2 has a similar influence on the calculation of heterogeneity, calculating much high interface concentrations of SiH than actually occurs. When SiH_2 is accounted for, the shift in the heterogeneity to below 0.5 can be seen (Figure 24b), particularly for thicker a-Si:H(i) layers, when deposition at higher pressures occurs in conjunction with low *rf*-power. This suggests a shift in the dominate hydride mode is taking place. Remembering that SiH_3 and poly-silyl hydrides are present at higher temperatures and located primarily within the bulk region as well, it can be understood that their inclusion in calculating heterogeneity would lead to incorrect compositional analysis of the a-Si:H(i) layers. By comparing to the bond densities in Figure 23, it may be concluded that the shift towards a bulk hydride dominant film occurs at higher pressures due to the presence of poly-silyl components.

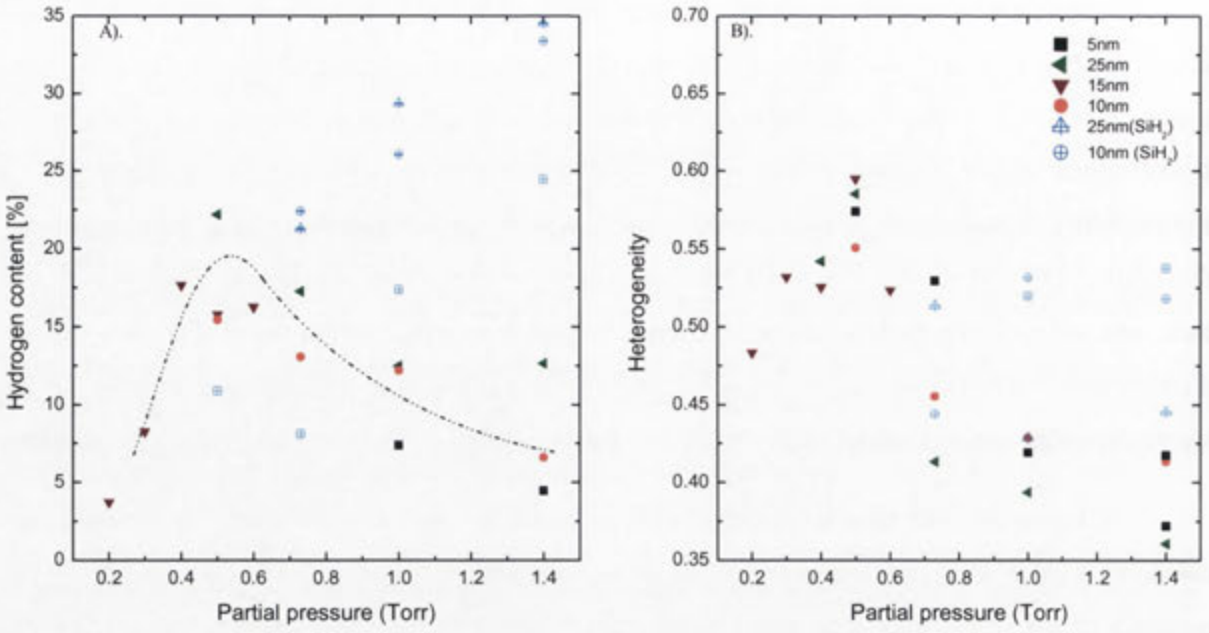

Figure 24: Dependence of a). hydrogen content and b). heterogeneity on the deposition partial pressure for 5nm, 10nm, 15nm and 25nm a-Si:H(i) layers onto 1.4Ωcm *FZ*. Hollow markers represent the as-deposited measurement.

Although some variation in the hydrogen content and heterogeneity of the a-Si:H(i) layers is apparent, it can be concluded that the effect of partial pressures during deposition between 400mT and 750mT on hydride composition and distribution are negligible.

The peak positions for TA, LA, LO, and TO modes from the Raman spectra of the a-Si:H(i) layers deposited at the different partial pressures are given in Figure 25. For layers deposited with partial pressure below 400mT, a stressed Raman response is observed by the low peak position of the TO-band below 480cm^{-1} and TA-band above 152cm^{-1}. As seen in FTIR, hydrogen was present within the a-Si:H(i) layers deposited below 400mT, indicated by the low ω_{LO}; however, the higher than expected measured ω_{LA} is more likely characteristic of a layer where hydrogenation is occurring [140], although not readily in the monohydride phase. Instead this profile describes a layer where hydrogen remains trapped within a stressed network, perhaps around closed silicon rings which can lead to the presence of microvoids. By comparison, Lebib and Roca i Cabarrocas [142] appear to report a similar increase in ω_{TO} for a-Si:H deposited under similar conditions.

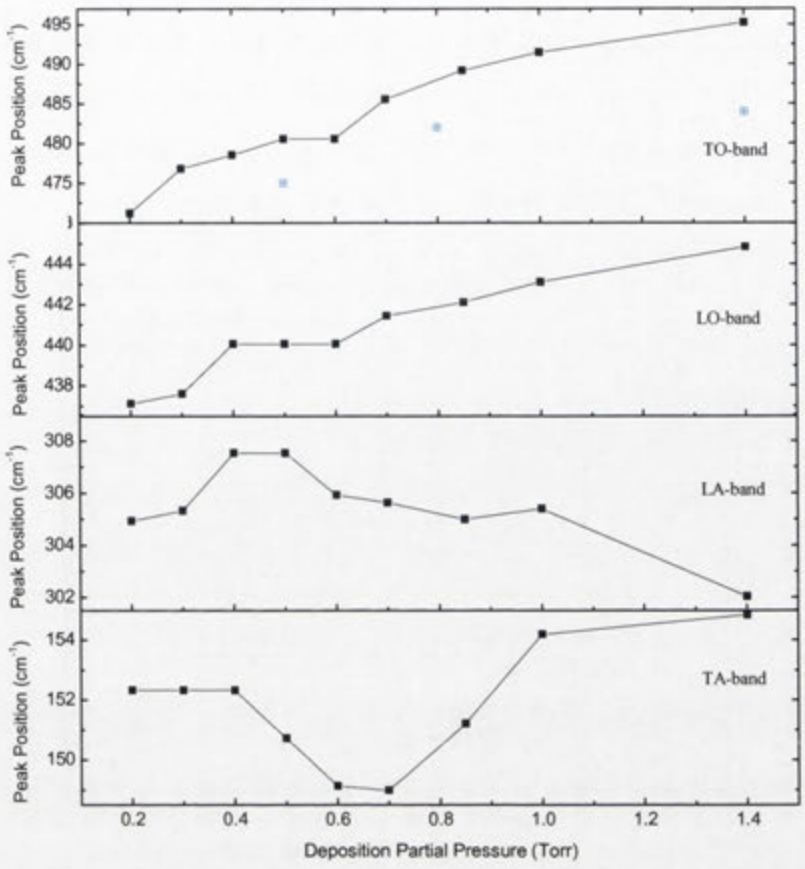

Figure 25: Peak position of TO, LO, LA and TA-bands from Raman spectroscopy measurements of a-Si:H deposited at different partial pressures between 200 mT and 1400 mT. Peak position of TO reported by Lebib and Roca I Cabarrocas [142] is given by blue/hollow markers.

For partial pressures above 1000mT, a distinctly different layer structure can be observed by the blue-shift in peak position of both the TO and LO-bands, characteristic of hydride clustering at micro-voids [101, 102]. This clustering is common in the presence of trihydride reported earlier in FTIR measurements. The slight, simultaneous shift in both ω_{TA} and ω_{LA} for a-Si:H layers deposited at higher partial pressures implies that network stresses are being reduced at the micro-void sites, when void-density is below 10%. The shift in ω_{LA} also indicates a lower hydrogenation of silicon bonds at the c-Si surface (i.e. monohydride).

To understand the importance of bonding arrangements and stress within the network for a-Si:H(i) layers, the raw and corrected profiles for mean deviation in bond angle ($\Delta\Theta$) against partial pressure is given in Figure 26. The significant decrease, approximately 6°, in the $\Delta\Theta$ (raw) for a-Si:H(i) deposited at higher partial pressures is typically interpreted as an improvement in SRO and MRO (i.e. crystallisation) due to the errors and assumptions in parameters for this model. Additionally, the trapping of hydrogen in stressed layers at low pressure (≤400mT) and the high-volume fraction of

poly-silyl hydride in layers deposited above 800mT can be misleading. The corrected profile for $\Delta\Theta$ indicates that a smaller decrease of approximately 3.5° in the mean deviation in bond angle actually occurs, remaining within the range of a-Si:H (9^0 up to 11.6^0). For partial pressures above 800mT, the lower value of $\Delta\Theta$ (corrected), below 9.7^0, is a feature of micro-void fractions which occur between 5% and 10% and not the improvement in SRO as assumed in the literature.

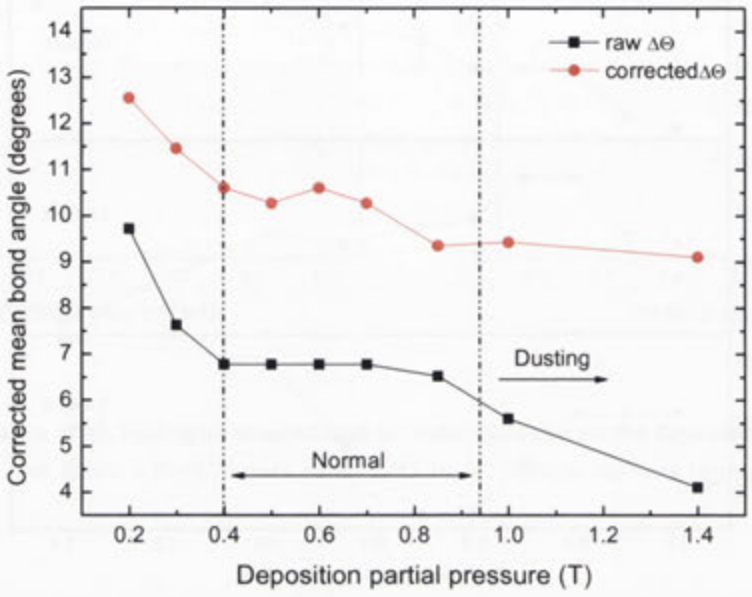

Figure 26: Raw and corrected mean bond angles for SiH calculated from ω_{TO} according to Eq. 1.10.

The results of the IR analysis go some way to explaining the surface passivation profile for a-Si:H(i) deposited for different partial pressures. However, it should be noted that partial pressure is considered a plasma-based parameter, and its influence is mitigated by deposition parameters like temperature and *rf*-power.

2.5.1 Gas flow rate and gas ratio

Maintaining partial pressure by regulating gas-flow rates into the system and exhaust of unwanted gases has been shown above to be most critical when deposition takes place outside a critical system range. In this work this range occurs between 400mT and 750mT. The capacity of the deposition chamber allowed for gas-flow rates below 30sccm and as high as 150sccm to easily be tested. No noticeable effect was observed in the passivation quality, FTIR or IR analysis when the gas-flow rate was varied, providing that plasma could be initiated and remained stable during

deposition. However, for larger systems, depositing over a wider area, the gas flow rate is likely to be more significant.

The deposition of a-Si:H(i) involved the introduction of silane (SiH_4) gas into the system. Unless, this gas is mixed with other gases, for example ammonia (depositing SiN), methane (depositing a-SiC_x:H), or phosphine (n-type a-Si:H) and diborane (p-type a-Si:H), the ratio was of little relevance to the outcomes of this study and is not reported here.

2.6 Multi-layer Plasma-Enhanced Chemical Vapour Deposition

The quality of the deposited a-Si:H layer has been linked to the temperature, *rf*-power and partial pressure of deposition. Given optimal conditions for the two last parameters, temperature has been shown to be the primary determining factor in the composition and distribution of hydrides within the a-Si:H layer. Also, it has been demonstrated previously in this work, the level of surface passivation does not improve with thickness. Ideally, in the case of thin a-Si:H, less than 10nm, a hydride-rich interface region is desired firstly; followed by a moderate-hydride a-Si:H bulk with a relaxed network. Certainly electronic properties at the interface with c-Si extend only a few nanometres into the a-Si:H layer itself [72, 143, 144]. Therefore the focus during deposition should be on improving hydrogenation within the interface region and reducing surface states. Achieving these conditions requires finer control of the PECVD process at the nano-scale.

The development, as part of this thesis, of a new deposition technique 'Multi-Layer PECVD' allows for very-thin a-Si:H layers (≤ 5nm) to be deposited successfully with higher interface hydride density than for bulk a-Si:H compared to standard PECVD. In ML-PECVD, a series of individual, 1nm sub-layers are deposited which are thermally cycled prior to the next sub-layer being deposited (see Figure 27). This continues until the desired total layer thickness, either 5nm or 10nm is obtained.

Two variations in the thermal treatment of sub-layers were investigated, *'constant temperature'* and *'inter-deposition cooling'*. In both cases, all depositions occur at 225°C, although for the second treatment condition, a cooling period[4] at 120°C for 20 minutes between sub-layer depositions is carried out.

[4] At 120°C, thermal annealing is unlikely to effect the a-Si:H, hydride or hydrogen within the layer. Hydrogen mobility is negligible at these temperatures.

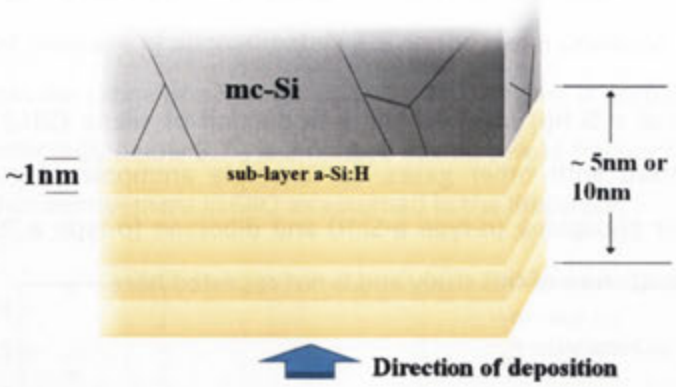

Figure 27: Illustration of ML-PECVD sub-layer deposition process

Initial testing increased the total deposition time (including: evacuation of chamber and heating/cooling) to 2 hours compared to 20 minutes (from start-up) for standard PECVD for a 10nm sample due to system setup. Following improvements to the heater-assembly and system including refinement of the process to running in a unique 'stand-by' mode for this system, total layer deposition times were reduced to 20 minutes using ML-PECVD, including evacuation of the chamber (standard PECVD times ≈ 8 minutes). It should be noted, that for the results presented here, ML-PECVD exists only as a research method, not presently applicable to industry.

The deposition of thin a-Si:H(i) layers are examined using each deposition technique. In some cases, the same wafers were re-used after undergoing a short re-etch of the previous a-Si:H(i) layer which may include a few μm of the c-Si surface. Therefore, passivation quality is reported in terms of S_{eff}.

In Figure 28, the effective surface recombination velocity profiles across a wide injection range for each technique are shown. ML-PECVD with thermal cycling to 120°C appears to demonstrate some improvement in S_{eff} in comparison to standard PECVD and more noticeably to ML-PECVD with constant temperature. IR spectra of a-Si:H(i) shows that monohydride (SiH) density is higher using ML-PECVD methods compared to standard PECVD, and thermal cycling appears to improve this further. The distinct difference of the constant temperature ML-PECVD method, suggested that the heating/cooling cycle may be the key to improving a-Si:H layers structural quality (i.e. density, network relaxation).

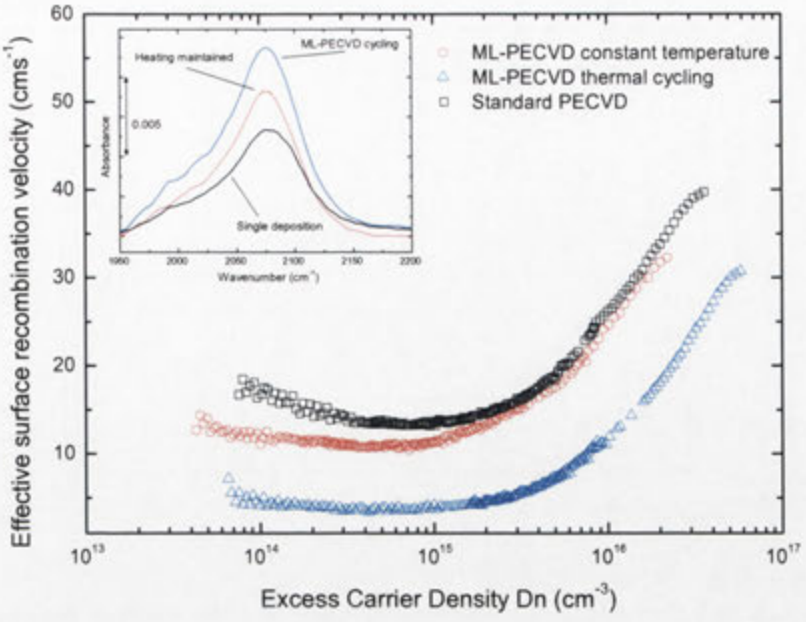

Figure 28: S_{eff} for deposition of a-Si:H(i) sub-layers by ML-PECVD at 225°C onto 138µm 1.4Ωcm c-Si(n). ML-PECVD shown in blue (triangle) for Inter-deposition cooling, red (circle) for constant temperature, standard PECVD in black (squares). (Insert): IR absorbance spectra for primary hydride bonds. Single deposition 10nm a-Si:H(i) onto 120µm is shown for comparison.

In Figure 29, the relationship of the thermal cycling temperature in ML-PECVD to the overall surface passivation quality with this minimal thermal annealing is shown for different injection ranges (standard PECVD does not undergo thermal cycling). For inter-deposition temperatures below 180°C, S_{eff} is noticeably lower. Although, standard PECVD also yields good passivation results in this experiment, a-Si:H deposited by ML-PECVD with thermal cycling to 120°C exhibited a substantially improved response.

Ideally, a balance is needed between the a-Si:H(i) layer thickness and reproducibility without compromising the excellent surface passivation. In Figure 30, improvements in the reliability of high quality surface passivation by 5nm ML-PECVD a-Si:H layers compared to standard PECVD is shown. This study included a population size of 14 sets of approximately 140µm wafers. Notable, is the significantly higher τ_{eff} which achieved using ML-PECVD involving inter-deposition cooling than for a-Si:H deposited by standard PECVD.

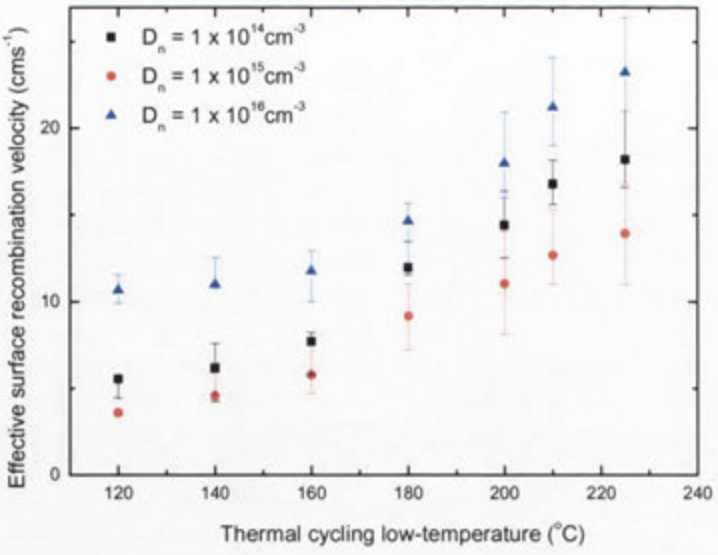

Figure 29: Surface recombination velocities at low, intermediate, and high injection regions for 5nm a-Si:H(i) deposited by ML-PECVD with thermal cycling at different temperatures.

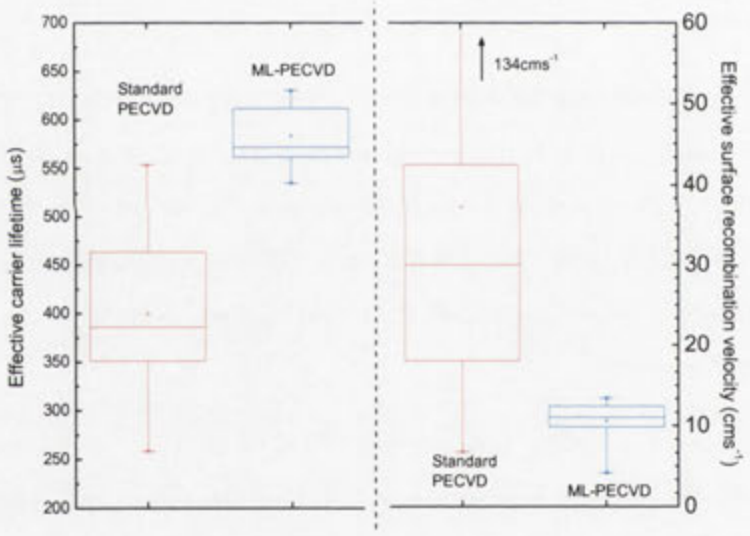

Figure 30: The variation in surface passivation in terms of τ_{eff} and S_{eff} according to deposition technique onto 1.4Ωcm c-Si(n) *FZ* with a average thickness of 128µm. Results for ML-PECVD (constant heating) are omitted.

ML-PECVD also displays an improvement in the reliability of this high quality surface passivation. Although high τ_{eff} above 1ms is achievable for standard PECVD, the median τ_{eff} value is significantly lower, below 400µs. By contrast, reduced deviations in surface passivation quality for ML-PECVD a-Si:H layers is evident, with median τ_{eff} above approximately 575µs in this early study. It can be said, the quality of surface passivation obtained for a-Si:H layers deposited by ML-PECVD with

inter-deposition cooling is significantly higher than for standard PECVD, highlighting one of the advantages of this new deposition technique.

To understand where the improved reliability of surface passivation using ML-PECVD may stem from, the hydride bonding content is examined compared to standard PECVD using a profiled mesa-type sample (Figure 31).

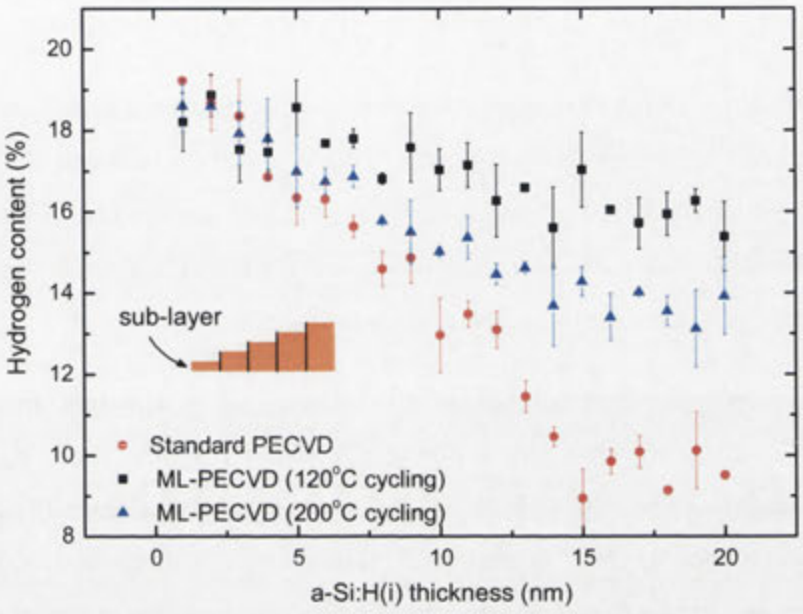

Figure 31: Hydrogen content of ML-PECVD a-Si:H with thermal cycling temperatures of 120°C and 200°C, Standard PECVD at 225°C is also shown for comparison.

The H% of ML-PECVD a-Si:H(i) demonstrates a clear improvement over standard PECVD. More so, with thermal cycling at 120°C, the H% content shows gains over 200°C thermal cycling accounting for the τ_{eff}/S_{eff} measured with different cycling temperatures. This indicates that the relaxation and optimal repacking of growing a-Si:H is likely dependent upon temperature, specifically, on the low temperature thermal cycling/anneal.

As the ML-PECVD is a modification to standard PECVD, yielding improved reliability and fine control of the critical deposition process for very-thin layers of a-Si:H (i.e. ≈ 5nm), further discussion of the technique as applied to stacked a-Si:H layers is made in Chapter 4 and to mc-Si surfaces in Chapter 5.

2.7 Chapter summary and conclusions

This chapter has examined the influence which the deposition conditions, namely, *rf*-power, temperature and partial pressure, have had on the a-Si:H(i) layer and its effectiveness in passivating the c-Si surface with this material. Each condition has been tested singularly and to some extent cooperatively, in order to determine the variations in structure and electronic properties with a goal of identifying the ideal deposition conditions for a-Si:H(i) at a range of thicknesses.

It has been shown that the depositions conditions for optimal a-Si:H(i) layer quality occur within a small range of values; these are *rf*-power <8W, temperature between 180°C to 240°C, and partial pressures approximately 650mT. In combination, the best achieved surface passivation using a-Si:H(i) is likely. Each of these parameters is optimised for the PECVD system in this work, however, each may be considered somewhat universal to many similar systems.

From the work presented throughout this chapter, it is apparent that surface-based parameters of *rf*-power and temperature during deposition play the most significant role in determining the quality of the a-Si:H(i) layer. It was demonstrated that lower *rf*-power, below 8W and ideally 4W (51mW/cm^2), reduced plasma-damage of the interface and limited abstraction hydride from the bulk of the a-Si:H layer, thereby, limiting any subsequent loss of monohydride at the interface. The dominant presence of SiH_2 in a-Si:H(i) deposited at lower temperatures, below 170°C, has shown that previous assumptions pertaining to higher hydrogen concentration at these temperatures is misleading. When the presence of SiH_2 in these layers is corrected for, hydrogen content and the distribution of active hydrides for a-Si:H(i) is much lower that initially speculated. Indeed, it may be concluded that SiH_2 actually reduces the presence of monohydride at the interface; thereby reducing passivation of the c-Si surface. Careful consideration should be given when choosing both *rf*-power and temperature for deposition by other PECVD systems.

Partial pressure has been shown here to exert less influence on the quality of a-Si:H(i) deposited in this work, provided that overall plasma quality is maintained. As such, this parameter is predominantly plasma-based, given ideal conditions characteristic to each system's setup. Dusting, a result of trihydride and poly-silyl hydrides could be observed at higher partial pressures above 900mT and should be avoided. This would be particularly critical for systems which deposit downwards onto the c-Si surface, unlike the inverted bias surface utilised throughout this thesis.

It has been demonstrated that Multi-Layer PECVD, developed as part of this work offers greater control over the deposition of thin a-Si:H(i), albeit with longer process times required still at

this early stage. The reliability in the quality of surface passivation by deposited layers with thermal cycling between sub-layer depositions was shown to improve significantly. Improvements in the equipment assembly were made to reduce total deposition times to approximately 20 minutes for 10nm layers; however, this process remains a laboratory technique at this stage. The use of ML-PECVD and its advantages for c-Si and mc-Si surfaces is discussed further in this thesis.

The observations in this chapter have many implications for both the deposition conditions and the passivation of the c-Si surface. The examination of the a-Si:H layers in this optimisation study provide evidence for the more dynamic role that hydrogen within a-Si:H has on surface passivation and raises questions concerning the current thinking about hydrogen and the mechanisms behind the passivation process.

3.

Thermal Annealing and Surface Passivation

Silicon based solar cell technology utilises the concept of surface passivation, usually by hydrogen, to reduce recombination at the surface of the silicon wafer. Provision of hydrogen to this surface has been shown to occur following the deposition of a-Si:H layers; however, the characteristics of a-Si:H are often overlooked. The presence of a non-homogenous distribution of hydrides in the a-Si:H, with the preference of the interface, highlights the possible dynamic nature of hydrogen within these layers and has interesting implications with respect to our thinking about hydrogen and the mechanisms governing passivation.

In this chapter, the thermal annealing process is analysed in detail, firstly to identify an ideal temperature and time required to achieve high quality passivation of the c-Si surface below 300°C. Secondly, with a view to understanding how this influences the optical and structural properties of the a-Si:H(i) layer. Thirdly, following a review of the commonly accepted mechanism governing passivation of the c-Si surface by a-Si:H, an alternative mechanism for surface passivation is presented.

The aim of this chapter is not to treat the properties of semiconductors rigorously from fundamentals. Rather it is to highlight those properties of semiconductors that are important to reducing recombination at the interface (e.g. reducing the density of interface states), without compromising the optical and structural properties of the a-Si:H. Although other processes may also be considered, including for example: band-bending and closed defects at the a-Si:H/c-Si interface [145], many of these are outside the scope of this work and are not investigated in this work.

3.1 Experimental procedure

In this chapter, the surfaces of n- and p-type *FZ* wafers are prepared according to the method described in Chapter 2. The deposition of a-Si:H(i) is onto both surfaces of the wafer and is under ideal conditions as discussed in Chapter 2 (i.e. 225°C, 4W applied, 650mT).

QSSPC and PCD measurements of the effective carrier lifetime (τ_{eff}) are undertaken at mid-injection ($\Delta n - 10^{15}cm^{-3}$). For accuracy, the absorption coefficient (α) and extinction coefficient (k) are measured by multi-wavelength spectral ellipsometry according to the method described in Appendix A. To simplify comparison, only results measured at 633nm are presented in this chapter. The refractive index (n) for the a-Si:H(i) is measured firstly on glass substrates, then on c-Si wafers due to the difficulty in distinguishing between very thin a-Si:H(i) and the c-Si surface. Corning 7059 glass slides are prepared under the conditions given in Chapter 2.

3.2 The need for post-deposition thermal annealing

Good quality passivation of the c-Si surface by a-Si:H(i) layers has been reported for as-deposited layers in commercial systems with τ_{eff} above 1ms [65, 71, 146]. However, in many cases it remains unclear the extent to which thermal annealing has occurred immediately following deposition. It has been reported that thermal annealing reduces the electronic defects and improves the electrical conductivity for a-Si:H deposited at low temperatures [77, 147, 148]. In chapter 2, it was shown that similarly high levels of surface passivation were achievable only following a thermal annealing step. Without this thermal anneal, as-deposited surface passivation was low with τ_{eff} repeatedly being measured below 100µs.

To understand the extent which thermal annealing following deposition has upon the overall passivation quality provided by the a-Si:H(i) layer, a range of thicknesses between 5nm and 150nm are initially annealed at the deposition temperature for up to two hours. The passivation results on the Si-H ($2000cm^{-1}$-$2100cm^{-1}$) peak heights for this anneal step are given in Figure 32. All a-Si:H(i) layers were deposited at 225°C, 4W applied and 650mT, before being removed immediately following the evacuation of process gases and argon flush. Post-deposition took place in a tube furnace with ambient Nitrogen.

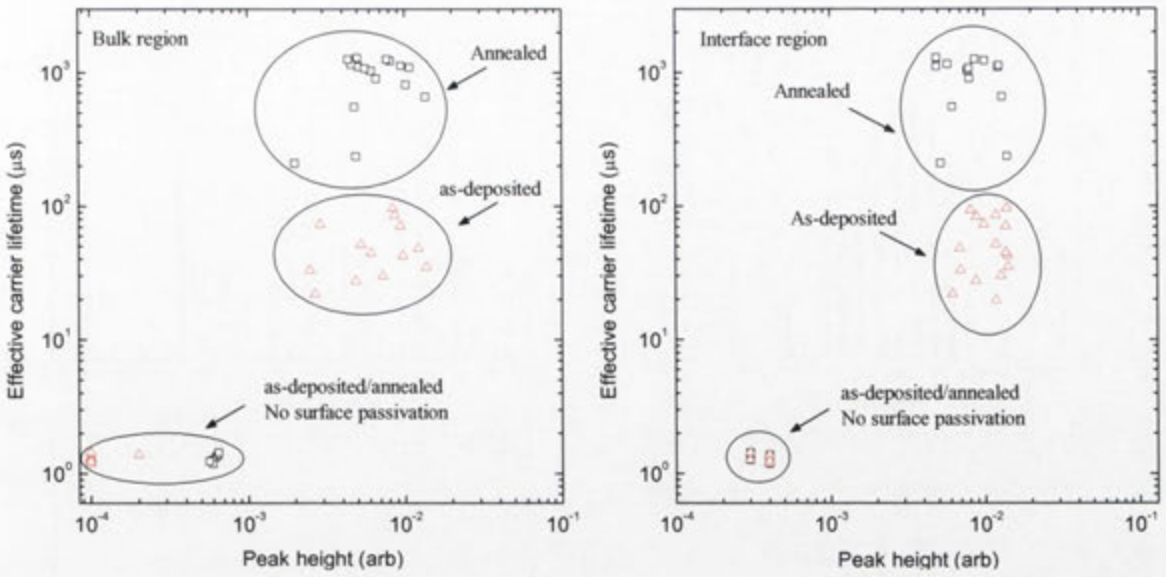

Figure 32: Peak heights for Si-H (2000cm^{-1}-2100cm^{-1}) within the a-Si:H(i) bulk (a) and at the interface (b) compared to effective carrier lifetime in as-deposited cases and following post-deposition thermal anneal at 225°C for one hour.

From Figure 32, the presence of the Si-H hydride bond within the a-Si:H(i) bulk and at the interface with c-Si is clearly observed. Importantly, no significant change in peak height (corresponding to bond concentration) of the bulk and interface hydrides before and after thermal annealing is observed, despite the significant improvement in passivation quality. This result is consistent with that reported by Lim *et. al.* [129], who showed that the concentration of Si-H does not vary for annealing temperatures up to 350°C. Samples deficient in Si-H hydrides exhibited almost no surface passivation, even following substantial post-deposition thermal annealing. It can be concluded that at temperatures below 300°C, thermal annealing is unable to create new Si-H hydride bonds. We can conclude from this that improvements in surface passivation following post-deposition thermal annealing are not simply caused by new hydride bond-formation as believed, and more likely a result of a 'healing' of mismatched or shallow-trapped hydrogen bonds.

According to the Defect-Pool model, any improvements in surface passivation following post-deposition thermal annealing are explained by a change in the defect distribution which remains influenced by thermal processes after initial deposition. Therefore, it can be surmised that improvements in the passivation quality from the thermal annealing process following deposition may occur for an ideal temperature and time; and may be critical to the surface passivation process above.

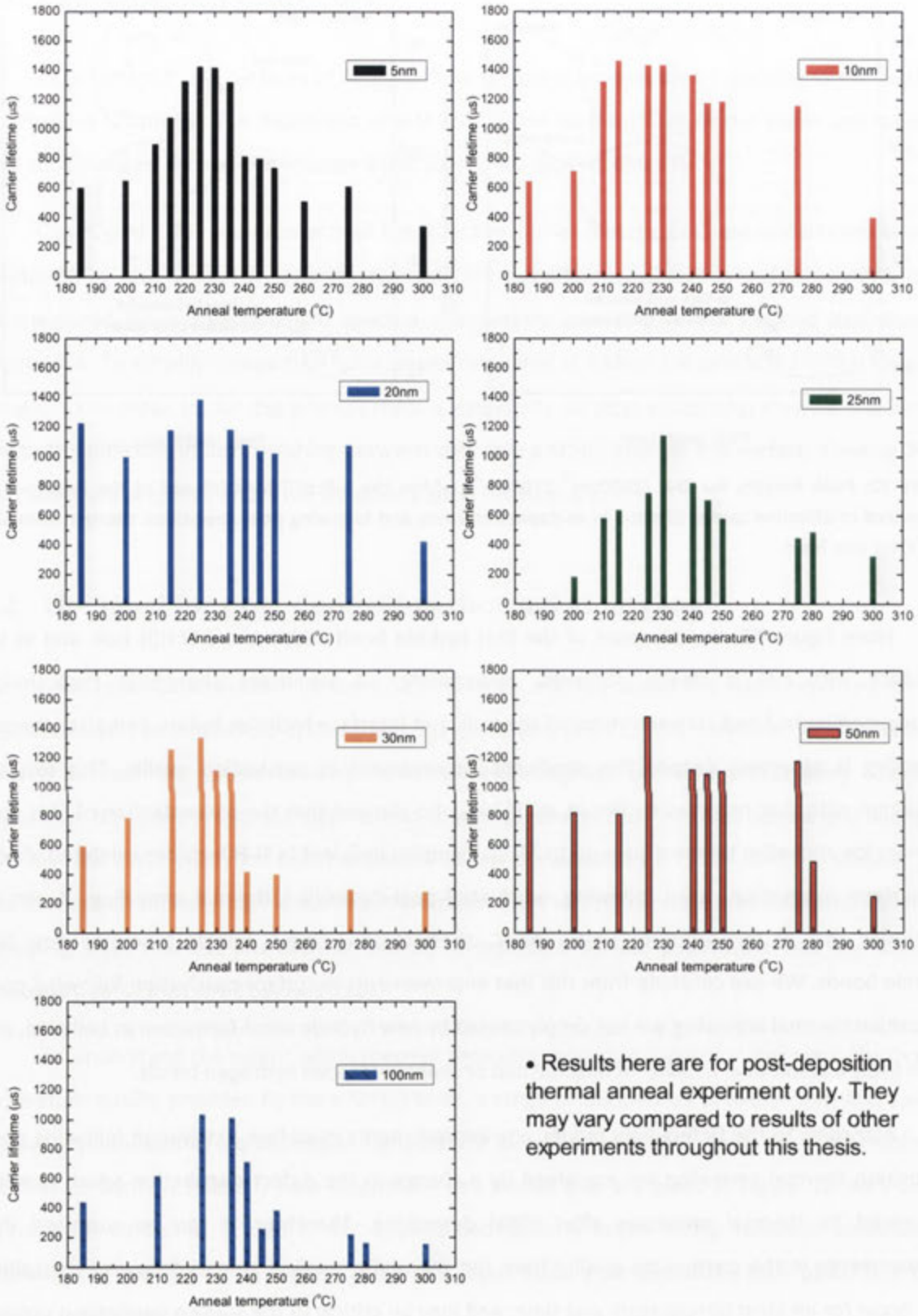

Figure 33: Surface passivation profiles for 5nm - 100nm a-Si:H(i) layers deposited onto 1.4Ωcm FZ c-Si(n) at 225oC, 4W applied, and 650mT; then thermally annealed at different temperatures between 185°C and 285°C. All measurements are at mid-injection ($\Delta n = 10^{15} cm^{-3}$).

It was observed that significant improvements in surface passivation occur when anneal temperatures equivalent to the deposition temperature or higher are utilised. The most effective annealing temperature required to produce high-quality surface passivation within minimal times is examined for a range for a-Si:H(i) thicknesses deposited onto 1.4Ωcm^{-1} *FZ* c-Si(n), the results of which are given in Figure 33.

The τ_{eff} in Figure 33 is measured at room temperature, in-between sequential anneal times. To aid in comparison between c-Si wafers of different thicknesses, S_{eff} is also calculated and displayed in Figure 34. Although some variation in the quality of the surface passivation is observed for τ_{eff}, a more accurate trend is revealed in using S_{eff} over the temperature range.

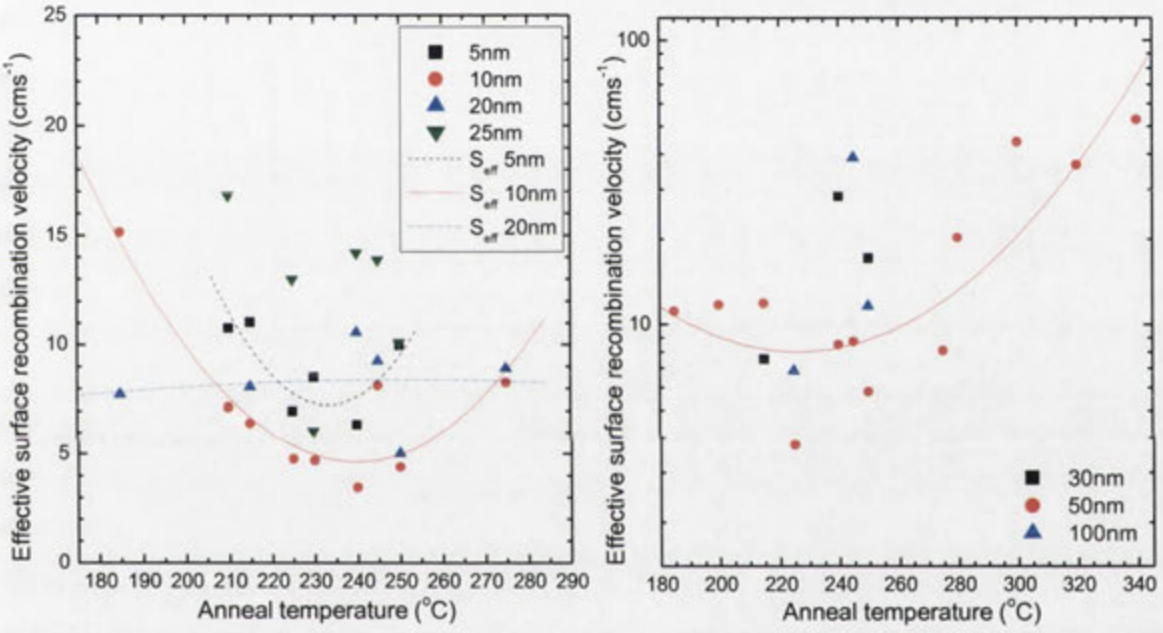

Figure 34: Surface recombination velocities a-Si:H(i) profiles displayed in Figure 33. All measurements are at mid-injection ($\Delta n = 10^{15}cm^{-3}$).

Anneal temperatures above 200°C are observed to yield the lowest recombination rates at the c-Si surface. As the anneal temperature is lowered, recombination increases indicating that Si-H hydrides at the interface are not in saturation. Similarly for higher temperatures above 260°C, the S_{eff} is seen to increase, thus giving an optimal thermal annealing temperature range between 220°C and 250°C. The profiles of most a-Si:H(i) layers do appear to indicate that distinct maxima in surface passivation occur for anneal temperatures within this range. Notably, we have demonstrated that within this anneal temperatures range it is possible to achieve an excellent S_{eff} of 3cms^{-1}.

Undoubtedly, thermal annealing improves surface passivation significantly across the temperature range studied; however, the overall time required to achieve these maxima in passivation quality is not clear. Indeed, provided that anneal times were long enough, similar values were achievable in some cases. In Figure 35, the overall time required until no further improvements in surface passivation are measured is displayed. It is clear that for annealing temperatures below that of deposition (i.e. 225°C), longer annealing times up to 1½ hours are required. By comparison, at temperatures above 225°C, the annealing time required is significantly shorter.

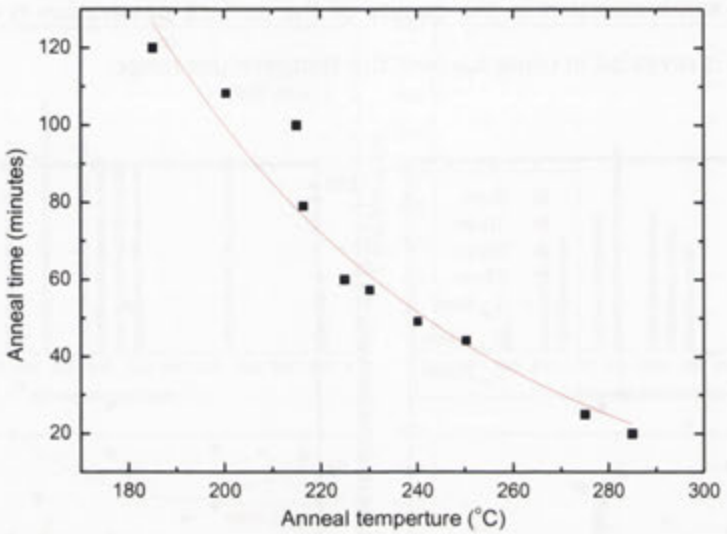

Figure 35: Thermal anneal time required to achieve maximum surface passivation of c-Si surfaces in Figure 33 with annealing temperature.

It is likely that many a-Si:H(i) films deposited using commercial systems undergo some form of thermal annealing, as the equipment often requires cooling to below 100°C before samples can be removed. In this case, many of these a-Si:H(i) layers would have undergone a thermal annealing step, which may contribute to the higher as-deposited τ_{eff} reported. For the PECVD system used throughout this work, samples were removed from the system within 10 minutes of deposition and may explain the low as-deposited surface passivation.

The importance of post-deposition thermal annealing in achieving high passivation quality of the c-Si surface is likely related to the deposition process itself. During PECVD, impinging hydrogen, with low relative mass, is not capable of altering the configurations of the c-Si surface. Therefore, it can only interact with the suitable surface bond states whose density is dependent upon surface preparation and orientation (i.e. 110, 100). Therefore, hydrogen is likely to be either free or shallow-trapped within the a-Si:H layer. Thermal annealing at suitable temperatures following deposition

would aid in surface diffusion and reconfiguration of silicon surface bond states. Ideally, this temperature has been shown to occur between the deposition temperature of 225°C and 275°C. Higher than this and the effectiveness of the passivation is reduced as proto-crystalline formation occurs (dependent upon deposition conditions and a-Si:H quality).

Additionally, thermally induced improvements in surface passivation of c-Si were previously thought only possible for a-Si:H(i) deposited and annealed at temperatures above 200°C [54, 64]. Below this temperature, surface diffusion of Si-H has not been reported. Instead, the formation of new hydride bonds was accepted as the cause for the reduction in surface recombination. However, improvements in surface passivation without new bond formation are clearly evident below this temperature. Alternatively, it has been suggested that hydrogen within the bulk of the a-Si:H(i) layer diffusing towards the c-Si surface is the origin of the improvement in passivation results following annealing. This supposition fails to give any explanation for why hydrogen would preferentially diffuse towards the interface with the c-Si surface when already within a region of higher defect density [149]. Certainly the longer times required for maximum passivation to be achieved when annealing at lower temperatures suggests that the mechanism governing surface passivation is more dynamic than bulk hydrogen diffusion. This concept is discussed in further detail in section 3.4.

Here, it may be concluded that post-deposition thermal annealing between 185°C and 285°C can improve surface passivation of c-Si significantly with no measureable shift for monohydride density in both the bulk and interface regions of the a-Si:H(i). This demonstrates that post-deposition thermal annealing below 300°C does not influence the profiles given in chapter 2, only the time required to achieve saturation of the c-Si surface by available hydrogen. In this way, the selected temperature is a trade-off between surface passivation properties and anneal time, in addition to preserving the quality of the a-Si:H(i). The higher the anneal temperature the less time is required; however, exceeding the optimal range discussed is likely to introduce phase changes within the layer itself. In this work, 240°C has been chosen throughout this work to minimise the time required to improve the surface passivation provided by as-deposited a-Si:H(i). Although there remains some latitude in the choice of anneal temperature.

, a trade-off is more likely between surface passivation properties and shortening anneal time. Also, it is proposed that surface passivation at temperatures below 300°C may be independent of bulk hydrogen diffusion and considering that no new interface hydride bonds or are formed or hydride migration towards the interface occurs.

3.3 Influence of annealing temperature on optical and structural properties

In photovoltaic devices, the passivating a-Si:H(i) layers are often deposited onto the front or illuminated side of the c-Si and in some cases, such as bifacial solar cells, onto both surfaces. Although the thickness of these thin layer(s) would require the presence of an anti-reflection coating as well, the optical properties of the a-Si:H(i) layer(s) themselves need to be considered in order to optimise light transmission through to the c-Si bulk. As previously discussed, the electronic properties are influenced by thermal processes; therefore, the optical properties with thermal annealing are investigated here in terms of absorption coefficient (α) and refractive index (n).

Myburg and Swanpoel reported an increase in the refractive index from 3.0 to 4.2 (at 633nm) as temperature was increased from -100°C to 400°C [124]. Freeman and Paul showed that for slight decreases in hydrogen content of *rf*-sputtered a-Si:H(i) layers, the value of n increases also [150]. In both studies, it was indicated, although not stated, that an inverse relationship exists between hydrogen content and the refractive index. However, when considering the deposition conditions of these two studies, a void-rich layer may also have been assumed. In comparison, Nobuo *et. al.* reported an increase in the absorption coefficient for increases in the annealing temperature between 100°C and 230°C [151], which taken with the statement above, implies the same relationship is occurring.

In this work, the refractive index and absorption coefficient for 633nm is examined over a broader range for first time on much thinner a-Si:H layers to establish a more complete optical profile of the a-Si:H(i) layer with temperature. The results of which are given in Figure 36.

For increase in temperature, both the refractive index and the absorption coefficient are seen to increase from 3.6 to 4.1, and $1x10^4 cm^{-1}$ to $5 x10^4 cm^{-1}$, respectively. In both cases, the results given here agree with those of Nobue *et. al* for a-Si:H(i) [151] and to some extent Myburg and Swanpoel [124]. Combined with those results presented previously in this thesis, an upward trend is established that correlates well with the shifts in FTIR and Raman which showed a relaxation in the network stresses with temperatures above 200°C. Of note, the increase in α at 633nm is not drastic, between $10^4 cm^{-1}$ and $10^5 cm^{-1}$.

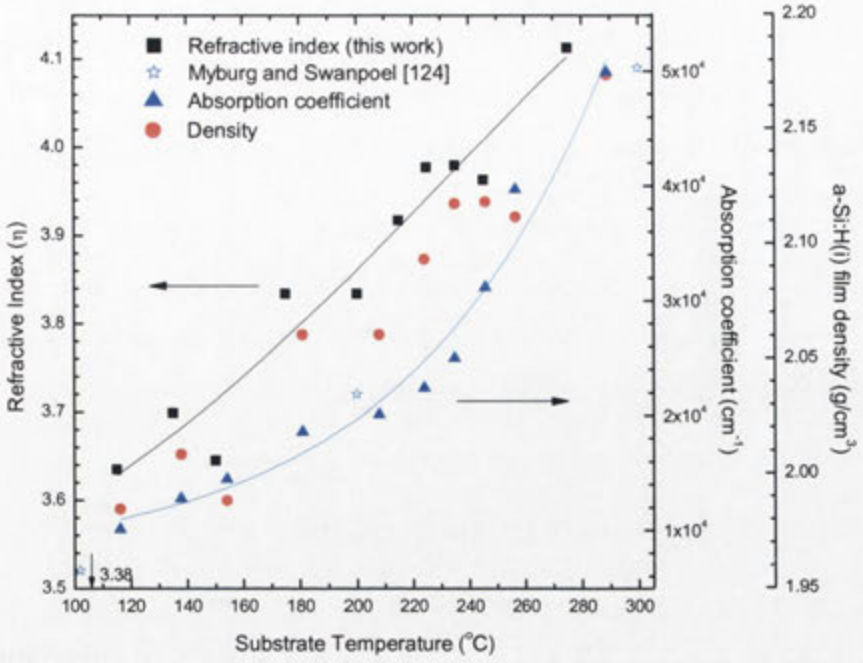

Figure 36: Profile for refractive index (n), absorption coefficient (α), and density (ρ) of a-Si:H(i) as a function of substrate thermal annealing temperature, measured at λ = 633nm.

Although in single crystal solar cells, increases in absorption coefficient of a-Si:H(i) are considered undesirable, and here α may be considered already high. The inverse of the absorption coefficient ($1/\alpha$) indicates that for the thicknesses where 66% of the light is absorbed, according to equation (3- 1).

$$\frac{1}{\alpha} \approx \begin{cases} 10^{-5} cm \rightarrow 1\mu m \\ \frac{10^{-5}}{5} cm \rightarrow 0.2\mu m \end{cases} \qquad (3\text{- }1)$$

To minimise absorption the a-Si:H(i) layer thickness should be kept <<0.1µm. As the layer thicknesses studied primarily throughout this work are between 5nm and 50nm, the significance of any increased absorbance in the a-Si:H(i) would be small.

It is commonly thought that for temperatures approaching 300°C, increases in micro-void density occur, characterised as a decrease in the density of the a-Si:H(i) [132, 152]. Indeed, at higher

temperatures above 300°C, decreases in the a-Si:H(i) layer density have been reported to occur in micro-void rich films during the onset of crystallinity [153]. In the same work, refractive index was also reported to decrease in the presence of micro-voids. However, no micro-void fraction was observed in this work for increases in temperature up to 300°C, as shown by FTIR and Raman results presented throughout this thesis.

The density (ρ) of the a-Si:H(i) layers deposited in this study can be determined from the refractive index according to equation (3- 2) [124, 152, 153]. The results given in Figure 36 are the first reported regarding the density of a-Si:H(i) below 300°C.

$$\rho = 0.0511\left(n_0^2 - 1\right) + 1.36 \qquad (3\text{- }2)$$

From Figure 36, the density of the a-Si:H(i) layer is seen to increase for temperatures between 100°C and 300°C, confirming that micro-void formation is negligible, consistent with IR spectroscopy in this work. This does not negate the influence of micro-voids if present, as for some a-Si:H(i) layers reported by other groups. Certainly, Myburg and Swanpoel have reported a decrease in the density of a-Si:H with higher refractive index for a-Si:H(i) with thicknesses above 900nm, attributed to hydrogen content but also to voids and holes within the layer [152].

Therefore, it may be concluded that the increase in refractive index and absorption coefficient are indeed due to hydrogen content in the a-Si:H(i) and not the presence of micro-voids. In considering the higher density for a-Si:H(i) layers deposited in this work, it can be suggested that the a-Si:H(i) layers and conclusions reported by Halindintwali *et. al.* [153] and similarly by Schropp *et. al.* [154] are likely for low quality a-Si:H(i) layers characteristically deposited at high temperatures, high *rf*-power and partial pressures. In the case of Myburg and Swanpoel [124], 1000nm are deposited between -100°C and 400°C which acknowledge a large range of structural effects may be unaccounted for in addition to significantly increase absorption expected for very thick layers.

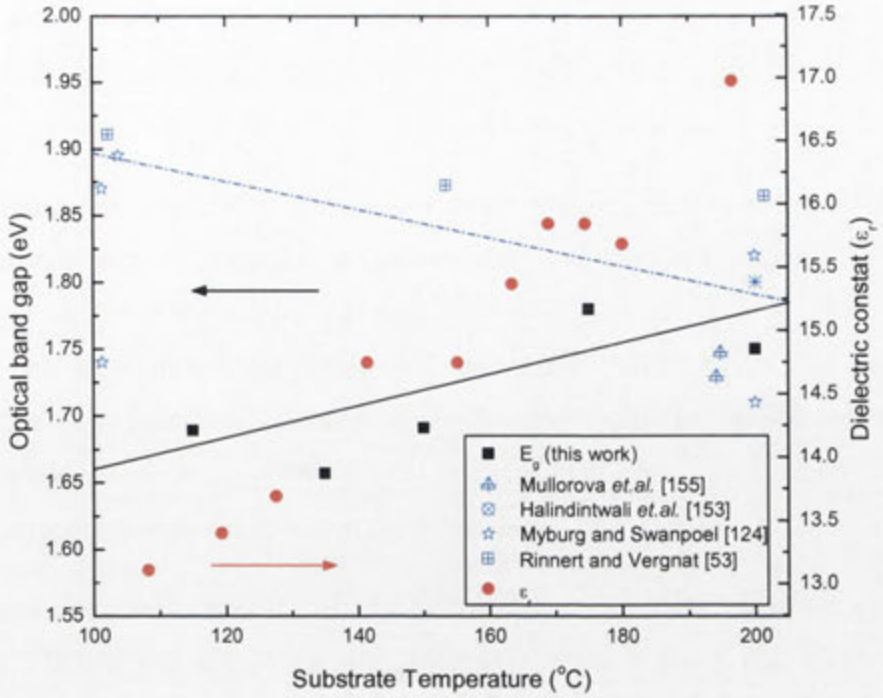

Figure 37: Optical band gap (E_g) for a-Si:H(i) layers thermally annealed at different temperatures following deposition at 225°C, 4W applied, and 650mT. The black guide line gives the trend for E_g in this work. The a-Si:H(i) layers reported by Müllerová *et. al.* [155] are at 400°C, 1000nm layers by Myburg and Swanpoel [124] are deposited between -100°C and 400°C (blue guide line), Rinnert and Vergnat [53] are by ion-assisted evaporation argon-hydrogen plasma. Note: In Halindintwali *et. al* .[153], the layer is 800nm in thickness by HWCVD at 410°C, 2Pa (diluted 92%) provided for comparison to other CVD techniques.

To understand further the significance that temperature has upon the optical properties of the a-Si:H(i), the optical band gap (E_g) is examined. The value of E_g has often been associated with the concentrations of Si and H but can also be related to the density of micro-voids [152]. In IR studies regarding E_g for relatively thick a-Si:H(i) layers, Müllerová *et. al.* [155], Halindintwali *et. al.* [153] have both reported lower E_g with increased ordering contrary to results reported by Myburg and Swanpoel [124, 152] who reported a decrease as occurring. However, as thinner a-Si:H(i) layers are preferred for passivating the c-Si surface, it is necessary to consider the influence of anneal temperature on E_g for these thinner layers. It is suitable to extrapolate this value from the separation of the band gap edges on Tauc's plot according to equation (3- 3) [43], where $\alpha_{(\hbar\omega)}$ is wavelength dependent absorption coefficient, ω is the angular wavelength, $\hbar$ is the reduced Plank's constant and A' is a proportional optical constant (2×10^4) [156, 157].

$$\left[\hbar\omega\alpha_{(\hbar\omega)}\right]^{1/2} = A'\left(\hbar\omega - E_G\right) \qquad (3\text{-}3)$$

The calculated values for E_g of a-Si:H(i) deposited in this work and annealed at different temperatures are given in Figure 37 as a function of the anneal temperature. The results for a-Si:H(i) layers deposited at optimised conditions in this work (i.e. 225°C, 4W applied, 650mT).

Previously unknown to occur, the trend shown here with anneal temperature following deposition exhibits a distinct increase in E_g, between 100°C and 300°C. The blue-shift relates well to the increase in density of the a-Si:H(i) layer with higher anneal temperatures (see Figure 36). This appears to contradict the results of Myburg and Swanpoel [124], and those of Maley and Lannin [97], who each reported that E_g decreases with higher temperatures. However, it should be firstly noted that both these studies attributed decreases in E_g to a decrease in density of the layer results from the presence of micro-voids, which if present would influence this optical property.

Secondly, the results of Myburg and Swanpoel were based were based upon large increments in temperature (i.e. 100°C steps), such that measurements were made only at 200°C and 300°C, in comparison to those reported in this work. Thirdly, at higher temperatures, above 300°C, it has been reported that E_g decreases rapidly with the onset of crystallinity as a consequence of high micro-void density [153, 158].

From the results of this work, a clear increase is observed over a large temperature range for a-Si:H(i) with no significant micro-void presence detected.

To explain the significance of this trend, the interaction of the a-Si:H(i) on the c-Si surface must be considered. From the work in chapter 2, it is known that a higher proportion of hydrogen occurs within the interface region. Although, bond density has been shown not to increase with post-deposition thermal annealing, a relaxation of the network stress does occur. This is likely to result in an improved efficiency in passivating dangling bonds, leading to a reduction in the band tail and appearance of an indirect gap of 3.3eV. Indeed, Maley and Lannin demonstrated that hydrogen influences E_g for a-Si:H(i) layers deposited by HWCVD despite the void-rich layer [97]. The trend reported in this work is explained by the increased proportion of hydrogen at the c-Si interface, which leads to reductions in band tails and the appearance of an indirect gap of 3.3eV, when the density of dangling bonds are reduced. This conclusion is supported by the similar increase in the dielectric constant (ε_r) (where: $\varepsilon_r = n^2-1$) shown in Figure 37 for simultaneous increases in density of the a-Si:H(i) layer; a result also reported by Freeman and Paul [150].

Of importance is the concurrent increase in E_g with α given here, indicating that for the a-Si:H(i) layers deposited and annealed in this work an improved transparency for lower energy

photons (i.e. longer λ) results from thermal annealing. From the viewpoint of front surface passivation by thin a-Si:H(i), high Eg within the passivating layer improves the transmission of longer λ light to the c-Si bulk underneath. As such, it can be concluded that post-deposition thermal annealing can yield benefits both electronically and optically to the a-Si:H(i) passivated c-Si device, provided that the layer is kept thin (i.e. ideally ≤10nm).

3.3.1 Stability of surface passivation by a-Si:H(i) undergoing thermal anneal

Previously is was reported in section 3.2 that rapid improvements in surface passivation occur when deposited a-Si:H(i) layers were thermally annealed at temperatures of 225°C and above. For lower temperatures, the anneal time increased from 20 minutes to more than 1 hour in a tube furnace. This extended thermal anneal time raises the question of thermal stability during longer thermal treatments. In 2002, Dauwe *et. al.* [65] reported low surface recombination velocities for 30nm a-Si:H(i) layers annealed at either 250°C or 375°C for up to 65 hours, with the latter temperature causing significant degradation of passivation. Further to this, the operational thermal stability of a-Si:H(i) layers in HIT solar cells has been commented on by Taguchi *et. al.* [159, 160].

The importance of long term stability is desirable in contact formation and represents an indication of the robustness of the a-Si:H(i) layers. Therefore, a selection of good-passivating a-Si:H(i) layers deposited at ideal conditions (225°C, 4W applied, 650mT) underwent a thermal annealing at 250°C for up to 80 hours with the results are given in Figure 38. Periodically, a-Si:H(i)/c-Si samples are removed from the tube furnace, allowed to cool to room temperature, before τ_{eff} was measured. Surface recombination velocities are given to aid in comparison between samples with different c-Si base wafer thicknesses and also to those reported in the literature.

For most layers shown in Figure 38 thermal annealing did not degrade the quality of the surface passivation. A similar outcome (not shown) was also observed when passivating 0.9Ωcm *FZ* c-Si(p). For both c-Si dopant types, the stable profile of surface passivation for extended annealing times is indicative of the deposition of high quality, robust a-Si:H(i) layers in this work. The results for a-Si:H(i) layer deposited and annealed in this work not only agree with that reported by Dauwe *et. al.* [65], they exhibit a lower level of degradation is achievable, even for layers as thin as 5nm.

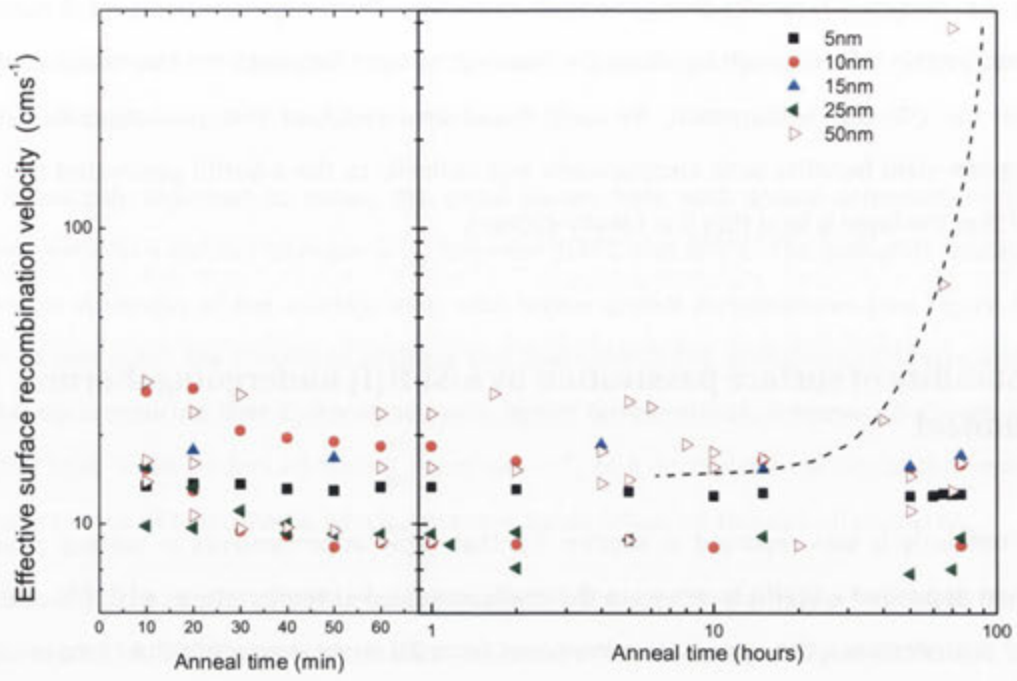

Figure 38: Surface recombination velocities for 1.4Ωcm *FZ* c-Si(n) deposited bifacially with a-Si:H(i) at ideal conditions and thermally annealed at 250°C for up to 80 hours. Note: scale change from minutes to hours.

To understand the excellent thermal stability demonstrated in this work, we refer to FTIR measurements made at room temperature during each incremental thermal anneal and the analysis presented in Figure 39.

For most layers deposited and annealed in this, no significant change in either the bulk or interface monohydride density is observable. Some initial shifts within the first hour occur as the network stress is relaxed; thereafter, remaining stable for the entire 80 hours of annealing. The hydrogen % content also remains stable between 10% and 18%, depending on the layer, during the length of the thermal anneal at 250°C. Similarly, no shift in heterogeneity occurs for most layers up to 60 hours, although, some slight decrease does appear to occur for longer times.

The thermal stability of the surface passivation provided by the a-Si:H(i) layers in this work appears to arise from the densities of the layers themselves and the dominance of monohydride in the both the interface and bulk regions of the a-Si:H(i). The consistency demonstrated indicates that Si-H bonding strain remains minimal following initial improvements within the first hour of thermal annealing, limiting the propensity for hydrogen to diffuse for longer times.

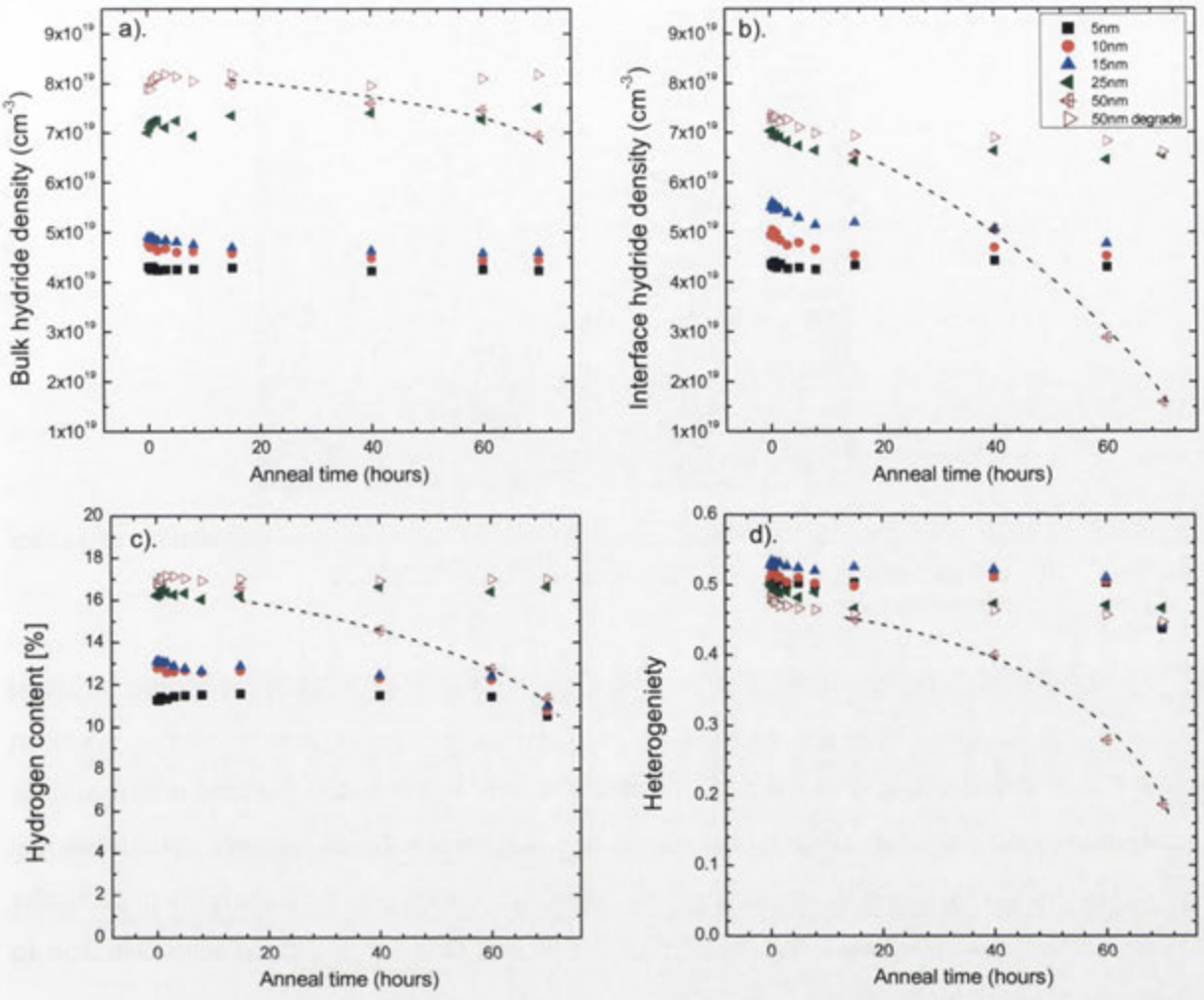

Figure 39: IR hydride bond density results a). Bulk monohydride, b). Interface monohydride densities, c). Hydrogen % content, d). Heterogeneity for a-Si:H(i) of different thicknesses on 1.4Ωcm *FZ* c-Si(n) and annealed at 250°C 80 hours. All layers were deposited at 225°C, 4W applied, and 650mT. Dotted line is a guide for degraded 50nm a-Si:H(i) layer.

The exception to the excellent thermal stability in this work is seen for a 50nm a-Si:H(i) layer in which blistering was evident (see Figure 40) and complete degradation in passivation occurred after 65 hours (Figure 38: dotted line). Blistering of a-Si:H(i) layers is known to occur for two common reasons, the formation of long hydrogen chains, and secondly delamination from surface defects or contaminates. No blistering had been observed on other 50nm layers deposited simultaneously with this degraded sample. Therefore, it is assumed that delamination, in this case, is the likely cause of the degradation in surface passivation. Although this would suggest contamination of the c-Si surface prior to deposition, it cannot be conclusively stated, that blistering has occurred for this reason.

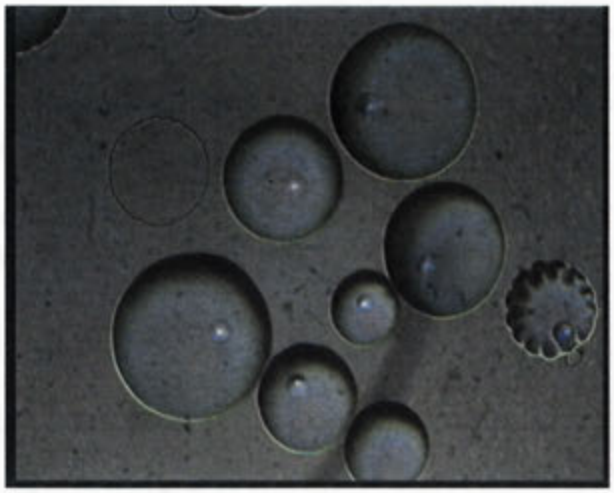

Figure 40: Micrograph of 50nm a-Si:H(i) layer on c-Si(n) that suffered complete degradation of surface passivation after 65 hours. Blistering of surface can be seen to cover the surface.

However, it can be concluded from this work that thin a-Si:H(i) deposited at ideal temperatures, so as to limit SiH_2 and higher-order hydride formation, onto a suitably prepared surface and thermally annealed at 225°C or above is suitable for yielding stable, robust surface passivation to the c-Si surface without compromising transparency. The significance of both thermal and optical improvements and stability for the a-Si:H(i) layers achieved in this study are of particular importance for their application to either the front or rear surfaces of bifacial solar cells and to where contact formation is required.

3.4 Surface passivation and the hydrogenation mechanism

Recombination of photogenerated charge carriers at the surface of c-Si is known to govern the overall performance of a solar cell. Deep energy levels or dangling bonds at the c-Si surface act as recombination centers for the photogenerated carriers from the c-Si bulk. Hydrogen has been widely discovered to be an essential ingredient for improving the electronic quality of the c-Si surface by passivation of dangling bonds at this surface. Although the benefits of hydrogenation at the c-Si surface have been known for more than two decades, there remains a considerable lack of understanding of many of the fundamental properties of hydrogen involved in passivation. The interaction of hydrogen at the c-Si interface with a-Si:H and the mechanisms by which it migrates to these sites is of particular importance for improving the effectiveness of surface passivation. In this section, a contribution towards improving our understanding of surface hydrogenation is presented.

3.4.1 Previous developments in surface passivation mechanisms

The standard picture of hydrogen migration is one in which hydrogen atoms, thermally activated from deep energy levels or trapping sites within the a-Si:H layer bulk diffuse towards the unpassivated c-Si surface [161-164], in a process commonly referred to as bulk hydrogen diffusion. However, this picture perhaps overlooks the origins of hydrogen involved in passivation of the c-Si surface and the energies required for this process.

If hydrogen is presumed to originate from the bulk of the a-Si:H layer then the potential source can be assessed as in either un-bonded or bonded states. As high levels of 'free' hydrogen are unlikely in a material such as a-Si:H, with a high defect density between $10^{15}cm^{-3}$ and $10^{17}cm^{-3}$ [149, 165, 166], bonded hydrogen is considered a more likely primary source. Numerous energies have been proposed for bonded hydrogen between 1.05eV and 3.60eV [167]. Initially, the spontaneous release of hydrogen was assumed as a possible source. Although it is reasonable to believe that hydrogen can be released from a 3-fold Silicon configuration[5] [43], this would require an energy of approximately 2.49eV [168], applicable only at higher temperatures than those studied in this work. Therefore, the 'spontaneous release' fails to explain the hydrogen saturation of dangling bonds at the c-Si surface at the lower temperatures observed and discussed earlier in this work as well as by others; and the disparity between hydrogenation of the c-Si surface by hydrogenated thin films without the breaking of Si-H bonds at low temperatures remains apparent.

To address the inconsistency between experimental results and theory a mechanism of lower energy than Si-H bond spontaneous release was necessary. Pantelides proposed a quasi-free hydrogen state where loosely bonded hydrogen atoms are able to diffuse via 'bond-interconversion' [149, 169]. This mechanism requires a lower energy of 1.5eV for hydrogen to move through a series of mobile states until it is captured by a dangling bond, ideally at the c-Si surface as illustrated in Figure 41.

In numerous experimental and theoretical studies this trap-limited model for hydrogen diffusion has been accepted for SiN passivation at high temperatures [57, 135, 162, 170-173]. In earlier work, Leihr et. al. [174] have shown, using temperature desorption spectroscopy for temperatures up to 700°C, that molecular hydrogen does not interact with the silicon surface or interfere with silane adsorption.

[5] A 3-fold Silicon configuration refers to most stable form of Hydrogen bonded to a single Silicon atom which is back-bonded to 2 additional Silicon atoms [43]

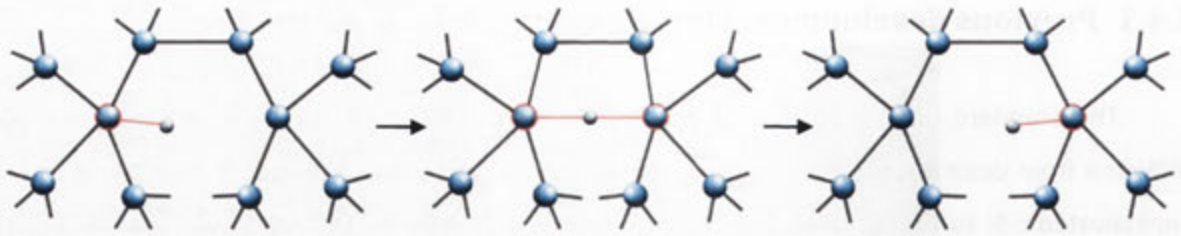

Figure 41: Schematic of the bond 'inter-conversion' process. Hydrogen is weakly bonded to a 5-fold coordinated Si atom, before being shared between two Si atoms within 2.3Å of each other. The hydride is then transferred to the second Si atom after any number of attempts.

For the temperatures common to improvements in surface passivation by SiN, the inter-conversion' process appears to explain how hydrogen migrates from the bulk of the thin film to the interface. A similar activation energy of 1.5eV for hydrogen diffusion in a-Si:H at temperatures above 500°C has also been reported. Consequently, this diffusion mechanism was also adopted to explain improvements in a-Si:H passivation of the c-Si surface at low temperatures below 500°C and has been drawn on to explain hydrogenation at temperatures as low as 200°C. Currently, the hypothesis concerning bulk diffusion of hydrogen towards the c-Si surface has been widely accepted as the primary mechanism by which hydrogen assists in reducing recombination at the c-Si surface in all materials [65-67, 69].

This assumption has in the past led to the widespread belief that hydrogenated thin film layers with high hydrogen contents are the most suitable for passivation of the c-Si surface [50, 175-178]. However, high hydrogen concentrations resulted in reductions in τ_{eff} and solar cell performance [176, 179, 180]. To overcome this duplicity in hydrogen, thicker layers above 50nm with lower overall hydrogen contents have commonly been utilised to increase the supply of hydrogen, believed to occur via bulk-diffusion, without increasing its concentration with the layer. Although this appeared to be an effective solution, given the assumptions of a bulk- diffusion model, it does not address the nature of hydrogenation at the c-Si surface in several ways:

- The preferential diffusion of hydrogen towards the c-Si surface, as opposed to other defect-rich regions throughout the a-Si:H contradicts experiments concerning the effusion of hydrogen from the thin film at high temperatures.
- Hydrogen is unlikely to remain in weakly bonded states within a high defect material
- The hydrogen bond-interconversion bulk diffusion mechanism for a-Si:H would be significantly inhibited by the high defect density of a-Si:H deposited at low temperatures below 280°C.

- Bulk hydrogen diffusion is time-thickness dependent with no significant limitation on diffusion distance for thin films.
- The minimum energy level for a bulk diffusion mechanism (E_d) is 1.5eV, severely limiting hydrogen migration to the c-Si surface at low temperatures, below 280°C. Hydrogenation of the c-Si at temperatures of 200°C and below is not likely according to the bulk diffusion mechanism's minimal energy requirements.

In chapter 2, high effective carrier lifetimes were shown to occur for a-Si:H/c-Si, deposited and then thermally annealed, at temperatures below 250°C. In addition, although thermal annealing at temperatures of 185°C required longer anneal times, high τ_{eff} was achieved, contrary to the predictions of the thermal diffusion mechanism. Furthermore, in section 3.2, FTIR revealed that no significant new bond formation or shift in hydride concentration from the a-Si:H bulk to the interface occurs during thermal annealing as would be expected for bulk hydrogen diffusion. Therefore, for the lower temperature range, where hydrogen lacks sufficient energy to undergo the bond interconversion process through the bulk, it is unlikely that a bulk diffusion mechanism is responsible for hydrogenation and passivation of the c-Si surface.

In both the work of Gupta *et. al.* [181] and Fujiwara *et. al.* [132] strong evidence concerning the presence of a hydrogen rich interface region over that of a stoichiometric a-Si:H layer is given. Indeed the results of Kolasinski *et. al.* [182, 183] support the concept of bulk and interface regions having different hydrogen concentrations. In the work presented earlier in this thesis, the occurrence of a hydrogen rich interface region, which may be suitable to passivate the c-Si surface without a thick bulk region was also evident. Certainly, a-Si:H layers as thin as 5nm with relatively low hydrogen content, were shown to achieve high passivation quality without the need of a thick bulk layer. This would appear to counter the need for thicker bulk regions and the necessity of bulk hydrogen diffusion to effectively passivate the c-Si surface.

Given the paradoxical conclusions presented by the bulk hydrogen diffusion model, a series of 1.4Ωcm *FZ* c-Si(n) wafers were prepared and deposited with a-Si:H(i) between 5nm and 100nm to determine the time dependence and activation energy for a surface passivation mechanism at temperatures below 300°C. All wafers were prepared according to the method outlined in chapter 2 for optimal conditions (i.e. 225°C, 4W applied, 650mT). Each set of a-Si:H(i)/c-Si(n) wafers were then annealed at one of five temperatures, 185°C, 215°C 225°C, 245°C and 275°C. Measurement of τ_{eff} by QSSPC/PCD ($\Delta n = 10^{15}cm^{-3}$) was undertaken at room temperature at set increments during the annealing process. In this analysis, the annealing temperature was assumed to be the determining

factor for the rate by which surface passivation is occurring as all other parameters were kept constant.

3.4.2 Time dependence of the thermally activated surface passivation

In Figure 42, τ_{eff} is observed to increase from a level below 100μs for the as-deposited a-Si:H(i)/c-Si(n) to above 1ms following post deposition thermal anneal at each of the temperatures investigated. As discussed previously in section 3.2, temperature directly influences the annealing time required to saturate the c-Si surface. For temperatures equal to or above the deposition temperature, this improvement in τ_{eff} is rapid compared to temperatures below 200°C as shown in Figure 42. The different rates of improvement in surface passivation shown here provide clear evidence for two flaws in the concept of a bulk diffusion mechanism:

- that significant improvements in surface passivation are achievable within this temperature range (if E_d = 1.5eV), and
- no significant temperature dependence for surface passivation should be evident.

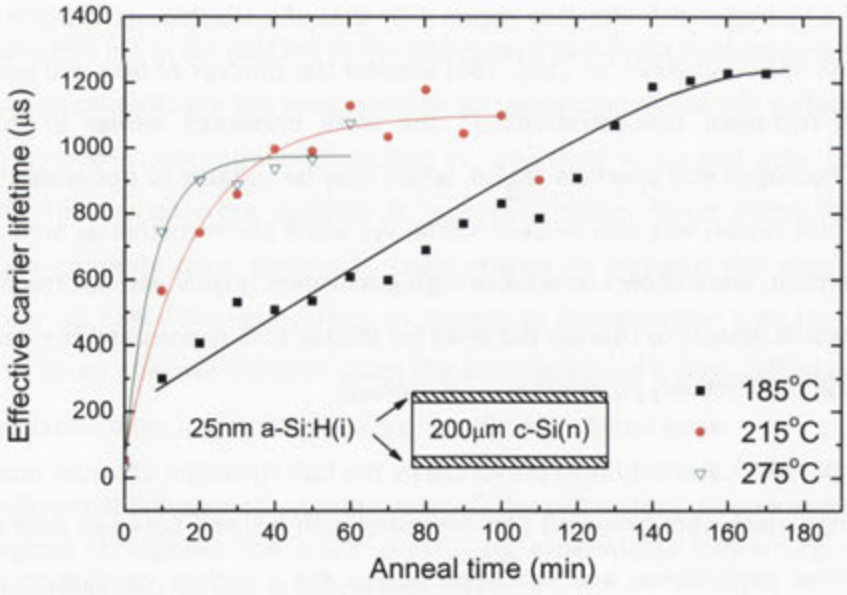

Figure 42: Measured annealing time dependence of τ_{eff} for 25nm thick a-Si:H(i) films, for three different annealing temperatures. Fitted lines are shown.

In Figure 43, the improvement in τ_{eff} for 10nm, 20nm and 50nm a-Si:H(i) on c-Si(n) thermally annealed at 225°C is shown. The reaction rate ($1/\tau_{reac}$) can be calculated by Sigmoidal fitting of the τ_{eff} by fitting equation (3- 4)(3- 3), where τ_{reac} is the reaction time constant, τ_b is the bulk carrier lifetime, t is the thermal anneal time, and A_1 is a pre-exponential factor determined during the fitting process.

$$\tau_{eff} = \left[\frac{1}{\tau_B} + A_1 \exp\left(\frac{-t}{\tau_{reac}}\right)\right]^{-1} \qquad (3\text{- }4)$$

The fitting process is illustrated in Figure 43 for the three a-Si:H(i) layer thicknesses shown, however, similar fits are made for other thicknesses and at other thermal anneal temperatures. The error bars represent the maximum and minimum fitted solutions of $1/\tau_{reac}$.

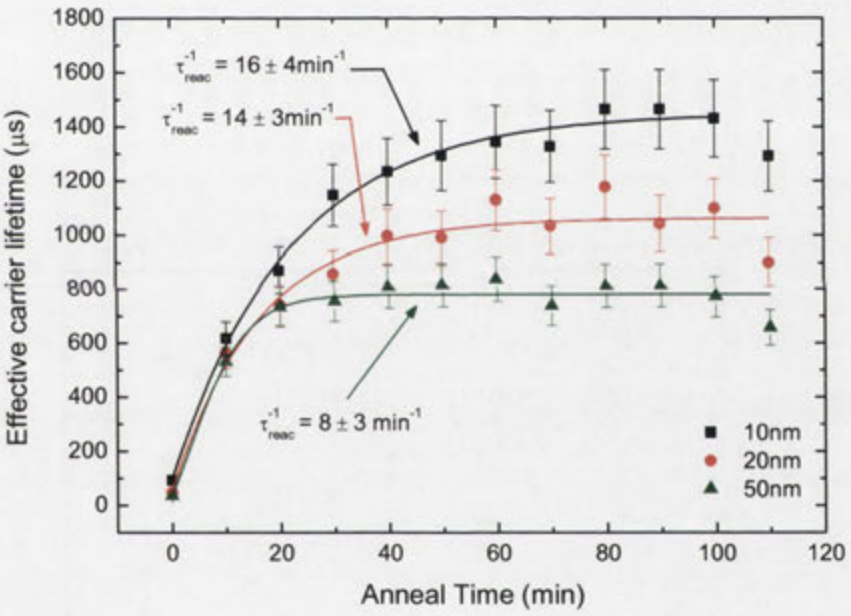

Figure 43: Improvements in τ_{eff} from post-deposition thermal annealing for three different a-Si:H(i) layer thicknesses at 225°C. Sigmoidal fits and the reaction rate are shown for each thickness.

Assessing the improvements in surface passivation quality for each thickness annealed at a particular temperature provides similar reaction rates, suggesting that the hydrogenation and subsequent surface passivation of c-Si is independent of a bulk diffusion mechanism. From this an alternative mechanism with a different energy may be derived.

3.4.3 Determination of thermal activation energy for low temperature surface passivation

The activation energy (E_A) for a temperature dependent surface passivation mechanism between the a-Si:H layer and the c-Si surface, which also occurs at lower temperatures unsuitable for a bulk diffusion mechanism, can be determined by an Arrhenius calculation. Using the previously fitted values of $1/\tau_{reac}$ the value of E_A for the surface passivation mechanism is determined from the slope of the fitted line using equation (3- 5). Here, A_2 is the pre-exponential factor determined by exponential fit (~10^6), k_B is the Boltzmann constant and T is the temperature. In Figure 44, the reaction rates for a particular a-Si:H(i) thickness, thermally annealed at different temperatures are plotted against the inverse temperature. The error bars represent the maxima and minima of the fitted solutions from equation (3- 5). The process was repeated for other thicknesses between 5nm and 100nm.

$$\frac{1}{\tau_{reac}} = A_2 \exp\left[-\frac{E_A}{k_B T}\right] \qquad (3\text{- }5)$$

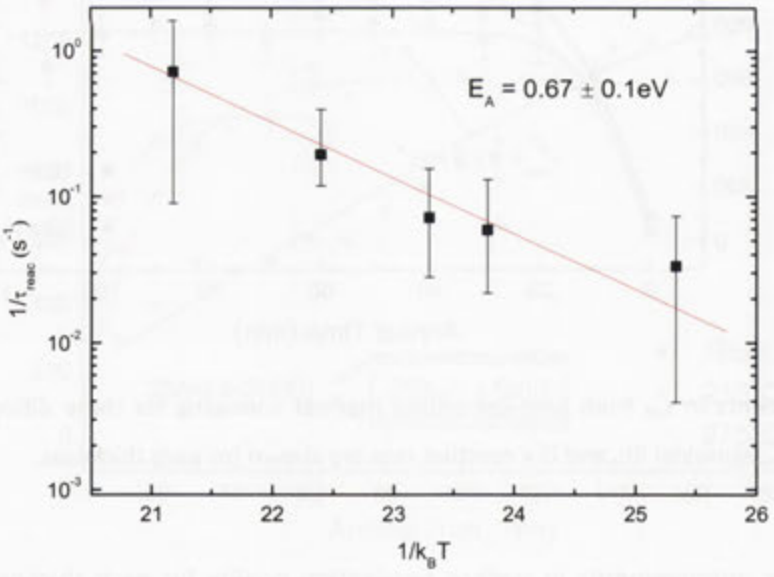

Figure 44: Arrhenius plot of reaction rate showing the fit for determining the activation energy of the surface passivation process. A 25nm a-Si:H(i) layer deposited onto a 200µm c-Si(n) wafer is shown. Fitted line according to equation (3- 5).

A clear temperature dependence is evident in Figure 44 for the 25nm a-Si:H(i) layers deposited onto c-Si(n) and thermally at different temperatures in agreement with results previously discussed in this chapter. For the 25nm a-Si:H(i) layer a value for E_A of 0.67eV is determined, well below the 1.5eV that is required for the bulk diffusion mechanism. The above method is repeated for other thicknesses between 5nm and 100nm to assess whether thickness dependence for the value of E_A relating to the surface passivation exists that would indicate a mechanism similar to bulk diffusion.

In Figure 45, the results for the determination of E_A for the surface passivation mechanism between a-Si:H(i) and c-Si is plotted against the layer thickness. It can be observed that the activation energy does not exhibit a strong dependence on the thickness of the a-Si:H(i) layer. Therefore, it can be inferred from this result that the mechanism for surface passivation is indeed independent of any bulk hydrogen diffusion mechanism.

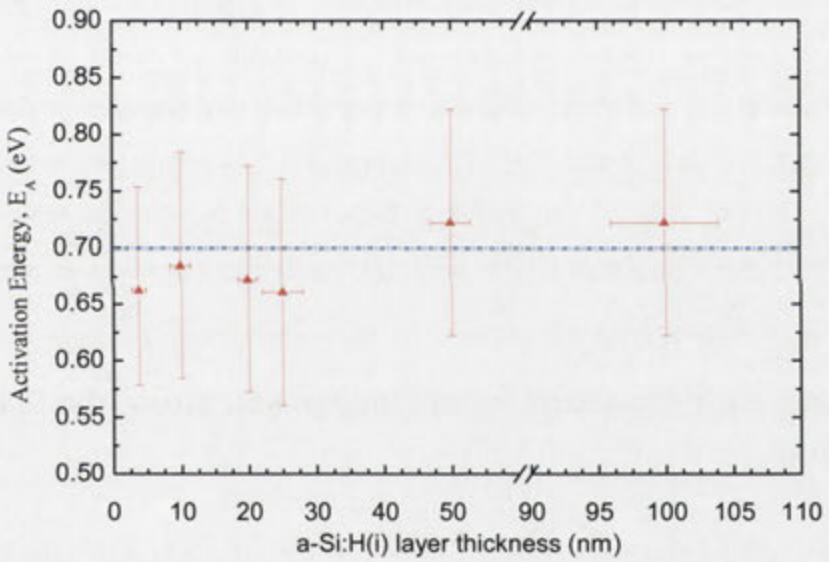

Figure 45: Calculated thermally activated surface passivation energies for different a-Si:H(i) layer thicknesses. Dotted line indicates the average value for E_A across all thicknesses.

An average E_A of 0.7 ± 0.1eV for the mechanism governing hydrogenation and passivation of the 1.4Ωcm <100> *FZ* c-Si(n) surface is calculated. This agrees well with the results in a parallel study by De Wolf *et. al.* which gave a value for E_A of 0.6eV for surface passivation of c-Si with a-Si:H(i) films deposited at low temperatures [64]. The value of $E_A \approx 0.7$eV determined here also agrees with that obtained by electron spin resonance measurements of silicon dangling bond density performed by Biegelsen [148] during thermal annealing up to 250°C [148]. Similarly, Brenig, Gross and Russ report

a value for E_A of 0.75eV, determined by theoretical simulations of hydrogen motion and passivation of the c-Si surface in terms of adsorption and desorption of hydrogen at this surface [184].

Importantly, the value of E_A determined in this work differs from that reported for bulk related long-range hydrogen diffusion processes in a-Si:H of approximately 1.5eV [149, 171] and the 2.49eV required for spontaneous hydrogen release [168]. Consequently, the lower E_A here and from similar experiments and simulations would suggest that surface passivation is primarily dependent upon available surface states, rather than the bulk diffusion processes commonly referred to in the literature [65-69]. While bulk hydrogen diffusion can still occur at higher temperatures, the results of this study indicate the existence of an alternative surface reaction-type mechanism for surface passivation by a-Si:H(i), involving hydrogen already very close to the interface, at lower temperature.

This possible explanation for the relatively lower activation energy found here for surface passivation reflects the bonded rearrangement of hydrogen already present at the interface prior to deposition (i.e. the final HF step) or else from hydrogen incorporated during the initial stages of deposition. In this case, only a localised surface diffusion of hydrogen atoms would be sufficient to produce improvements in surface passivation. Importantly, this explanation does not rely on hydrogen diffusing from the bulk of the a-Si:H layer through a highly defective material to selectively passivate the c-Si surface states. It can therefore be concluded that for low temperatures, below 300°C, that surface passivation would be very unlikely explained by a bulk related mechanism.

3.5 Alternative mechanisms for surface passivation of c-Si by hydrogen

If we consider that hydrogen, already present at the c-Si surface or within the interface region, is the likely foundation for improvements in the surface passivation quality, then the interaction of hydrogen with surface-states is of interest to improving our understanding. In this, hydrogen reactivity at the c-Si surface would be dependent upon its arrival at either bonding or anti-bonding sites, in other words the orientation of Si-Si bonds to accept incident hydrogen.

The reconfiguration of both silicon and hydrogen at the interface has been suggested in different models based on a similar fundamental assumption, that of a thermally activated surface-state. In simulations by Brenig, Groβ, and Russ, a prediction of a strong phonon assisted trapping of hydrogen using a local lattice relaxation model was proposed [184]. Here they showed that although in principle 'detailed balance' is valid, it cannot be applied to very large energy releases occurring

from lattice distortions, in-effect hydrogen mobility is localised. Bratu *et. al.* [185, 186] has shown, by using IR-analysis of second-harmonic generation, that excitations of lattice vibrations influence the dynamics of hydrogen interaction with the c-Si surface. Importantly, for temperatures from 277°C and upwards, a thermally activated process regarding dissociative adsorption with energy of 0.7 ± 0.1eV, matching the E_A determined in this work, was reported. In similar studies, state-specific detection of hydrogen desorbed from the Si <100> surface passing through transition states has also been discussed [183, 187, 188]. Indeed, Fujiwara *et. al.* has reported strong evidence by spectral ellipsometry and attenuated total reflection spectroscopy on a surface diffusion process concerning hydrogen as a part of a smoothing mechanism which promotes a dense a-Si:H network to aid in hydrogenation [132].

In each of these models, the interaction of hydrogen with the c-Si surface was found to be influenced by the rate of adsorption. Although this commonality seems logical, it does not answer several questions relating to hydrogen pairing with silicon; namely, the reported decrease in adsorption probability at higher anneal temperatures following deposition [174, 182, 186] and despite shorter anneal times [72, 189]. Also, no explanation is specified on the increased energy requirements for hydrogen desorption between trapping sites reported by Jing *et. al.* [157], which has been attributed to the temperature dependent phononic excitations at 0.75eV [184].

3.5.1 Surface transport model for passivation of c-Si by hydrogen

"Millions saw the apple fall, but Newton was the one who asked why"

Bernard M Baruch

In order to improve our understanding concerning the physical process of surface passivation driven by a surface reaction limited mechanism, the low value of $E_A \approx 0.7$eV determined in this work is extended to the development of a hydrogen surface mobility model based on the work by Tuttle and Adams [190] ,Bratu *et. al.* [186, 191], Branz [172], Fedders [192], and Street [43]. In Figure 46, the essential concept of the model in this work is illustrated.

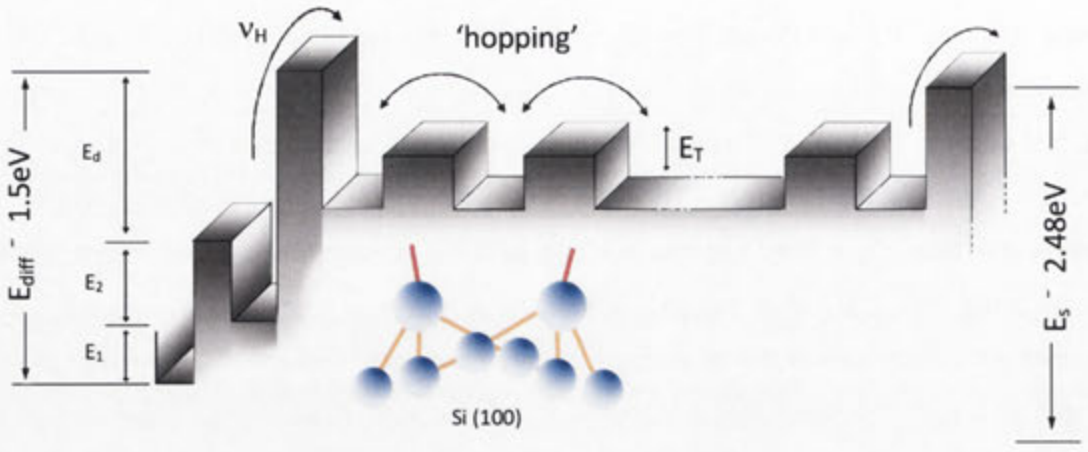

Figure 46: Diagram of hydrogen desorption and surface diffusion mechanism via shallow trap sites. The E_{d1-3} denotes the energy for each desorption configuration of hydrogen, from trap → intermediate → transport level. E_T represents the energy of hopping at the transport level, between 0.2-0.4eV. E_{diff} and E_S denote the energy for bulk diffusion and spontaneous release of hydrogen, respectively. υ_H is the desorption rate, and υ_d° represents the hopping frequency.

This model is aimed at explaining the results observed throughout this thesis and those reported by other groups. It is proposed in this model, that hydrogen surface diffusion occurs on c-Si and beneath an a-Si:H(i) layer by localised hopping, where the hydrogen absorbed at one site jumps to another site on the surface via shallow trapping states. For this, hydrogen is considered to be mobile between traps through a transport level, and also that surface diffusion is a random walk in 3-dimensions which may be influenced by phonon scattering. As described, hydrogen from intermediate trapping sites with energies E_{d1-3}, move to the transport level where diffusion across the surface can occur, via a series of shallow traps, with energies between 0.2eV and 0.4eV.

Indeed post-hydrogenation studies of a-Si:H films by IR and SIMS spectroscopy have reported hydrogen migrations through a series of weak-bonded interstitial or shallow trap sites at energies between of 0.23eV and 0.31eV [166]. These and other activation energies between 0.2eV and 0.5eV have been reported for transport process of hydrogen across the surface [135, 166]. However, the model for the surface diffusion mechanism presented in this work is the first consistent with the transport of hydrogen from an interstitial site to a deeply trapped site within the value E_A of 0.7eV determined as part of this work, in agreement with thermal annealing results presented here and with no significant dependence on bulk-diffusion.

In the following sections, the derivation for the surface-diffusion model is first presented, followed by a discussion of the model output. The multidisplinary approach includes established chemisorption and probabilistic based formulae, where referenced, and others are found through this work. In order to simulate the measured behaviour for this model, whenever possible, experimentally determined numerical values are utilised for the parameters.

3.5.2 Hydrogen adsorption and desorption at the c-Si surface

The role of surface states on the passivation mechanism is likely to be governed by the nature of adsorption and desorption of hydrogen at the interface with c-Si. Adsorption of mobile hydrogen at a favourable site can be determined when considering the probability of trapping; which itself compares the rate of adsorption to the relative rate of desorption of hydrogen at the surface. The probability of hydrogen being deeply trapped on the c-Si surface may depend on many factors; foremost is the existing coverage of hydrogen (θ), and secondly the presence of any activation barrier to adsorption.

In terms which concern the trapping of hydrogen at a bonding site, either interstitial (shallow) or deep (dangling bond), the trapping potential can be given according to the relation:

$$\text{Trapping probability} = \frac{\text{rate of adsorption at a site}}{\text{rate of trapping at a site}}$$

Under the first condition, the number of sutiable sites available to trap hydrogen can be expected to decrease as surface coverage increases, reducing the probability of trapping according to equation (3- 6). In this, the probability of mobile hydrogen becoming deeply trapped (s) is proportional to the fractional hydrogen coverage(θ), given a trapping coefficient (s_o) for the material.

$$s = s_o(1 - \theta) \qquad (3\text{-}6)$$

The trapping coefficient, which governs the adsorption of mobile hydrogen at favourable sites[6], has been shown to be temperature dependent in laser induced thermal desorption

[6] Favourable site is defined as a silicon dangling bond, correctly aligned (i.e. π-bond), to accept a mobile hydrogen.

experiments by Kolasinski *et al.* [182]. Thermally activated, an Arrhenius expression for s_o can be made in equation (3- 7), where site-blocking by Si-H and σ-bond is applicable. In this, the pre-exponential factor (A_o) is $7 \times 10^{-2 \pm 0.5}$, relating to hydrogen chemisorption [182, 184]. E_A is 0.7eV from this work, Boltzmann's constant is given as k_B and T_s is the substrate temperature.

$$s_o = A_o \exp\left[\frac{-E_A}{k_B T_s}\right] \qquad (3\text{-}7)$$

Typically, a very low trapping coefficient is considered a good indication of widespread hydrogen bonded coverage of the c-Si surface, a consequence of the apparently large adsorption barrier near equilibrium when site-blocking is accounted for.

Slight increases in s_o with increasing substrate temperature describes for a thermally dependent hydrogen adsorption at the c-Si surface. The question concerning the defect passivation by hydrogen being independent of the network stress remains. Although, the height of the adsorption barrier is known to be influenced by the Si-H bond stress; during thermal annealing, a-Si:H undergoes structural relaxation so the contribution of network stress is likely to be minimal.

In the model presented, hydrogen passivation is considered a balance between the probabilities of desorbed, mobile hydrogen from the a-Si:H being shallow trapped and deeply trapped. Here it is assumed that the initial hydrogen-coverage[7] of the c-Si surface is minimal due to low, initial passivation measurements prior to thermal annealing. This would denote a scenario where the *'rate of desorption'* of hydrogen is slower than the *'rate of adsorption'* of hydrogen, a condition for which the principle of detailed balance is not applicable. Therefore, to understand the importance of decreasing s_o with temperature, it should not be thought that the adsorption rate[8] (k_a) increases due to a lowering of the barrier, instead it is more reasonable to consider that the desorption rate (k_d) increases relative to k_a (i.e. $k_a << k_d$) for the monolayer. This is the case when hydrogen located at interstitial bonding sites is sufficient for maximum monolayer coverage. Also, that when considering the increased probability that hydrogen located at interstitial sites, will have sufficient energy to overcome the dissociation barrier and diffuse across the surface to a favourable

[7] Hydrogen coverage is defined as bonded (deeply-trapped) hydrogen at the c-Si surface.

[8] Adsorption rate relates to the rate at which a single hydrogen atom may be adsorbed at either shallow or deep traps. Desorption rate relates to the rate at which a single hydrogen may be released from shallow or deep trap sites.

site with no adsorption barrier. Consequently, as anneal temperature is increased, more interstitial hydrogen can be released into the transport level inherently linking increases in s_o with anneal temperature to the decreased availability of suitable bonding sites. The process is self-regulating, continuing until most dangling bonds at the c-Si surface are passivated.

However, the observed behaviour in s_o can also be attributed to temperature dependent phononic (lattice) excitations with a similar apparent activation energy of 0.75eV which dissipates the energy of the desorbed hydrogen though silicon-phonons [184]. This suggests that hydrogen transitions from being interstitially-trapped to being deeply-trapped with no surface transport. In both cases, a reconfigured surface state occurs with the value of E_a and s_o determined here. To ascertain which of these may be responsible, it is necessary to examine hydrogen coverage with time.

3.5.3 Dependence of hydrogen coverage on surface-reaction states

The dynamic interaction of hydrogen in surface states through adsorption and desorption barriers centers on the effective coverage of the c-Si surface. The relationship between anneal temperature and time (section 3.4.2), points toward a surface diffusion of hydrogen according to the Langmuir isotherm [193]. This is often used to describe the surface coverage as a function of both time and temperature, and allows the effective hydrogen coverage for different temperatures to be estimated from the trapping potential given the activation energy. Accordingly, the conditions of the surface-state model are:

- Adsorption cannot proceed beyond the monolayer coverage,
- All surface sites are treated as equivalent on a uniform surface, and
- The ability of hydrogen to be adsorbed at any site remains independent of the occupation of neighbouring sites.

The use of this isotherm is logical given that passivation of the c-Si surface by hydrogen at the low temperatures explored throughout this work has shown that no bulk diffusion of hydrogen occurs with the significant improvement in τ_{eff}. As indicated by FTIR measurements made in this work, a hydrogen rich interface region already exists during deposition, where a reservoir of hydrogen is available to effectively passivate the c-Si surface. Also, according to the results presented in Chapter 3, the improvement in surface passivation is thermally activated by an energy

of 0.7 ± 0.1eV, indicating that hydrogenation is not through a bulk diffusion process (E_A = 1.5eV) and may already be present at or within a few nanometres of the c-Si surface. Although already present, incident hydrogen during rapid deposition simply does not have sufficient energy of 0.1eV (c-Si <100> [194]) to flip an asymmetric c-Si dimer into a suitable configuration for adsorption, an otherwise slow process.

Two additional assumptions are applied to this analysis; that,

- Mobile hydrogen transport can occur across shallow traps with a minimum energy of 0.2eV [195, 196], and
- Hydrogen can be sourced from above the monolayer.

In Langmuir adsoption, a reliance on surface coverage often applies to the temperature dependent trapping coefficient such that $s_o = s_o(T_s)f(\theta_{(t)})$, where $f(\theta) = (1-\theta)^2$. However, as the relevive extent of the monolayer coverage considered here is approximately 0.14ML, concerning the interaction of hydrogen with the c-Si surface (i.e. $f(\theta_{(t)}) \approx 1$), the surface coverage is unlikely to have any influence on s_o. As such, we maintain the relation for s_o given in equation (3- 7).

Desorption of hydrogen from interstial sites

Hydrogen present at the surface in a shallow trap for low temperatures is likely to remain in this state almost indefinitely according to the first assumption. However, as the temperature of the substrate is increased, the thermal energy of the shallow trapped hydrogen will also increase, and desorption to a mobile state is increasingly likely to occur.

According to the principle of microscopic reversibility, a reaction must follow the same reaction pathway [193]; therefore, the desorption rate of hydrogen (k_d) from trapped sites is expressed by the rate law (3- 8) according to Langmuir kinetics; where k is a rate constant, $\theta_{(t)}$ the surface coverage over time and m the reaction order.

$$k_d(T_s) = \frac{-d\theta_{(t)}}{dt} = k\theta_{(t)}^{m} \qquad (3\text{-}8)$$

When considering hydrogen mobility on the c-Si surface, it is more informative to consider the factors controlling the desorption and adsorption processes at the molecular level. The desorption rate of hydrogen from a shallow trap is assumed temperature-dependent as *k* is a rate limiting value which follows an Arrhenius relationship expressed in equation (3- 9). Here, ν_d^o is a desorption prefactor considered to be an attempt frequency, commonly $10^{13}s^{-1}$ [197-199] at 580K.

$$k_d(T_s) = \nu_d^o \exp\left(-E/k_b T_s\right) \tag{3-9}$$

Considering that k_d is determined through temperature-dependence and the maximum surface coverage (θ_{max}) of 0.8 for 0.14ML [182, 186, 200], where $k_d \rightarrow 0$, according to equation (3- 9), we can now rewrite equation (3- 8) as:

$$k_d(T_s) = \nu_d^o \exp\left(-E/k_b T_s\right)\theta_{max} \tag{3-10}$$

Given the time-dependence likely to occur in this case, the rate by which hydrogen is emitted from a shallow trap can be expressed according to the Polyanyi-Wigner model [193] in equation (3- 11).

$$k_d(\theta_{(t)}, T_s) = \theta_{(t)}^m k_d(T_s) = \theta_{(t)}^m \nu_d^o \exp\left(-E/k_b T_s\right) \tag{3-11}$$

The desorption process is often rate-limited according to the attempt frequency preceding hydrogen release from a shallow trap, a factor dependent upon the desorption site. Therefore, the reaction order is determined by the desorption kinetic, either 1st or 2nd order [169]. For <100> c-Si, surface desorption undergoes both 1st and 2nd order kinetics as two different desorption sites are present. In the first, desorption of hydrogen occurs from adjacent silicon atoms of a single dimer [183, 200]. For the second, the formation of a secondary, intermediate dihydride phase to faciliate the desorption process from two monohydrides simultaneously occurs [201-203]. As a constant rate of desorption occurs for any given temperature, it is reasonable to assume that desorption proceeds by a 1st order process. However, in most cases, a value of 1.56 [204, 205] is chosen as midway between monohydride and dihydride desorption. For monohydride dominated a-Si:H(i) layers, a value for *m* closer to 2 would be more likely.

The attempt frequency ν_d is often expressed according to equation (3- 12), where α is the 'hopping' distance between surface silicon trapping sites of 2.4×10^{-8}cm [156, 157, 182].

$$v_d = \frac{3 D_o}{2 a^2} \quad (3\text{-}12)$$

For undoped a-Si:H, D_o is often reported to be approximately $10^{-3}cm^2s^{-1}$ [162]. We will return to this parameter in a moment.

Adsorption of hydrogen at favourable trapping sites

Also from Langmuir kinetics, the adsorption rate (k_a) of hydrogen at the c-Si surface follows a similar expression to desorption, and can be usually expressed by equation (3- 13). However, as k_a is related to the concentration of mobile hydrogen and the probability of trapping, noting that the influence of $f(\theta)$ is negligible for the monolayer.

$$k_a(T_s) = \Phi_{(t)}(T_s)\, s_o(T_s)\, f(\theta_{(t)}) \quad (3\text{-}13)$$

Here $\Phi_{(t)}$ is a time-dependent flux and $s_o(T)$ is the temperature-dependent trapping coefficient. As k_a is Arrhenius in nature, it should be noted that the activation energy for adsorption may itself be influenced by the surface coverage with time. Noting that the barrier to adsorption is minimal for an unpassivated site.

3.5.4 Dependence of hydrogen coverage on transport states

The c-Si surface coverage by hydrogen is ruled by the simple relation between the rates of adsorption and desorption:

$$k_a(T_s) = k_d(T_s) \quad (3\text{-}14)$$

Since $k_a << k_d$, is the likely scenario for low temperatures the adsorption rate is limiting. As adsorption only occurs when mobile hydrogen interacts with a favourable site, mobile hydrogen density is governed by the surface coverage over time and the desorption rate of hydrogen from shallow trap sites. In this, the maximum surface coverage serves as a limiting parameter when $T_s > T_d$. Therefore mobile hydrogen relates to time-dependent coverage, fractional coverage and desorption

probability for all local reaction pathways. If the rate of adsorption is assumed constant, the flux of the mobile hydrogen ($\Phi_{(t)}$) within the monolayer for any given pathway is given by equation (3- 15).

$$\Phi_{(t)} = v_d \theta^m \left[2 \pi m k_b T_s\right]^{-1/2} \theta_{(t)\max} \tag{3-15}$$

To determine the realistic flux of mobile hydrogen states, the equilibrium between adsorption and desorption states needs to be considered (i.e. surface coverage with time relative to total surface coverage). Assuming fractional hydrogen coverage, midway between 1st and 2nd order kinetics, the flux of mobile hydrogen can be expressed by equation (3- 16).

$$\Phi_{(t)} = 0.8 v_d \exp\left[-E/k_b T_s\right] \theta^m_{(t)} \left[2 \pi m k_b T_s\right]^{-1/2} \tag{3-16}$$

At any given time and temperature, the cumulative hydrogen coverage would be determined by the rates of adsorption and desorption, limited by mobile hydrogen density.

$$\theta_{(t)} = \int_0^t \left[k_a(\theta, T, t) - k_d(\theta, t)\right] dt \tag{3-17}$$

According to Fick's Law [193], the mobile hydrogen density remains proportional to the first derivative of the concentration in order for the condition $dk_d/dt = 0$, otherwise from equation (3- 8), mobile hydrogen density will be independent of heating rate (i.e. $d^2\theta/dT^2 = 0$). It is known from chapter 3 (Figure 42) that this is not the case. Therefore, by evaluating equation (3- 17), the hydrogen coverage towards equilibrium can be expressed according to the flux of mobile hydrogen, trapping coefficient, and temperature-dependent desorption rate given in equation (3- 18).

$$\theta_{(t)} = \left[\frac{\Phi_{(t)} S_o}{v_d^o \exp\left[-E/k_b T_s\right]}\right]^{1/m} \tag{3-18}$$

As the concentration of mobile hydrogen is assumed low, relative to the immobile SiH, the density of mobile hydrogen will vary linearly with the square root of the concentration such that Kohlrausch's

Law can be applied to equation (3- 18). This gives the time-dependent surface coverage by hydrogen through a Langmuir adsorption kinetic, where the adsorption reaction is related to the flux of mobile hydrogen for any given pathway as a ratio of total hydrogen coverage (equation (3- 19)).

$$\theta_{(t)} = \theta^{m}\left[1 - \exp\left(\frac{-s_o \Phi t}{\theta_{(t)\max}}\right)\right] \qquad (3\text{- }19)$$

Zafar and Schiff [165] have suggested two equally possible configurations of hydrogen for this scenario; firstly, that 6 hydrogens are clustered in close proximity; secondly, that hydrogen remains spatially isolated. In either case, for the Si <100> surface a value of 8 $x10^{14}cm^{-2}$ is apparent for hydrogen diffused through a series of surface states [182, 191, 206]. With 2 x $10^{21}cm^{-3}$ hydrogen atoms being considered the upper limit, if no termination of silicon dangling bonds is present initially; and as such, both cases are likely for the a-Si:H layers deposited in this work.

3.5.5 Effective hydrogen surface diffusion in dimensional space

Assuming that hydrogen desorption and transport across the surface (via shallow steps) primarily follows thermal activation, the temperature dependence of the hydrogen diffusion coefficient (D_m) is also defined by its Arrhenius behaviour with mobile energy of E_H.

$$D_m = D_o \exp\left[-E_H / k_b T_s\right] \qquad (3\text{- }20)$$

Where D_o is the diffusion coefficient for mobile hydrogen (within the monolayer) regulated by mean inter-atomic 'hopping' distance [156, 157, 182] and hopping frequency, and is roughly equivalent to that reported for hydrogen diffusion relating to the c-Si [162, 207].

If the substrate temperature (T_s) is greater than the temperature for desorption of hydrogen (T_d) (i.e. $T_s > T_d$) then diffusion of mobile hydrogen across the surface will continue to occur and can be thought of as a trap-limited process when the mobile hydrogen density is small relative to the immobile hydrogen density [208]. Surface diffusion is defined by the relation:

$$N_m D_m = N_H D_H \quad (3\text{-}21)$$

Here, N_m is the mobile hydrogen density, D_m is the mobile hydrogen diffusion coefficient within the transport level, N_H is the immobile hydrogen density for a-Si:H (i.e. 5 x $10^{21}cm^{-3}$), and D_H is the effective hydrogen diffusion coefficient within a-Si:H(i) [208].

Given that the trapping rate of mobile hydrogen by dangling bonds is a function of desorption rate and deeply trapped hydrogen according to equation (3- 22) we can consider the temperature dependence of the above relationship.

$$R_{db} = k_{db} N_m N_{db} \quad (3\text{-}22)$$

, where $k_{db} = 4\pi\alpha D_m$, and N_{db} is the dangling bond density that varies inversely with N_H, although initially it would be approximately $10^{16}cm^{-3}$ for silicon below 300°C [165, 208]

If the thermal emission rate is expressed by the Arrhenius expression where ν_{th}^{o} is a prefactor ~$10^{8\pm1}s^{-1}$ between 180°C and 300°C).

$$R_{th} = N_H \nu_{th}^{o} \exp\left[-E_H / k_b T_s\right] \quad (3\text{-}23)$$

Substituting R_{th} and R_{db} into equation (3- 21) we re-arrange to obtain the mobile hydrogen density as:

$$N_m = \left(\frac{N_H \nu_{th}^{o}}{k_{db} N_{db}}\right) \exp\left[-E_H / k_b T_s\right] \quad (3\text{-}24)$$

Here, we find two solutions for determining D_H; firstly through the thermal emission rate; secondly according to the kinetic formula for diffusion.

In the first, substituting N_m and k_{db} into equation (3- 21), D_H can be expressed as:

$$D_H = \left(\frac{\nu_{th}^{o}}{4 \pi a N_{db}} \right) \exp \left[- E_H / k_b T_s \right] \quad (3\text{-}25)$$

, and ν_{th} can be expressed from the rearrangement of equation (3- 24) as:

$$\nu_{th}^{o} = \left(\frac{k_{db} N_{db} \left(N_m \exp \left[- E_H / k_b T_s \right]^{-1} \right)}{N_H} \right) \quad (3\text{-}26)$$

Alternatively, the kinetic formula for diffusion, where $\nu_H = R_{th}(N_H)^{-1}$ is the emission rate of one mobile hydrogen per Si-H, and the mean distance of mobile hydrogen before re-trapping is given by $\lambda_{(t)}$as in equation (3- 27).

$$D_H = \nu_H \lambda_{(t)}^2 = \frac{R_{th} \lambda_{(t)}^2}{N_H} \quad (3\text{-}27)$$

As the diffusion of mobile hydrogen across the c-Si surface is only terminated by capture at a deep-trap site, surface diffusion may be thought of as trap-limited when the concentration of mobile hydrogen is small relative to that of immobile hydrogen. For a random walk in 3 dimensions the mean distance travelled by mobile hydrogen before being trapped can be expressed according to [208] as:

$$\lambda_{(t)} = (6aN_{db})^{-1/2} \quad (3\text{-}28)$$

According to the Stokes-Einstein theory, the D_H can be written for hydrogen mobility in 3 dimensions without violating the monolayer. By substituting $\lambda_{(t)}$ and R_{th} into equation (3- 27) the following result for D_H is obtained.

$$D_H = \left(\frac{\nu_{th}^{o}}{6 a N_{db}} \right) \exp \left[- E_H / k_b T_s \right] \quad (3\text{-}29)$$

The emission rate of hydrogen to the mobile state can be derived from above as:

$$v_H^o = 6aN_{db}\left(\frac{D_H}{\exp\left[-E_H/k_bT_s\right]}\right) \quad (3\text{-}30)$$

Residence time of hydrogen in the transport level

The surface diffusion time of mobile hydrogen concerns the average time hydrogen is mobile before re-trapping. Given that mobile hydrogen can only permanently be trapped by a dangling bond at low-moderate temperatures, the relation between surface diffusion to distance and time is given by the kinetic formula for diffusion given in equation (3- 27)). By rearranging this we can determine the mean distance travelled by mobile hydrogen and substitute into equation (3- 21) to give:

$$D_H N_H = R_{th} \lambda_{th}^2 \quad (3\text{-}31)$$

Now, the kinetic formula for diffusion can be written in terms of R_{th}, $\lambda_{(t)}$ and N_H. The relation between diffusion of mobile hydrogen to distance and time is given by the Einstein-Smoluchowski equation [193]:

$$D_m = \frac{\lambda_{(t)}^2}{2\tau_H} \quad (3\text{-}32)$$

The Einstein-Smoluchowski equation, importantly, associates the individual details regarding particle motion with the microscopic parameter relating to diffusion through a network (i.e. linking D_m with Stokes-Einstein). Further to this, the average 'hopping' time of mobile hydrogen between shallow traps can also be determined from this expression.

3.6 Applied surface-state diffusion model

In the surface diffusion model, a number of key parameters were defined concerning the dynamic relationship between the desorption, transport and adsorption of hydrogen on the c-Si surface beneath an a-Si:H layer. Discussed here, is the determination of these values and the

outcomes of the surface diffusion model presented in this work for improving surface coverage and consequently passivation of dangling bonds.

A suitable value for s_o is determined across the temperature range studied in this work for a-Si:H(i). For the anneal temperatures investigated, using an E_A of 0.7eV, values for s_o from 2×10^{-9} up to 3.5×10^{-8} are determined as the temperature increases, from equation (3- 7). Bratu *et. al.* [186] has reported a similar trend in s_o for temperatures up to 1000°C with the only comparative temperature being for 277°C. Liehr *et. al.* [174] reported a similar value of s_o of 1×10^{-8} for a temperature below 170°C, even though there is some indication of that SiH_2 dominates the a-Si:H layer for this result. For temperatures below 300°C, Kolasinski *et. al.* shows that very little change in s_o is likely to occur [182], however, slight decreases in s_o remain important for weakly-bonded hydrogen to diffuse across the c-Si surface to preferred sites. Following the principle of detailed balance, Kolasinski *et. al.* [183] and Nachtigall *et. al* [202, 209] have shown that a low barrier to adsorption can be described as an indication that energetic and structural factors are involved in Si-H pairing. For the Si <100> surface, low values of $s_o \leq 10^{-8}$ denote good surface passivation due to the limited availability of dangling bonds or favourable bonding sites [174, 183, 186].

For the reaction order (m), in most cases a value of 1.56 is chosen as midway between monohydride and dihydride desorption [204, 205]. For monohydride dominated a-Si:H(i) layers a value for m closer to 2 would be more likely. The iterative analysis in this work shows a value of 1.7 is more appropriate for a monohydride dominated a-Si:H layer on an unpassivated c-Si surface. Similarly, for undoped a-Si:H, D_o is assumed to be approximately $5 \times 10^{-3} cm^2 s^{-1}$ by fitting equations (3- 20) and (3- 12) to experimental results at temperatures within the range of this study and remains in agreement with the literature values of $2 \times 10^{-3} cm^2 s^{-1}$ to $10^{-2} cm^2 s^{-1}$ [171, 182]

In determining the thermal prefactor for hydrogen desorption from a trapping site (i.e. interstitial or shallow) ν_{th}° is altered slightly from $5 \times 10^2 s^{-1}$ to $6 \times 10^3 s^{-1}$ for temperatures between 185°C and 275°C by an iterative approach of equation (3- 23).

The effective hydrogen surface coverage (i.e. Si-H deep trapping) in terms of post-deposition thermal annealing time and temperature according to the surface diffusion model presented in equation (3- 19) of the previous section, is shown in Figure 47. Hydrogen coverage of the surface rapidly proceeds within the first few minutes, particularly at higher temperatures due to the increased desorption rate; as the distance between interstitial and deep trap sites is likely only a few nanometres

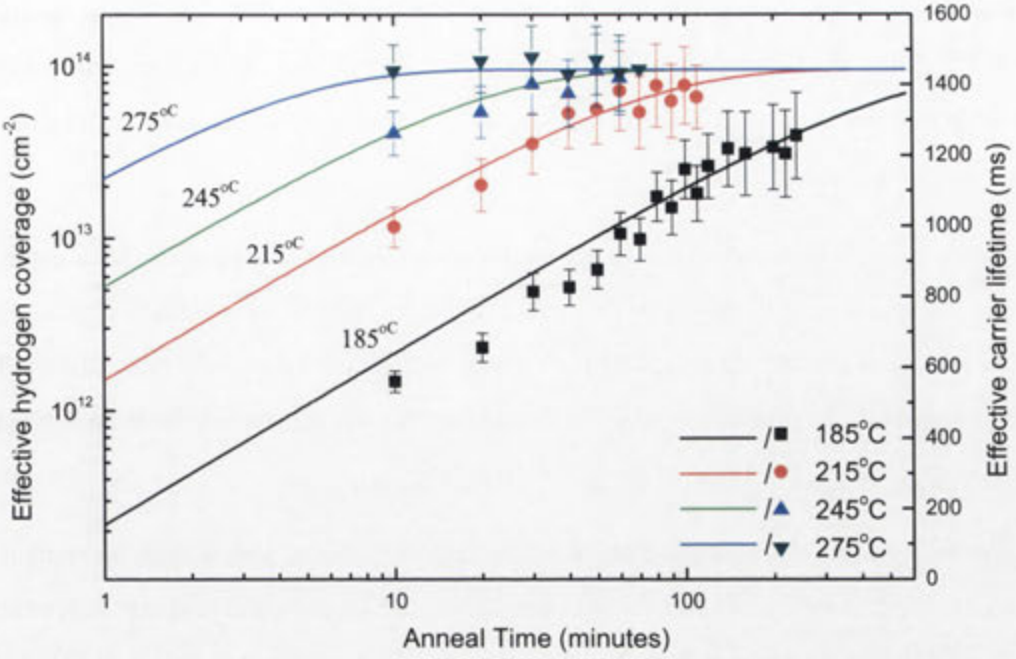

Figure 47: Effective hydrogen coverage over time with respect to post-deposition thermal annealing temperature according to equation (3- 19) and compared with the effective carrier lifetime of a-Si:H(i)/c-Si(n) annealed under similar temperatures.

As hydrogen coverage approaches equilibrium, adsorption is slowed since the probability of mobile hydrogen locating a deep trapping site is reduced. This 'saturation' of the c-Si surface by hydrogen which occurs here at approximately $10^{14}cm^{-2}$ assuming a fractional coverage following deposition, is consistent with the results for anneal times at different temperatures until no further gains in passivation quality are achieved. Similar fits were made for different thicknesses of a-Si:H deposited onto c-Si using the surface diffusion model presented here, highlighting the non-bulk related nature of surface passivation.

The output of the surface-diffusion model here remains consistent with kinetics of adsorption versus desorption, where the initial probability of a silicon dangling bond interacting with mobile hydrogen increases sharply for higher temperatures; however, as k_d approaches k_a, equilibrium is reached. Therefore, it is logical to assume that the hydrogen passivation mechanism is likely bounded by the surface equilibrium and s_o, which becomes high (10^{-5}), as indicated by Kolasinski *et. al.* [182] according to the principle of detailed balance.

Next, the mobile hydrogen released from an interstitial site, and moving through the transport level is given in Figure 48. The calculated effective flux of mobile hydrogen in the monolayer is determined according to equation (3- 16) and is seen to increase rapidly at higher anneal temperatures for an initially fractionally passivated c-Si surface. Mobile hydrogen densities within

the transport level (N_m) decrease for higher anneal temperatures. This seemingly contradictory behaviour is a result of the increased probability for mobile hydrogen to be trapped by a dangling bond with higher temperature. From equation (3- 21) it can be understood that Φ will increase with temperature, N_m decreases for an increased D_m.

It should be considered that $\Phi_{(t)}$ is not simply a measure of hydrogen in the transport level itself; it is also a measure of the average mobility of hydrogen moving between sites in the transport level, independent of surface corrugation or phononic (lattice) excitations. As adsorption will occur rapidly for an unpassivated surface, relative to desorption, $\theta_{(t)}$ will approach saturation of the surface quickly for temperatures above that of the initial deposition.

D_m linearly increases with temperature at these temperatures, and is likely to remain at this level for a partially passivated c-Si surface until equilibrium between k_d and k_a is reached; whereby, it will decrease further to a value similar to D_H of 2 x 10^{-18}cm^{-1} [189, 208]. Branz *et. al.* [172] reported a similar value for D_m for mobile hydrogen within the transport level at 210°C using a higher E_A and lower ν_o, that also results in N_m being one order higher in magnitude than reported in this work. Given the deposition conditions, the difference is likely attributed to the uncompensated presence of SiH_2 in those a-Si:H layers.

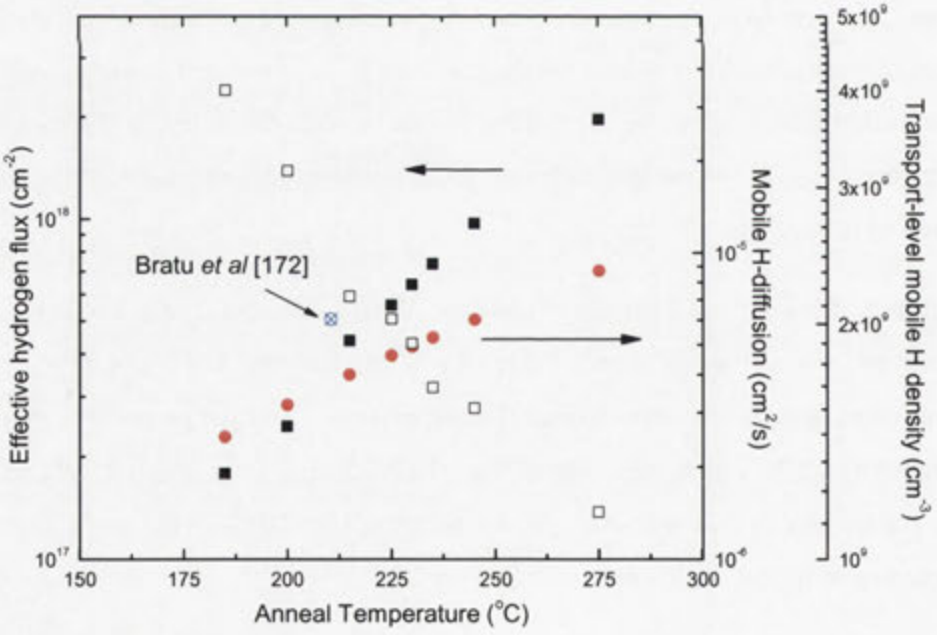

Figure 48: (Φ) Effective hydrogen flux (solid squares), (N_m) transport-level mobile H-density (hollow squares) and (D_m) mobile hydrogen diffusion coefficient (circles). Branz *et al* has shown similar D_m at 210°C [172].

Reported in both cases however, is $N_m << \Phi_{(t)}$ for temperatures below 300°C, which is understood by considering that the mobile hydrogen moving in a given reaction pathway for the monolayer is likely to be higher than the density of mobile hydrogen for the monolayer given the initially unpassivated surface. This remains the case at least until approaching 'saturation' of the surface by hydrogen.

The average diffusion length of mobile hydrogen (λ_H) moving in the transport level between the desorption site and the deep-trap site can be calculated according to the kinetic formula for diffusion given in equation (3- 27), using the value of D_H determined from equation (3- 21). In this it has been assumed that the length corresponds to deep-traps only as the number of shallow-trap pathways is considered to be very large.

In Figure 49, the mean distance for hydrogen travelling across the surface is shown to increase linearly with increase in thermal anneal temperature, up to 300°C. Importantly, hydrogen within the first few monolayers is evidently capable of diffusing across the c-Si surface to passivate local dangling bonds. Hydrogen bulk-diffusion from within the a-Si:H is clearly unnecessary provided sufficient hydrogen at the interface with c-Si and a-Si:H is available.

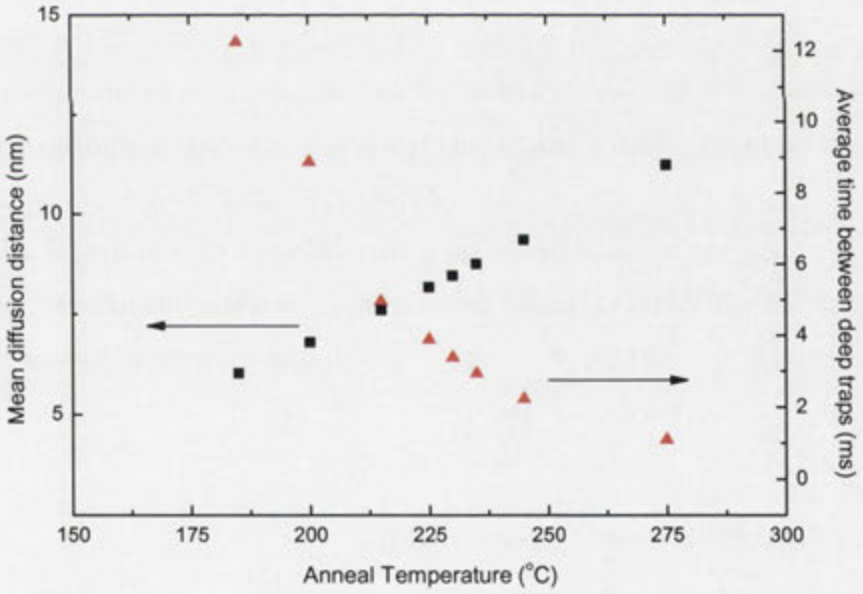

Figure 49: Mean diffusion length of hydrogen (λ_t) before becoming trapped at a deep-defect (i.e. dangling bond) and the average time of hydrogen (τ_H) spent between deep trapping sites (i.e. shallow trapping and mobile).

The average time (τ_H) spent by mobile hydrogen desorbed from an interstitial site before being trapped at a suitable site (i.e. dangling bond) on the c-Si surface can be calculated according to the Einstein-Smoluchowski equation according to equation (3- 32) and is also displayed in Figure 49. Unlike λ_H, the average hopping time until becoming deeply trapped is not linear. Here, we see that τ_H rapidly decreases with small incremental increases in annealing temperature from 170°C and 225°C; after which little gain can be achieved as the probability of mobile hydrogen locating a favourable site decreases significantly.

The increased rate of hydrogen adsorption at dangling bond sites for increasing temperatures was predicted according to Langmuir's isotherm for a monolayer and agrees with the experimental rates of passivation previously shown in this work [189]. The small diffusion distances at low temperatures in combination with the low activation energy and similarly low initial s_o (≤300°C) provides strong evidence in support of a surface transport process as the most likely mechanism for the surface passivation of c-Si at low-temperatures.

The results of this model and analysis do not contradict existing experimental results for annealing temperatures above 400°C, which support a bulk diffusion-limited mechanism [65-69]. Instead, the misconception surrounding the importance of the diffusion-limited process has been identified in this work. At significantly higher anneal temperatures (≥400°C) the average diffusion distance of hydrogen, according to the surface-model discussed in this work, increases rapidly to above 25nm, suitable for bulk mobile hydrogen to reach the c-Si surface. Hydrogen diffusion lengths in this range agree with those reported for the diffusion-limited mechanism within the higher temperature region and also account for the rapid passivation of the c-Si surface after only a few seconds of thermal annealing at these higher temperatures. Therefore, the influence of the diffusion mechanism can simply be considered to have masked the underlying surface-state reaction responsible for passivation of the c-Si surface.

Composition of the thermal activation energy (E_A)

Previously, the activation energy of 0.7 ± 0.1 eV for the surface passivation mechanism was determined to be well below the energy required for bulk-diffusion from the a-Si:H(i); also, it was found that the effective hydrogen coverage is temperature dependent. It is likely, according to Brenig, Groβ and Russ [184], passivation occurs through a reconfiguration of surface-states, where mobile hydrogen may be trapped by a dangling bond at the c-Si surface without experiencing a large

barrier to adsorption [182, 183]. This provision is valid, since surface-states in the Si bandgap are known to reduce the adsorption barrier as Si-Si bond lengths increase when hydrogen is adsorbed [186]. Accordingly, only three types of transition are relevant for hydrogen at the surface:

- From a trapped state to the transport level,
- transport between traps within the transport level, and
- from the transport level to a trapped state.

Earlier, E_A has been reported to represent the thermal activation energy for the improvements in surface passivation quality between as-deposited and post-deposition thermal annealing observed throughout this work. It is known that the minimum energy value for 'hopping' of hydrogen between shallow traps across the c-Si surface (E_H) is 0.2eV [41]. Also, the approximate energy required for hydrogen to overcome the potential barrier to desorption from interstitial sites (E_I) has been reported to be 0.47eV [148]. Therefore, any remaining, residual energy (E_R) could possibly be associated with the probability that mobile hydrogen will continue across the shallow-traps at the c-Si surface until a suitable deep-trap site is located.

Hence, the surface diffusion model is extended to show that the value of E_A may represent the sum of different energies for each of these transitions.

$$E_A = E_H + E_I + E_R \tag{3-33}$$

If we assume that the energy to overcome any desorption barrier for the interstitial site is constant, the approximate value of E_R can be calculated from the above equation.

In Figure 50, the residual energy available to assist hopping transport across shallow-traps for annealing temperatures below 300°C is seen to be only slightly below the energy required for mobile hydrogen (0.2eV) to move across shallow traps. However, this additional energy is likely to further improve trapping probability through shallow-trap pathways. This is understood by considering that for anneal temperatures below that of deposition; hydrogen which is able to just overcome the dissociation potential is more likely to return to the interstitial site instead of a deep-trap site or diffuse across the surface to a new site.

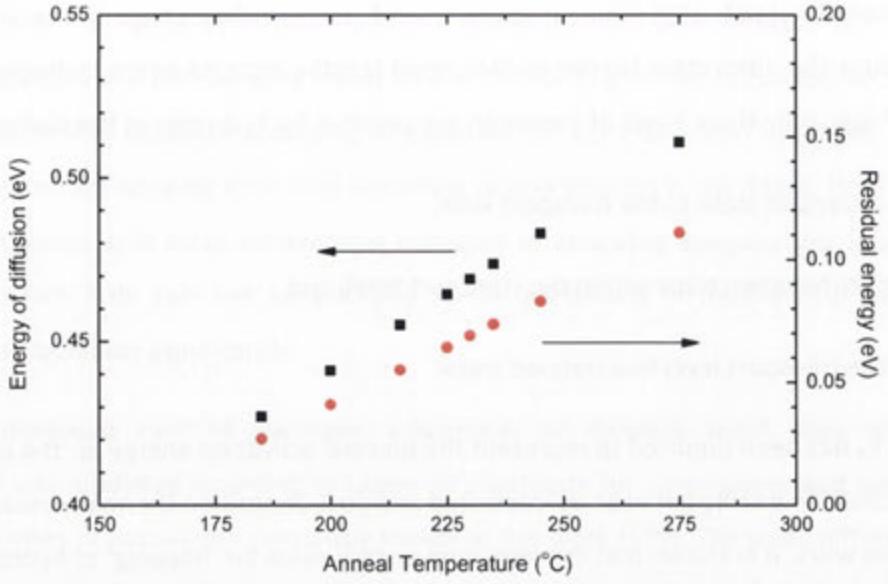

Figure 50: Comparison between energy of mobile H-release and residual energy available for hopping mechanism. The residual energy was calculated from equations (3- 33), representing the additional energy available to the hopping transport reaction mechanism.

This would also explain the slow, but eventual, passivation of the c-Si surface by a-Si:H below 200°C [72]. The probability that mobile hydrogen becomes trapped at an interstitial or shallow trap site would be higher for low temperatures. As the thermal anneal temperature is increased above 200°C, the probability that mobile hydrogen will continue to diffuse across the surface until a suitable deep trap is located also increases, as does the probability of interstitial hydrogen overcoming the dissociation potential. Therefore, E_R regulates the increased probability that hydrogen will diffuse across the c-Si surface, until it can be adsorbed at different trapping site and representing the relaxation energy of the Si-H bond.

The surface diffusion mechanism for hydrogen proposed in this work is consistent with interstitial transport of hydrogen with a distribution of E_A over a range of energies 0.2 - 0.5eV as reported in [135, 166]. From this analysis the differences in these energies is accounted for by E_R [195, 196, 210]. Therefore, if little of no adsorption barrier is assumed, E_A will be primarily associated with desorption and transport of mobile H.

This model also explains the lack of passivation for as-deposited layers observed throughout this work. Although the energy required to flip an asymmetric dimer into a suitable configuration for hydrogen adsorption is only 0.1eV for Si<100>, the process is slow and cannot be forced by incident hydrogen during deposition [20]. Due to the relatively high deposition rate ($4 Å s^{-1}$), there is insufficient time for the Si surface to reconfigure for hydrogen adsorption. Post-deposition thermal

annealing, shown previously in this work, improves the surface state configurations and relaxes the a-Si:H network. This lowers the adsorption barrier [43, 44] which influences surface-state reconfigurations. This goes part-way to explaining some of the energies associated with the previously determined values of E_A, although there remains some uncertainty regarding the energy required for dissociation and transport of hydrogen.

3.7 Chapter summary and conclusions

In this chapter, post-deposition conditions regarding thermal annealing have been mainly studied to optimise passivation of c-Si surfaces by stable a-Si:H(i) and to understand the structural and optical properties of these layers.

The post-deposition thermal annealing process at temperatures between 225°C and 280°C of a-Si:H(i) layers previously deposited onto the c-Si surface has been presented. Evident, is the improvement in the surface passivation quality illustrated by the significant increase in the effective carrier lifetime from an initial value below 50μs, to well above 1ms following annealing. Furthermore, it was concluded from this study, that the achievable surface passivation exhibits no strange dependence upon the anneal temperature chosen (provided T_{anneal} above 170°C), except to determine the anneal time required to saturate the c-Si surface with Si-H hydrides. Following extensive testing of both anneal temperature and the time required to achieve a maximum surface passivation, it can be surmised that the improvements in surface passivation obtained from thermal annealing occur not from a single anneal step, but instead from the thermal cycling between temperatures. This thermal cycling, in some way, likely relaxes the network stresses inherent in the deposition process.

In the previous chapter and throughout this study, post-deposition had been observed to significantly improve the carrier lifetimes of a-Si:H(i) deposited on c-Si. Although, the temperatures during deposition and thermal annealing have similar effects on the hydrogen concentration within the regions of the a-Si:H(i) layer, it remains the deposition temperature that governs the density and composition of the a-Si:H(i) layer; and the thermal annealing temperature which governs the relaxation of the network. Significantly, monohydride bonds at the interface and within the bulk region are critical to the surface passivation process. Passivation of the c-Si surface was shown to be and continued to be negligible in the absence of these hydrides, even following extensive annealing. Counter to this, the highest surface passivation occurs for interface regions dominated by

monohydride bonds and for when the concentration exceeds that of the bulk region. Importantly, no shift in monohydride concentration from the a-Si:H bulk to the interface region was evident, indicating that the improvements in passivation are not simply a result of new hydride bond formation. This also signifies that hydrogen does not preferentially diffuse towards the interface with the c-Si surface, and it may be concluded that surface passivation due to bulk-diffusion is unlikely to occur for temperatures below 300°C.

A review of the currently accepted hypothesis surrounding the mechanism responsible for the passivation of the c-Si surface by hydrogen present within a-Si:H(i) was examined in light of the observations throughout this chapter. As discussed, the surface passivation mechanism does not demonstrate the hydride concentration temperature-time dependence as predicted by the bulk-diffusion process, whereby, passivation only occurs above 200°C and shifts concentration from the bulk to the interface as new bonds are formed. Instead, passivation occurs at a range of anneal temperatures inversely proportional to the anneal time required for saturation without significant formation of new bonds or shifts in the hydride concentration throughout the a-Si:H layer. Therefore, a surface-diffusion model has been introduced in this chapter as a likely explanation for the previous observations in this thesis.

As discussed in this model, hydrogenation of the unpassivated c-Si surface is governed by the balance between the rates of desorption and adsorption, with hydrogen movement through a probabilistic transport level. Thermally, increased desorption of hydrogen from interstitial trapping sites occurs, with the hopping distance travelled between the emission site and dangling bond site dependent upon coverage at any given time. The model presented here, gives a series of values for mobile hydrogen flux, effective hydrogen coverage with time, hopping distance and the average time between traps which agree with the time and temperature requirements for achieving the high passivation observed in this work. This model, presents an alternative hypothesis supported by experimentation for hydrogen surface passivation of the c-Si surface.

This chapter has focused on some of the several possible mechanisms that contribute to surface passivation, including recombination defects at the a-Si:H/c-Si interface and structural defects, like micro-voids which form from unpassivated silicon dangling bonds forming closed rings. Other factors which would also need to be taken in account to further our understanding would include band bending, and heterostructure effects (i.e. discontinuities in the energy bands), the latter, is in some way addressed in the next chapter.

4

Surface Passivation using Stacked a-Si:H Intrinsic and Doped Layers

Contemporary designs for crystalline silicon solar cells include the formation of a junction which facilitates the collection of photogenerated charge carriers. This junction is often formed by thermal diffusion of a dopant, either phosphorous or boron, into the surface at temperatures up to and exceeding 900°C [211]. However, this high temperature diffusion step can limit the use of the much more fragile, thinner c-Si wafers (<150μm) due to thermal stresses, and in the case of boron diffusion, may deteriorate the c-Si bulk in the presence of contaminants [212, 213]. A key problem in using n-type silicon as the base in solar cells is that the sun-facing emitter, doped with boron, is the formation of the Boron-Oxygen complex, making it difficult to use conventional passivating layers such as SiO_2 or SiN_x (although recently progress in this has made with Al_2O_3 and boron-emitters [214, 215]). In addition, many high temperature steps, including contact formation, are still required before the solar cell is complete, placing restrictions on the order of processing steps and leading to more complicated devices and time consuming processes.

In the past, silicon oxide has been shown to be suitable for reducing surface recombination with reported laboratory efficiencies of 25% (4cm^2) [33]. More recently, silicon nitride has gained popularity due to a lower processing temperature of 400°C and laboratory efficiencies of 19.5% [216]. However, efficiencies are often below 20% for industrial production as replicating this processing technology in industry remains difficult. Certainly for SiN_x, shunting through parasitic induced junction formations on p-type back surface layers is a common difficulty [36]. Hybrid devices using a-Si:H stacked layers with Al-BSF, μc-Si:H, SiO_x, SiN_x [61, 88, 110, 217, 218], a-SiC_x:H [87, 219, 220], and SiN_x, SiO_x/Al rear layers [219], have achieved similarly limited results.

Alternatively, a-Si:H has shown substantial promise when doped a-Si:H is combined with the excellent passivation provided by a-Si:H(i) at temperatures below 300°C [160, 221], although challenges remain. In this chapter, the a-Si:H stacked layers are investigated for their effectiveness in passivating the c-Si surface, firstly in the presence of a diffused dopant on the surface, then absent of one (i.e. bare surface). The influence the doped a-Si:H layers have upon the passivating intrinsic layer is also assessed in terms of electrical and internal structural properties of the stack, with the hope of developing an ideal format for the dual a-Si:H layers. Although the conversion efficiency of solar cells is most relevant in comparing devices, this chapter instead concentrates on the aspect of surface passivation and design only.

4.1 Junction formation at interfaces

The formation of the p-n junction is commonly done through thermal diffusion, implantation or epitaxy of a dopant, commonly phosphorus or boron. The diffusion of dopant is notably the most popular method, involving temperatures above 750°C (up to 1000°C), although requiring clean methodologies to avoid contamination. Comparatively, for a-Si:H, it is relatively easy to add dopant during deposition by PECVD using phosphorus or boron gases at low temperatures below 300°C. Combined with a high level of control in layer deposition, defined junctions are able to be formed. With c-Si, a stacked a-Si:H is required involving intrinsic and doped a-Si:H layers. It is reasonable to assume that a junction forms between the two materials, given the band offset which exists involving c-Si and a-Si:H(i/n or i/p), provided that dangling bonds are well passivated which would otherwise pin the Fermi energy level.

4.2 Experimental preparation and procedure

Two surface preparation methods are used throughout this chapter to study passivation quality of the a-Si:H layers on planar c-Si surfaces.

- Thermal diffusion of n+ emitter
- Standard non-diffused bare c-Si surface

The details for the preparation of each of these are given separately below. All c-Si surfaces initially underwent the procedure outlined in section 2.1.2. This included HF/HNO_3 etch to remove surface damage, RCA clean, and oxide removal in HF. High-quality *FZ* c-Si wafers are used to reduce the influence of Shockley-Read-Hall recombination within the c-Si bulk to negligible levels.

4.2.1 Thermal diffusions of c-Si

Following the Si-damage etch and RCA cleaning, previously described here, a series of 40Ωcm p-type *FZ* c-Si wafers with an average thickness of 200μm have been loaded into a quartz tube furnace and the surfaces thermally diffused by phosphorus at temperatures between 750°C and 940°C. The dopant source is vaporised $POCl_3$, which forms an n^+ region at both surfaces of the c-Si(p) wafer. The thermal profile is illustrated in Figure 51. During emitter diffusion, constant gas flows of 1.5L/min N_2, 2L/min O_2 and 1L/min $POCl_3$ are maintained. In this way, the peak temperature determines the final sheet resistance of the n^+ emitter. For some wafers, a 25nm thermal oxide was grown at 900°C for 30 minutes in a separate quartz tube furnace, simultaneously 'driving-in' the diffusion.

All c-Si(p) wafers with diffusion surfaces were then deglazed in 10% HF solution at room temperature until hydrophobic and the sheet resistance of the n^+ emitter measured using a 4-point probe [222]. Sheet resistances ranged between 7Ω/□ and 350Ω/□. A final RCA cleaning and removal of any oxide layer was performed immediately prior to deposition of the a-Si:H layers.

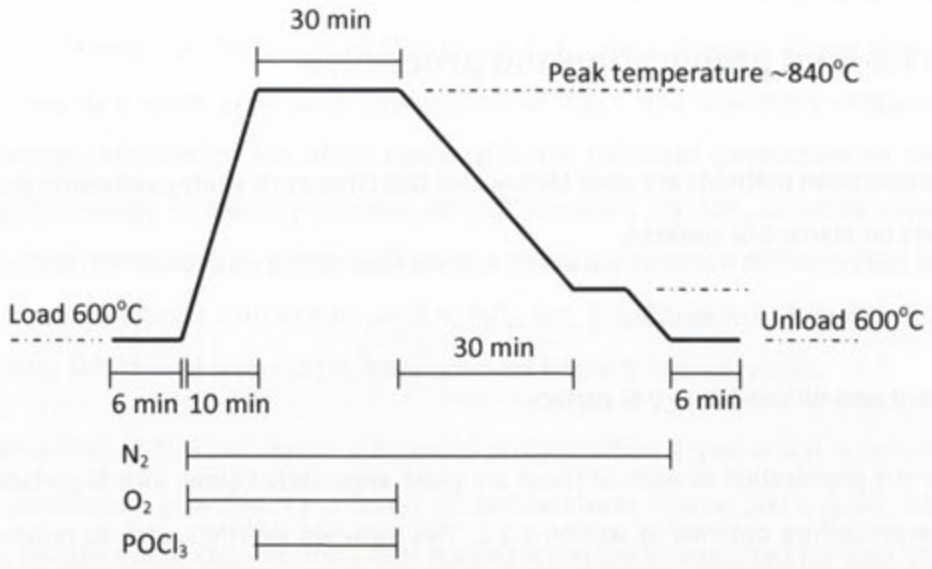

Figure 51: Thermal profile of $POCl_3$ extended gettering process. Peak temperature is used to control the sheet resistance of the diffused emitter region.

4.2.2 Non-diffused c-Si surfaces

Non-diffused 1.4Ωcm n-type and 0.9Ωcm p-type (100) FZ c-Si wafers have been prepared according to section 2.1.2. Native oxide is removed immediately prior to deposition. As thinner wafers are of interest in reducing the material budget of PV production, different thicknesses of c-Si were tested ranging between 100μm and 200μm, allowing for the benefits of low temperature passivation by a-Si:H to be evaluated in comparison to high temperature SiO_x and SiN_x.

4.2.3 Deposition of intrinsic and doped a-Si:H by PECVD

All a-Si:H layers, except where specified, are deposited by PECVD at the conditions given in Chapter 2 identified to form a high-quality passivating layer. These are 225°C for temperature, 4W applied (50mW/cm^2) for *rf*-power, and 650mT for partial pressure. For 40Ωcm c-Si wafers with a diffused n+ emitter surface, a-Si:H(i) layers between 5nm and 50nm are deposited directly onto this surface. The low-deposition temperature is unlikely to result in any redistribution of phosphorus in the c-Si.

The formation of intrinsic/doped a-Si:H stacked layers first involves the deposition of 5nm or 10nm a-Si:H(i) inter-layers by ML-PECVD onto the bare c-Si surface for passivation. This is then followed by either phosphorus-doped a-Si:H (n-type) or boron-doped a-Si:H (p-type) layers between 5nm and 100nm in thickness. The doping of a-Si:H is accomplished by premixing phosphine (PH_3) or diborane (B_2H_6) with silane (SiH_4) prior to entering the deposition chamber and plasma ignition.

As deposition temperature was shown in chapter 2 to have the greatest influence on the quality of the a-Si:H layer, a similar optimisation was also undertaken for doped a-Si:H layers. To avoid repetition, the results are not presented in this work, although it was found that 230°C for these layers was optimal. Partial pressure and *rf*-power were chosen within the ideal range described for a-Si:H(i) layers. Post-deposition of all a-Si:H layers was at 240°C to improve as-deposited surface passivation.

4.2.4 Additional characterisation parameters

Measurement of the effective carrier lifetime (τ_{eff}) is by QSSPC and PCD for mid-injection ($\Delta n = 10^{15}cm^{-3}$). Surface recombination velocity (S_{eff}) is again calculated from τ_{eff} according to the method described in Appendix A. However, the presence of an n^+ emitter region makes direct comparison of results here with others using τ_{eff} and S_{eff} difficult. Therefore, a new parameter is introduced, the saturation current (J_o), which represents recombination at both surfaces. This J_o is calculated from the slope of the inverse carrier lifetime (τ_{eff}^{-1}) for $\Delta n = 10^{16}cm^{-3}$ according to Kane and Swanson [223], and automatically decouples the c-Si bulk recombination from the c-Si surface recombination.

The emitter current density (J_{oE}) is approximated by halving J_o to represent a single c-Si surface passivated by a-Si:H. Direct comparison of J_{oE} is possible without modelling, as in the case of S_{eff}. Although the concepts of J_{oE} and S_{eff} are interchangeable, the former is more appropriate for characterising surface regions where a p-n junction exists. It should be noted however, that diffusion-limited surface recombination can affect the determination of J_{oE}; as such, measurements are performed in high-injection ($10^{16}cm^{-3}$) where a suitable fit can be obtained.

Limitation in carrier diffusivity can be neglected in the determination of J_{oE} if the condition in equation (4- 1) is satisfied. In this, n_i is the intrinsic carrier density (cm^{-3}), q is the magnitude of electron charge (1.6×10^{-19} C), W is the thickness of the substrate, N_A is the acceptor doping density

(cm^{-3}) and Δn is the excess carrier density (cm^{-3}). For the conditions in this work, an upper limit for J_{oE} of 4.5pA/cm^2 can be determined from equation (4- 1)

$$J_{oE} << \frac{6qn_i^2 D_A}{W[N_A + \Delta n]} \tag{4- 1}$$

For a-Si:H stacked layers, the effectiveness of the surface passivation of c-Si can be given in terms of J_{oE} for n-type c-Si (equation (4- 2)) and for p-type c-Si (equation (4- 3)). Each of these illustrate that J_{oE} remains constant, while S_{eff} remains dependent upon wafer doping and the carrier injection level [224].

$$S_{eff} = J_{oE} \frac{N_D + \Delta p}{qn_i^2} \tag{4- 2}$$

$$S_{eff} = J_{oE} \frac{N_D + \Delta p}{qn_i^2} \tag{4- 3}$$

Hence, J_{oE} is not simply suitable for the comparison of surface passivation, it is also more accurate for assessing the surface recombination in the presence of a junction.

An additional characterisation parameter is introduced in this chapter, the open-circuit voltage (V_{oc}) limit, to compare the use of different a-Si:H stacks. Under illumination, the stacked a-Si:H/c-Si is known to be in non-equilibrium conditions and a quasi-steady-state occurs at the a-Si:H and c-Si interface [225]. Therefore, inadequately passivated c-Si surfaces will likely exhibit a reduced V_{oc}-limit. From the value of J_{oE} determined from by the above method, and assuming ideal photogeneration (J_{ph}) of 0.043A/cm^3 (an upper limit[9]) without any significant bulk a-Si:H, the V_{oc}-limit can be calculated according to equation (4- 4), where kT/q is the thermal energy. Although, it is also possible to determine the potential current density according to equation (B 1) in Appendix B, which also includes the effect of bulk recombination.

$$V_{oc}\text{ - limit} = \frac{kT}{q} \ln\left(\frac{J_{ph(\max)}}{J_{oT}}\right) \tag{4- 4}$$

[9] In the case of thin a-Si:H layers used in this work, light absorption is negligible (see section 3.3) and any influence on J_{ph} is likely negligible.

For very low J_{oE}, the limit in V_{oc} may be higher than the Auger limit as the bulk Auger recombination is not included in this surface orientated expression. Therefore, S_{eff}, J_{oE} and V_{oc}-limit must be considered together as indicators of the effectiveness of the a-Si:H/c-Si heterostructures.

4.3 Passivation of diffused n+ surfaces by a-Si:H(i)

The reduction of minority charge carriers at a diffused c-Si surface region is an important step in reducing recombination losses limiting device efficiency. Heavy diffusions at the surface are effective in repelling minority carriers from the surface. For n^+ diffusions, the ohmic contact is even assisted by the tunnelling barrier between the metal and silicon bulk [224]. Diffused regions are also needed to reduce the lateral resistance between contacts. Therefore, any passivation layer is required to be compatible with a range of diffusion, heavier near metal contacts, and lighter in other areas. To date, SiO_x and SiN_x have served well in this regard.

In this section, the suitability of a-Si:H(i) as a passivating layer on a range of diffused n^+ emitters for 40Ωcm *FZ* c-Si(p) is examined. Deposited under ideal conditions, a-Si:H(i) up to 50nm in thickness for a structure shown in Figure 52 of a-Si:H(i)/ c-Si(n^+)/c-Si(p). The range of sheet resistances tested extended from 10Ω/□ to 340Ω/□, which include common emitter values used in screen-printed contacts (40Ω/□), evaporated contacts (100Ω/□), and inter-contact regions in selective emitter designs (above 150Ω/□). In considering the higher absorption characteristics of a-Si:H particularly for front surfaces, it is noted that all layers in this study have thickness of 50nm or less. As shown in section (3-3), this is well below any absorptive effects posed by the material.

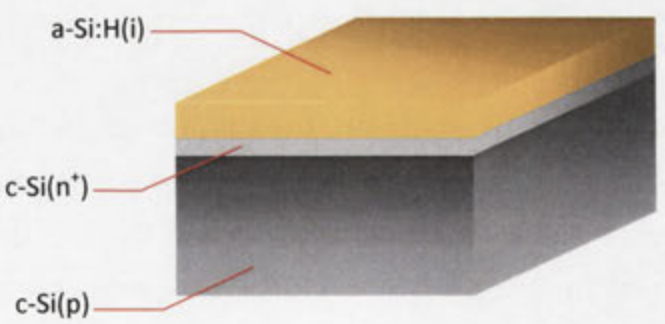

Figure 52: Illustration of intrinsic a-Si:H layer deposited by ML-PECVD onto a thermally diffused n^+ emitter surface of 40Ωcm c-Si(p) wafer.

Presented in Figure 53 is the complete profile for J_{oE} of n^+ emitters for a range of sheet resistances passivated by the a-Si:H(i) layers following post-deposition thermal annealing. The profiles of the more standard SiN, FGA thin oxide, alnealed thin oxide [213], and a-SiC_x:H [226] passivation layers for similarly diffused c-Si(p) surfaces are also shown for comparison. The main trend indicated by the line can be attributed to the surface doping density of the c-Si wafers.

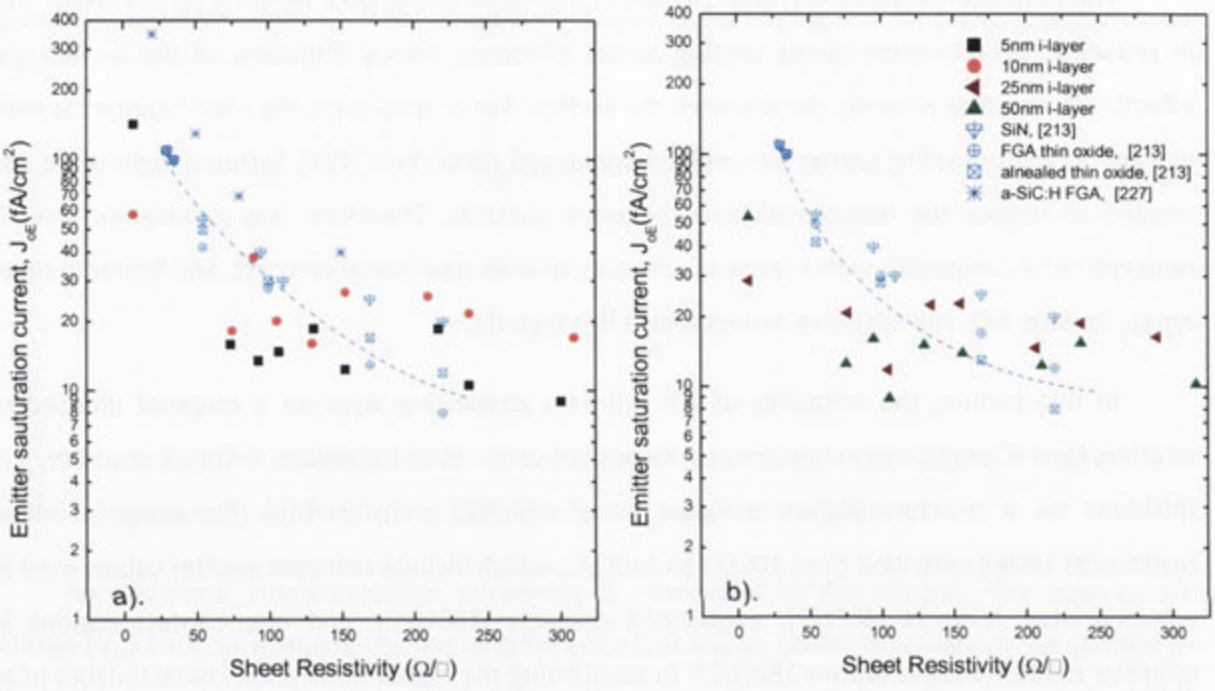

Figure 53: Profile of J_{oE} of phosphorus diffused emitters passivated with a-Si:H(i) layers of either 5nm, 10nm (shown in a.), or 25nm, 50nm (shown in b.) onto planar c-Si surfaces. The J_{oE} for more common passivating layers including SIN, FGA thin oxide and alnealed thin oxide [213] and a-SiC_x:H [227] on similarly diffused c-Si(p) surfaces are shown for comparison. The line is a guide for the dependence of these passivating schemes on the doping density of the c-Si surface.

In Figure 53, two distinct features can be observed, firstly that J_{oE} is mostly independent of the thickness of the a-Si:H(i) layers; secondly, a similar dependence to that reported for other passivating schemes occurs. Indeed for a-Si:H(i) layers between 5nm and 50nm thick, J_{oE} decreases at higher sheet resistances (i.e. lightly diffused n^+ emitter) as expected. For sheet resistances above 50Ω/□, using an a-Si:H(i) layer thickness of 5nm, J_{oE} remains below 20fA/cm^2, with a minimum of 9fA/cm^2 recorded for a sheet resistance of 100Ω/□, common for devices employing evaporated aluminium or indium tin oxide contacts.

Comparatively, values of J_{oE} for PECVD-SiN, FGA thin oxide, alnealed thin oxide reported by Kerr [213] tend to be higher than those for a-Si:H(i) layers in this work. For these other passivating layers on low sheet resistances (i.e. deeply diffused n^+ emitter), the high J_{oE} reported is explained due to recombination within the emitter bulk being dominant. For thin a-Si:H(i), charges at the interface are less likely to be an influencing factor, which may account the improvement in J_{oE} seen here. For lightly diffused emitters, J_{oE} is governed more by surface recombination. In both cases, when using a-Si:H(i), the reduction in current density at the emitter surface does not appear to exhibit the same dependence on sheet resistance (dotted line) as reported for SiN_x and SiO_x [14]. This may indicate a strong reduction in the carrier density at the emitter surface which extends minimally into the bulk.

In a parallel study, Ferre *et. al.* [227] reported on similar decreases in the J_{oE} for 8nm and 12nm a-SiC_x:H layers (FGA at 400°C for 20 minutes) for higher sheet resistances. Although low J_{oE} was reported, a-SiC_x:H deposited onto emitters with high sheet resistances, following FGA, J_{oE} is higher than those observed for a-Si:H(i) layers deposited in this work.

It is clear that the J_{oE} for most a-Si:H(i) passivated diffused c-Si surfaces is lower than those reported for conventional passivation schemes. Noteworthy are those values achieved at 75Ω/□ and 350Ω/□. In the latter circumstance, J_{oE} for a-Si:H(i) as low as 10fA/cm^2 is achieved here with minimal processing and all at temperatures below 260°C. By comparison, J_{oE} as low as 3fA/cm^2 has been reported using oxide/nitride stacks and high temperature steps [17], although this was only achievable after extensive processing steps.

Looking closely at the calculated V_{oc}-limit for the n^+ emitter surface passivated by the a-Si:H(i), similar profiles are observed across the range of sheet resistances for layers of different thicknesses (see Figure 54). Again, a-Si:H(i) layers exhibit similar results to those reported for other passivation schemes. It also appears that 5nm and 10nm are overall better suited to passivation than thicker layers for the range of sheet resistances tested. It should be noted that while, the main trend observed in J_{oE} and V_{oc}-limit is mainly attributed to the surface doping density, the higher the sheet resistance, surface passivation becomes easier with the lower the surface doping density.

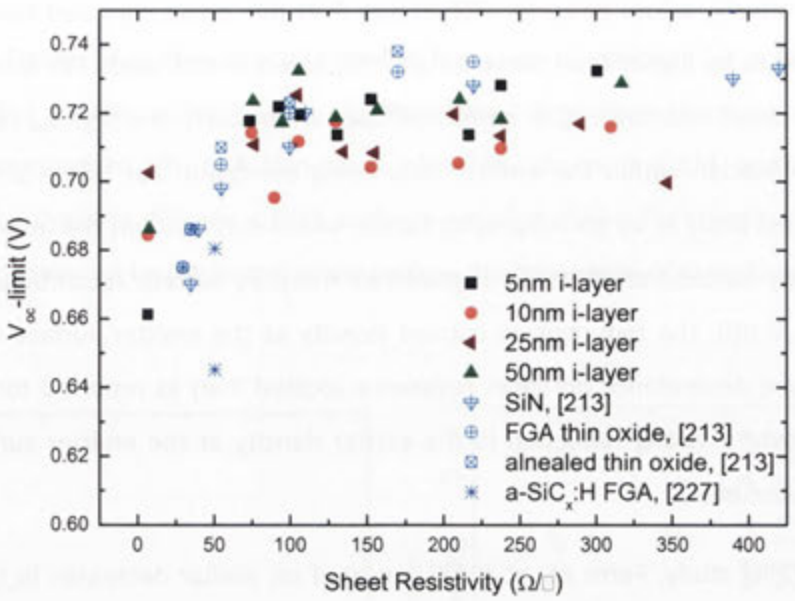

Figure 54: Implied-V_{oc} for phosphorus diffused n^+ emitter surface on 40Ωcm *FZ* c-Si(n) passivated by a-Si:H(i) layers between 5nm and 50nm. V_{oc}-limit for SiN, FGA thin oxide and alnealed thin oxide layers [213] and 12nm a-SiC$_x$:H FGA [227] are also shown for comparison.

The excellent passivation quality of a-Si:H(i) deposited in this work has until now been demonstrated by low surface recombination velocities, linked to Si-H bonding at the c-Si surface. In this section, it has been shown that significant reductions in the current density at the n^+ emitter also occur. Comparable J_{0E} and V_{oc}-limits are reported for other higher temperature passivation materials. Therefore, it may be concluded that, although SiN, FGA or alnealed thin oxide layers, and to some extent a-SiC$_x$:H, are well established, the a-Si:H(i) demonstrates potential for where low thermal conditions are required, for example on thin c-Si wafers 100μm or less.

4.4 Passivation of non-diffused c-Si surfaces by bifacial a-Si:H stacks

Sanyo's HIT (Heterojunction with Intrinsic Thin-layer) solar cell has reported record conversion efficiencies of 22% (100cm^2) in 2007 and most recently 23% for n-type [221]. Since then many research groups have raced to reproduce similar results on both n-type and p-type c-Si with an assortment of success (see Introduction). In many cases the general uptake of a-Si:H heterostructure designs in solar cells has been somewhat limited, primarily due to the intellectual property held by Sanyo, and secondly due to a somewhat limited understanding of the material. Despite recent advances in HIT-like solar cells, the gap which exists in our understanding of the surface passivation for a-Si:H(i/doped) stacks merits further investigation.

Earlier in this work, it had been demonstrated that a-Si:H(i) can provide high-quality, stable passivation of the bare c-Si surface, even in the presence of an n^+ emitter. Therefore, the study of surface passivation using a-Si:H(i/doped) stacks on bare c-Si surfaces, absent of a diffused n^+ emitter, is investigated here.

The a-Si:H(i/doped) stack or heterostructure consists of a thin a-Si:H(i) inter-layer which is deposited onto the bare c-Si surface, followed by either an a-Si:H(n) or a-Si:H(p) layer. Illustrated in Figure 55, is the structure of a-Si:H bifacial stacks deposited in this work by standard PECVD and ML-PECVD onto either bare 1.4Ωcm n-type *FZ* c-Si or similar 0.9Ωcm p-type *FZ* c-Si (not shown). For the a-Si:H(i) inter-layer, two thicknesses of 5nm and 10nm were deposited and discussed; although others between 1nm and 20nm were also investigated. For optimised doped a-Si:H layers, thicknesses between 5nm and 100nm were deposited.

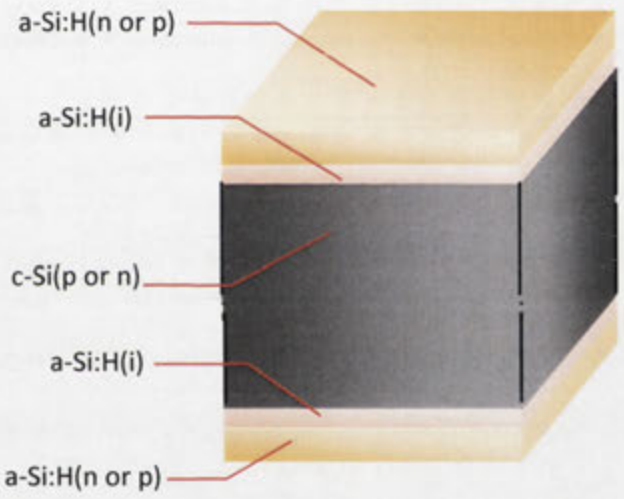

Figure 55: Schematic of a-Si:H heterostructure on c-Si wafer, c-Si base wafer can be either n- or p-type. Doped a-Si:H layers are either n- or p-type deposited onto a-Si:H(i) inter-layer.

In this way, the doped a-Si:H layer is expected to perform as an emitter if the c-Si wafer is oppositely doped (i.e. a-Si:H(n)/a-Si:H(i)/c-Si(p), or visa versa). It should be noted that, deposition of a doped layer directly onto the c-Si surface is not desirable due to the higher defect density of these layers, and also limitations to V_{oc} which result from tunnelling losses [30]. The inclusion of an optimised, thin a-Si:H(i) inter-layer to provide high-quality passivation and serve as a barrier between the doped a-Si:H layer and c-Si surface is therefore prudent.

As part of this study, a preliminary result for the V_{oc} for cell-like devices is also made by depositing a suitable heterostructure stack. This is achieved by magnetron sputtering of a 70nm thick 99.99% indium tin oxide (ITO) and evaporation of 0.5μm thick dot-like aluminium contacts onto the top-most a-Si:H layer. Post deposition thermal annealing is performed at 240°C for 40 minutes, prior to any metallisation step, to prevent the formation of an aluminium alloy with the a-Si:H from occurring [228].

4.4.1 Bifacial a-Si:H(i/n) stacks on n-type c-Si

In Table 1, a summary of reported results for other groups on a-Si:H stacks for c-Si(n) is given for comparison with the results of this study. With the exception of De Wolf *et. al.*[71], many of the results are well below what can be expected of this material.

Table 1: Summary of a-Si:H(i/n) stacks deposited onto *FZ* c-Si(n). S_{eff} is calculated for unknown base wafer thicknesses assuming 300μm width according to method described in Appendix A. Where Al-BSF is indicated, the S_{eff} is assumed to represent the front non-metal sides surface.

Group	Dopant (*FZ*)	c-Si thickness	a-Si:H(i) thickness	Front surface	Rear surface	Technique	τ_{eff} (μs)	S_{eff} (cms^{-1})
Rau et. al. [229]	1Ωcm (n)	250μm	a-Si:H(i)	a-Si:H(n)	a-Si:H(n)		--	20
Wang et. al. [110]	1Ωcm (n)	--	a-Si:H(i)	a-Si:H(n)	Al-BSF	HWCVD	900	~15.57
Garin et. al. [230]	1Ωcm (n)	--	10nm (i)	10nm a-Si:H(n)	10nm (n)	PECVD	40	~437
Garin et. al. [230]	1Ωcm (n)	--	10nm (i)	10nm a-Si:H(n)	30nm (n)	PECVD	70	~232
De Wolf et. al. [71]	0.7Ωcm (n)	300μm	5nm (i)	4nm a-Si:H(n)	4nm (n)	PECVD	880	~13
Rau et. al. [229]	0.3Ωcm (n)	375μm	a-Si:H(i)	a-Si:H(n)	a-Si:H(n)	PECVD		150
Garin et. al. [230]	1Ωcm (n)	--	10nm (i)	10nm a-Si:H(n)	30nm (p)	PECVD	40	~437
Fujiwara [61]	2.6Ωcm (n)	525μm	4nm (i)	5nm a-Si:H(p)	Al-BSF	PECVD	728	36
Fujiwara [61]	4.1Ωcm (n)	525μm	4nm (i)	5nm a-Si:H(p)	Al-BSF	PECVD	717	37

In Figure 56, the results of a-Si:H(n)/a-Si(i) stacks deposited bifacially onto bare, planar 1.4Ωcm *FZ* c-Si(n) are given with comparison to De Wolf *et.al.* [71] and Garin *et. al.* [230] as described in Table 1. The incorporation of a 5nm a-Si:H(i) inter-layer achieves a *'reliable'* τ_{eff} measurement of 1.2ms when combined with a top-layer a-Si:H(n) up to 20nm in thickness. For the a-Si:H(n) layers above 50nm, the effective surface passivation appears to be slightly compromised. A

similar response in passivation quality can also be seen when using a 10nm a-Si:H(i) inter-layer. Therefore, it can be concluded that, provided the intrinsic inter-layer is not compromised, similar levels of high quality passivation are achievable for thin inter-layers in the presence of a-Si:H(n) layers up to 50nm thick.

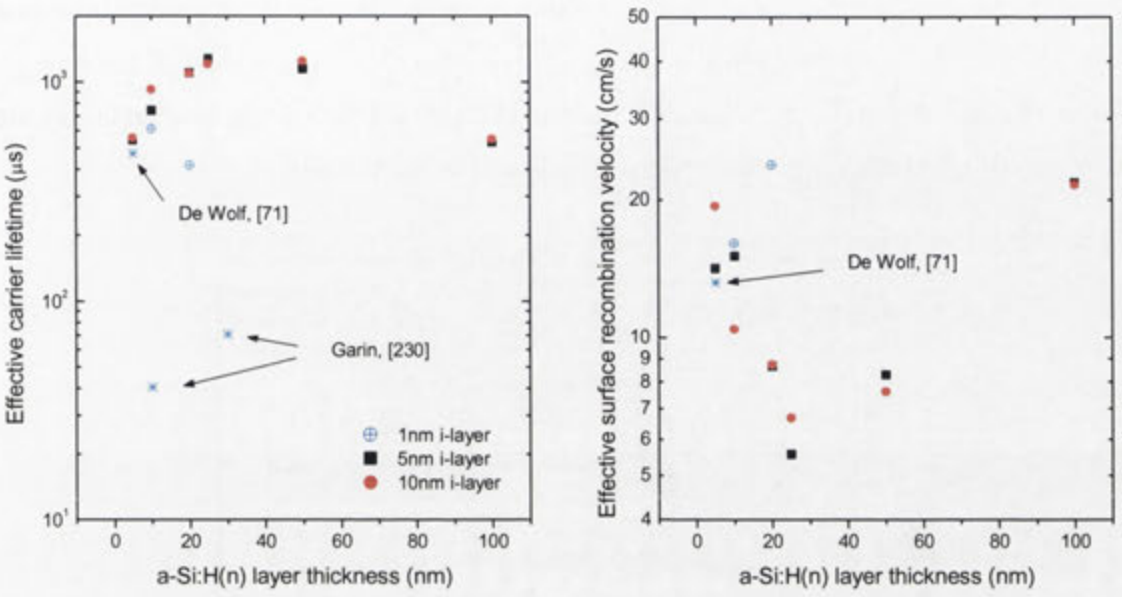

Figure 56: Passivation quality profile, in terms of a). τ_{eff}, and b). S_{eff}, for a-Si:H(n)/a-Si(n) stacked layers on 1.4Ωcm c-Si(n) according to the doped layer thickness. The a-Si:H(i) inter-layer thickness is 5nm or 10nm, although singular results for a 1nm inter-layer are also shown. Results for similar a-Si:H stacks by Garin *et. al.* [230] on 0.7Ωcm and De Wolf *et. al.* [71] on 1Ωcm on 300μm c-Si(n) are provided for comparison.

Several reasons for the decrease in surface passivation quality when using a-Si:H(n) layers above 50nm can be hypothesised; attenuation of incident light by the n-layer and compromises to the interface layer during deposition or annealing are the most likely cause. In the latter case, charge carriers would be able to overcome the potential barrier via thermionic emission or by tunnelling into the a-Si:H band tail states, effectively finding an efficient recombination pathway in dangling bonds within this layer. This is also possible due to inhomogeneities in the coverage of the a-Si:H(i) on the c-Si surface; however, the consistency in passivation quality by 5nm and 10nm a-Si:H(i) inter-layers with a-Si:H(n) below 50nm would demonstrate that layer coverage is not the cause.

The contrast to similar a-Si:H stacks reported by other groups (see Table 1), makes clear the quality of the a-Si:H stacks in this work. In Figure 56, τ_{eff} up to 1.3ms (S_{eff} of 5.5cms^{-1}) for this work compared to Garin *et. al.* [230] who reports values of 40μs (S_{eff} of 437cms^{-1}); or even those reported by De Wolf and Beaucarne [71] for τ_{eff} of 500μs ($S_{eff} \approx$ 13cms^{-1}), are shown. Indeed, despite the

difference in surface preparation, the results of a-Si:H(i/n) stacks presented here are more similar to those reported by Sanyo with a τ_{eff} of 1.1ms or 1.7ms [205, 231], respectively.

From the calculated S_{eff} described in Figure 56b, the ideal stack layer thickness is for a 25nm a-Si:H(n) on either 5nm or 10nm a-Si:H(i). Further characterisation of the a-Si:H(i/n) stack is by the emitter saturation current density (J_{oE}) given in Figure 57 using 5nm and 10nm a-Si:H(i) inter-layers. Early analysis describes similar reductions in J_{oE} at the c-Si surface, independent of the inter-layer thickness of 10nm or less. From this, it can be concluded that a 5nm a-Si:H(i) is suitable as a inter-layer in the a-Si:H(i/n) stack with a-Si:H(n) layers up to 100nm in thickness.

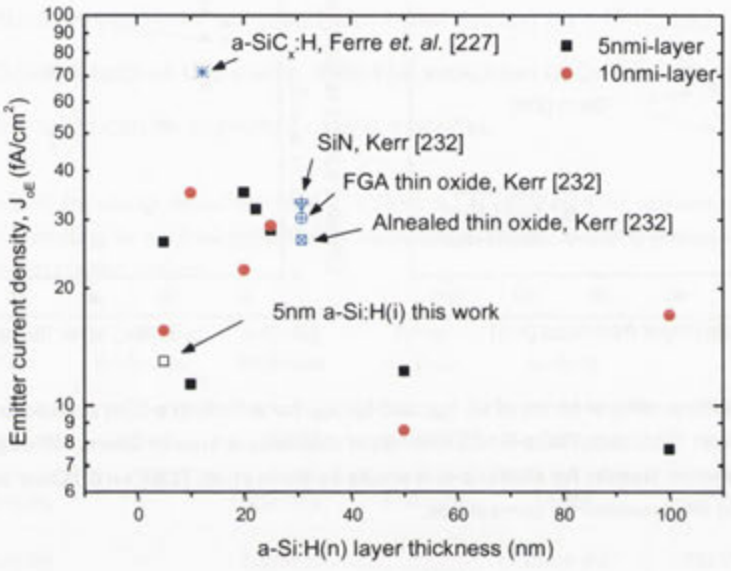

Figure 57: Influence of a-Si:H(n) layer thickness in a-Si:H(i/n) stacks on the J_{oE} for 1.4Ωcm *FZ* c-Si(n). The thickness of the a-Si:H(i) inter-layer is 5nm and 10nm. For comparison, references Kerr [232], and Ferre *et. al.* [227] are given. Also displayed in this J_{oE} for 5nm a-Si:H(i) on the n+ emitter in this work.

Comparison to other passivating schemes which use an n^+ emitter is possible given that for lightly diffused emitters, surface recombination is dominant. J_{oE} as low as 10fA/cm^2 is achieved here for a-Si:H(i/n) deposited at 230°C, comparing well with J_{oE} reported for SiN_x layers deposited at temperatures above 400°C and SiO_x passivation layers above 800°C on lightly doped n^+ emitters [213]. Noteworthy is that no n^+ emitter is required to achieve this result for the a-Si:H (i/n) stacks as part of this work.

The reductions in emitter current density above are reflected in the calculation of the V_{oc}-limit for a-Si:H(i/n) stacks shown in Figure 58. For the case of 5nm or 10nm inter-layers, the V_{oc}-limit appears to improve slightly when combined with a thicker a-Si:H(n) layer (i.e. ~40nm). Nevertheless,

the V_{oc}-limit for a-Si:H(i/n) stacks on the non-diffused c-Si surface is approximately 733mV. The results presented here compare well with the calculated V_{oc}-limits reported using SiN_x, FGA and alnealed thin oxides on 100Ω/□ n^+ emitters [213], and are higher than those for a-SiC_x:H [227]. Although the V_{oc}-limit continues to be influenced by the thickness of the a-Si:H(n) layer, the significance of these results (i.e. reduction in J_{oE} and high V_{oc}-limit) are noteworthy in that no diffused n+ emitter is present, and all processing is performed in one system at temperatures below 250°C. An achievement compared to other more intensive passivation and junction formation schemes.

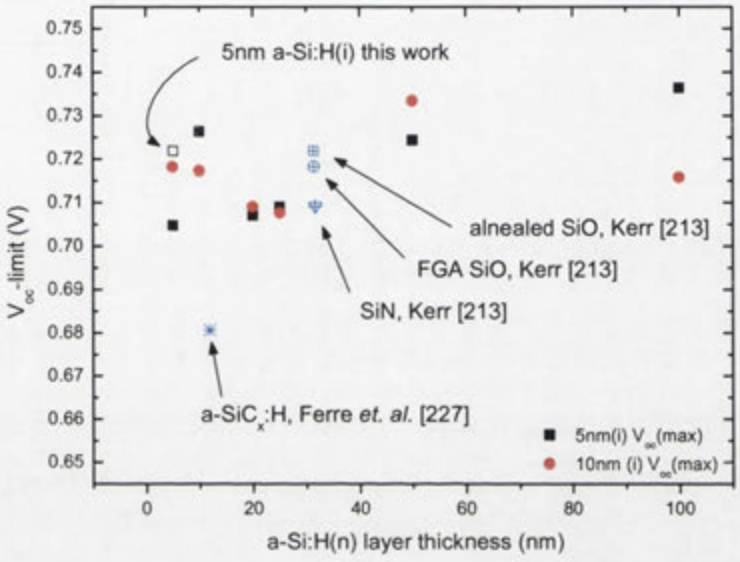

Figure 58: Implied-V_{oc} at non-diffused surface of 1.4Ωcm *FZ* c-Si(n) deposited and passivated by a-Si:H(i/n) stacked layers according to a-Si:H(n) layer thickness. A-Si:H(i) inter-layers are 5nm or 10nm. For comparison, references for Kerr [213] Ferre *et. al.* [227] are also shown. Also displayed is the V_{oc}-limit for 5nm a-Si:H(i) on the n+ emitter in this work.

The high V_{oc}-limit would suggest that the passivation quality and reductions in current density at the c-Si surface are dependent upon the quality and stability of the a-Si:H(i) in the presence of the a-Si:H(n) layer. Earlier in this thesis, the role which hydride bond density and the composition of the a-Si:H layer has upon the a-Si:H/c-Si interface's electronic properties was discussed. It is necessary therefore, to assess the influence which the a-Si:H(n) may have had on this aspect of the passivating layer. The results of FTIR spectroscopy on post-deposition thermally annealed a-Si:H(i/n)/c-Si(n) stacks is given in Figure 59.

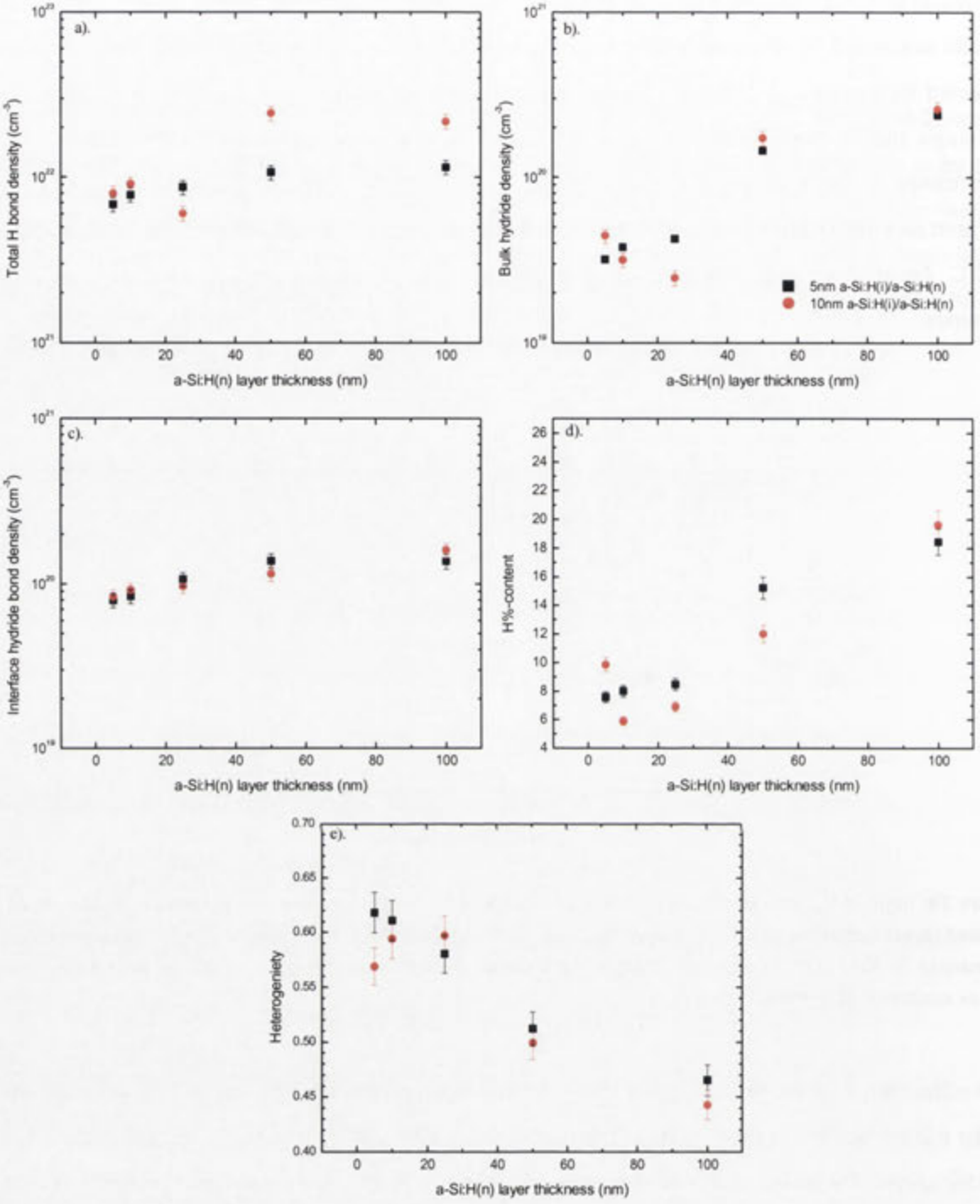

Figure 59: IR hydride bond density results a). Total bond density, b). Bulk monohydride, c). Interface monohydride densities, d). Hydrogen % content, e). Heterogeneity for a-Si:H(i/n) stacks of different thicknesses on bare, planar 1.4Ωcm *FZ* c-Si(n) and annealed at 240°C for 40 minutes.

The slight increase in the total bond hydrogen is expected for stacks with thicker n-type a-Si:H layers, and is similarly seen in the measurements for bulk hydride density. No significant change in

the hydride density can be observed within the interface region between the a-Si:H(i) layer and the c-Si(n) surface. Increases in the H%-content from 7% to 18%, for thicknesses can therefore be attributed to the thicker a-Si:H(n) layer, in a similar way to thicker a-Si:H(i) have been shown to increase H%-content (see section 2.2).

Despite the induced stress of the thicker a-Si:H(n) layer, the interface hydride density remains consistent with earlier results for a-Si:H(i) only layers, suggesting that although the a-Si:H(n) layer has a higher defect density it does not compromise the quality and stability of the a-Si:H(i) layer on the c-Si(n) surface.

A shift in heterogeneity from 0.61 to 0.46 for a-Si:H(i/n) stacks using 5nm inter-layers is observed, reflecting a swing in the dominant hydride composition from the interface to the bulk. A similar change is observed when a 10nm inter-layer is used, and allows an equivalence point for shifts in hydride density from the a-Si:H(n) to the a-Si:H(n) bulk above 0.5 to be deduced. From this the effective limit for the a-Si:H(i/n) stack dimensions is approximated, and agrees well with the results in τ_{eff}/S_{eff} and J_{0E} (see Figure 56 and Figure 57, respectively). Ideally, it would appear that the total thickness of the a-Si:H(n) layer should be limited to a maximum of 40nm to prevent degradation of the a-Si:H(i)/c-Si interface.

In addition, as heterogeneity remains above 0.35 for all a-Si:H(i/n) stack thicknesses examined here, effusion of hydrogen is not likely to occur at these temperatures, and it can be concluded that passivation quality is maintained for a-Si:H(n) layers up to 100nm in thickness when using a-Si:H(i) inter-layers as thin as 5nm.

4.4.2 Bifacial a-Si:H(i/p) stacks on n-type c-Si

The separation of photogenerated charges injected from the crystalline bulk requires the passivation the c-Si(n) surface in the presence of a p^+ region. In many conventional solar cell designs the p^+ region is accomplished by boron diffusion at temperatures above 800°C. As in the previous section, the removal of the diffused p^+ region in favour of the a-Si:H(i/p) stack would present a significant improvement in processing efficiencies (i.e. reductions in thermal budget, complexity and time). Sanyo has demonstrated that good passivation, J_{0E} and V_{oc} are achievable using the a-Si:H(i/p) stack in its HIT solar cell. However, according to many research efforts, the achieved surface passivation of these stacks on c-Si(n) is somewhat variable (Table 2).

De Wolf and Kondo have reported τ_{eff} up to 300µs ($S_{eff} \approx 200 cms^{-1}$) for 6nm/150nm a-Si:H(i/p) deposited at 150°C on a 300µm *FZ* 0.7Ωcm c-Si(n) [146], degrading when annealed at temperatures above 220°C linked to hydrogen effusion. Conversely, for similar a-Si:H(i/p) stacks on c-Si(n), Garin *et. al.* [230] reported significantly lower τ_{eff} of 40µs (S_{eff} = $437 cms^{-1}$), and it was surmised that the passivation quality provided by the a-Si:H(i) layer on the c-Si(n) surface was degraded in general, in the presence of the doped a-Si:H. Indeed, Fujiwara and Kondo have reported a higher τ_{eff} of 728µs when using Al-BSF for c-Si(n) instead of the a-Si:H(i/p) stack on 2.5Ωcm and 4.1Ωcm c-Si(n) [61].

Table 2: Summary of a-Si:H(i/p) stacks deposited onto *FZ* c-Si(n). S_{eff} is calculated assuming a thickness (if not provided) of 300µm width (Appendix A). For Al-BSF, S_{eff} is assumed to represent the front non-metal surface.

Group	Dopant (*FZ*)	c-Si thickness	a-Si:H(i) thickness	Front surface	Rear surface	Technique	τ_{eff} (µs)	S_{eff} (cms^{-1})
De Wolf & Kondo [233]	0.7Ωcm (n)	320µm	7.3nm a-Si:H(i)	8.3nm a-Si:H(p)	88.3nm a-Si:H(p)	PECVD, 155°C	~ 80µs	~ 200
De Wolf & Kondo [71]	0.7Ωcm (n)	300µm	4-5nm a-Si:H(i)	~ 4nm a-Si:H(p)	~ 4nm a-Si:H(p)	PECVD, 180°C, 5/15W	90µs	~384
Garin *et. al.* [230]	1Ωcm (n)	--	10nm a-Si:H(i)	10nm a-Si:H(n)	30nm a-Si:H(p)	PECVD	40µs	~437
Fujiwara [61]	2.6Ωcm (n)	525µm	4nm a-Si:H(i)	5nm a-Si:H(p)	Al-BSF	PECVD	728µs	36
Fujiwara [61]	4.1Ωcm (n)	525µm	4nm a-Si:H(i)	5nm a-Si:H(p)	Al-BSF	PECVD	717µs	37

Given the disparity between passivation quality of the c-Si(n) using a-Si:H(i/p) stacked layers reported in the literature and the achievements of Sanyo, the a-Si:H(i/p) heterostructure on c-Si(n) is investigated here. Similar to the deposition process in the previous section, a 5nm or 10nm a-Si:H(i) inter-layer is bifacially deposited, followed by an a-Si:H(p) layer between 5nm and 100nm onto both front and rear surfaces, then thermally annealed at 240°C for 40 minutes. The surface passivation results for these a-Si:H(i/p)/c-Si(n) heterostructures are given in Figure 60.

Contrary to results reported in the literature, passivation of the c-Si(n) surface by the a-Si:H(i/p) layer stack is significantly higher than previously thought. Measured τ_{eff} for the stacked layers in this work, achieved values of approximately 1.4ms ($5 cms^{-1}$), even when a thin 5nm a-Si:H(i) inter-layer is used. Although, the a-Si:H(i) appears to decrease slightly when a thicker a-Si:H(p) layer up to 100nm is used, the passivation quality remains substantially higher than those reported by other groups. Although not shown in this section, thicker a-Si:H(p) layers above 150nm displayed significant reductions occur in the passivation of the c-Si surface by the a-Si:H(i) layer.

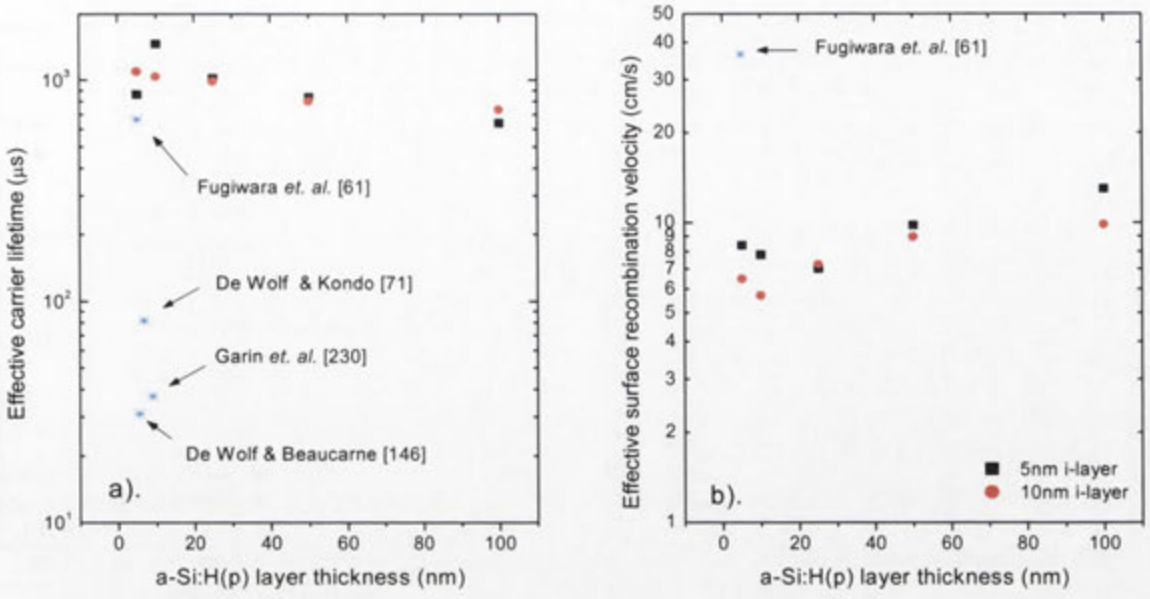

Figure 60: Passivation quality profile for a-Si:H(n)/a-Si(p) stacked layers on 1.4Ωcm c-Si(n) according to the doped layer thickness in terms of a). τ_{eff}, and b). S_{eff}, The a-Si:H(i) inter-layer thickness is 5nm or 10nm. For comparison, results for similar a-Si:H(i/p) stacks by Garin *et. al.* [230] on 0.7Ωcm c-Si(n), Fujiwara *et. al.* [61] using Al-BSF with a-Si:H(i/p) 525μm 2.6Ωcm *FZ* c-Si(n) (5nm i) are given.

It can be concluded from the results of Figure 60 that a-Si:H(i/p) layers less than 100nm in overall thickness maintain high levels of passivation of the c-Si(n) surface when optimised a-Si:H layers are deposited. Furthermore, a range of a-Si:H(p) were tested and appeared suitable, however, the best results achieved occurred for layer dimensions ≤20nm. The surface recombination velocity of 5cms^{-1} achieved for a-Si:H(i/p) stacked layers in this work are some of the lowest reported to date.

In Figure 61, low values below 20fA/cm^2 of J_{oE} are calculated for the c-Si(n) surfaces using a-Si:H(i/p) layer stacks. For thicknesses up to 100nm the a-Si:H(p) layers deposited in this work are seen to exert little influence on the current density of the c-Si surface. The improvement in J_{oE} using 10nm a-Si:H(i) inter-layers might also be viewed as an improvement in reducing any thermionic emission or tunnelling by charge carriers given the higher levels of passivation exhibited by the 5nm a-Si:H(i) compared to the 10nm a-Si:H(i).

In either case, the V_{oc}-limit for a-Si:H(i/p)/c-Si(n) heterostructures presented in Figure 61b, demonstrate that a high V_{oc} is possible using the optimised layers deposited in this work. For overall a-Si:H(i/p) thicknesses, below 100nm, the V_{oc}-limit appears unaffected and values of approximately 740mV are calculated.

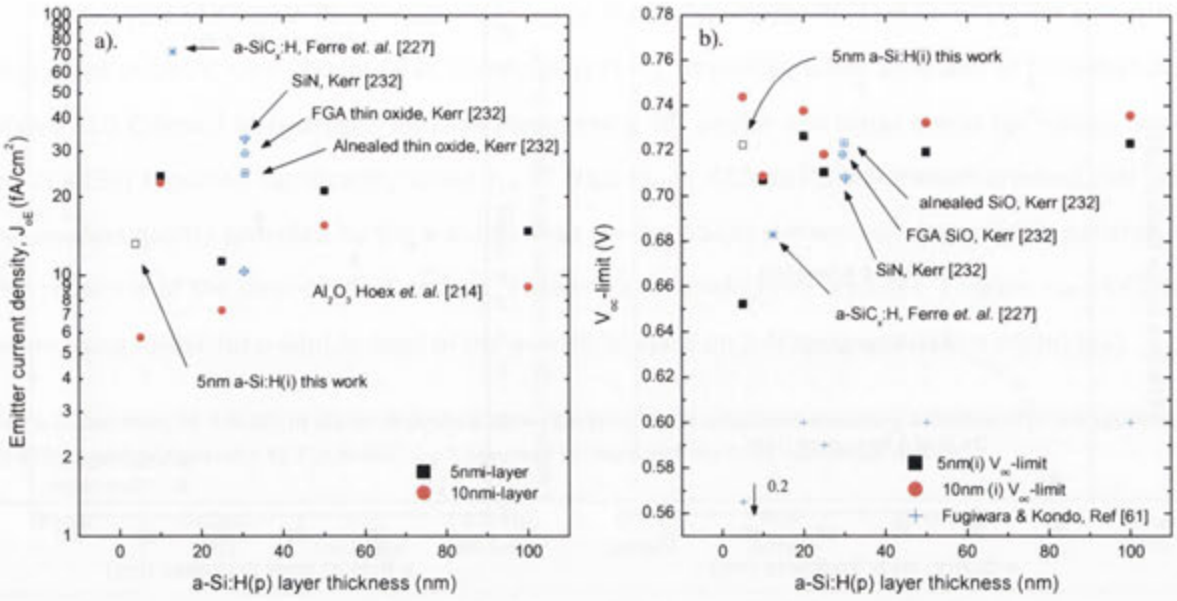

Figure 61: Influence on the a). J_{oE} and b). Implied-V_{oc} by a-Si:H(p) layer thickness in a-Si:H(i/p) stacks on non-diffused surface for 1.4Ωcm *FZ* c-Si(n). The a-Si:H(i) inter-layer is 5nm or 10nm. For comparison, J_{oE} of SiN_x, FGA and alnealed SiOx reported by Kerr [232], 30nm Al_2O_3 Hoex *et. al.* [214] , and 12nm a-SiC_x:H by Ferre *et. al.* [227] on 100Ω/□ n^+ emitters is provided for comparison to more conventional solar cell designs. Also displayed in this J_{oE} and V_{oc}-limit for 5nm a-Si:H(i) on the n+ emitter in this work.

The a-Si:H(i/p) stacked layers deposited in this work have been shown to measure J_{oE} and V_{oc}-limits at low temperatures on bare c-Si(n) surfaces similar to those by SiN_x, FGA and alnealed thin-oxide passivating layers on n^+ emitter surfaces demonstrating the tremendous advantage that a-Si:H represents in terms of c-Si(n) solar cell design.

4.4.3 Bifacial a-Si:H(i/n) or a-Si:H(i/p) stacks on p-type c-Si

In solar cells, the c-Si(p) wafer material is often favoured due to the high carrier diffusion length of electrons in this material and relative ease in forming a diffused n^+ emitter at the front surface compared to that of a boron emitter required for c-Si(n). For compatibility with front-surface contact formation, local diffusions of phosphorus beneath metal contact are utilised with some degree of complexity [234], while at the rear surface an Al-BSF layer is formed. In this section, the passivation and suitability of a-Si:H stacks on the c-Si(p) is investigated by removal of the diffused emitter and Al-BSF at the surface, instead replacing them with either a-Si:H(i/n) or a-Si:H(i/p) stacked layers respectively.

A broad summary of the stacked layer a-Si:H of each type reported in the literature onto the bare *FZ* c-Si(p) surfaces is given in Table 3. De Wolf and Kondo [71] and Beaucarne [146] report similarly high τ_{eff} corresponding to S_{eff} of 22.6cms^{-1} on 3Ωcm c-Si(p) and 11.56cms^{-1} on 1.5Ωcm c-Si(p) using both a-Si:H(i/n) and a-Si:H(i/p) respectively. Garin *et. al.* [230] also report similar passivation results using the a-Si:H(i/p) stack on 0.6Ωcm c-Si(p), higher than is achieved using the a-Si:H(i/n) layer stack. By comparison other passivating schemes listed, including a-SiC$_x$:H, have yielded mixed results between 60μs on 0.4Ωcm c-Si(p) using (i/n) layers and 585μs with (i/p) on 3.3Ωcm c-Si(p).

Table 3: Summary of a-Si:H(i/n) and a-Si:H(i/p) layer stacks deposited onto *FZ* c-Si(p). S_{eff} is calculated for unknown base wafer thicknesses assuming 300μm width according to method described in Appendix A. Where Al-BSF is indicated, the S_{eff} is assumed to represent the front non-metal side surface.

Group	Dopant (*FZ*)	c-Si thickness	a-Si:H(i) thickness	Front surface	Rear surface	Technique	τ_{eff} (μs)	S_{eff} (cms^{-1})
De Wolf & Kondo [71]	3Ωcm (p)	300μm	4-5nm	4nm a-Si:H(n)			650	22.6
Vetter et. al. [220]	0.4Ωcm (p)	390μm	--	a-SiC$_x$:H(n)	a-SiC$_x$:H(n)	PECVD	60	392
Garin et. al. [230]	0.6Ωcm (p)	--	10nm (i)	10nm (n)	10nm (n)	PECVD	300	49
Garin et. al. [230]	0.6Ωcm (p)	--	10nm (i)	10nm (n)	30nm (n)	PECVD	400	36.62
Martin et.al. [87]	0.9Ωcm (p)	--	pm-Si:H(i)		a-SiCx:H	HWCVD	139	109.2
Janz et. al. [219]	1.0Ωcm (p)	--	a-SiCx:H(i)	70nm a-SiC$_x$:H(n)	SiO/Al		1200	11.38
Rau et. al. [229]	0.3Ωcm (p)	375μm	a-Si:H(i)	a-Si:H(p)	a-Si:H(p)			90
Garin et. al. [230]	0.6Ωcm (p)	--	10nm (i)	10nm (p)	30nm (n)	PECVD	150	100
De Wolf & Kondo [71]	0.7Ωcm (n)	300μm	7.3nm a-Si:H(i)	8.3nm a-Si:H(p)	88nm a-Si:H(p)	PECVD, 155°C		
De Wolf & Beaucarne [146]	1.5Ωcm (p)	300μm	6nm (i)	150nm a-Si:H(p)	150nm a-Si:H(p)		30	447
De Wolf & Beaucarne [146]	1.5Ωcm (p)	250μm	5-6nm (i)	150nm a-Si:H(p)	150nm a-Si:H(p)	PECVD	800	14.4
De Wolf & Beaucarne [146]	1.5Ωcm (p)	250μm	3-4nm (i)	150nm a-Si:H(p)		PECVD	200	62
De Wolf & Beaucarne [146]	1.5Ωcm (p)	250μm	50nm (i)	150nm a-Si:H(p)			1000	11.56
Einsele et. al. [235]	1.0Ωcm (p)	250μm	30nm a-Si:H(i)	μc-Si:H(p)	30nm a-Si:H(i)	PECVD	600	13
De Wolf & Kondo [71]	3Ωcm (p)	250μm	<6nm (i)	4nm a-Si:H(p)			<110	139
De Wolf et. al. [146]	3Ωcm (p)	300μm	4-5nm (i)	5nm a-Si:H(p)	5nm a-Si:H(p)	PECVD	~850	30
Martin et. al [51]	3.3Ωcm (p)	--	--	70nm a-SiC$_x$:H			585	30
Martin et.al. [87]	14Ωcm (?)		pm-Si:H(i)		Al-BSF	PECVD	2000	6.0

As in the previous sections, the variability in the passivation quality of the c-Si(p) surface with different doping concentration, layer thicknesses, deposition conditions and structure make defining a standard a-Si:H stacked layer structure difficult to discern. Therefore, the a-Si:H(i/n) and a-Si:H(i/p) layer structures are investigated on the bare, planar 0.9Ωcm *FZ* c-Si(p) between 120μm and 150μm. Two a-Si:H(i) inter-layer thicknesses, 5nm and 10nm, are deposited followed by the doped a-Si:H layer between 5nm and 150nm. The passivation quality profiles for both stack layer structures are given in Figure 62.

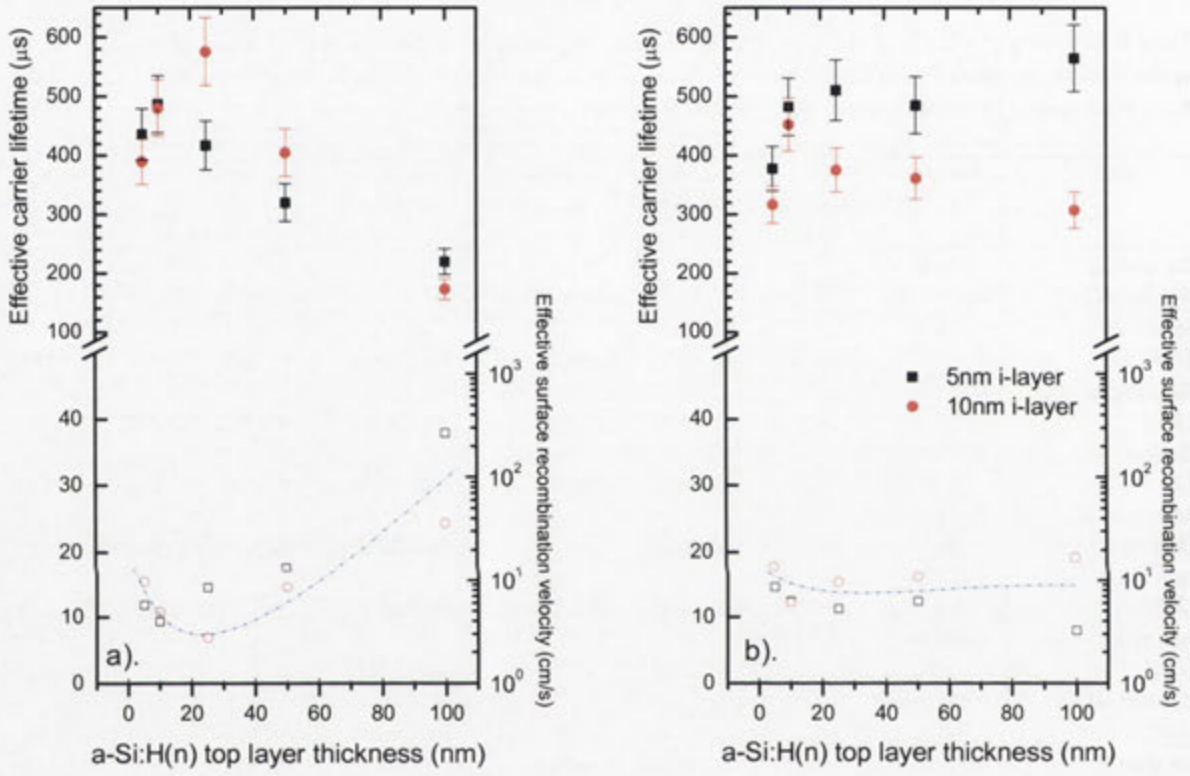

Figure 62: Passivation quality profile for a). a-Si:H(i/n) and b). a-Si:H(i/p) in terms of both measured τ_{eff} and calculated S_{eff} on bare, planar 0.9Ωcm c-Si(p) according to the doped layer thickness. The a-Si:H(i) inter-layer thickness is 5nm or 10nm.

In Figure 62, the a-Si:H(i/n) stacked layer or heterostructure on c-Si(p) the best passivation quality is realised using the thin a-Si:H(n) layers 40nm and less, achieving S_{eff} of 3cms^{-1} for 25nm thicknesses. Similarly, for the a-Si:H(i/p) stacked layer, S_{eff} below 15cms^{-1} is achievable for most thicknesses of the a-Si:H(p) layer on both 5nm and 10nm a-Si:H(i) inter-layers. Increases to the thickness of the a-Si:H(n) appear to degrade the quality of the surface passivation provided by the a-Si:H(i). The differences in S_{eff} using 100nm a-Si:H(n) may be indicative of tunnelling through the thinner 5nm a-Si:H(i) compared to 10nm a-Si:H(i), not observable with a-Si:H(p).

Comparatively, the passivation results for the a-Si:H(i/n) heterostructure and the a-Si:H(i/p) stacked layers outperform most similar a-Si:H stacks listed in Table 3. It may be concluded from this that, the a-Si:H(i) inter-layer and both a-Si:H(n) and a-Si(p) layers in this work are deposited under ideal conditions and that the inter-layer is not degraded by the deposition or presence of the doped a-Si:H layer. No epitaxial growth for processing temperatures up to 240°C is observable, contrary to Fujiwara *et. al.* [92].

Further, it is suggested that a suitable junction may indeed be formed using the a-Si:H(i/n) heterostructure on the bare c-Si(p) surface. To ascertain the extent to which this occurs, the current density (J_{oE}) and V_{oc}-limit for both structures on c-Si(p) are presented in Figure 63 and Figure 64.

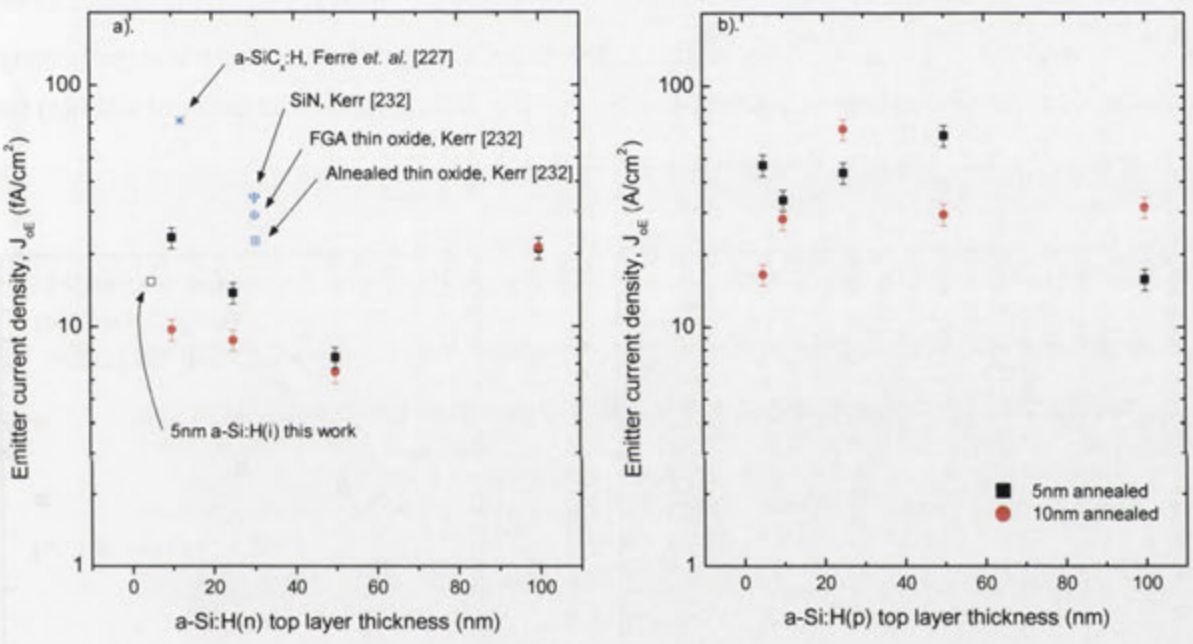

Figure 63: Influence of layer thickness for a). a-Si:H(n) in a-Si:H(i/n) heterostructure and b). a-Si:H(p) in the a-Si:H(i/p) layer stacks on the J_{oE} at the non-diffused surface for 0.9Ωcm *FZ* c-Si(p). The thickness of a-Si:H(i) inter-layer is 5nm and 10nm. For comparison, references for Kerr [232] and Ferre *et. al.* [227] are also given. Also displayed are the J_{oE} and V_{oc}-limit for 5nm a-Si:H(i) on the n+ emitter in this work.

Low J_{oE} less than 10fA/cm^2 are shown to occur for the a-Si:H(i/n) heterostructure between 10fA/cm^2 and 60fA/cm^2 for the a-Si:H(i/p) stacked layer structure (see Figure 63). Indeed a decrease in J_{oE} is observed for thicker a-Si:H(n) up to 50nm. Conversely, the thickness of the a-Si:H(p) layer appears to increase J_{oE}. Although thermionic emission or tunnelling may still occur through the inter-layer at these layer thicknesses, this is unlikely to be the cause. The V_{oc}-limits shown in Figure 64 signify that the thickness of the doped a-Si:H layer does not strongly influence the V_{oc}-limit, although

a thinner a-Si:H(p) (approximately 25nm) would appear to achieve higher values. From these results, two observations can be surmised:

- The a-Si:H(n) and a-Si:H(p) layers deposited onto 5nm or 10nm a-Si:H(i) do not contact with the c-Si(p) surface, remaining electronically isolated
- Diffused n^+ emitters or Al-BSF are not a necessary requirements of the solar cell structure when a-Si:H(i/p) and a-Si:H(i/n) stacks are used

For comparison, the V_{oc}-limit for similar a-Si:H stacked layers deposited by Jensen *et. al.* [32] on 0.5Ωcm *FZ* c-Si(p), Fujiwara and Kondo [61] on 0.5Ωcm *Cz* c-Si(p) and Janz *et. al.* [219] using a-SiC_x:H on 1.0Ωcm are shown. The V_{oc}-limit for SiN_x, FGA and alnealed SiO_x reported by Kerr [232] and 12nm a-SiC_x:H by Ferre *et. al.* [227] on 100Ω/□ n^+ emitters is provided for comparison with more conventional solar cell designs. It should be noted that the unfavourable band offset of a-Si:H(n) for p-type c-Si is likely to decrease the V_{oc}-limit somewhat.

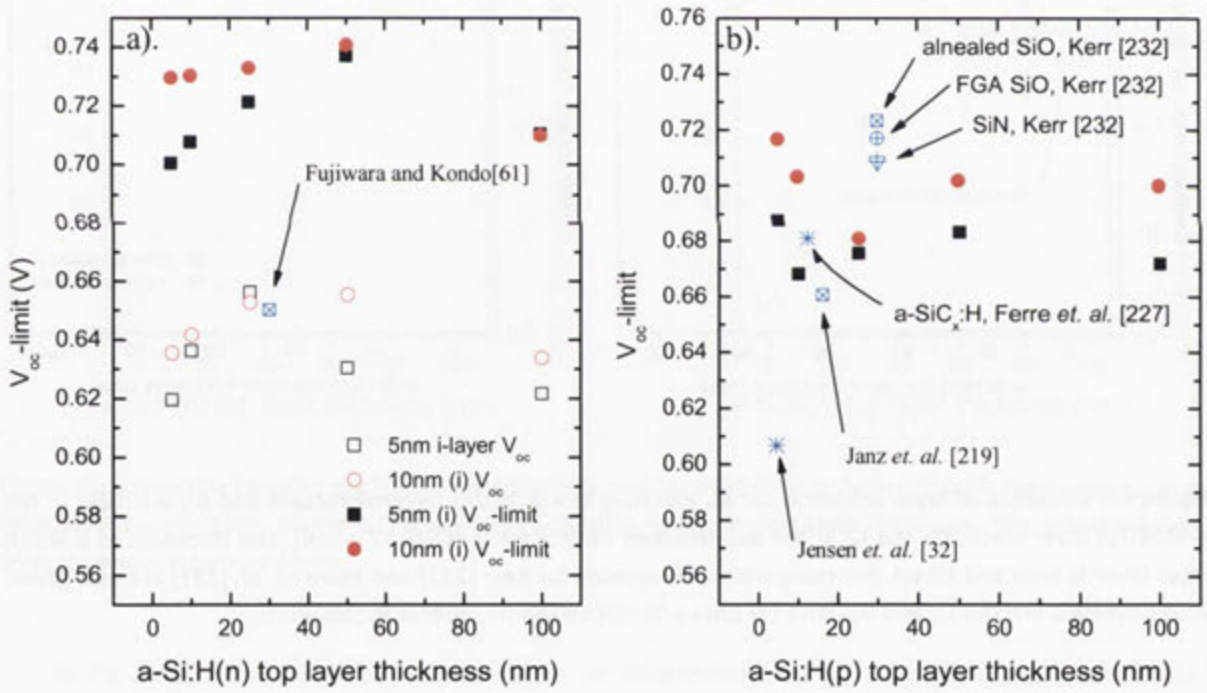

Figure 64: Influence of layer thickness for a). a-Si:H(n) layer in a-Si:H(i/n) heterostructure and b). a-Si:H(p) in a-Si:H(i/p) layer stacks on the Implied-V_{oc} at the non-diffused surface for 0.9Ωcm *FZ* c-Si(p). The thickness of the a-Si:H(i) inter-layer is 5nm and 10nm.

IR spectroscopy of the a-Si:H(i/n) heterostructure and a-Si:H(i/p) stacked layers on the c-Si(p) surface are given in Figure 65.

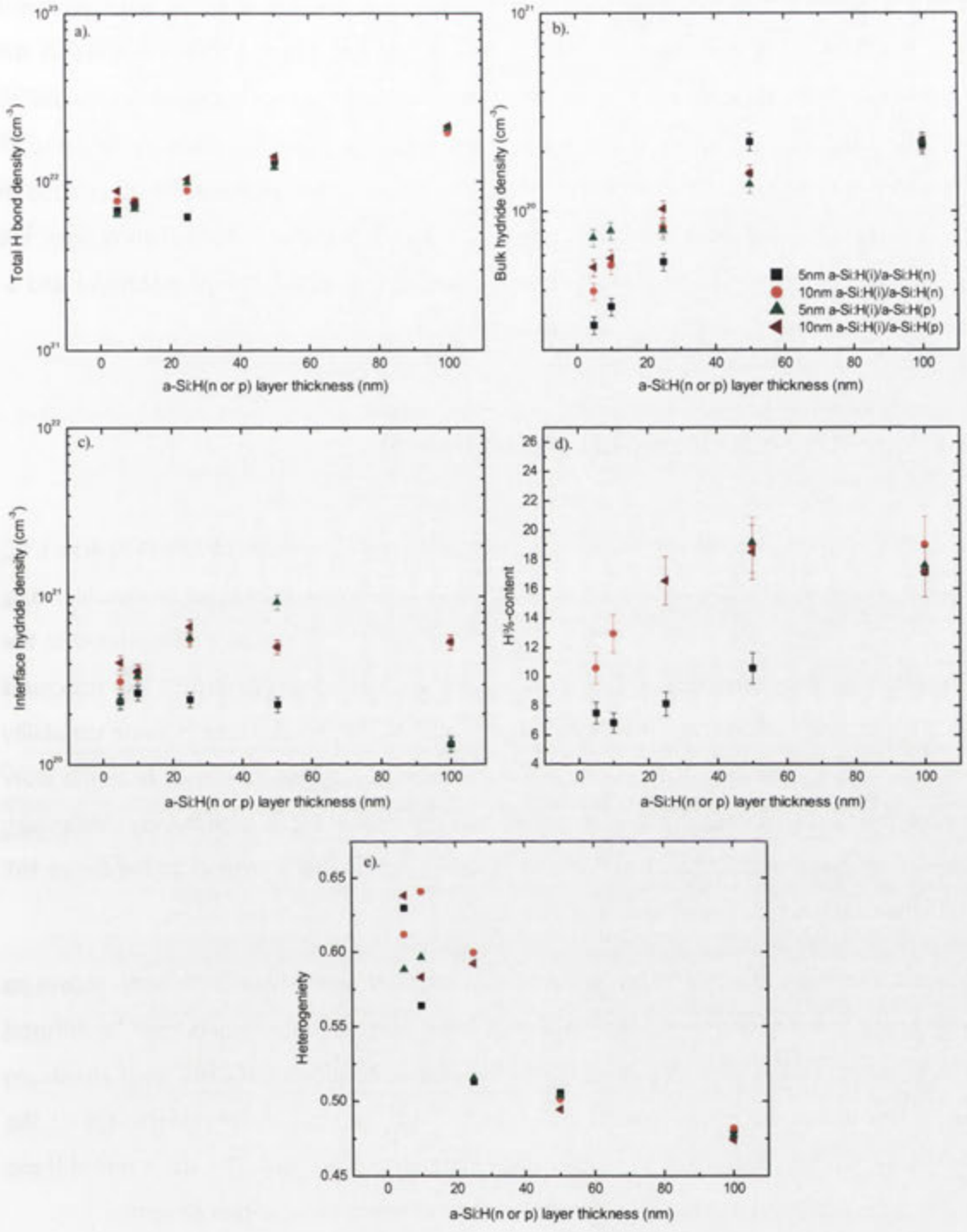

Figure 65: IR hydride bond density results a). Total bond density, b). Bulk monohydride, c). Interface monohydride densities, d). Hydrogen % content, e). Heterogeneity for a-Si:H(i/n) heterostructure and a-Si:H(i/p) stacked layer of different thicknesses on bare, planar 0.9Ωcm *FZ* c-Si(p) and annealed at 240°C for 40 minutes.

As for a-Si:H stacked layer structures on the c-Si(n) surface, similar minimal increases in bond density occur at either the interface or bulk regions; and, the distinct increase in H%-content for

thicker layers persists. Heterogeneity sharply decreases from 0.65 to 0.45 as layer thickness increases, despite no significant loss in surface passivation quality and is a likely response to the doped layer (see Figure 62).Although not presented, the stability of surface passivation provided by both a-Si:H(i/n) and a-Si:H(i/p) stacked layers during post-deposition thermal annealing for up to 80 hours at 250°C was assessed. The results of this thermal cycling are similar to that reported in Section 3.3.1. No significant changes in monohydride density within the interface or bulk regions, H% content or heterogeneity could be observed, demonstrating that stable, robust a-Si:H(i/n) and a-Si:H(i/p) layers have been successfully deposited in this work.

4.5 Asymmetric bifacial a-Si:H stacks on c-Si

The success of the Sanyo HIT solar cells with reported record efficiencies of 23% (100.4cm^2), V_{oc} of 742mV is well known [35, 221]. Although some success has been made by other groups, including Sawada *et. al.* [29] and Taguchi *et. al.* [159], they are difficult to achieve as demonstrated in the results reported by many others listed in Table 7 (Appendix C). For devices with HIT-like structures [29, 236, 237] average efficiencies of 14% are often obtained. Although, there is some variability between doping concentration, surface area and thickness of the c-Si wafers used, from the work presented in this thesis thus far, it can be surmised that one critical factor in achieving similar high quality surface passivation, charge collection and other electronic characteristics of the Sanyo HIT device is in the quality of the deposited a-Si:H layers.

In previous sections, the a-Si:H(i/n) and a-Si:H(i/p) stacked layers have both been shown to effectively passivate the n- or p-type c-Si surface and appear to remove the requirement for diffused n+ and/or p+ emitters. Subsequently, the asymmetric deposition of both stacked layer structures achieved in this work onto either side of c-Si(n) and c-Si(p) wafers and the assessment of the resulting overall HIT-like structure in terms of surface passivation is prudent. The structures of these HIT-like devices are illustrated in Figure 66, and follow two different front-to-rear designs:

- Si:H(p)/a-Si:H(i)/ c-Si(n)/a-Si:H(i)/a-Si:H(n), and
- Si:H(n)/a-Si:H(i)/c-Si(p)/a-Si:H(i)/a-Si:H(p)

The c-Si(n) and c-Si(p) wafers in each case are high-quality *float-zone*, planar with no phosphorus or boron diffusion (i.e. no emitter) and are 140μm and 120μm thick, respectively. All intrinsic and

doped a-Si:H layers are optimised according to outcomes shown previously in this work. Inter-layers are 5nm or 10nm a-Si:H(i) deposited prior to doped a-Si:H layers of thicknesses between 5nm and 50nm. To prevent dopant contamination[10] by diborane, the a-Si:H(p) layer is deposited first to one side, followed by the a-Si:H(n) layer on the reverse side. As a dielectric material, the a-Si:H layers are compatible with current extraction and where necessary 70nm of ITO is *rf*-sputtered onto the surface following initial characterisation and thermal annealing, followed by 0.5μm Al dots.

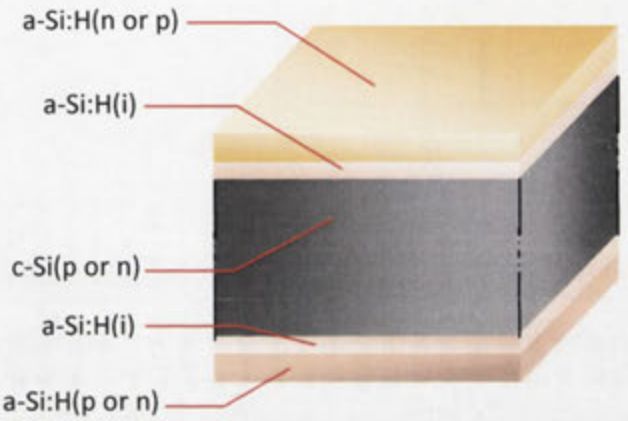

Figure 66: Schematic of asymmetrical a-Si:H heterostructure on c-Si wafer. The c-Si base wafer can be either n- or p-type and determines the emitter and BSF-layer structure, (e.g. p-based heterostructure for emitter and n-based heterostructure for BSF on c-Si(n)). The heterostructures are reversed for c-Si(p).

The quality of surface passivation of either c-Si(n) or c-Si(p) using the HIT-like a-Si:H stacked layers is shown in Figure 67. As expected, no degradation in the surface passivation quality is seen to occur when using the asymmetric a-Si:H layer stacks. Certainly, high quality passivation is shown for these HIT-like structures which exhibit τ_{eff} above 1ms corresponding to S_{eff} below 6cms^{-1}. Although similar results have been reported for similar structures they are often for thicker a-Si:H layers and c-Si bulk of different concentrations [236].

[10] Diborane partially breaks down at approximately 200°C in the absence of a plasma and may contaminate the other side of the c-Si prior to deposition of the a-Si:H(n) layer. Phosphine requires a plasma to decompose and does not contaminate the side to be deposited with a-Si:H(n).

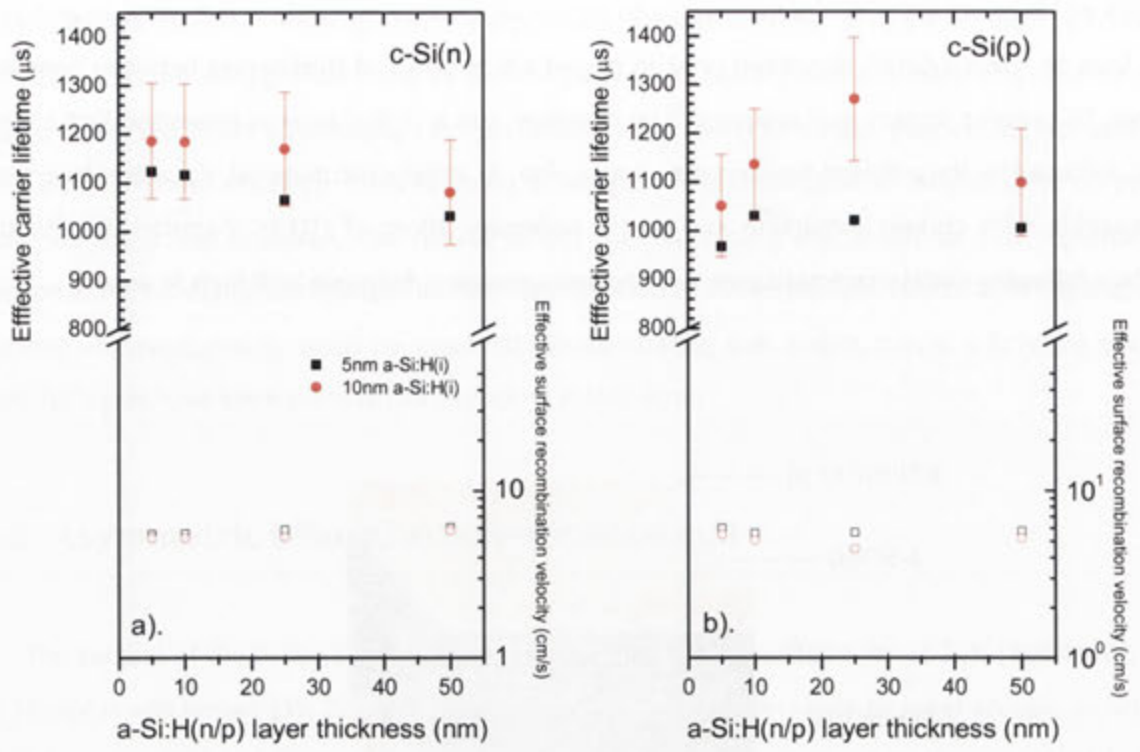

Figure 67: Passivation quality profile for a). a-Si:H(n/i)/c-Si(n)/a-Si:H(i/p) and b). a-Si:H(p/i)/c-Si(p)/a-Si:H(i/n) in terms of both measured τ_{eff} and calculated S_{eff} on bare, planar 1.4Ωcm c-Si(n) and 0.9Ωcm c-Si(p) according to the doped layer thickness. The a-Si:H(i) inter-layer thickness is 5nm or 10nm.

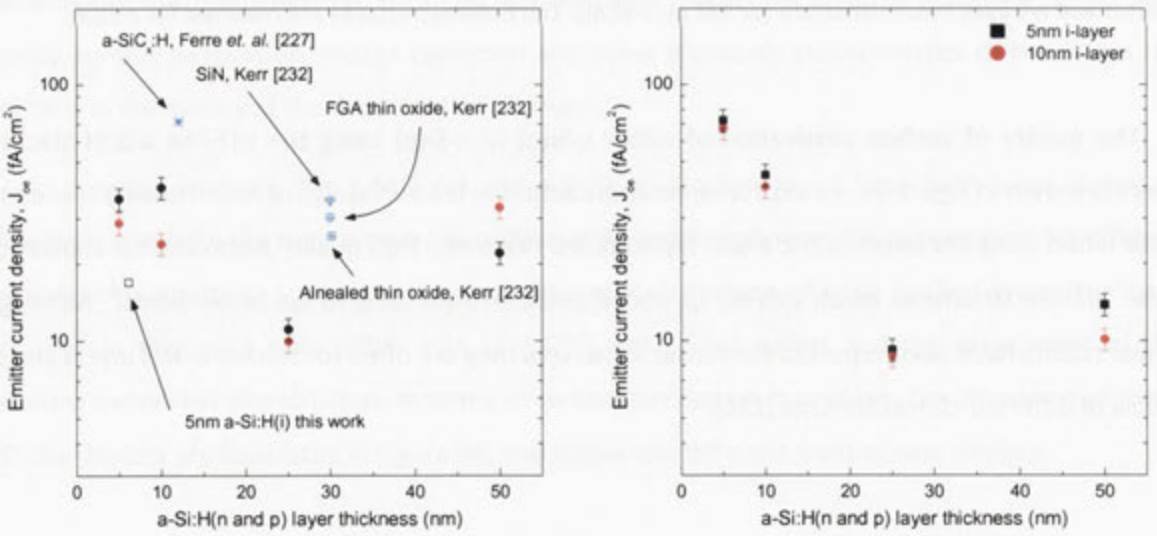

Figure 68: Influence the doped a-Si:H layer thickness has on J_{oE} for a). a-Si:H(n/i)/c-Si(n)/a-Si:H(i/p) and b). a-Si:H(p/i)/c-Si(p)/a-Si:H(i/n) layer stacks deposited bifacially onto the non-diffused, planar surface for 1.4Ωcm c-Si(n) and 0.9Ωcm *FZ* c-Si(p). The thickness of the a-Si:H(i) inter-layer is 5nm and 10nm. For comparison, references for Kerr [232] and Ferre *et. al.* [227] are also shown. Also displayed in this J_{oE} and V_{oc}-limit for 5nm a-Si:H(i) on the n+ emitter in this work.

The average J_{oE}, corresponding to either the front or rear surface on both c-Si(n) and c-Si(p) is given in Figure 68. In both instances, a minimum J_{oE} below 10fA/cm^2 is achieved, respectively, 9.96fA/cm^2 and 8.7fA/cm^2 when 25nm doped a-Si:H layers are deposited with 5nm or 10nm a-Si:H(i) inter-layers. This shows that the recombination properties of the HiT-like emitter are independent of the substrate acceptor density. The low J_{oE} and exceptional S_{eff} for non-textured, non-diffused c-Si demonstrates that the a-Si:H layers deposited in this work are suitable for HIT-like devices given equally high quality ITO and metal contact formation steps. In Table 4, the calculated V_{oc}-limit, representing an upper bound, and the actual V_{oc} measured, following contact formation are given. These results assume that a junction is formed by either the a-Si:H(i/p) stacked layer on c-Si(n) or the a-Si:H(i/n) stacked layer on c-Si(p), with the rear-side a-Si:H stacked layer performing as a back-surface-field layer.

Table 4: V_{oc}-limit calculated from J_{oE} and measured V_{oc} for HiT-like a-Si:H stacked layers bifacially deposited onto non-diffused, planar 140µm *FZ* 1.4Ωcm and 120µm 0.9Ωcm *FZ* c-Si(p).

c-Si doping	c-Si thickness	a-Si:H(i) layer thickness	a-Si:H(n/p) layer thickness	V_{oc}-limit (mV)	V_{oc}-measured (mV)
N	131µm	5nm	25nm	725	714
N	150µm	10nm	25nm	723	711
P	120µm	5nm	25nm	723	676
P	122µm	10nm	25nm	749	678

Measured results indicate that a high V_{oc}, 714mV and 678mV for c-Si(n) or c-Si(p) respectively, may be achievable using the optimised a-Si:H layers deposited and presented in this work. The difference between the V_{oc}-limit and measured V_{oc} when using c-Si(p) is particularly significant. This may be a consequence of the unfavourable band offset for a-Si:H(n) on c-Si(p) which is more evident when thicker intrinsic layers are used, a low fill factor would also result in this case. In considering the similar V_{oc}-limits calculated from J_{oE} of the a-Si:H structures on both c-Si(n) and c-Si(p) the possible impact of the non-optimised ITO and Al contacts formed here cannot be ignored and it is likely that a completed device would require further experimentation.

Difficulty in defining the surface area for the above devices made attempts to measure efficiencies unsuitable for comparison. However, comparison of the measured V_{oc} here to those in references [32, 205] which give corresponding efficiencies would suggest conversion efficiencies

above 15% at minimum may be estimated for the devices in Table 4. Initial conversion efficiencies do seem to indicate up to 18% are likely although only approximated for an undefined surface area.

The results of the HIT-like a-Si:H structures deposited using optimised a-Si:H layers in this thesis indicate that further improvements to HIT solar cell performance may be achievable other than through surface texturing and developments in ITO and ARC coatings. Once the understanding of the characteristics for a-Si:H layers themselves and the role they play is more extensive, thinner layers, less processing and more reliable efficiencies are possible.

4.6 Summary and conclusions

The application of intrinsic and stacked intrinsic/doped a-Si:H layers to both diffused and non-diffused *FZ* c-Si surfaces in this chapter have identified some of the unique advantages which a-Si:H offers. A first study of thermally diffused phosphorus emitters of various sheet resistances on c-Si(p), equivalent levels of passivation was conducted using a-Si:H(i) deposited by ML-PECVD and standard PECVD. For lightly doped emitters, a J_{oE} similar to and in some cases lower than those achieved with a-SiC_x:H, SiN, FGA thin oxide and alnealed oxide has been measured. No depletion conditions were observed for the a-Si:H(i) layers in this work. Additionally, the influence of sheet resistance on the reduction in emitter current density is negligible for all but the lowest sheet resistance tested. In general, it may be surmised that the thickness of the a-Si:H(i) layer does not appear to influence the reduction in J_{oE} achieved provided interface passivation is suitable. From calculations of the V_{oc}-limit, passivation by the a-Si:H(i) layers in this work demonstrated similar results to those achieved with other higher temperature passivation materials which require more involved processing.

By this result, the combination of intrinsic and doped a-Si:H to form a stacked layer design similar to SANYO HIT-like solar cells was examined in terms of surface passivation, *potential substitution* of the diffused emitter and Al-BSF layer technologies.

For a-Si:H(i/n) stacked heterostructures, S_{eff} as low as 5.5cms^{-1} has been reported here using 25nm a-Si:H(n) layers with 5nm a-Si:H(i) inter-layers, although, similarly low surface recombination has been shown for the range of a-Si:H(n) thicknesses tested. A notable improvement upon the results reported for thermally diffused and metallised-BSF. An average J_{oE} below 20fA/cm^2 (min of 8fA/cm^2) is given for this structure, a preliminary result surpassing those reported for a-SiC_x:H, SiN and SiO_x layers, and is reflected in calculation of the V_{oc}-limit, where values between 720mV and

740mV can be expected. Within reason, a $V_{oc} \approx 687$mV is achievable when using a-Si:H(i/n) as both a passivating and emitter layer.

The a-Si:H(i/p) stacked heterostructure demonstrated similar improvements in surface passivation with $\tau_{eff} \approx 1$ms ($S_{eff} < 10 cms^{-1}$) being reported. J_{oE} and V_{oc}-limit equivalent to that reported for SiN and SiO_x passivated diffused emitters has been shown here, demonstrating that substituting with a-Si:H(i/p) heterostructure deposited by ML-PECVD or standard PECVD on bare c-Si(n or p) can perform as does the diffused emitter or metallised BSF without high temperatures and more involved processing. For both a-Si:H(i/n) and a-Si:H(i/p) layers, $S_{eff} \leq 10 cms^{-1}$ ($min \approx 2.74 cms^{-1}$) are easily achievable, corresponding to J_{oE} below $20 fA/cm^2$ for the former, and as high as $60 fA/cm^2$. The V_{oc}-limit exhibited a slight decrease from 720mV when using 10nm inter-layers, to 650mV with 5nm inter-layers. Although many more results have been reported for a-Si:H heterostructures and hybrid designs on non-diffused c-Si, the n- and p-based heterostructure deposited in this work have shown a superior level of passivation quality on the non-diffused surface. The suppression of surface recombination remains excellent using these heterostructures indicating the stability of the 5nm and 10nm a-Si:H(i) inter-layers deposited by ML-PECVD in the presence of doped a-Si:H layers is not compromised. In all, no thermally diffused emitter, metallised BSF or other high temperature steps were required.

According to FTIR, the bond density, H%-content and the distribution of hydrides between the interface and bulk regions for both a-Si:H(i/n) and a-Si:H(i/p) stacked layers is consistent on both the c-Si(n) and c-Si(p) surfaces. Any shifts in passivation quality of these surfaces would then appear to be unrelated to the doping type and concentration of the c-Si wafer. It can be concluded that the quality of the intrinsic and doped a-Si:H layers deposited and annealed on the c-Si surface govern the passivation quality directly and results for a final device are largely determined by these a-Si:H layers.

In the final stage of this investigation, asymmetric a-Si:H heterostructures were deposited onto either side of n- and p-type c-Si wafers, with a-Si:H(i) inter-layers. Both BSF and emitter a-Si:H heterostructure layers were successfully deposited without contamination of either side and low S_{eff} ($<10 cms^{-1}$) and a J_{oE} of approximately $8 fA/cm^2$ has been shown. The V_{oc}-limits determined from J_{oE}, indicated that further improvements in surface passivation and charge collection by the a-Si:H heterostructures is achievable. in addition to enhancements in the ITO and Al layers. Upon sputtering and evaporation of ITO and Al layers, V_{oc} was measured. Assuming metallisation steps are optimised and no significant recombination losses are introduced into the fabrication of a complete

device it is logical to conclude that high conversion efficiencies, between 15% and 20%, are achievable using the a-Si:H heterostructures deposited in this work. Although improvements in surface passivation are indicated by using ML-PECVD a-Si:H heterostructures further experimentation is required. In both cases, the results of this study display an excellent agreement with the leading results for a-Si:H heterostructure based design and with SANYO's textured HIT cells.

5.

Surface Passivation of Multicrystalline Silicon Surface by a-Si:H Layers

Introduced in 1976, multicrystalline silicon (mc-Si) shares many of the properties of single crystalline silicon for photovoltaic applications without the high purity requirements [9, 238]. In photovoltaics, p-type mc-Si solar cells dominate the market despite the indications of high carrier lifetimes being exhibited by phosphorus doped n-type mc-Si. Indeed production of mc-Si(n) solar cells in industry is virtually non-existent, due to the relative inexperience with boron diffusions necessary to form emitter regions for such devices [239]. Although the conversion efficiencies of the either type of mc-Si solar cell typically remain below that of *float-zone* and *Cz*-grown devices, this result is mainly due to impurities located at the defects and grain boundaries acting as a recombination centres for photogenerated charge carriers. Progressive bulk passivation and impurity gettering processes [240] have led to conversion efficiencies up to 17.5% [241] and, more recently reported, 22.0% [242] in the laboratory.

For mc-Si wafers, the lower quality of the material, including recombination along grain boundaries, interstitial iron, structural strength and so on, are significant limitations to the use of this material in solar cell manufacture. Principally, the higher temperature steps and metallisation processes required can often introduce complications to the device structure leading to breakages and poor junction formation for thinner wafers. Additionally, the risk of impurities through high temperature processing and damage to mc-Si wafers have often meant passivation is carried out by depositing SiN_x by PECVD [17, 213, 243, 244] and metallisation through stress-inducing metal pastes. In many cases, the passivation of the mc-Si surface is secondary to reducing recombination within its bulk, thereby improving τ_b.

A number of novel techniques have been applied to the mc-Si solar cell the in hope of reducing the detrimental impact that high temperature processing has on the structural stress during metallisation [245] while maintaining passivation quality. Despite these improvements, many of the processes employed adhere to similar principles regarding design.

Alternatively, a different strategy is presented throughout this chapter for passivating the mc-Si surface and to form a junction with the mc-Si for charge collection absent of a diffused emitter or metallised BSF. Here, the a-Si:H(i) passivating layer and intrinsic/doped a-Si:H stacked layers are deposited and annealed onto the mc-Si surface at temperatures below 240°C. Three benefits of this are immediately:

- Relatively simple device structure design.
- The low temperature processes required for the a-Si:H stacked layers, below 250°C, limit stress within the mc-Si wafer and at the surface.
- Aluminium and ITO contact formation at low temperatures, below 300°C, are ideally suited to the a-Si:H layer, removing need for metallised pastes, and further reducing mechanical stresses on the mc-Si

Given the requirement for optimised contact formation, only the effectiveness of the surface passivation and potential device characteristics are assessed here. The use of the a-Si:H layer for this purpose represents the first known study regarding this material application in mc-Si solar cell devices.

5.1 Experimental preparation and procedure

The preparation of the mc-Si prior to deposition of a-Si:H is similar in many of the processes, as described earlier for *FZ* c-Si (see 2.1.2). However, some additional steps have been added to improve the initial quality of the mc-Si used throughout this chapter.

A consecutive series of 250μm thick 125mm x 125mm 1Ωcm mc-Si wafers from the mid-ingot, either p-type or n-type, are HF/HNO_3 damaged etched. This is followed by RCA cleaning, HF-dip and rinsing in deionised water until hydrophobic and dried by N_2 before being loaded into a tube furnace at 600°C. A phosphorus gettering of the mc-Si material for 30 minutes using $POCl_3$ is performed according to the thermal profile illustrated in Figure 69. This gettering step is extended for 5 hours at 700°C in N_2 before unloading.

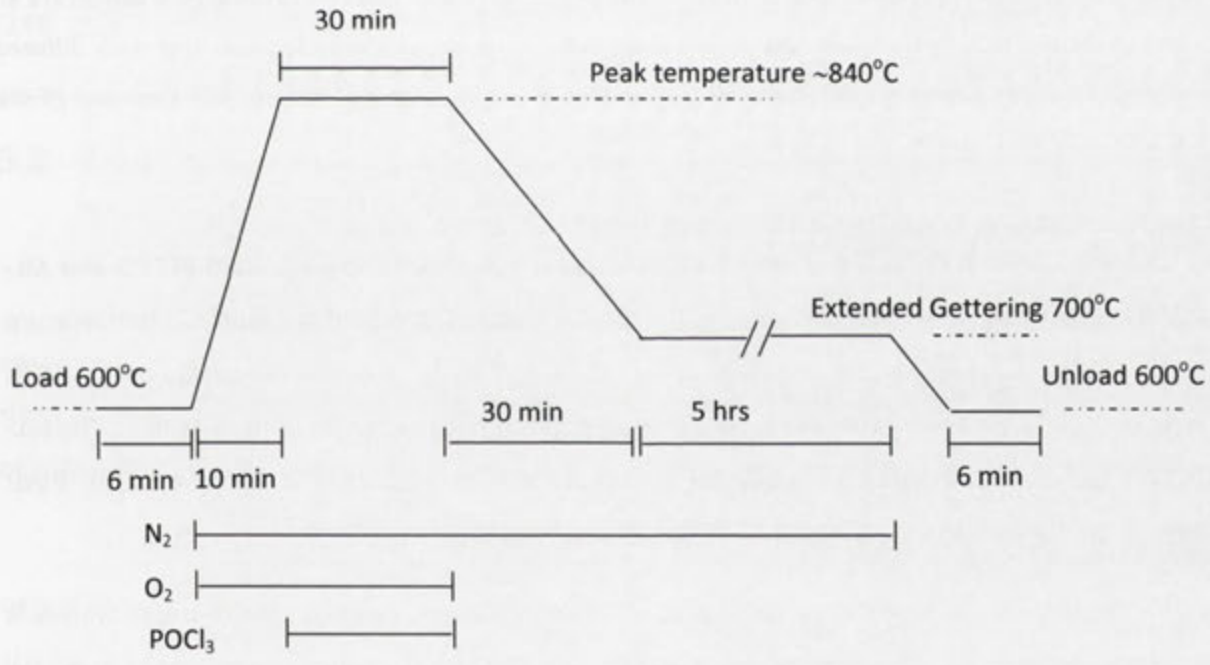

Figure 69: Thermal profile of $POCl_3$ extended gettering process

After gettering by phosphorus, all wafers were deglazed in 10% HF/DI-water solution followed by two additional acid etches; the first to remove the n^+ region; the second to reduce crystallographic dislocations at the mc-Si surface. These wafers are considered 'planar-like' compared to the starting mc-Si wafer surface. Between these two etching steps, the 125mm x 125mm wafers are divided into 12 smaller wafer pieces 35mm x 26m (see Figure 70). Adjacent

pieces, hence called wafers, which present the same grain orientation, are grouped together. An equal distribution of initial bulk lifetimes (τ_b) is assumed for each set of wafers. All wafers received a third and final RCA clean, HF-dip, DI-water rinse and N_2 dry before being loaded into the PECVD chamber and brought to high vacuum.

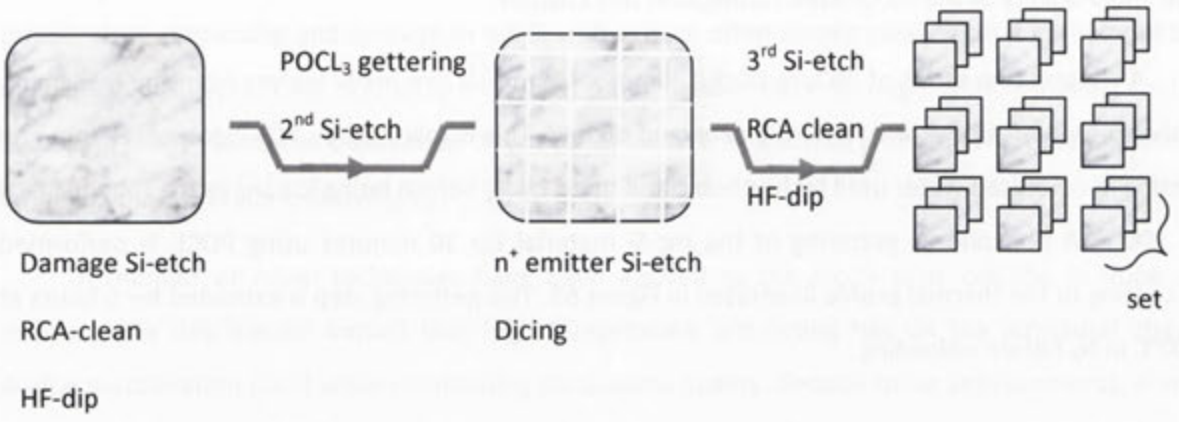

Figure 70: Pre-depositions processing steps for n- and p-type mc-Si wafers. 125 x 125mm mc-Si wafers are Si-damage etched, RCA-cleaned and HF-dipped before $POCl_3$ gettering in a tube furnace. Thermally diffused surface is removed, prior to dicing into smaller wafer sizes which undergo a 3rd etching, RCA-clean and HF-dip to reduce surface features.

Deposition of a-Si:H(i) and doped a-Si:H layers is completed using standard PECVD and ML-PECVD techniques. All depositions were at the ideal conditions identified in chapter 2; temperature 225 ± 4°C, partial pressure 650mT and *rf*-power 4W (52mW/cm^2). To assess the quality of the a-Si:H layer deposited, a *FZ* c-Si wafer was simultaneously deposited with each set of mc-Si wafers. The ML-PECVD technique was used primarily for the deposition of all 5nm and 10nm a-Si:H(i). Post-deposition thermal annealing was at 240°C for up to 1 hour.

The initial thickness of each wafer is approximately 180µm. However, the re-use of wafers is done by the etching of any previously deposited a-Si:H layer(s) to insure consistency in τ_b for measurements across depositions. This causes the thickness to reduce further by an average of 30µm. As the thickness of the mc-Si reduces to 96µm, the s_{eff} remains a useful parameter for comparisons between mc-Si wafers at different thicknesses, despite the lower quality of the bulk mc-Si material. Determining J_{oE} and the V_{oc}-limit is by the method described in section 4.2.4.

IR spectroscopy (FTIR and Raman) is again used to calculate the bond densities, hydrogen content, heterogeneity and degree of crystallinity of the a-Si:H layers deposited here. Photoluminescence imaging at 1 Sun using an 815nm laser has also been performed on a

representative sample of a-Si:H/mc-Si from this study to determine whether improvements in the carrier lifetime were due to the a-Si:H passivation, bulk hydrogenation or gettering alone. A detailed description of the photoluminescence technique is available in the references [246, 247].

5.1.1 Gettering to improve mc-Si

Reducing metal contamination is one of the most important aspects in the preparation of mc-Si wafers for use in solar cells and involves the effective removal of trace metals such as Iron which are contained within the material during formation [248]. Gettering using $POCl_3$ thermal diffusion is a common technique in the solar industry for removing and neutralising interstitial iron [Fe_i]. At temperatures above 700°C, [Fe_i] is soluble and precipitation towards the mc-Si n^+ diffused surface occurs, whereby, it can be removed when the top few µm are etched away. The gettering process (see Figure 51) has been reported to yield significant improvements in bulk lifetime for mc-Si wafers [249, 250].

5.2 Passivation of the n- and p-type multicrystalline surface by intrinsic a-Si:H

The optimised a-Si:H(i) layers were deposited to study the effectiveness of the layers to passivate both n-type and p-type mc-Si surfaces. Two deposition techniques are considered for a surface involving crystallographic dislocations; standard PECVD and ML-PECVD. Although the focus of this work is on a-Si:H(i) 25nm or less, a full range of thicknesses have been examined.

The effectiveness of the a-Si:H(i) layers of thicknesses between 5nm and 100nm deposited onto the 1Ωcm n- or p-type mc-Si surfaces is shown in Figure 71 in terms of τ_{eff} and S_{eff}. The results shown are following post-deposition thermal annealing at 240°C, although as-deposited τ_{eff} are also provided to illustrate the improved passivation achieved.

A significant improvement in passivation by both deposition techniques is clearly seen in Figure 71, particularly when thicknesses below 20nm are deposited. It is evident that a-Si:H, carefully deposited by either deposition technique is capable of passivating the dangling bonds at the mc-Si wafer surfaces simply, and at low temperatures. Here, the s_{eff} achieved may be considered a good response, comparable to other passivating materials.

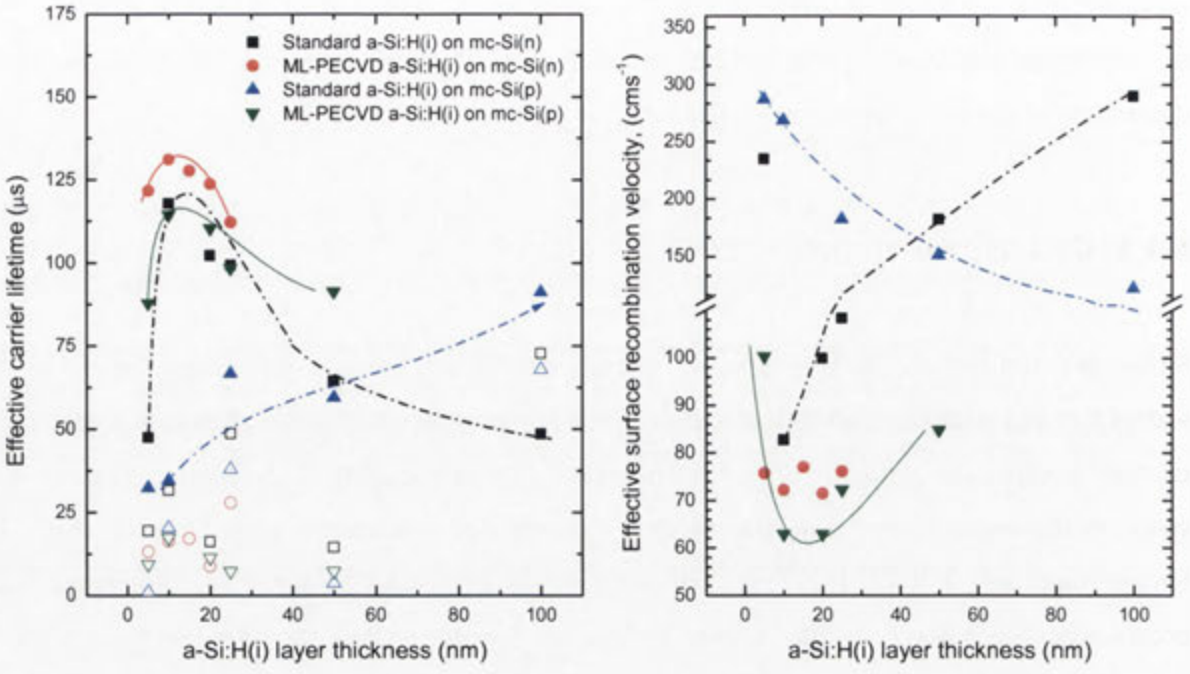

Figure 71: Passivation profile for n-type or p-type mc-Si deposited with either 5nm or 10nm a-Si:H(i) layers by standard PECVD or ML-PECVD at 225°C, 650mT and 4W applied. The calculated surface recombination velocity is given in b) to assist in comparing passivation quality for the mc-Si wafer thicknesses between 120μm and 180μm given.

Analysis of the results for passivation reliability of each deposition technique at different thicknesses for all 50 samples (i.e. 10 of each type) is provided in Figure 72. The ML-PECVD a-Si:H(i) layers appear to more successful in passivation, resulting either from improved coverage across crystallographic dislocations or improved quality of the layer itself, compared to those by standard PECVD. For a-Si:H(i)/mc-Si(n), a relatively consistent S_{eff} of 75cms^{-1} is achievable for a-Si:H(i) between 5nm and 25nm by MLPECVD.

Although S_{eff} = 80cms^{-1} could be achieved using a 10nm a-Si:H(i) layer deposited by standard PECVD, the deviation in the passivation results for a-Si:H(i) by this deposition technique were larger. This is apparent when considering that for thicker a-Si:H(i) layers deposited by standard PECVD, the passivation quality does not appear to improve. Although for SiN passivating layers any hydrogenation of the bulk m-Si via grain boundaries when using a-Si:H(i) layers remains unlikely and is addressed in section 5.2.2.

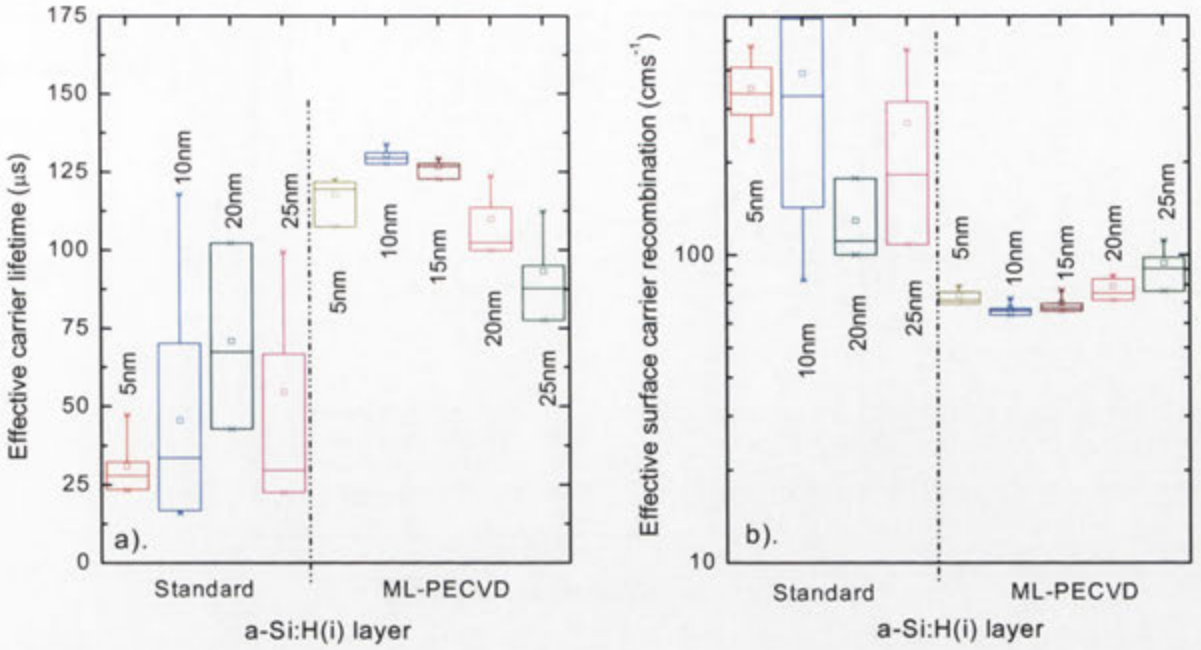

Figure 72: Reliability of surface passivation a). τ_{eff} and b). S_{eff}, for deposition of a-Si:H(i) layers onto mc-Si(n) wafers by standard PECVD and ML-PECVD.

Clearly for all a-Si:H(i) layers deposited onto the mc-Si surface, the ML-PECVD technique does achieve an improvement in the reliability of passivation quality and is most notable for thinner layers. It is therefore likely that the difficulty in coverage and passivation across crystallographic defects, is the mitigating factor in the surface passivation of mc-Si by a-Si:H(i) and not the quality of the a-Si:H(i) layer.

Therefore, two conclusions are made;

- Si:H(i) layers are suitable for passivating the n- or p-type mc-Si surface, and
- Layer thickness below 25nm is ideal in each case,
- with ML-PECVD proving a preferred choice for reliability and quality

Although no diffused emitter region is present, it is possible for estimate by calculation the likely implied V_{oc}-limit from J_{oE} according to the method described in section 4.2.4. The result for the ML-PECVD a-Si:H(i) layers on both n- and p-type mc-Si is given in Figure 73.

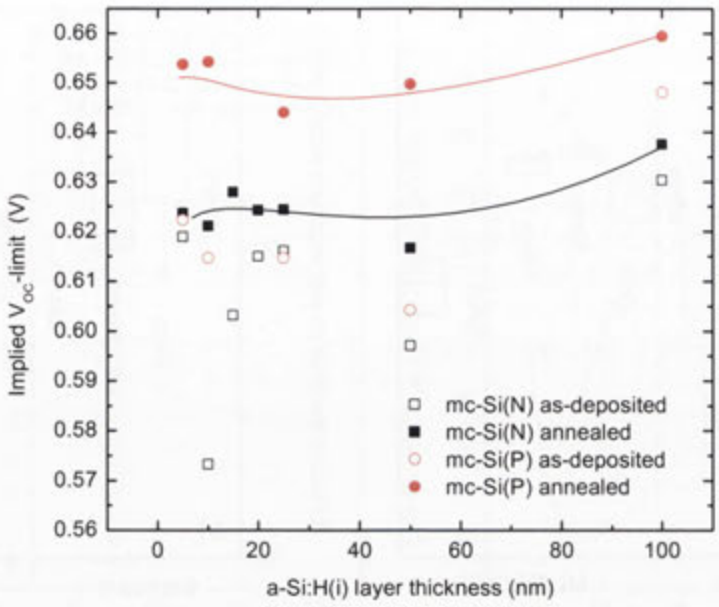

Figure 73: Implied V_{oc} of 1Ωcm n- and p-type mc-Si wafers passivated with a-Si:H(i) ML-PECVD layers between 5nm and 100nm thick. Lines are guide for eye.

A high V_{oc}-limit using ML-PECVD a-Si:H(i) layers deposited and annealed on either the n-type or p-type mc-Si surfaces following post-deposition thermal annealing. There appears to be no dependence on the thickness of the layer, and provided the mc-Si surface is suitably passivated the additional thickness of the a-Si:H(i) may only serve to improve the robustness of the a-Si:H(i) layer.

In context to the more common passivation schemes using SiN, the a-Si:H(i) layers deposited in this work onto the mc-Si surface appear to demonstrate a similar proficiency in passivation efficacy using lower temperatures. Indeed, Schmidt *et. al.* reported V_{oc}-limits approximating 655mV on comparable mc-Si using silicon-rich SiN and process temperatures in excess of 400°C [17].

5.2.1 IR spectroscopy of a-Si:H(i) on the mc-Si surface

Although the a-Si:H(i) layers deposited in this chapter are similar to those in previous chapters, this work represents the first reported application of a-Si:H(i) to passivating the mc-Si surface. Therefore, it is prudent to consider the influence that the crystallographic dislocations at the mc-Si surface may have upon the hydride composition of the a-Si:H(i). Results for both ML-PECVD and standard PECVD layers are given to determine what, if any, differentiation may occur for the mc-Si surface. The mc-Si dopant type is not likely to influence the a-Si:H structure or composition. The

FTIR spectra for 5nm to 15nm a-Si:H(i) layers deposited by both techniques onto the mc-Si(n) wafer surface are given in Figure 74.

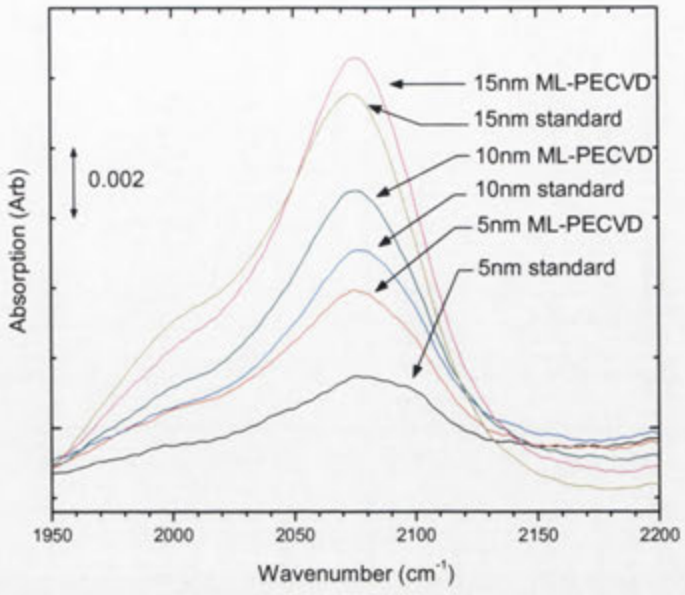

Figure 74: Profile of FTIR hydride spectra between 1950cm^{-1} and 2200cm^{-1} of both standard PECVD and ML-PECVD a-Si:H(i) layers between 5nm and 15nm thick deposited onto mc-Si(n) wafers.

For both standard PECVD and ML-PECVD, the bulk monohydride (2000cm^{-1}) and interface monohydride (2080cm^{-1}) peaks are both clearly visible, and in agreement with the good passivation quality reported for these layers (see Figure 71). For each thickness shown, the ML-PECVD a-Si:H(i) layers have higher absorbance's in the 2070-2085cm^{-1} band, describing a higher density of interface monohydride, compared to those by standard PECVD. The increased presence of SiH_2 (2090 - 2100cm^{-1}) for 5nm a-Si:H(i) by standard PECVD, not seen on the *FZ* c-Si surface (see Figure 13) infers that the first few monolayers are most affected by the mc-Si surface.

To consider this further, the FTIR calculation of bond densities, H% content and heterogeneity are provided in Figure 75 for the a-Si:H(i)/mc-Si(n) in this work.

An increase in the total hydride bond density occurs for thicker a-Si:H(i) in-line with increases reported previously on the bulk hydrides for ML-PECVD layers. Minor improvements in the interface density are also observed, consistent with the sub-surface displacement growth process which improves packing density. Consequently, the H% content increases for a similar range as reported previously for a-Si:H(i) on *FZ* c-Si.

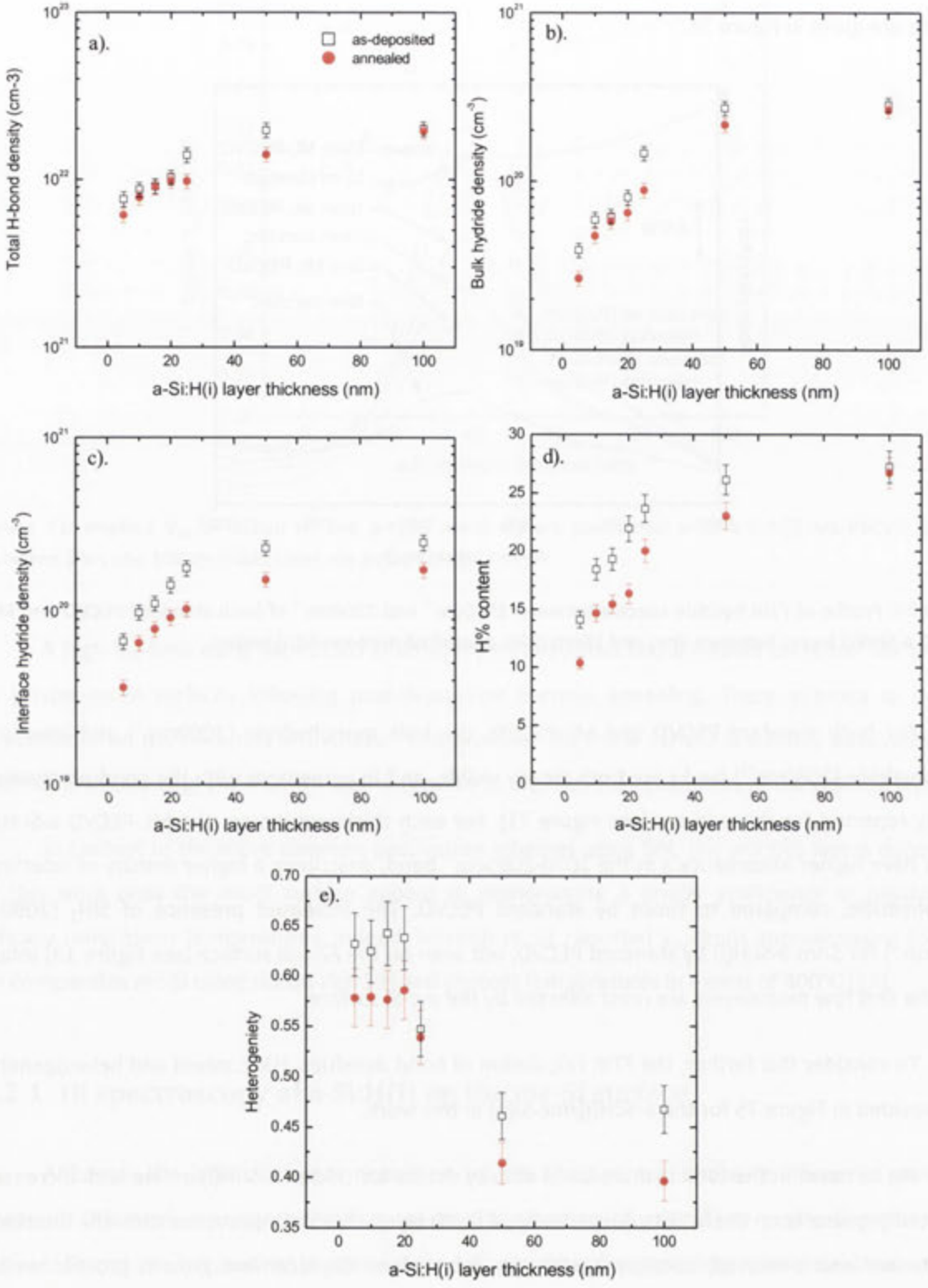

Figure 75: As-deposited and post-deposition thermal anneal FTIR measurements of a). total H-bond density, b). bulk hydride bond density, c.) interface hydride bond density, d). H% content, and e). Heterogeneity of a-S:H(i) layers deposited by ML-PECVD onto mc-Si(n) wafers. The interface region is within the a-Si:H(i) layer.

The marginally higher monohydride bond densities at the interface and within the bulk for ML-PECVD a-Si:H(i) layers compared to those by measured for standard PECVD may be indicative of both the sub-surface ion displacement[11] occurring with each new sub-layer deposition in ML-PECVD and repacking during thermal cycling[12]. Both would yield further improvements in the quality of the a-Si:H layer. If sub-surface ion-assisted growth by displacement is occurring, then rapid increases within the first few nanometres of a-Si:H(i) would occur for interface and bulk hydride densities. This is observed in Figure 75b/c. Despite the bulk SiH density being high, any hydrogen would be expected to remain relatively immobile in a relaxed a-Si:H network for temperatures below 300°C.

Calculation of heterogeneity shows that hydrides at the mc-Si surface and near-interface region are dominant in both deposition techniques for a-Si:H(i) layers of 20nm thickness and less. However, the ratio of interface to bulk monohydride shifts sharply from 0.65 to below 0.5 for thicker layers. This shift of monohydride towards the bulk region correlates with decreases in the surface passivation quality. It remains unknown at this stage what the causes this shift, given that hydrogen effusion to the bulk region is not likely while heterogeneity remains above 0.3. While a degree of uncertainty, approximately 10%, occurs as part of the hydride bond density determination by FTIR, a clear trend is apparent in the thickness of the a-Si:H(i) layer by ML-PECVD and by standard PECVD on the mc-Si surface.

Certainly, it appears that a-Si:H(i) layers deposited by the ML-PECVD method are superior in both passivation quality and interface hydride density compared to the standard PECVD a-Si:H(i) layers. This is not to say that standard PECVD is not suitable for a-Si:H deposition onto mc-Si for the purpose of surface passivation. The ML-PECVD technique offers a superior level of fine control over the deposition of thin a-Si:H(i), and its use is warranted for 5nm a-Si:H(i) layers. The importance of this technique will be discussed further for stacked a-Si:H layers in section 5.3.

[11] Sub-surface ion assisted growth by displacement occurs when ions impinging the growing a-Si:H layer are able to abstract hydrogen from the first 2-3 monolayers which are in various non-optimal configurations in the packing order. This effectively makes available a bond for a suitable hydrogen configuration.

[12] Thermal cycling occurs during ML-PECVD of sub-layers as the substrate is cooled to below 120°C then reheated to deposition temperature of 225°C for the next sub-layer. As shown in chapter 3, thermal annealing does not show any significant increases in hydride density (i.e. no new bonds are formed). Repacking reduces network stress in the deposited a-Si:H layers.

5.2.2 The limitation of bulk hydrogenation of mc-Si by a-Si:H

Compared to *FZ* c-Si wafers, the mc-Si wafers are of lower quality, and as such the bulk carrier lifetime is also lower. Hydrogenation of the mc-Si bulk is one process frequently utilised to improve bulk carrier lifetime. In this, hydrogen, usually from the SiN layer, is diffused through the mc-Si surface and into the mc-Si bulk during high temperature annealing to passivate defects within the wafer [8, 243, 251-253]. Typically, hydrogenation of the mc-Si bulk is often completed during a firing process at temperatures of 700°C and above. While this has obvious complications regarding thermal degradation of the mc-Si material, particularly at the top and bottom of the ingot where interstitial iron concentration is highest, it also raises the question of hydrogenation at lower temperatures.

For a-Si:H(i), the significantly lower process temperatures, below 300°C, have been shown in chapter 3 to limit hydrogen mobility to a few nanometres within the a-Si:H layer. Although, hydrogen is capable of surface diffusion at low temperatures (i.e. 140°C-300°C), the likelihood of hydrogen migration to the mc-Si bulk from the a-Si:H(i) layer is not known. Any significant migration of the hydrogen into the mc-Si bulk itself is likely to be observed by improvements in the bulk carrier lifetime directly, with the improvement in bulk carrier lifetime influencing (through QSSPC measurements) the effective carrier lifetime. Therefore, for this purpose, photoluminescence imaging of mc-Si wafers passivated and annealed with 5nm and 10nm a-Si:H(i) layers is presented in Figure 76.

As shown, hydrogenation of the mc-Si bulk appears negligible for both as-deposited and thermally annealed a-Si:H(i)/mc-Si samples, despite improvements in the measured effective carrier lifetime. It is therefore unlikely that hydrogen migration from the a-Si:H(i) layer is occurring at these temperatures. Although some isolated regions show some enhancement, this would not account for the improvements in overall surface passivation for all wafers deposited by a-Si:H(i), and it may be assumed that these areas result from a feature corresponding to the surface instead.

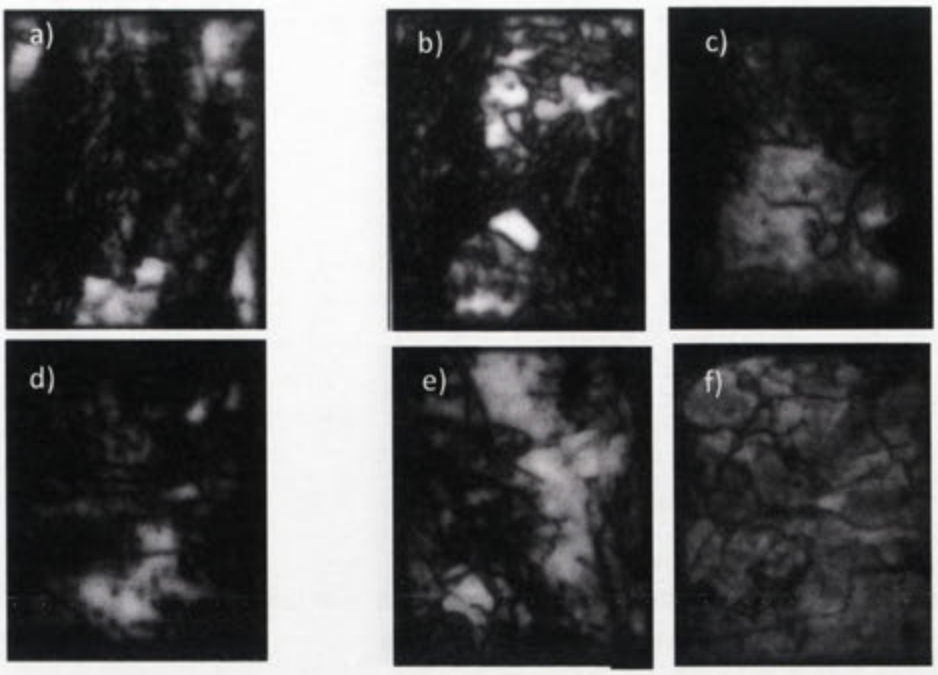

Figure 76: Photoluminescence imaging of mid-ingot 35 x 26mm mc-Si(n) wafers with 5nm and 10nm a-Si:H(i) layers deposited by ML-PECVD. Images are for a). 5nm as-deposited, b). 5nm annealed d). 10nm as-deposited, e). 10nm annealed. Both c/f). are sourced from a different part of the wafer and annealed, respectively.

To understand the lack of hydrogenation of the mc-Si bulk and its significance for the use of a-Si:H(i) layers, the diffusivity of hydrogen (D_H) and the solubility of hydrogen (K_H) at both high and low process temperatures is considered. In the high temperature region, D_H can be determined according to equation (5- 1). This was originally derived for diffusivity at high temperatures by Van Wieringen and Warmoltz in 1956 [210] and has been commonly assumed until the present day to be the case for all temperatures [254]. However, according to the work discussed in chapter 3 a more realistic approximation for D_H at lower temperatures is given by equation (5- 2) which is likely a more accurate appraisal of hydrogen diffusivity for temperatures up to 350°C. In Figure 77, a comparison of the two approximations is given in terms of process temperature.

$$D_H = 9.4\times10^{-4}\exp^{0.48eV/kT} \quad (5\text{- }1)$$

$$D_H = 5\times10^{-3}\exp^{0.3eV/kT} \quad (5\text{- }2)$$

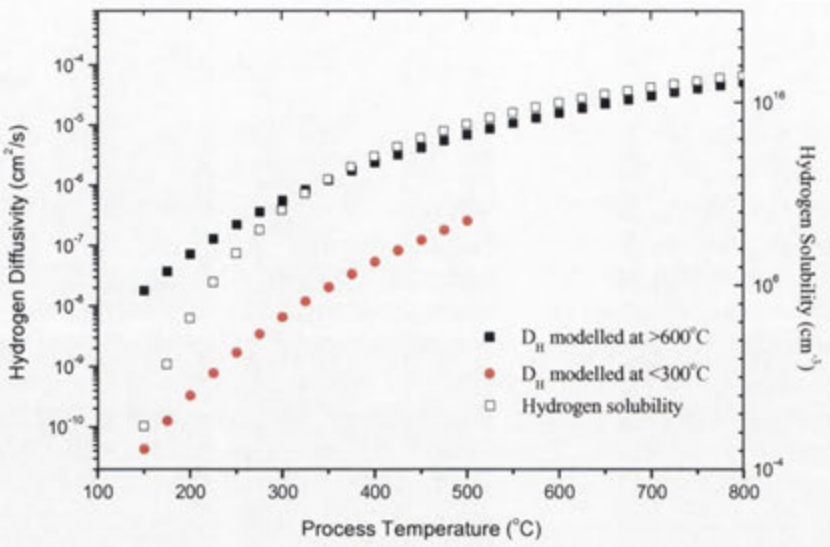

Figure 77: Diffusivity and solubility of Hydrogen at temperatures ≥600°C calculated from Equation (5.1). The change in D_H is also shown for temperatures ≤ 350°C (chapter 3).

According to the standard approximation in equation (5- 1), the diffusion of hydrogen rapidly decreases as temperature is lowered. This is consistent with experimental observations for temperatures down to 500°C [250, 255-257], indicative of hydrogen becoming increasingly trapped within the mc-Si bulk. However, using the approximation given by equation (5- 2) from the work here, the previously unknown mobility for quasi-bonded hydrogen at lower temperatures is accounted for. From this, the diffusion of hydrogen in mc-Si for T < 300°C would be far less than previously thought; below $10^{-7}cm^2s^{-1}$ at temperatures below 400°C. Although not shown in Figure 77, the approximation in this work does exhibit some agreement with the standard estimate for higher temperatures (i.e. T > 650°C).

Also shown in Figure 77 is the solubility of hydrogen, according to the mobility of hydrogen, as a function of process temperature [210, 258, 259]. At high temperatures, above 600°C, the solubility of hydrogen is $9.6 \times 10^{15}cm^{-3}$, consistent with firing temperatures used in mc-Si bulk hydrogenation with SiN layers. As the temperature is decreased, the solubility also decreases, gradually at first then rapidly at temperatures below 350°C. For process temperatures of a-Si:H layers, (i.e. ≤250°C) this value is $6 \times 10^{6}cm^{-3}$. From this, it may be surmised that the ability of hydrogen to migrate into the mc-Si bulk from the surface is limited to temperatures above 450°C. Subsequently, thermal processes including annealing and metallisation are very unlikely to cause hydrogenation of the mc-Si bulk, and as such, any improvement in carrier lifetime is a result of surface passivation only. For mc-Si wafers sourced from the top and bottom of the ingot, a-Si:H passivation may be of some benefit since interstitial iron at the lower process temperatures is less problematic.

5.3 Passivation of mc-Si surface with intrinsic/doped a-Si:H stacked layers

In chapter 4, intrinsic/doped a-Si:H stacked layers were shown to effectively passivate the *FZ* c-Si surface, reducing current density at the a-Si:H/c-Si interface without a n^+ emitter or Al-BSF; essentially replacing the need for the diffused emitter and Al-BSF in a final device. Here for the first time, the a-Si:H stacked layer design as applied to the mc-Si surface, is investigated and discussed. In each case, no diffused emitter region or metallised BSF layer is utilised, and the effect that the crystallographic dislocations have upon the a-Si:H(i)/a-Si:H(doped) structure is reported here for the first time.

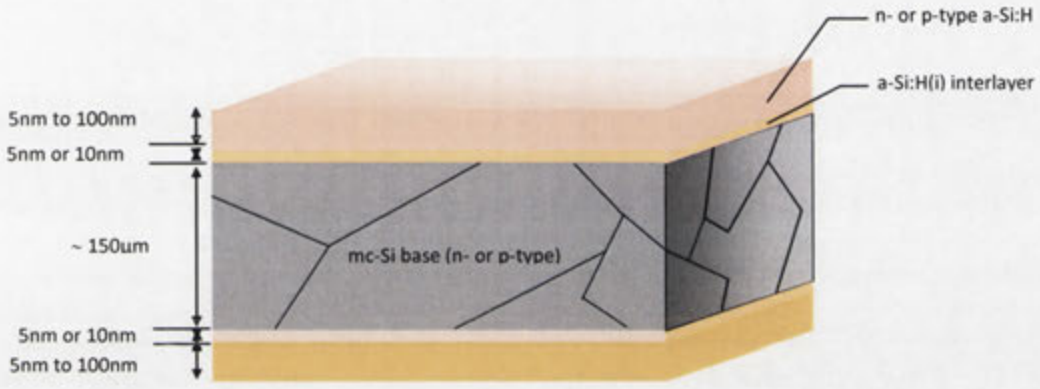

Figure 78: A schematic of a bifacial a-Si:H heterostructure consisting of an intrinsic inter-layer deposited by ML-PECVD onto a mc-Si surface followed by either a layer of n- or p-type a-Si:H. The same stacked layer structure deposited on both sides.

An illustration of the intrinsic/doped a-Si:H layer is given in Figure 78. Both ML-PECVD and standard deposition of a-Si:H layers are undertaken for comparison of the two techniques. All depositions are at 225°C, 650mT and 4W applied *rf*-power. Thermal annealing at 240°C, following deposition of the layers to improve as-deposited passivation, is standard.

Three structures are considered in the following sections:

- a-Si:H(n)/ a-Si:H(i)/mc-Si/ a-Si:H(i)/ a-Si:H,
- a-Si:H(p)/ a-Si:H(i)/mc(n)/ a-Si:H(i)/ a-Si:H(p), and
- a-Si:H (p)/ a-Si:H(i)/mc-Si(n)/ a-Si:H(i)/ a-Si:H(n)

5.3.1 Bifacial a-Si:H(i/n) stacks on n-type mc-Si

Firstly, the bifacial deposition of a-Si:H(i/n) on the mc-Si(n) is considered. In Figure 79, for thinner a-Si:H(n) layers, higher τ_{eff} is achieved using ML-PECVD a-Si:H(i) inter-layer than those by standard PECVD, although this difference is negligible for a-Si:H(n) layer thicknesses above 60nm.

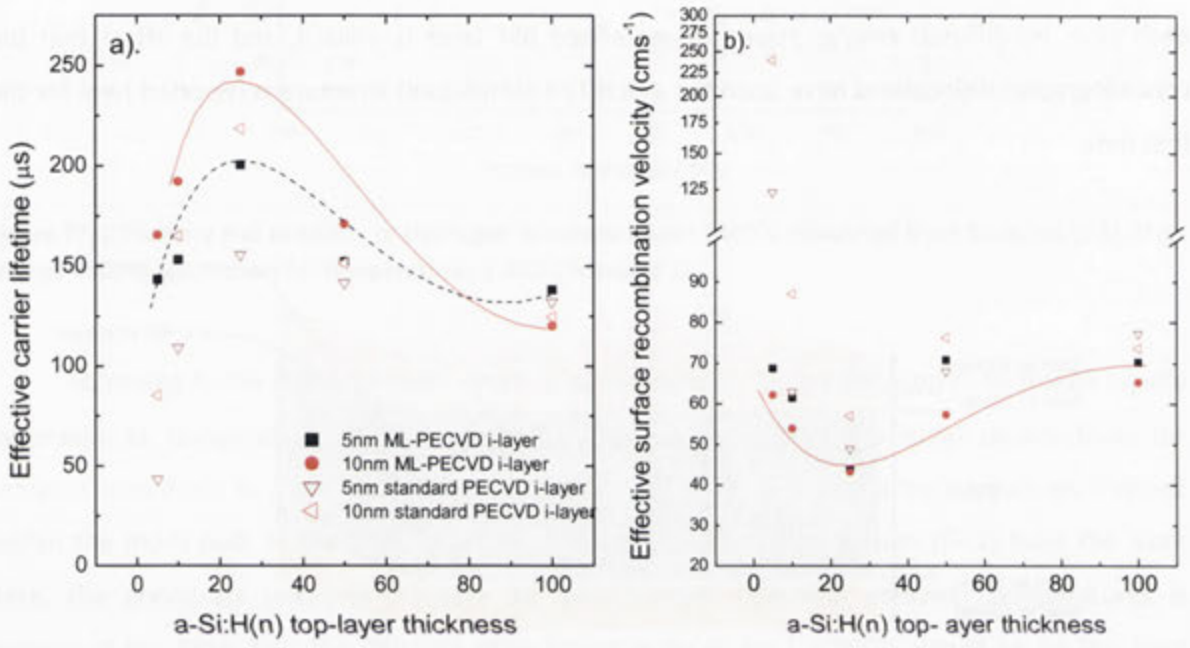

Figure 79: Passivation quality profile for bare, 1Ωcm mc-Si(n) bifacially deposited with a-Si:H(i/n) in terms of both measured τ_{eff} and calculated S_{eff} according to the a-Si:H(n) layer thickness. The a-Si:H(i) inter-layer thickness is 5nm or 10nm.

The best surface passivation, from both τ_{eff} and S_{eff}, can be seen to occur for a-Si:H(i/n) stacked layers using a 25nm a-Si:H(n) layer. The relatively low S_{eff} of 41cms^{-1} according to the thickness of the stacked layer demonstrates that a significant surface passivation of the mc-Si surface does is achievable using a-Si:H. The reliability of the passivation achievable using a-Si:H(i/n) stacked layers by either deposition technique is given in Figure 80. Similar results are achievable using both deposition techniques; however, those layers deposited by ML-PECVD demonstrate a distinct improvement in obtaining consistently good passivation of the mc-Si surface.

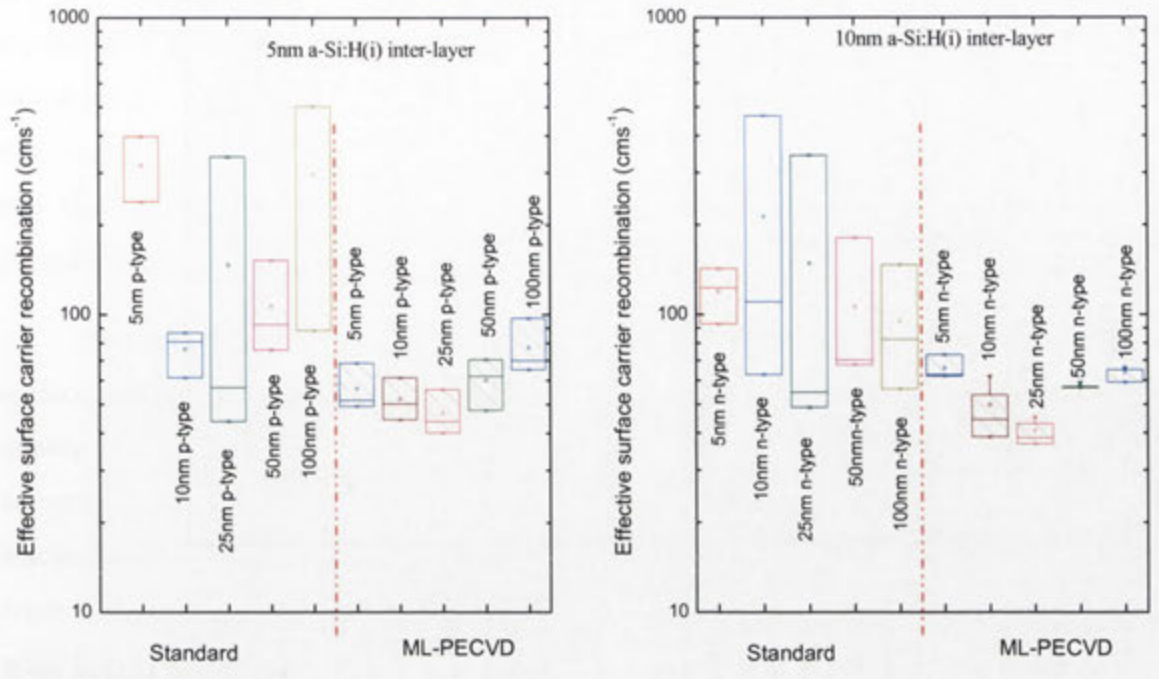

Figure 80: Reliability of mc-Si(n) surface passivation a). τ_{eff} and b). S_{eff}, for deposition of a-Si:H(i/n) stacked layers by standard PECVD and ML-PECVD. The population size of each thickness is 25 samples, for both deposition techniques.

The higher τ_{eff} measured for mc-Si(n) using a-Si:H(i/n) stacked layers compared with a-Si:H(i) alone (see section 5.2) indicates that improvements in reducing current density at the mc-Si surface occur in the presence of a a-Si:H(n) layer. In Figure 81, the influence of the a-Si:H(n) layer thickness for the a-Si:H(i/n) stacked layer reveals that J_{oE} improves when thicknesses similar to the a-Si:H(i) inter-layer and above are deposited. This improvement is greatest for layers deposited by ML-PECVD and appears to be best achieved using the 10nm a-Si:H(i) inter-layer and a 25nm a-Si:H(n). Although, it is also evident that a thicker a-Si:H(n) layer, up to 100nm, does not compromise the a-Si:H(i) inter-layer or is less effective in reducing current density at the interface. These results are comparable to that of Schmidt *et. al.* [17], in which optimised SiO_2/SiN stacks and alnealed SiO_2 onto p-type mc-Si with n^+ emitter sheet resistances between 20Ω/□ and 15Ω/□.

The implied V_{oc}-limit for the above bifacial a-Si:H(n)/a-Si(i)/mc-Si(n) structure is given in Figure 82. For a-Si:H layer deposited by ML-PECVD a limit between 660mV and 700mV is indicated, likely a result of improvements in the a-Si:H(i) inter-layer at the mc-Si surface. For a-Si:H(i/n) layers, with 10nm layers, the value for V_{oc}-limit appears to reach a maximum. It is likely, that with improvements in the τ_b of the mc-Si wafer, further increases in the achievable V_{oc} would be likely.

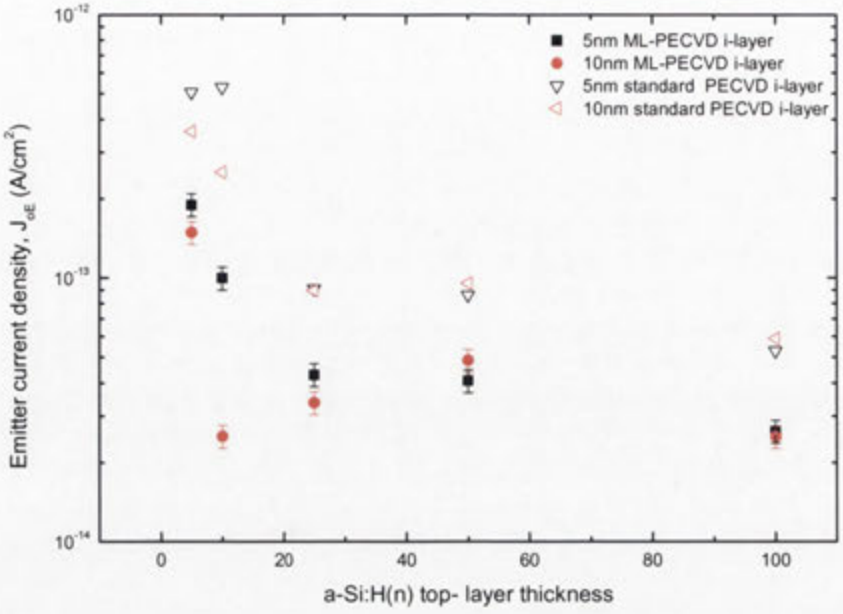

Figure 81: Influence of the a-Si:H(n) layer thickness on reducing J_{oE} at a single, non-diffused 1.0Ωcm mc-Si surface when deposited with a-Si:H(i/n) stacked layers by standard PECVD or ML-PECVD. Heterostructures consist of 5nm or 10nm a-Si:H(i) inter-layer and a-Si:H(n) emitter layers between 5nm and 100nm thick.

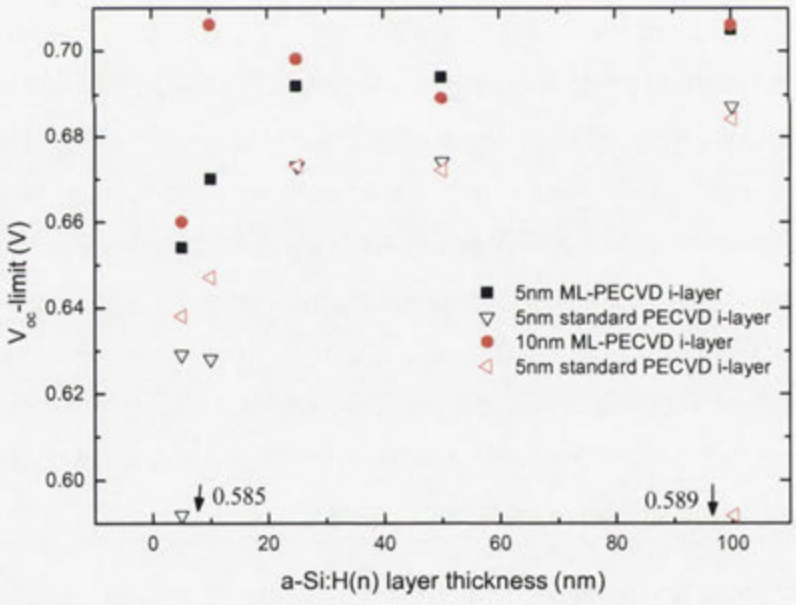

Figure 82: Implied-V_{oc} for non-diffused 1Ωcm mc-Si(n) wafers deposited with a-Si:H(i/n) stacked layers deposited by standard PECVD and ML-PECVD. Mc-Si wafer thickness is approximately 150μm.

The relatively high calculated limit for V_{oc} demonstrates two important aspects; that the a-Si:H(i) inter-layer performs well as a passivating layer for the mc-Si surface; and as a barrier layer

between the mc-Si(n) and the a-Si:H(n) layer, both in the presence of crystallographic dislocations on the mc-Si(n) surface. For this reason, a 25nm a-Si:H stacked layer with either a 5nm/10nm a-Si:H(i) is suited to both passivate and perform as a back-surface field for mc-Si(n) devices. The simplicity of this stacked a-Si:H layer design in achieving relatively good τ_{eff} and S_{eff}, significant reductions in J_{oE} and likely good V_{oc}, formed at low temperatures. This is an attractive option to using an n^+ phosphorus diffused region at the back of n-type cells.

Although, it remains unclear as to the influence crystallographic dislocations at the mc-Si surface are likely to have on the composition and distribution of the layers it is known that the quality of the a-Si:H layers are primarily determined by the PECVD technique, deposition and annealing conditions. In understanding the effect the mc-Si surface has upon the a-Si:H(i)/a-Si:H(n) stacked layer composition, the FTIR spectroscopy hydride bond analysis is presented in Figure 83. From FTIR, the total hydride density is shown to remain consistent with results given earlier for the a-Si:H(i) only layers. A 1% increase is observed when a-Si:H(n) is added to the a-Si:H(i) as expected for n-type a-Si:H. As there is little difference in the total hydrogen bonded within the thin-film layers, any improvement in the surface passivation is unlikely to have occurred from additional hydrogen into a-Si:H(i)/mc-Si(n) interface region.

The sharp increase in the H%-content observed in Figure 83d does not yield any improvement in surface passivation, as often misinterpreted, and is simply an artefact of the a-Si:H(n) bulk with increased optical absorption and IR multiple passes. Even so, this likely indicates a defined interface existing between the a-Si:H(n) layer and the a-Si:H(i) interface region. As a-Si:H(n) has little influence on the mc-Si passivation, the evident 'drop-off' may offer some additional information concerning the a-Si:H layers and the mc-Si surface.

Comparing Figure 83 to surface passivation in Figure 80, where 20nm thick a-Si:H(n) layers appear to achieve the best and most consistent results, a layer with mid-range hydride densities. If a two layer structure is considered, where two interfaces and two a-Si:H regions occur, hydride densities in this range continue to be ideal, and the a-Si:H(n) bulk does not compromise the thinner a-Si:H(i) hydride distribution, which remains at the mc-Si interface. This may also help us understand how the surface passivation and heterojunction formation over crystallographic dislocations relates to the surface coverage of the mc-Si surface

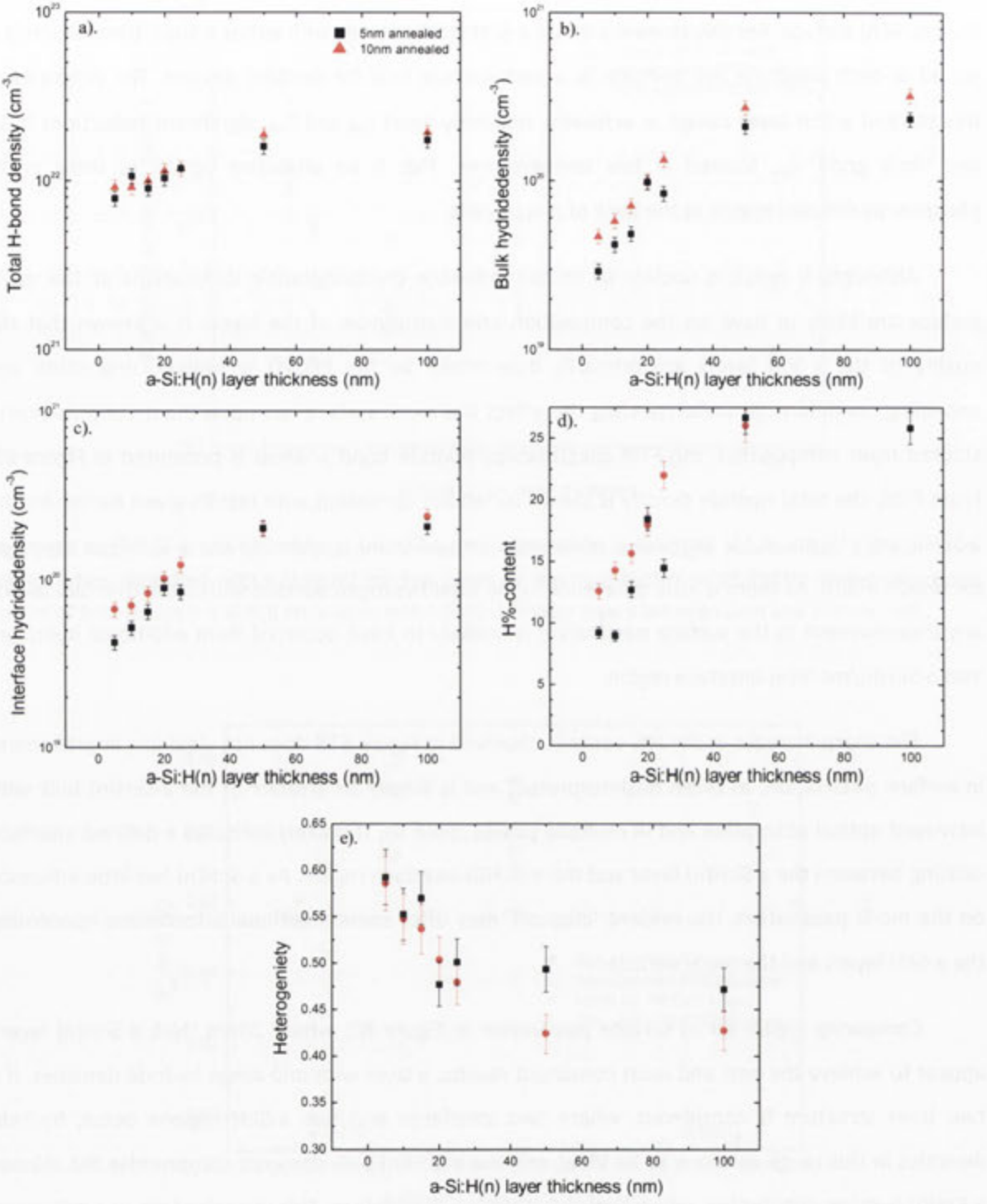

Figure 83: IR hydride bond density results a). Total bond density, b). Bulk monohydride, c). Interface monohydride densities, d). Hydrogen % content, e). Heterogeneity for a-Si:H(i/n) stacked layer of different thicknesses on bare 1.0Ωcm mc-Si(n) and annealed at 240°C for 40 minutes.

Previous studies concerning the interface between a-Si:H(i) and the rough c-Si surface have shown that rough interfaces can occur [64, 110], and would be increasingly problematic for

deposition of the doped a-Si:H layer in a HIT-like design on a mc-Si surface. Here, it has been shown that the a-Si:H(i)/a-Si:H(n) interface exists over a defined area of a few nanometres, and not as an extended gradient compromising the a-Si:H(i) layer nearer to the interface with mc-Si(n). ML-PECVD of the first few nanometres of each a-Si:H layer in this case would provide greater control in the quality of the two interface regions.

5.3.2 Bifacial a-Si:H(i/p) stacks on n-type mc-Si

To fabricate a functional bifacial mc-Si solar cell using a-Si:H stacked layers, high quality passivation of the mc-Si surface and possible formation of an emitter using an a-Si:H(p) layer is required. As in the previous section, the mc-Si surface is deposited bifacially with a-Si:H(i) inter-layers between 5nm and 10nm, followed by an a-Si:H(p) layer between 5nm and 100nm. The 1Ωcm mc-Si(n) wafers here averaged 120μm in thickness, following all Si-etch, RCA cleaning and gettering steps. The mc-Si(n) wafer surfaces remained bare (i.e. no diffused emitter was present).

Shown in Figure 84 is the profile for passivating the mc-Si(n) surface using a-Si:H(i/p) stacked layers according to the a-Si:(p) layer thickness. The highest measurement for τ_{eff} was achieved when thinner a-Si:H(p) layers, with thicknesses between 5nm and 25nm were deposited onto the a-Si:H(i) inter-layer, although good passivation results are also achievable for thicker doped layers. There is no indication that the lower defect density of the a-Si:H(p) compared to a-Si:H(n) influences the passivation results here. Surface recombination of the a-Si:H(p)/a-Si:H(i)/mc-Si(n) structure increases from 45cms^{-1} to 65cms^{-1} as the layer thickness increases from 5nm to 100nm. A similar response occurs for stacked layers with a 10nm a-Si:H(i) inter-layer. It is apparent that the a-Si:H(i) inter-layer is a suitable barrier separating the a-Si:H(p) layer from the mc-Si surface, and the performance is not compromised by the presence of this layer.

Notably, the passivation response for mc-Si(n) by a-Si:H(i/p) achieved at temperatures below 250°C, compares well with other passivation materials previously discussed in chapter 4 including SiN deposited by PECVD at temperatures of 400°C and above.

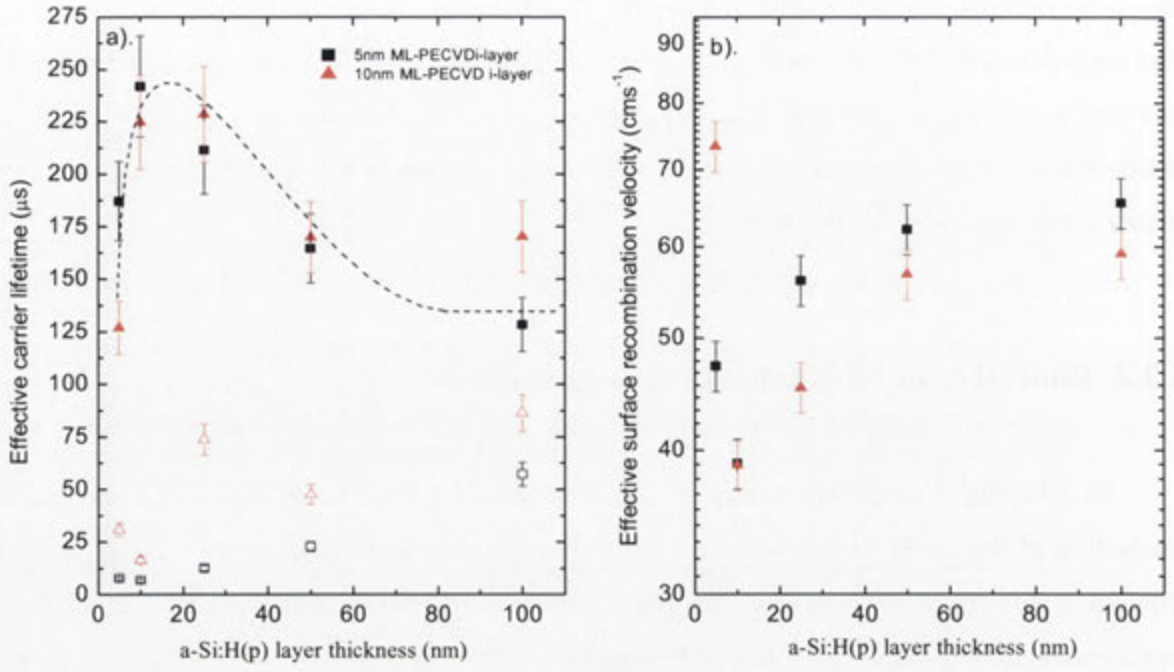

Figure 84: Passivation quality profile for bare, 1Ωcm mc-Si(n) bifacially deposited with a-Si:H(i/p) in terms of both measured τ_{eff} and calculated S_{eff} according to the a-Si:H(p) layer thickness. The a-Si:H(i) inter-layer thickness is 5nm or 10nm.

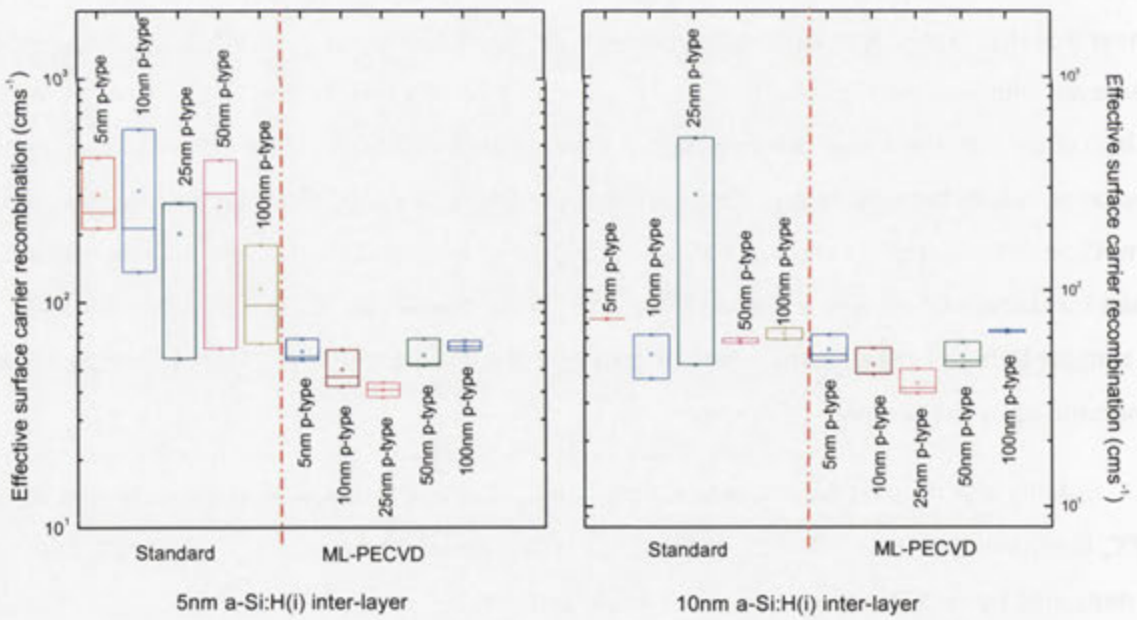

Figure 85: Reliability of mc-Si(n) surface passivation a). τ_{eff} and b). S_{eff}, for deposition of a-Si:H(i/p) stacked layers by standard PECVD and ML-PECVD. The population size of each thickness is 25, for both deposition techniques.

The reliability in achieving good, high-quality passivation of the mc-Si(n) surface by either PECVD or ML-PECVD deposited a-Si:H(i/p) stacked layers is shown in Figure 85. As in the previous section, the recombination velocity is observed to be consistently lower using the ML-PECVD technique. Indeed a significant improvement can be observed between the two deposition methods for this stacked layer design.

In Figure 86, the J_{oE} achieved, using different a-Si:H(p) thicknesses in the heterostructure stack, is given.

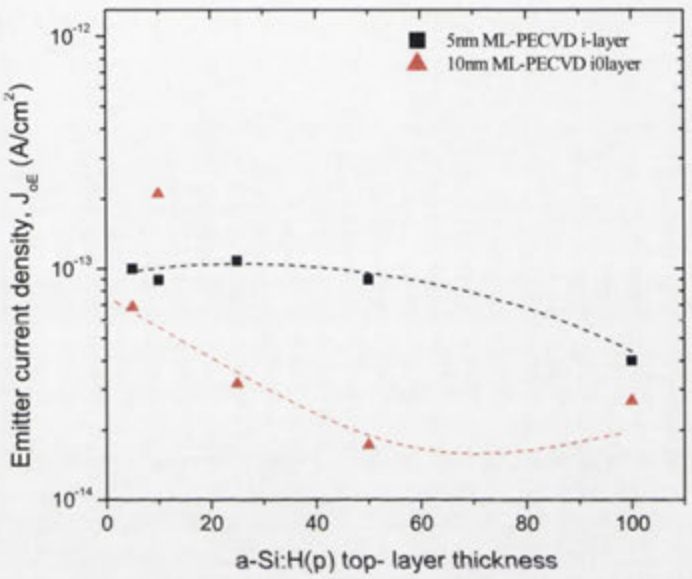

Figure 86: Influence of the a-Si:H(p) layer thickness on reducing J_{oE} at a single, non-diffused 1.0Ωcm mc-Si surface when deposited with a-Si:H(i/p) stacked layers by standard PECVD or ML-PECVD. Heterostructures consist of 5nm or 10nm a-Si:H(i) inter-layer and a-Si:H(p) emitter layers between 5nm and 100nm thick.

The significant difference between using 5nm or 10nm a-Si:H(i) inter-layers for a-Si:H(p) above 50nm suggests that the a-Si:H(p) layer itself may be influencing the mc-Si interface here, perhaps by reducing charge carriers at the mc-Si surface. Here, low J_{oE}, below $1x10^{-13}Acm^{-2}$ for a-Si:H(i/p) heterostructure stacks occurs, decreasing for thicker doped layers. The influence of the a-Si:H(p) thickness is most noticeable when a 10nm a-Si:H(i) inter-layer is used instead of a 5nm a-Si:H(i) one. Indeed J_{oE} as low as $20fAcm^{-2}$ are achievable for the thicker a-Si:H(p) on this inter-layer thickness, suggesting that the doped layer does reduce charge density at the a-Si:H(i)/mc-Si interface. As the a-Si:H(i) layer is slightly n-type compared to the a-Si:H(p) layer, the effect of a thicker inter-layer may likely enhance any influence on the interface, although this remains unclear.

In the V_{oc}-limits shown in Figure 87, a higher result is achieved using a 10nm a-Si:H(i) with a thicker a-Si:H(p) layer approximately 50nm thick is observed, although similar results are calculated for other thicknesses. For the 5nm a-Si:H(i) inter-layer with a-Si:H(p) a V_{oc}-limit of 675mV was determined, and a higher value of 710mV using the 10nm a-Si:H(i) inter-layer. Further testing in this stacked layer design is likely to yield improvements in the maximum V_{oc} achieved.

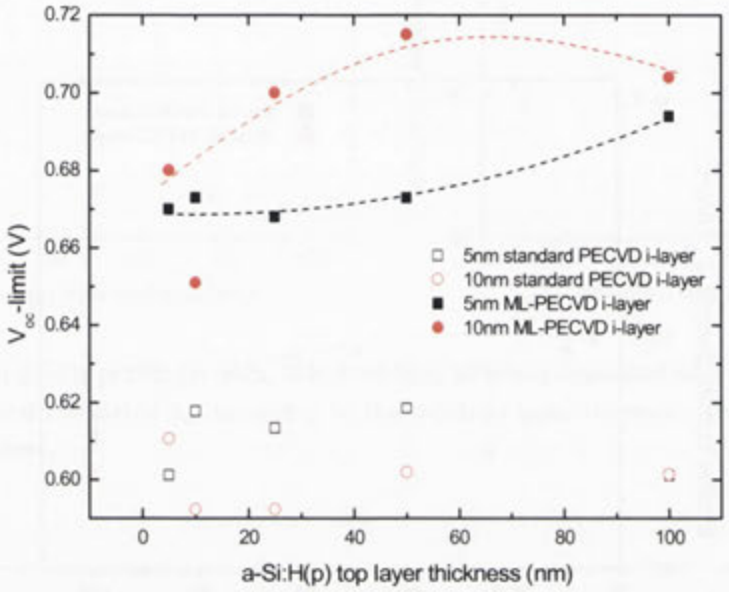

Figure 87: Implied-V_{oc} for non-diffused 1Ωcm mc-Si(n) wafers deposited with a-Si:H(i/p) stacked layers deposited by standard PECVD and ML-PECVD. Mc-Si wafer thickness is approximately 120μm.

As in the previous section, the FTIR analysis shows little change in hydride bond density, H%-content or heterogeneity for the a-Si:H(p)/a-Si:H(i)/mc-Si(n) heterostructure stacked layer (see Figure 88). H%-content and heterogeneity are ideally similar to other a-Si:H stacked layers, and correspond well with the highest passivation achieved here.

A rapid increase in the bulk hydride concentration helps to identify the interface thickness between the a-Si:H(i) and the a-Si:H(p) layers. Minimal improvements in the interface hydride density at the mc-Si surface show that this interface remains ideally uncompromised by the a-Si:H(p) layer. It can be understood that factors influencing the mc-Si surface interface region can extend up to 20nm into the a-Si:H layer. Accounting for the additional variations in surface geography over crystallographic dislocations, a suitable a-Si:H(i) sufficient to prevent tunnelling from mc-Si surface into mid-gap states present in the uppermost monolayers of the a-Si:H heterostructure would be required.

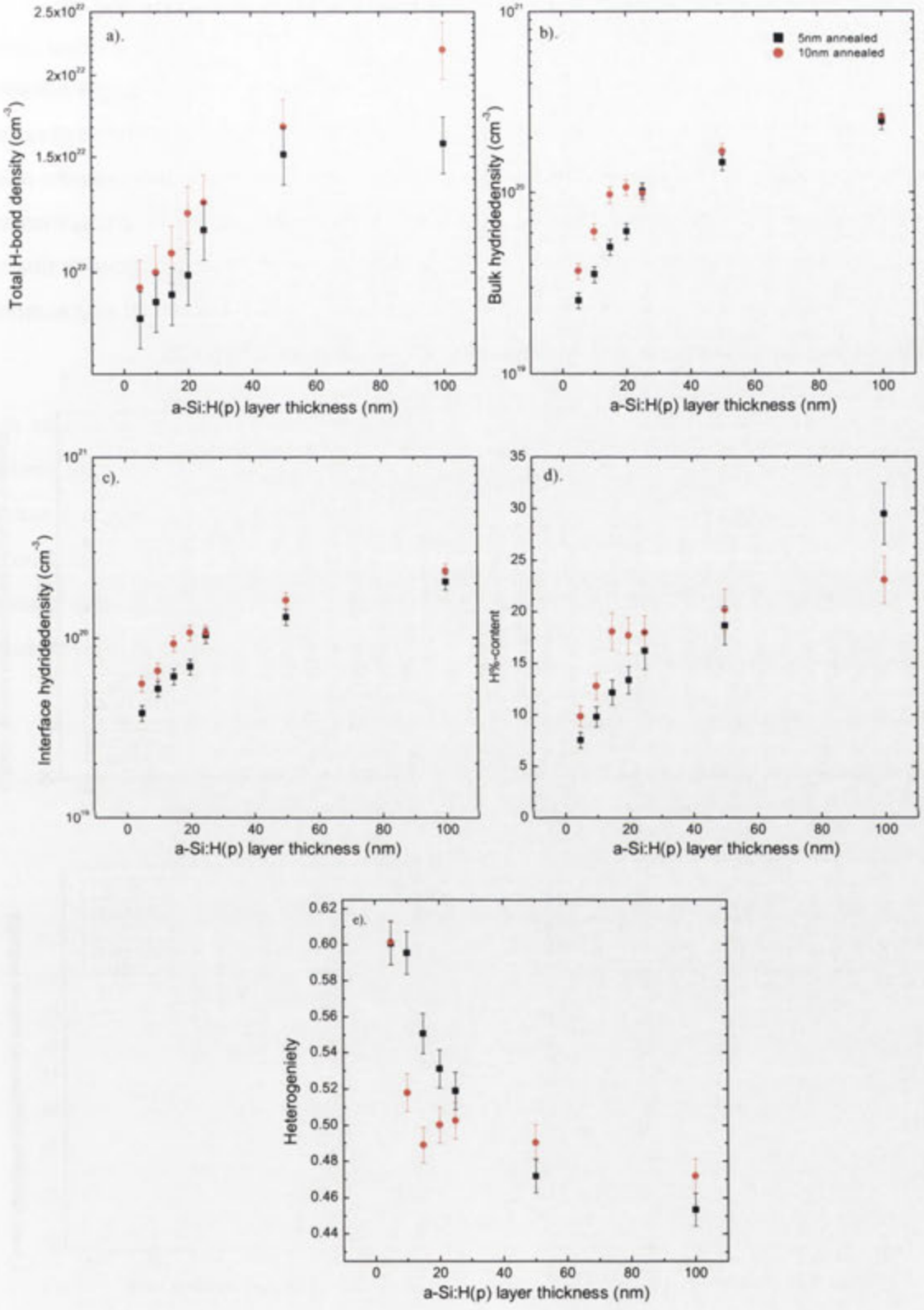

Figure 88: IR hydride bond density results a). Total bond density, b). Bulk monohydride, c). Interface monohydride densities, d). Hydrogen % content, e). Heterogeneity for a-Si:H(i/p) stacked layer of different thicknesses on bare 1.0Ωcm mc-Si(n) and annealed at 240°C for 40 minutes.

5.3.3 Bifacial a-Si:H(i/n) or a-Si:H(i/p) stacks on 100µm n-type mc-Si

In many cases, the passivation of the mc-Si surface is secondary to reducing recombination within its bulk, essentially, the focus has been on improving τ_b. Therefore, the importance of surface recombination becomes only relevant for significantly thinner mc-Si wafers. In this case, the a-Si:H stacked layers are deposited onto 100µm mc-Si(n) to assess their effectiveness for passivation and reducing the density of charges at the mc-Si surface in the absence of either a diffused emitter or metallised BSF. The surface passivation quality for the two types of a-Si:H stacked structures on the mc-Si(n) following post-deposition thermal annealing at 240°C is given in Figure 89.

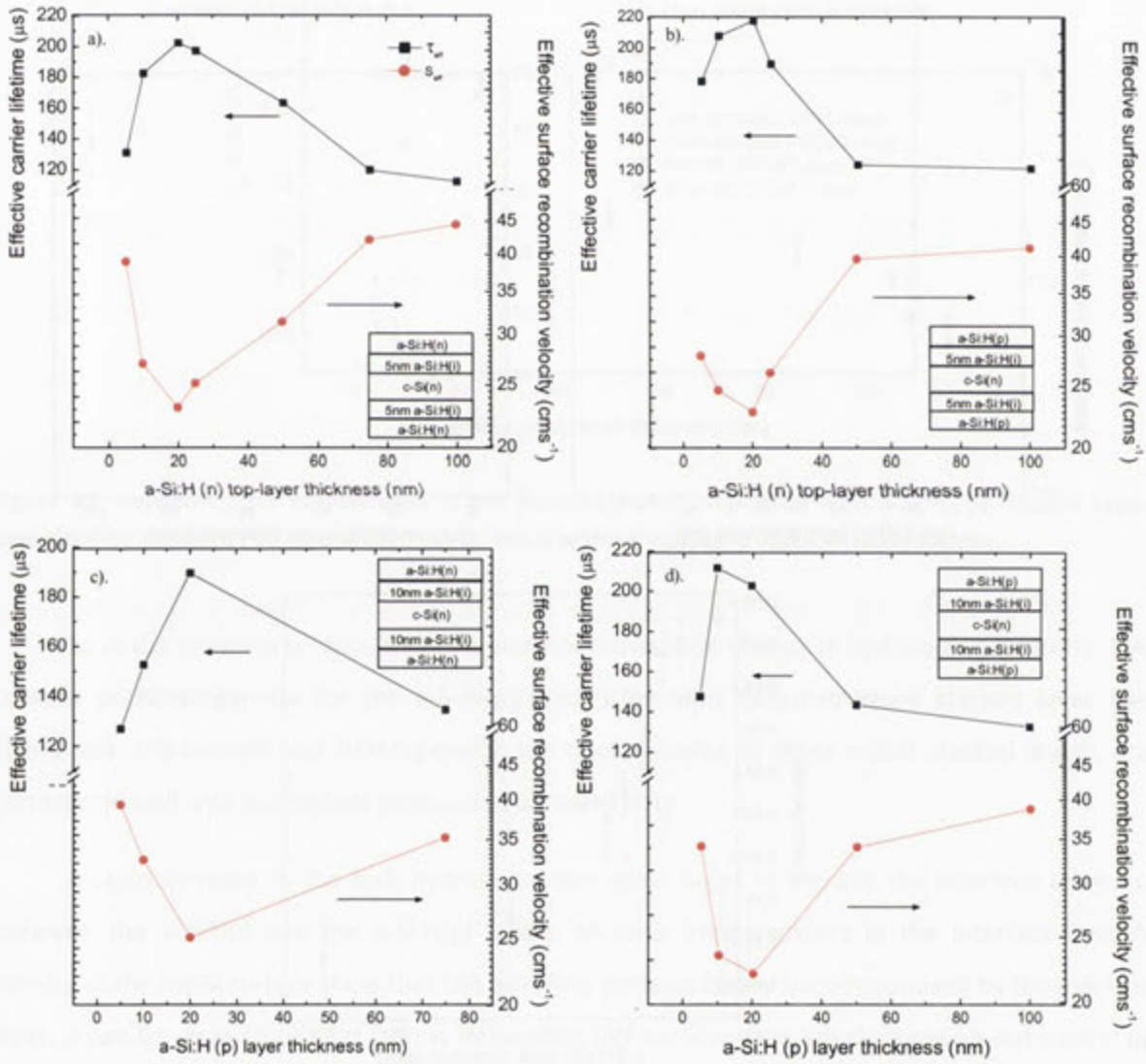

Figure 89: The τ_{eff} (squares) and S_{eff} (circles) for a-Si:H heterostructures with either n- or p-type a-Si:H top layers forming a BSF or emitter layer, respectively, deposited by ML-PECVD onto 100µm 1.0Ωcm mc-Si(n). An inter-layer of 5nm is used in (a/c) and 10nm in (b/d).

No significant change in the maximum τ_{eff} (220µs/23cms^{-1}) can be observed for 20nm a-Si:H(n) layers when using either 5nm or 10nm a-Si:H(i) inter-layers on the thinner 100µm mc-Si(n or p) wafers Figure 89a/b. A similar result for the 10nm to 20nm a-Si:H(p) layers on the mc-Si(n or p) with a minimum of S_{eff} of 22cms^{-1} being achieved (Figure 89c/d). The similar results for a-Si:H stacked layers on both n-type and p-type mc-Si for 100µm compared to thicker mc-Si wafers in the previous section demonstrate that the surface recombination velocity is less dependent on the bulk carrier lifetime. Therefore, the evaluation of S_{eff} gives a more robust assessment of the quality of the a-Si:H interface with mc-Si.

The constant values for τ_{eff}, may at first imply that these results are strongly impacted by bulk recombination and that if surface recombination is dominant, then some dependence of lifetime on thickness may be expected. However, as previously shown throughout this work, the thickness of the a-Si:H layer has little impact on the surface passivation. Additionally, if the surface recombination velocity is of increased importance for thinner mc-Si wafers, the consistent τ_{eff} would similarly give a low s_{eff}. This is apparent when examining the following expression and assuming constant bulk and effective lifetime, for the case where τ_{eff} is constant and τ_b is constant for lower W.

$$\text{Recombination} = \frac{\Delta nW}{\tau_b} + 2\Delta nS \equiv \frac{\Delta nW}{\tau_{eff}} \rightarrow \frac{1}{\tau_{eff}} = \frac{1}{\tau_b} + \frac{2S}{W} \qquad (5\text{-}3)$$

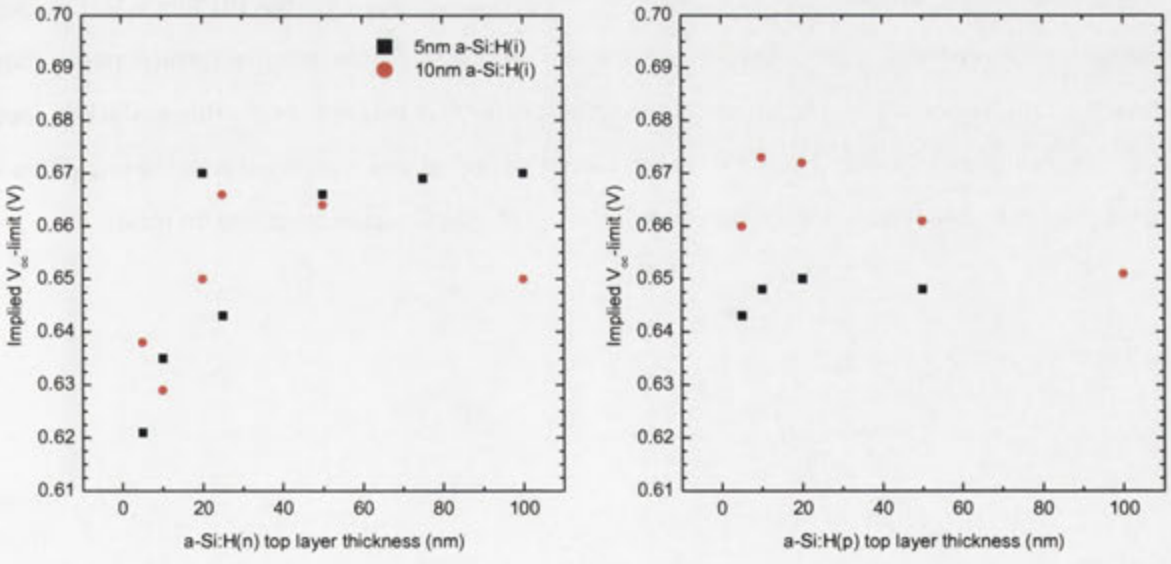

Figure 90: Limit in open-circuit voltage for a-Si:H(n or p) top layers atop 5nm or 10nm intrinsic inter-layers deposited onto 1.0Ωcm n- and p-type mc-Si with an average thickness of 100µm.

The implied V_{oc}-limits for these stacked layers on mc-Si(n) given in Figure 90 show that for thicker a-Si:H(n) above 20nm, a higher V_{oc} is likely to be achieved. The more pronounced dependence for 100μm mc-Si(n) may be attributed to the increased significance of the mc-Si surface recombination over that of the bulk. By comparison, the a-Si:H(p) layer below 20nm may be better suited as no dependence on a-Si:H thickness is apparent.

5.3.4 Asymmetric bifacial a-Si:H stacks on mc-Si

Utilising the good passivation results for both a-Si:H(i/n) and a-Si:H(i/p) stacked layers on mc-Si(n), the two are paired into an asymmetrical, bifacial a-Si:H stack onto both mc-Si(n) and mc-Si(p). The resulting device presented here is the first reported application of the HIT-like structure to the mc-Si wafer.

As before the a-Si:H(p) layer is deposited onto the a-Si:H(i) inter-layer before the a-Si:H(n) layer is deposited on the other side to prevent contamination. Both n- type and p-type mc-Si wafers utilised for this investigation are 100μm in thickness following re-etching of all a-Si:H layers from earlier depositions. The surface passivation quality for the asymmetric stacks a-Si:H stacks on the mc-Si(n) or mc-Si(p), following post-deposition thermal annealing at 240°C, are given in Figure 91 and Figure 92, respectively.

Very good passivation of the mc-Si surfaces by the a-Si:H stacked layers is demonstrated. High τ_{eff} of up to 300μs, corresponding to S_{eff} down to 50cms^{-1} is achieved for the HIT-like a-Si:H stacked layer structure on the 100μm mc-Si(n) and mc-Si(p). A clear profile for the surface passivation, similar to that presented in earlier sections in this chapter, is evident. From this a stacked layer design involving ideal 5nm and 10nm a-Si:H(i) layers and doped a-Si:H layers approximately 20nm in thickness appear the optimal choice for the a-Si:H HIT-like stacked layer structure on mc-Si.

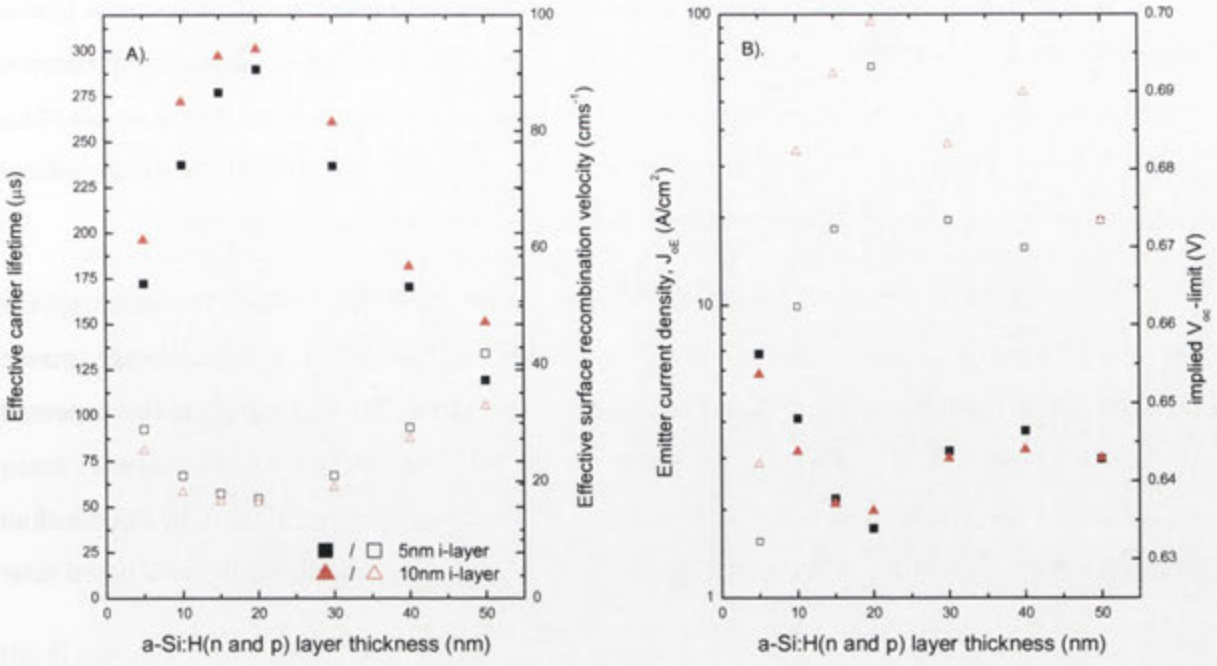

Figure 91: Quality of passivation provided by bifacial Hit-like a-Si:H stacked layers (i.e. a-Si:H(p)/a-Si:H(i)/c-Si(n)/a-Si:H(i)/a-Si:H(n)) following thermal anneal at 240°C for 30 minutes, a). measured using τ_{eff} (solid) and S_{eff} (hollow) on bare 100μm mc-Si(n), and b). J_{0E} (solid) and implied V_{oc}-implied (hollow).

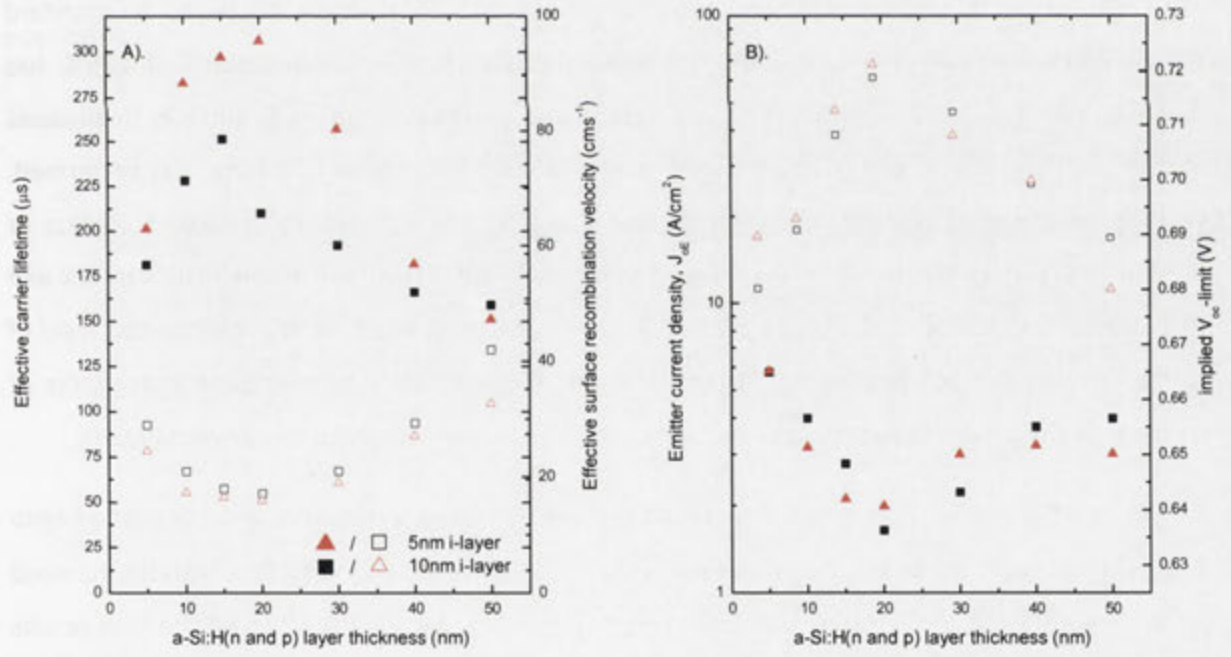

Figure 92: Quality of passivation provided by bifacial Hit-like a-Si:H stacked layers (i.e. a-Si:H(p)/a-Si:H(i)/c-Si(p)/a-Si:H(i)/a-Si:H(n)) following thermal anneal at 240°C for 30 minutes, a). measured using τ_{eff} (solid) and S_{eff} (hollow) on bare 100μm mc-Si(p), and b). J_{0E} (solid) and implied V_{oc}-implied (hollow).

Also shown in Figure 91b for mc-Si(n) and Figure 92b for mc-Si(p) are the measured J_{oE} and implied V_{oc}-limits for the mc-Si surfaces deposited with the asymmetric, bifacial stacked a-Si:H layers. As the asymmetric a-Si:H stacked layers are more representative of a completed device, levels of J_{oE}, below 10fA/cm^2 reveal the potential of the design in reducing current density at the mc-Si surfaces and are noteworthy in that this is achieved without diffused emitter or metallised BSF.

At this stage, the major drawback is the requirement for ITO/Al contact formation on the thinner 100μm mc-Si; and the difficulty in maintaining the a-Si:H layer coverage across crystallographic dislocations given the higher work function of the ITO/Al. Progress in this aspect of the design is likely to lead to functional mc-Si solar cells suitable for characterisation. However, it can be concluded that the introduction of mc-Si/a-Si:H HIT-like design for thin 100μm, by PECVD of all necessary layers, potentially offers a substantial cost reduction and convenience in mc-Si based solar cells.

5.4 Summary

The first study concerning the deposition of intrinsic a-Si:H layers deposited by standard PECVD and ML-PECVD onto a suitably prepared mc-Si surface at temperatures of 225°C has demonstrated that a-Si:H can achieve good passivation qualities of the mc-Si surface. In all cases post deposition thermal annealing at temperatures below 240°C for up to 1 hour was performed, yielding further improvements in carrier lifetimes. Despite the significantly reduced thickness of these layers, surface passivation is comparable to or better than many achievable results by SiN and SiO_x layers. The ML-PECVD technique was shown to be the most effective at achieving this level of surface passivation reliably, owing to the ability of this technique to overcome the effects of crystallographic dislocations on layer coverage during deposition compared to standard PECVD.

In a first application, n-based and p-based a-Si:H stacked layers have been deposited onto 150μm thick n-type mc-Si and they displayed significant passivation of the surface without the need for dopant diffusion of the mc-Si. Stacked layers deposited by ML-PECVD achieved the best results with S_{eff} of 43cms^{-1} with 25nm a-Si:H(n) layers and 38cms^{-1} with a-Si:H(p) layers between 5nm and 10nm. This corresponded well with a heterogeneity slightly above 0.5, representing an ideal ratio of interface to bulk hydride bonds. Saturation current densities at the mc-Si surfaces are in the range of 4.5×10^{-14} Acm^{-2} to 1×10^{-13}Acm^{-2} for n- and p-type a-Si:H layers, respectively, when deposited onto a-Si:H(i) inter-layers. Corresponding to an implied-V_{oc} of 624mV using both n-based and p-based

heterostructures with 150-180μm mc-Si wafers. The advantages of the a-Si:H stacked layer for mc-Si were demonstrated by depositing layers onto 100μm thick n-type mc-Si wafers. S_{eff} as low as $22cms^{-1}$ was calculated leading to higher V_{oc}-limit of 672mV using a-Si:H(n) layers and 673mV with a-Si:H(p) top layers.

IR-studies showed the presence of two interface regions, the a-Si:H(i)/mc-Si and the a-Si:H(i)/a-Si:H(n or p) region. ML-PECVD of the layers in both regions offered a method for fine control of these regions so as not to compromise the mc-Si passivation when very-thin a-Si:H(i) inter-layers are used. From this, FTIR was shown to be an effective method in determining the quality of passivation achievable and measuring the optimal hydride distribution for n-based a-Si:H heterostructures deposited onto mc-Si wafers.

Importantly, the a-Si:H heterostructure has been shown to be suitable for passivation of the mc-Si surface and is particularly appropriate for very thin mc-Si wafer dimensions. It has been shown that a a-Si:H heterostructure, consisting of a passivation layer, and either an emitter or BSF layer can be deposited onto, and with minimal stress to the mc-Si wafers at low temperature. This reduced the likelihood of breakage, more common for SiN passivated mc-Si, from occurring. The a-Si:H is compatible with low-temperature evaporation of aluminium or ITO contacts, providing the possibility of manufacturing mc-Si based solar cells using a-Si:H all at low temperature.

Several conclusions can be drawn from the results presented throughout this chapter:

- Thinner a-Si:H stacked layers (i.e. below 30nm) are suitable for passivating the mc-Si surface compared to thicker SiN_x and SiO_x passivating layers.
- Significant reductions may have been made in the density of interface states at the mc-Si surface by using intrinsic a-Si:H and stacked (intrinsic/doped) a-Si:H layers without any diffused emitter or metallised BSF layer.
- No precipitation of interstitial iron is likely to occur at the temperatures required for full device fabrication using a-Si:H stacked layers.
- As the mc-Si wafer thickness is reduced, the importance of surface recombination increases compared to the bulk recombination.
- Significant reductions in charge density at the mc-Si surface occur when using a-Si:H stacked layers in the absence of any diffused emitter or metallised BSF layer.

6.

Overview and Technical Applications

The scope of industrial applicability has narrowed in the last few years, with the demands on materials like a-Si:H to replace current technologies becoming more defined. Recently, the efforts by groups worldwide have shown that a-Si:H on c-Si surface in a HiT-like structure can yield high efficiencies. While many strategies achieve this main aim, the final product often falls short of the expectation, a consequence of the limited understanding concerning the material. The mechanisms and close interactions between initial deposition conditions and post-deposition processes of a-Si:H/c-Si, and indeed for many other passivating materials, is critical to our efficient manufacturing of next generation photovoltaic devices. In this light, the technical feasibility of merging a-Si:H with c-Si and the strategies involved to fabricate high efficiency photovoltaic solar cells has been investigated in this work.

Various manipulation processes have been examined throughout this thesis, to clarify and understand the critical pathways towards high-efficiency, low-cost photovoltaic applications of a-Si:H. The focus of this work has been in four key areas:

- The influence of conditions during deposition and the identification of the optimal deposition ranges for a-Si:H and the properties of such layers,
- The role of post-deposition thermal annealing in improving the passivation quality of c-Si using a-Si:H, and the properties of the a-Si:H during thermal processing,
- The a-Si:H(i) inter-layer in HiT-like stacked a-Si:H(i/n) or a-Si:H(i/p) layers and the application of this structure to non-diffused c-Si surfaces,
- The substitution of multicrystalline silicon for crystalline silicon in HiT-like stacked a-Si:H layer designs.

In chapter 2, the influence of the deposition parameters on the final passivation quality of the a-Si:H for c-Si were investigated, focusing on *rf*-power, temperature, and partial-pressure. For the system configuration in this work, a temperature of 225°C, an applied *rf*-power of 4W (), and partial pressure of 650mT have been shown to be ideal. Additionally, distinct conditions were revealed to occur for the optimal deposition of a-Si:H which meet the principal criteria for passivation of c-Si; namely, the suitable provision of hydrogen to the c-Si surface.

In this thesis, it has been identified that temperatures from 200°C to 250°C are most suitable for deposition, resulting in the highest and most easily achieved effective carrier lifetimes. Although similar results may be possible at lower or higher settings than these temperatures, the difficulty in obtaining comparable levels of passivation quickly becomes apparent by either, necessary longer healing times or an increase in dihydride concentration. Indeed, low temperatures below 170°C have mistakenly been reported as optimal in the literature due to the higher hydrogen-hydride densities measured, although no account of the hydride configuration had previously been linked to this. Here, it has been shown that increases in SiH_2 below 170°C are responsible for this reported high hydrogen content; noting that SiH_2 provides only minor and indirect surface passivation benefits. A prominent tendency towards the formation of bulk hydrides was exhibited by a-Si:H layers deposited at temperature at or exceeding 250°C. This can yield improvements in quality of this region so as not to interfere with the interface hydride. However, deposition above 300°C will result in the loss of hydrogen from the interface region, significantly reducing surface passivation quality. Unlike other studies, no crystallisation of the a-Si:H was observed in the range of temperatures investigated in this work, owing to the absence of microvoids and the presence of SiH_2 within the optimal range. It can be concluded that the temperature of deposition, a surface-dependent parameter, directly influences the quality of the a-Si:H and thereby the level of surface passivation.

For *rf*-power, depositions between the Paschen limit (for this system 2W) and an applied 8W demonstrated similarly high results in measured carrier lifetimes and no observable plasma related degradation of the a-Si:H during growth. Through analysis of bond configurations, it was found that monohydrides dominate the a-Si:H layer within this ideal range. Provided that *rf*-power is kept within these limits, the temperature during deposition governs much of the growth conditions for a-Si:H involving the composition and concentration of hydrides. The thresholds between the high-intermediate-low *rf*-power regimes were identified by hydride analysis. Shown was the shift in hydride configuration, and the rapid decrease in the density of monohydride as *rf*-power transitioned into intermediate (+120mWcm^2) and high (+240mWcm^2) regimes. The presence of dihydride occurred when *rf*-power was above or below the ideal range, with SiH_2 density increasing sharply. Thus, accounting for the higher reported hydrogen - hydride densities listed as optimal in some literature. The occurrence of trihydride when using *rf*-power regimes above 300mWcm^2 further increases the likelihood of forming microvoids within the a-Si:H layer; a condition which provides no passivation of the c-Si surface and may actually degrade it further.

For a-Si:H, the deposition temperature and *rf*-power were identified in this study as the main parameters to influence the quality of the layer and the passivation provided, followed by partial pressure. Although partial pressure does not exhibit the same influence on the quality of the a-Si:H layer(s) as do temperature and *rf*-power, a range between 400mT and 750mT provided similar results in passivation quality for the system in this work. The highest and most consistent results are obtained using a partial pressure of 650mT. Below 400mT and above 750mT, the undesired presence of dihydride occurs and the SiH_2 density increases noticeably. Of more concern is the occurrence of trihydride and polsilyl hydrides for depositions above 750mT. Although this 'dusting' region should be avoided, many large scale area depositions have difficulty in preventing it without compromising the quality of a-Si:H in other ways.

From all these observations, it is concluded that the surface-related parameters of temperature and *rf*-power, are the most critical in attaining the density, composition and distribution of hydrides within the a-Si:H layer for quality passivation of the c-Si. Ideally, a monohydride rich interface region is most likely to reduce dangling bond density at the c-Si surface. Although the presence of dihydride does reduce the effectiveness of this passivation, it is trihydride and polymeric hydrides which need to be avoided. For systems where the growth surface is on the lower electrode, the inclusion of dihydride and to a lesser extent trihydride is likely to take place.

Chapter 3 deals with improvements in the surface passivation quality observed during post-deposition thermal annealing. FTIR measurements on hydrides within the a-Si:H layers showed that no measureable increase in new bonds takes place despite considerable improvements in the effective carrier lifetimes measured. This result is significant, as for almost 20 years it has been assumed that new hydride bonds are formed at the c-Si surface through the preferential diffusion of hydrogen from the a-Si:H bulk. Indeed, for many years this has driven the development of hydrogen-rich passivating layers as an improved source for the c-Si surface, despite the negative side-effects of high hydrogen contents above 20%. Furthermore, the substantial improvements in the passivation of the interface observed throughout this work showed that little difference occurs in the hydride density, composition or distribution during thermal annealing. If hydride diffusion through the bulk towards the c-Si surface, or shifts from SiH_2 to SiH at the c-Si surface were responsible, then evidence in one of these would easily have been identified, however, no such changes occurred. This does not rule out other causes at least partly accounting for the improvement in surface passivation. However, the necessity of a hydrogen rich interface region is most likely the foundation for the improvements given the results presented in chapters 2 and 3. From this, it can be realised that bulk hydrogen diffusion, preferentially through a high-defect material like a-Si:H towards the c-Si surface does not agree with the many observations concerning the improvements in surface passivation. It is from these observations, in which a theoretical model for the surface-diffusion of hydrogen, already present at and within the interface region with c-Si, is offered as an explanation for the improved passivation quality.

For c-Si surfaces coated with a-Si:H(i), thermal annealing revealed a surface-limiting improvement in surface passivation dependent upon temperature. The Arrhenius relationship that exists, showed that the thermal activation energy for the passivation of c-Si by a-Si:H occurs at approximately 0.7 ± 0.1eV with no significant dependence on the thickness of the layer. Comparatively, bulk hydrogen diffusion would require 1.5eV, and 2.4eV for spontaneous hydrogen release, ruling these processes out.

The introductory physical model given in this thesis, details the surface-based mechanism by which hydrogen, present at the interface between a-Si:H(i) and c-Si can be transported through a series of shallow-traps across the c-Si surface to suitable deep-trapping sites. Complete hydrogenation of the c-Si surface occurs through the provision of hydrogen to all deep trapping sites. For high quality passivation, hydrogen coverage has been estimated to approximately 80%. Extending hydrogen adsorption to include near interface hydrogen as a source, a more accurate approximation of the passivation mechanism has been described. The expected surface-diffusion

lengths of hydrogen have been calculated for increases in temperature, revealing the underlying misconception concerning hydrogen and the c-Si surface passivation; that bulk diffusion is required. The mean hydrogen diffusion length and time necessary for surface diffusion of hydrogen until deep trapping occurs was shown to directly relate to the energy available during transport between interstitial sites. This temperature dependence agrees with thermal anneal times and links hydrogen mobility with passivation, indicating that bulk diffusion within hydrogenated materials at higher temperatures may simply mask the actual passivation mechanism. The impact of this model is that layers with hydrogen-rich bulks are not necessary to achieve high-efficiency passivation. Providing that sufficient hydrogen is contained within this bulk, the bulk serves only to stabilise the interface region.

IR-spectroscopy of hydrides in chapters 2, 3 and 4 has shown that well defined interface and bulk regions exist. The threshold in hydride distribution between the interface and bulk regions of the a-Si:H layers to achieve stable, high-quality passivation occurs when hydrides within the interface are dominant. A distinct lack of hydride bonds for the topmost a-Si:H, can result in depletion of the hydrides from within the intrinsic inter-layer and even from the interface with the c-Si surface itself. This unwanted effusion of hydrogen in this way has been observed experimentally during temperature processing. The effect is most critical when very thin a-Si:H(i) inter-layers are deposited, and/or when coverage across crystallographic dislocations, as is the case with mc-Si, is an issue.

Throughout this thesis, FTIR has been demonstrated as an effective method for monitoring hydride density, composition, H% content and distribution for a-Si:H layers; linking FTIR hydride bond analysis with the quality of achievable surface passivation on c-Si and mc-Si surface. The application of this technique to in-line manufacturing and quality control of a-Si:H layers is desirable. From a manufacturing standpoint, hydride-rich interface regions are recommended over increasing hydride content throughout the entire a-Si:H bulk. Although, little impact from the latter occurs for thicker a-Si:H layers, or is likely with thinner layers. More advanced design applications of a-Si:H benefit greatly from this conclusion.

Multi-layer Plasma Enhanced Chemical Vapour Deposition (ML-PECVD), a new technique developed as part of the post-deposition annealing studies during this thesis has been demonstrated to achieve substantial improvements in efficient surface coverage, hydride composition and distribution that reliably lead to high-quality passivation of the c-Si surface. The deposition of sequential sub-layers, with thermal cycling allows for optimal repacking of the growing a-Si:H layer

improving stability. Although deposition time does increase, due to the thermal cycling of the simple system utilised in this work, a clear advantage in reliability and stability for thin ML-PECVD a-Si:H layers over standard PECVD a-Si:H results was obtained. Fine control of the deposition process and quality of each region (i.e. interface or bulk) allows the a-Si:H layer to be designed more effectively for its intended application. This technique is not only limited to the aspects of photovoltaic designs discussed in this work and further system development of ML-PECVD is an attractive possibility.

The optical and structural properties of a-Si:H layers reported in chapter 3 indicated that for increases in substrate temperature from 100°C to 280°C:

- The absorption coefficient increases simultaneously with the optical energy gap, and
- The density of the thin film layer increases.

For thin a-Si:H, below 20nm, the attenuation of incident light is limited, encouraging the use of very thin a-Si:H for front-surface passivation. Provided that a-Si:H layers are very thin and do not contribute to photogeneration, the Staebler-Wronski effect is negligible. Importantly, the first complete picture concerning the densification of a-Si:H over a broad range of temperatures has been reported here; more so, these results are reported in the absence of micro-voids. Compared to micro-void rich layers, the higher density of the a-Si:H deposited in this work lead to a reduction of intrinsic stress within the a-Si:H, improving stability. The repacking of SiH with temperature explains the distinct improvements in surface passivation above and below 200°C. Additionally, micro-void formation has been shown to be atypical for a-Si:H layers deposited below 280°C, whose presence is more attributable to a lower deposition quality forming closed silicon rings, on the surface, than for temperature within this range.

The effectiveness of the intrinsic a-Si:H layer in passivating a diffused emitter surface over a wide range of emitter sheet resistances, between 7Ω/□ to 340Ω/□ has been proven in this thesis. Unlike SiO_2 and SiN passivating layers, the a-Si:H(i) does not appear to exhibit the same strong dependence on sheet resistance in reducing the saturation current density at the emitter surface. For emitter sheet resistance above 60Ω/□, similar J_{oE} between 7fA/cm^2 and 30fA/cm^2 have been reported here for most a-Si:H(i) layer thicknesses. Lightly diffused emitters, above 200Ω/□, coated with a-Si:H(i) layers displayed similar J_{oE} as that achieved using FGA alnealed SiO_2. The unique capacity of a-Si:H(i) to passivate both lightly and heavily doped emitter surfaces was discussed, and offers advantages in the large surface area deposition of a passivating layer at temperature below 300°C, including underneath metal contacts.

A next step, the replacement of the diffused emitter by a HiT-like stacked a-Si:H layer involving n-type or p-type a-Si:H has a distinct advantage of single process, low temperature junction formation for this type of solar cell. In this design, the a-Si:H(i/n) or a-Si:H(i/p) would perform as an emitter or BSF depending on the base c-Si wafer. For both types of stacked layers, an average S_{eff} as low as $5cms^{-1}$ (minimum $3cms^{-1}$) has been measured. Similarly, low J_{oE} of $10fA/cm^2$ have also been shown in each case, comparable to the best results achieved using diffused emitters and other passivating materials like SiO_x and SiN. Several benefits of a-Si:H stacked layers are immediately apparent for reducing manufacturing costs and production times:

- No complicated structural techniques (e.g. heavy doping, partial oxidation), allows a-Si:H stacked layer to be deposited over large areas and underneath metal contacts (ITO, AL)
- Surface passivation can be accomplished in a single, simple step process.
- Improved rear surface performance compared to aluminium alloyed BSF
- Possible simultaneous illumination of a bifacial device design
- Straight-forward use of n-type c-Si avoiding degradation through boron-oxygen metastable defects in c-Si(p).

Given that no distinct change in the hydride composition with the further deposition of stacked a-Si:H(i/n) or a-Si:H(i/p) layers could be observed, it may be concluded from the FTIR analysis of the deposited layers in Chapter 4, that the stability and surface coverage of the intrinsic layer remains the most important factor in the stacked layers. Not only does the passivation quality of c-Si or mc-Si surface depend on the fidelity of the a-Si:H(i) layer, but also to some extent on the n-type or p-type a-Si:H layers also. Although the production of complete solar cells devices was outside the scope of this work, some precursors were fabricated using non optimised Al/ITO contacts evaporated onto asymmetric, a-Si:H(n)/a-Si:H(i)/c-Si(n or p)/ a-Si:H(i)/a-Si(p). High open-circuit voltages of 714mV for 1.4Ω *FZ* c-Si(n) and 678mV for 0.9Ωcm *FZ* c-Si(p) were achieved, indicating the potential for a-Si:H layers deposited throughout this thesis using a relatively simple PECVD system.

Following the encouraging results for stacked a-Si:H layers on single-crystal silicon, and the more precise control offered by ML-PECVD, the a-Si:H(i) and HiT-like a-Si:H stacked layers were applied for the first time to the mc-Si surface. The a-Si:H(i) layer was shown to reduce recombination occurring at the mc-Si surface with S_{eff} below $100cms^{-1}$, stable for up to 1 hour of thermal annealing above 240°C. This is despite crystallographic dislocations, suggesting a more homogenous surface

coverage can be achieved using very thin a-Si:H(i) layers . According to the conclusions in chapter 3, regarding thermal annealing and hydrogen mobility, it can be calculated that for temperatures below 450°C rapidly decreased, limiting bulk hydrogenation of mc-Si in this case. As deposition and processing temperatures remain below 300°C, bulk hydrogenation of the mc-Si can be ruled out as the cause of the high surface passivation achieved here.

The deposition of stacked a-Si:H layers in the absence of a diffused emitter region achieved one of the most prominent outcomes in this thesis. For a-Si:H(i/n) using a 25nm a-Si:H(n) layer, an S_{eff} of 43cms^{-1} has been achieved, increasing slightly when using thicker layers. Similarly, 39cms^{-1} is reached using instead a-Si:H(p) layers between 5nm and 10nm, also increasing with thickness. In terms of reducing carrier density at the interface for these stacked layers, J_{oE} below 4.5 x 10^{-14}Acm^{-2} and implied-V_{oc} between 650mV and 700mV was demonstrated. Applied to thin 100µm n- or p-type mc-Si where bulk recombination is less important, a lower S_{eff} below 25cms^{-1} and V_{oc}-limit of 670mV have been reported here. When combined with Al/ITO evaporation, it is possible to manufacture a complete mc-Si solar cell at a temperature below 250°C (not including the temperature of an essential gettering which takes place prior to deposition). Owing to the reduced thermal stress and processing requirements, the potential yield per mc-Si wafer can be increased if applied to thinner mc-Si substrates correctly.

The outcomes of this thesis represent a series of steps forward in improving our understanding of a-Si:H and its application to photovoltaic devices. As with all fundamental investigations into emerging materials and their uses, some aspects can benefit from further study and development. These areas are listed below:

- Necessity to reduce the total ML-PECVD deposition time for complete layers by improving thermal cycling between sub-layer depositions for the practicality in using this method.
- Applying the a-Si:H stacked layers to a complete solar cell for the assessment of device properties.
- Heterojunction development of new structure designs and how the interface defect density for these may be influenced by hydrogen.
- Optimisation of a-Si:H fabrication has identified the role which hydrogen and its mechanisms, particularly hydride composition and concentration throughout the a-Si:H layer may affect surface passivation to some degree. However, other mechanisms and processes

may also influence surface passivation. To better complete our understanding, these should also be investigated in context with the work presented here.

- In this investigation, some aspects of deposition parameters, for example, the silane gas concentration, or radio frequency of the PECVD system were not fully examined. These may influence the electrical and physical characteristics of a-Si:H. Specifically, the use of trisilane which has been shown in early studies to improve plasma deposition quality.

- Low S_{eff} and J_{oE}, and expected high V_{oc} are only part of a complete solar cell. So it is necessary to revisit the heterojunction further and in the presence of TCO and Al contacts for these and 3D structures.

- Observe and characterise the atomic structure for as-deposited and thermally annealed a-Si:H layers using Rutherford Backscattering (RBS) and Elastic Recoil Detection (ERS).

- Verification of interface hydride composition during PECVD (*in situ*) and comparison to the expectations of the model presented in this work would be the next step in confirming the nature of surface passivation.

- Examine the defect chirality by Nuclear Magnetic Resonance (NMR) and Electron Spin Resonance (ESR) to which hydrogen is interacting with Si at the c-Si surface to reduce recombination

- Yield statistics for ML-PECVD versus Standard PECVD of a-Si:H or SiN on c-Si and mc-Si should be investigated further for textured, random pyramids and other features.

- Overall device performance is governed by more than simply surface passivation quality, or the electronic and optical properties of the a-Si:H layer. The base wafer bulk and surface quality, as well as the thickness remain an important factor. The suitability of high quality, very thin a-Si:H layers may be beneficial on other surfaces than mc-Si or c-Si.

- Understanding and a finer control of the deposition layer has been shown possible in this work, however, it is not only applicable to the aspects of these particular solar cell designs. Other devices, including nanowires, ARC coating and quantum dot structures may also be fabricated and it is recommended that further investigation into this be undertaken.

A.

Appendix A: Electrical and Optical Characterisation Techniques

Throughout this thesis, a variety of electrical and optical characterisation techniques are drawn on to understand the potential for hydrogenated amorphous silicon thin film layers to effectively passivate the crystalline silicon surface. In this appendix, a brief overview of each of these techniques is given as a foundation for interpreting the measurements presented in this work. More extensive details regarding the techniques are also referenced here.

A1. Effective carrier lifetime (τ_{eff})

The electronic quality of the surface passivation and therein the optimal a-Si:H layer deposition parameters are determined by measurement of the effective carrier lifetime (τ_{eff}) by quasi-steady-state photoconductance (QSSPC) [225], operating in generalised mode according to equation (A 1). In this Δn is the excess electron density (cm^{-3}) and G is the generation rate ($cm^{-3}s^{-1}$) with time.

$$\tau_{eff} = \frac{\Delta n(t)}{G(t) - \partial \Delta n / \partial t} \quad \text{(A 1)}$$

If G(t) = 0, the above expression descirbes Transient Photoconductance Decay (PCD), which is also performed on the same apparatus when higher τ_{eff} are achieved and has the advantage of limiting the effects of optical absorption in the a-Si:H layer [223]. This is of particular importance for when thickner a-Si:H layers are deposited and/or under infra-red illumination.

The experimental apparatus used for minority carrier lifetime measurments is illustrated in Figure 93. The sample to be measured is inductively coupled wut the tuned radio-frequency coil to and *rf*-bridge sensitive to changes in the inductive field of the coil which occur when the sample is not in steady-state conditions. Samples are illuminated with a time-dependent light source, into non-steady-state, where the light intensity is calibrated to a reference cell. The photoconductance is then determined by the measured induced electrical field as the excess carrier density within the illuminated sample decreases.

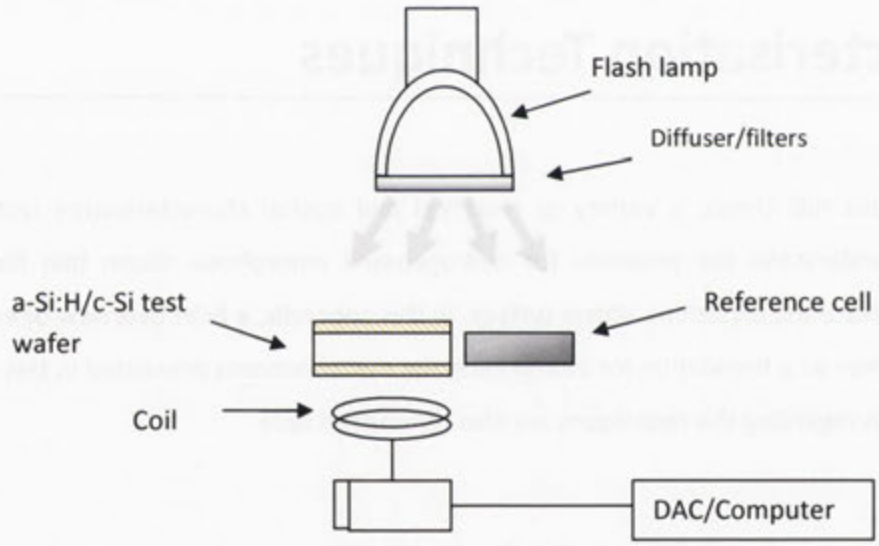

Figure 93: Schematic of inductively coupled photoconductance equipment.

The effective carrier lifetime can be considered to be a direct measure of the c-Si surface passivation quality in this work. For all samples, carrier lifetime measurements relating to the variations in surface passivation occuring from different deposition and post-deposition process parameters are performed in mid-injection ($10^{15}cm^{-3}$). In this way, the influence of other recombination pathways such as Auger recombination which can occur in high-injection ($10^{16}cm^{-3}$) are limited.

A2. Surface recombination velocity (S_{eff})

In order to evaluate the influence of process variables as closely as possible, c-Si and mc-Si wafer thickness ideally need to be equivalent. Throughout this work, the wafer thickness varied due to the re-etching of previous a-Si:H layers and some c-Si or mc-Si for re-use, leading to reductions in thickness of 40μm each time prior to new a-Si:H depositions. In certain cases, the thickness of the c-Si and mc-Si wafers were as thin as 100μm. In this case, surface recombination becomes increasingly important as the diffusion lengths of photogenerated charges begin to exceed the dimensions of the wafers themselves. Therefore, direct comparison between measured τ_{eff} is difficult between wafers of significantly different thicknesses. Surface recombination velocity (S_{eff}) is calculated from the measured τ_{eff} and presented along-side, providing a more accurate basis for comparison between samples.

For well-passivated surfaces associated with high-quality c-Si, where the effect of minority carrier diffusion towards the surface can be assumed to be negligible, τ_{eff} is dependent only upon recombination at the surface and within the c-Si bulk. This simplifies the calculation for low S_{eff} to that given in equation (A 2) ([224], pp 10), where τ_b is the bulk carrier lifetime and W is the c-Si wafer thickness.

$$\frac{1}{\tau_{eff}} = \frac{1}{\tau_b} + \frac{2S_{eff}}{W} \qquad \text{(A 2)}$$

Alternatively, a very high S_{eff} leads to a low τ_{eff} under steady-state conditions and the effective lifetime can be approximated as described by equation (A 3) [224]. Noticing that this is only the case for when low τ_{eff}, limited by high surface recombination velocities, occurs.

$$\frac{1}{\tau_{eff}} = \frac{1}{\tau_b} + D_n \frac{12}{W^2} \qquad \text{(A 3)}$$

For measurements of high τ_{eff} under transient conditions, the mathematical derivation concerning the influence of minority carrier diffusion is slightly different and is given in equation (A 4) [222, 224].

$$\frac{1}{\tau_{eff}} = \frac{1}{\tau_b} + D_n\left(\frac{\pi}{W}\right)^2 \quad \text{(A 4)}$$

More generally, by combining equation (A 2) and equation (A 4), both high and low S_{eff} can now be calculated from the measured τ_{eff} for any given thickness if τ_b is known according to the expression given below [224]. In this D_n is determined by either the diffusivity of minority carriers , electrons (D_n, shown below) or holes (D_p) within the c-Si wafers depending upon base wafer doping. Equation (A 5) is used to determine both the low and high value of S_{eff} throughout this work.

$$S_{eff} = \sqrt{D_n\left(\frac{1}{\tau_{eff}} - \frac{1}{\tau_b}\right)}\,Tan\left[\frac{W}{2}\sqrt{\frac{1}{D_n}\left(\frac{1}{\tau_{eff}} - \frac{1}{\tau_b}\right)}\right] \quad \text{(A 5)}$$

Shockley-Read-Hall recombination within the bulk can frequently be assumed negligible compared to recombination at surface defects if the quality of the c-Si wafer is high and and the dimensions are below approximately 500μm. Importantly the choice of τ_b [13] in equation (A 5) has a significant impact on the calculated value of S_{eff}, and care needs to be taken when comparing directly with other S_{eff} in the literature, particularly for low S_{eff}. The sensitivity of the S_{eff} calculation to the chosen τ_b manifests as either an upper limit (when $\tau_b \rightarrow \infty$), or a lower limit which may represent the ideal case; for example where $\tau_b \approx 2$ms, as is the case for the best experimental vaule reported for 1Ωcm c-Si [14]. Throughout this work, a conservative approach is adopted in the calculation of S_{eff} and the upper limit is only reported here. It can be assumed that the most significant measure of S_{eff} will occur at the interface between the a-Si:H layer and the c-Si surface, and that recombination at the a-SI:H/air interface is negligible by comparison.

A3. Fourier transform infra-red spectroscopy (FTIR)

Fourier transform infra-red spectroscopy (FTIR) is an optical absorption technique sensitive to hydride bonds both within the bulk a-Si:H and at the a-Si:H/c-Si interface. In this work, the the Perkin-Elmer Spectrum One FTIR instrument (see Figure 94), based on the Michelson interferometer, is used for determing bond type and concentration. Scanning frequencies from 400cm^{-1} to 4500cm^{-1}

[13] τ_b represents intrinsic recombination, consisting of radiative (τ_r) and Auger recombination (τ_A).

(resolution = $4cm^{-1}$) are made available by interference through 'moving mirror' which can lengthen or shorten the beam path.

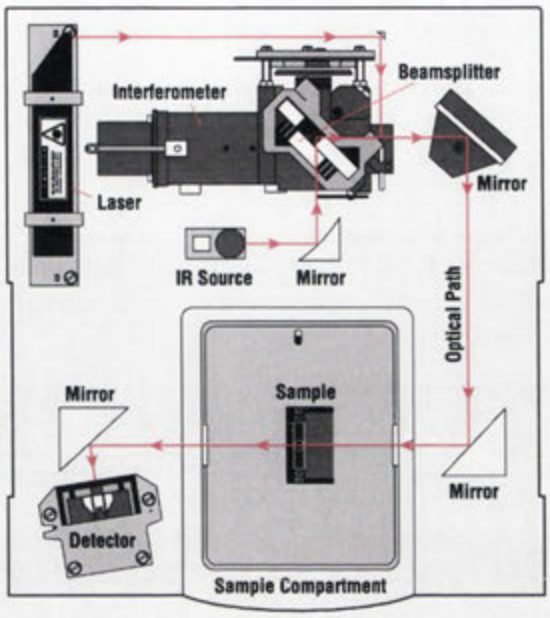

Figure 94: Schematic of Perkin-Elmer Spectrum One FTIR, adapted from Perkin Elmer [260].

The concentration and bonding state of hydrogen in a-Si:H can have signigificant influence on the structural and electronic properties at the a-Si:H/c-Si interface and the layer as a whole [261-263]. Conditions for PECVD and post-deposition thermal annealing of the a-Si:H layer(s) can be characterised by variations in the concentrations of hydride bonds ($Si\text{-}H_x$, $x \geq 1$). As infra-red absorption by hydride bonds occurs, insight into the importance of processing parameters for a-Si:H layers can be experimentally studied.

The sensitivity of IR spectroscopy to hydride bonds stems from the diametrically opposed electronegativity of the vibrating dipole. Hydrogen bonding to the Si-tetrahedral has a slightly negative charge, contrasting with the slightly positively charged neighbouring Si atoms. Viewing this arrangement as a harmonic oscillator, the SiH_x dynamic dipole moments can be altered using resonant infrared photons that are absorbed by the oscillator. Quanta of IR-light interacting with diatomic molecules ($Si\text{-}H_x$) via absorption cause an increase in their excitation for distinct vibrational modes dependent upon the incident photon frequency. The absorption excites the dipole to a higher vibrational state, where the state change matches to a specific spectral line. The intensity of this spectral absorption line directly corresponds to the number of hydride bonds. Experimentally,

hydrogen concentrations between 1% and 10% of dominant bonding configurations are clearly and directly observable by FTIR [264].

Represented by a wavenumber (cm^{-1}), each spectral absorption line corresponds to a particular hydride bond configuration. A select range of these for monohydride, dihydride and others, relevant to this study, are given Table 5 and the vibrational modes listed are illustrated on the FTIR spectra given in Figure 95.

Table 5: Relevant vibrational frequencies (ω) of different bonding configurations in a-Si:H measured at room temperature are given in terms of wavenumber. Additional ω for other hydrogen bonds (i.e. SiH_2, SiH_3, etc) are also shown [98, 104, 120, 140, 265-268].

Vibrational Mode	Wavenumber (cm^{-1})	Details
SiH bend	610-640	Total bonded hydrogen [101]
SiH stretch (bulk) – lf	2000-2020	Predominately monohydride in the bulk [269]
SiH stretch (surface) – hf	2070 – 2085	Monohydride [267, 270, 271]
SiH stretch (bulk) – hf_2	2090-2120	Dihydride (bulk and surface) [265, 267, 269]
Higher hydrides $SiH_{x>2}$	2200 - 2370	Surface and bulk [267, 269]

The presence of peaks at approximately $2000cm^{-1}$ and $2080cm^{-1}$ relate to the monohydride (SiH) located within the a-Si:H bulk and at the interface with the c-Si surface, respectively. Monohydride densities for these two regions are commonly reported with respect to the SiH bending mode located between $610cm^{-1}$ and $640cm^{-1}$, which can also represents the total bonded hydrogen and the degree of crystallinity/medium-range order of the a-Si:H.

For the primary peak between $1950cm^{-1}$ and $2150cm^{-1}$, the lower wavenumber region is often differentiated into three distinct Gaussian peaks [269] between $1950cm^{-1}$ to $2033cm^{-1}$. This range represents platelet-like configurations of Si-H stretching vibrations common to observations of a-Si:H deposited at higher temperatures [119]. The presence of this IR band is also known to be an indication of micro-voids within the a-Si:H [267]. However, at low temperatures this 3-peak band is preferentially removed in favour of the $2000cm^{-1}$ peak which correponds to bond-centered hydrogen (BCH) or Si-H stretching vibrations within the a-Si:H bulk.

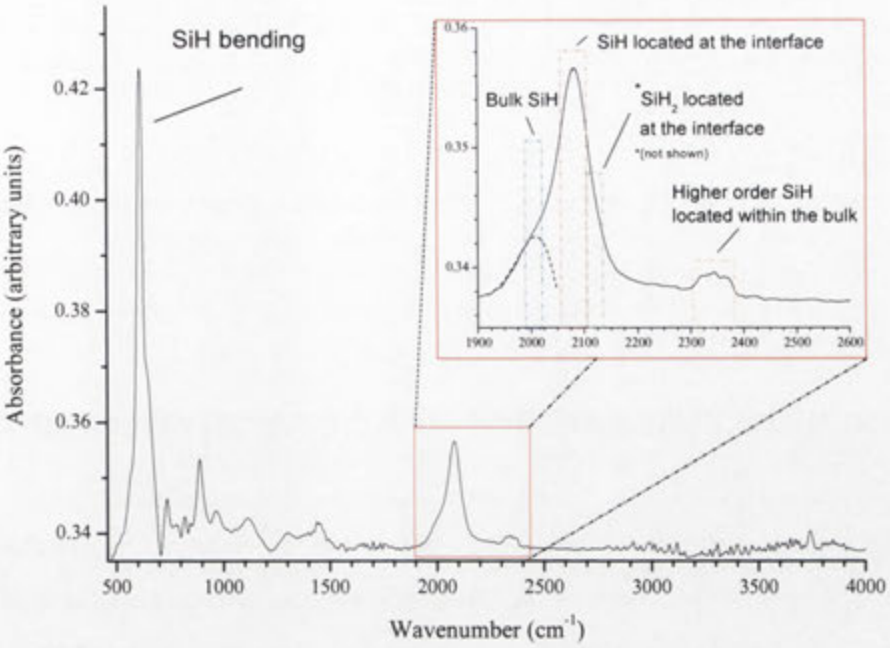

Figure 95: FTIR spectra illustrating common vibrational modes present in a-Si:H. Dihydride (SiH_2) occurs as a double peak (in most cases) in the region indicated, although not shown above. Other peaks characteristic to a-Si:H are also shown although they are not relevant to the IR analysis for surface passivation in this work.

Monohydride-terminated c-Si surface are characterised by an absorption peak located at 2084cm^{-1} which represents the ideal surface passivating bond [267]. Dihydride (SiH_2) measured between 2090cm^{-1} and 2120cm^{-1} in some cases is present at the interface region and within the bulk a-Si:H. Further to this, Gaussian fits within the higher frequency region also give details as to the region the SiH_2 or trihydride (SiH_3) occupy. In this occurence 2091cm^{-1} for bulk SiH_2, 2099cm^{-1} for surface SiH_2, and 2135cm^{-1} for surface SiH_3 [269]. Higher poly-hydride (Si_yH_x, $y \geq 1$, $x > 2$) with wavenumbers above 2220cm^{-1} [267, 269] are not common to FTIR spectra for a-Si:H in this work and therefore not shown.

A degree of spectral overlap for vibrational modes can occur between SiH vibrational states within the a-Si:H layer bulk and for those located at the a-Si:H/c-Si interface. Gaussian fits to the relevant hydride modes are used to determine the peak position and any shifts resulting from variation in the processing parameters (see insert Figure 95). In this way, the calculations of hydride bond concentrations are easier to define for each vibrational state.

Hydrogen bond concentrations are proportional to the absorption strength $N_{(H)}$ for specific vibrational modes in millimoles/cm^3 or bonds/cm^3 according to equation (A 6) [140], where ω is the resonant wavenumber and $\alpha_{(\omega)}$ is the absorption coefficient dependent on the mode frequency.

$$N_H = A\int \alpha(\omega)\omega^{-1} d\omega \qquad \text{(A 6)}$$

The proportional constant for absorption (*A*) is listed below according to the hydride bond-type and vibrational mode:

- SiH_{bend}: 2.1 x $10^{-19}cm^{-3}$ [120],
- $SiH_{stretch}$: 7.4 x $10^{-18}cm^{-3}$ (simulated: SiH 1.78 x 10^{17}, for SiH_2: 2.1 x $10^{-17}cm^{-3}$) [272]

The total bonded hydrogen content can be determined by equating the densities of both the interface and bulk hydrides with that of the SiH bending mode density, giving a total for diatomic hydrogen bond in the a-Si:H as a percentage according to equation (A 7) (adapted from [273]).

$$[H_{total}] = \frac{[Si-H]_{Bulk} + [Si-H]_{Interface}}{[Si-H]_{Bending} - [Si-H]_{Bulk} + [Si-H]_{Interface}} \qquad \text{(A 7)}$$

In this, *'bulk'* describes monohydride bonds within the a-Si:H bulk (ω = 2000-2020cm^{-1}), and *'interface'* describes monohydride bonds at the a-Si:H/c-Si interface (ω ≈ 2080cm^{-1}). As FTIR is insensitve to monatomically bonded hydrogen (H_2) and free hydrogen, these are not reflected in this calculation[14]. The basis for this asumption is that any H_2 within the a-Si:H layer is not passivating silicon dangling bonds, it may be disregarded. Also, the relatively high defect density (10^{15} - $10^{17}cm^{-3}$) within a-Si:H is assumed to rapdily eliminate any *free* hydrogen.

Throughout this thesis, the position and concentration of the spectral lines within the 2000cm^{-3}-2100cm^{-3} band can shift slightly under changing deposition and processing conditions not relevant to the analysis presented. Therefore, the wavenumbers corresponding to the bulk and interface regions are designated as low and high frequency, respectively; low frequency (*lf*) peaks for the stretching mode located within the a-Si:H layer bulk (2000 – 2020cm^{-1}), high frequency (*hf*) for monohydride stretching modes at the a-Si:H/c-Si interface (2070-2090cm^{-1}). In some cases SiH_2 (2100cm^{-1}) can also be included within this regions, particularly at void surfaces, and is taken into account where relevant. The near-interface region for very thin a-Si:H layers (<10nm), is called

[14] FTIR is not sensitive to monatomically bonded hydrogen like H_2 (H-H), which has no dipole moment. This also applies to free hydrogen.

the'pseudo-bulk' throughout this thesis, as it posesses bulk-like characteristics and does not directly interacting with the interface, but has insufficient thickness to prevent indirect influence on the interface.

Heterogeneity (r'), a measure of the hydride distribution between the interface and bulk regions of the a-Si:H layer according to equation (A 8) (adapted from [155, 263]). The inverse of this relation allows the inherent film stress to also be determined.

$$r' = \frac{[hf]}{[lf]+[hf]} \tag{A 8}$$

The value of r', gives the fraction of interface hydride to bulk hydride concentration as a ratio between a bulk dominated ($r' = 0.3$) and interface dominate ($r' = 0.7$). A value of 1 would be the case for a stoichiometric a-Si:H layer.

FTIR spectroscopy of all samples is performed for as-deposited and post-deposition thermal annealing to monitor the changes in bonding concentration of hydrides from process conditions. Although hydride bond densities and configurations represent an important characterisation tool concerning the a-Si:H layer, it remains difficult to determine some structural details including crystallinity. For this another complementary IR measurement technique is needed.

A4. Raman spectroscopy

Raman spectroscopy is an IR absorption technique that concentrates on phonon excitation in the target material typically at room temperatures by a laser source, with a measurable radial distribution function. In this work, Raman scattering is used to determine the microstructure of the as-deposited and thermally annealed a-Si:H layers. This technique is particularly beneficial for a-Si:H studies on crystalline silicon which has only one Raman active peak at 520cm^{-1} [94], whereas, all phonon modes in a-Si:H are Raman active [137]. Certain features in the Raman spectra are highly sensitive to structural properties of the a-Si:H. Therefore, measurements at room temperature can produce suitable spectral comparison between the phonon density-of-states for a-Si:H, which can be significantly modified by changes in short-range order (SRO) [47] and also medium-range order (MRO) [181]. In Table 6, the vibrational frequencies for a-Si:H and related modes are given.

Table 6: Raman modes for a-Si:H and c-Si corresponding to phonon density-of-states [101, 104, 140, 268].

Raman Mode		Wavenumber (cm^{-1})	Details
Transverse acoustic	TA	~150	Bond bending (Temperature-relaxation), MRO [97-99]
Longitudinal acoustic	LA	~280 – 330	Rocking mode (decreases as H content increases) [140]
Longitudinal optical	LO	~380 – 420	a-Si:H mode [101]
Transverse optical	TO	~470 – 490	Short-range order and bond angle [101-103]
c-Si	c-Si <100> (LO-mode)	520	Relates to crystalline structure of c-Si wafer [94-96]
D-Band		1360	Disordered microcrystalline
G-Band		1530	Sp^2 weak Si-Si bonds

For the Raman modes listed, information concerning the a-Si:H structure can be assessed by either a single mode scattering, or simultaneous effects on two or more modes. Principally, the two phonon modes, transverse optical and transverse acoustic, are of most interest for the information concerning the mean bond angle deviation, dihedral angle, SRO and MRO. These are discussed below. The mean bond angle for a-Si:H is approximately $108.6^0 \pm 0.2^0$, and $109.56^0 \pm 0.2^0$ for c-Si.

Transverse Optical (TO)

Depolarised Raman scattering of the TO-mode can be used to establish the mean bond angle ($\Delta\Theta$), and short-range order (SRO). Shifts in the TO-mode are known to correspond to variations in the density of the nearest-neighbour bond angle [103]. According to the work of Beeman *et. al.* [102] the linear relationship between the linewidth (Γ) full-width at half-maximum (FWHM) of the TO-mode and $\Delta\Theta$ can be expressed as:

$$\Gamma = 15 + 6\Delta\Theta \qquad \text{(A 9)}$$

However, the models used to derive this relationship are based on 238-atom simulated structures using only even numbered silicon arrangements. Simulations of a-Si:H often describe an abundance

of 5- and 7-fold configrations for silicon [274]. Consequently, equation (A 9) can be subject to large discrepancies when estimating $\Delta\Theta$. Therefore, a semi-experimental approach is adopted where the vibrational density-of-states of a 1000 atom model are fitted to experimental results. A new expression is derived in equation (A 10) which provides a more accurate estimation of $\Delta\Theta$.

$$\Gamma = 18.4 + 6.6\Delta\Theta \tag{A 10}$$

The observed intensity is determined according to equation (A 11), where R(ω) is the Raman intensity with thermal corrections, n(ω) the vibrational density-of-states , and ω the wavenumber.

$$I(\omega) = \frac{n(\omega)+1}{\omega} R(\omega) \tag{A 11}$$

Using the semi-experimental approach, the relation in equation is made for intensity.

$$I(\omega) = 0.0078\Delta\theta + 0.0626 \tag{A 12}$$

The $\Delta\Theta$, may also be expressed by using the least squares fit relation, equation (A 13), to the wavenumber (ω_{TO}).

$$\omega_{TO} = -2.5\Delta\Theta + 505.5 \tag{A 13}$$

Ideally, $\Delta\Theta$ should be approximately 11^0 for a-Si:H at the interface with c-Si, although may fluctuate between 9.7^0 and 11.6^0 as the a-Si:H relaxes. In well-annealed, realxed network of a-Si:H $\Delta\Theta = 10^0$ at temperatures up to 300°C, and as high as 14^0 for the non-relaxed case. For c-Si, the value of $\Delta\Theta = 0$. For reference, the mean bond angle (Θ) for tetrahedral silicon in a-Si:H is between $108.5^0 \pm 2^0$, and in c-Si is $109.55^0 \pm 2^0$.

Tanino *et. al.* showed that increases in SRO can be determined by simultaneous increases in the peak position and narrowing of peak width in the TO-band [47, 99]. Therefore, the TO mode in a-Si:H can be considered representative of the SRO for this material. The lower the peak position of TO and the wider the Γ, the lower SRO. Conversely, narrowing of the peak width indicates increased SRO. If the TO peak position is unchanged then the Si-Si bond length and angle remains unchanged

by hydrogen. It should be noted that minor shifts in the TO peak wavenumber ($480cm^{-1}$) can result from temperature increases from the laser during long measurements. However, acceptable Raman spectra are achievable within 60 seconds limiting the effect.

Transverse Acoustic (TA)

Following corrections to remove the influence of Raleigh scattering, the intensity and width of the transverse acoustic (TA) band occur from variations in the dihedral angle [97, 275, 276], representing changes in medium-range order (MRO) [99, 103, 276]. It can be assumed that no change in the TA peak position would indicate no change in the MRO. The sensitivity of the TO peak and TA peak are useful in observing changes in the Si-H bond-angle throughout the a-Si:H layer. The relative areas of both these bands provide information on the role hydrogen in bending and stretching modes when bonded with silicon [97, 277].

Longitudinal Optical (LO) and Logitudinal Acoustic (LA)

Cluster-Bethe-lattice calculations by Yndurian and Sen [278] have suggested that the LO-mode and LA- mode are due to the presense of closed rings of Si-atoms in the presence of void-rich films, which do not influence transverse modes. However, the presence of LA and LO modes are also typcial of a-Si:H layers absent of voids. Subsequently, decreases in the LA-band have since been associated with any increase in hydrogenation and the breaking of silicon-rings within an amorphous network [140]. This provides a measure of the hydrogenation process and the extent of voids within the deposited a-Si:H layer.

D-band and G-band

Although not heavily discussed, further information regarding the presence of microcrystallites within the a-Si:H matrix and the nature of the Si-Si bonds wihtin the a-Si:H layer can also be provided by two higher bands. The first is the D-band ($1360cm^{-1}$) corresponding to disordered microcrystallites within the amorphous layer for mixed-phase materials [279]. The second, G-band ($1530cm^{-1}$) relates to weakly-bond Si-Si bonds. The absence of the D-band if a G-band is detected often indicates that the a-Si:h layer is composed of weakly bonded Si-Si (sp^2) instead of strong Si-Si (sp^3) bonding.

A5. Spectroscopic ellipsomtery

Spectral ellipsometry is a non-destructive techniques that can accurately measure the refractive index and complex dielectric function of a given material. This is acheived by observing changes in the polarisation which occurs from the different attenuation and phase shifts of the electric fields for the incident light (see Figure 96).

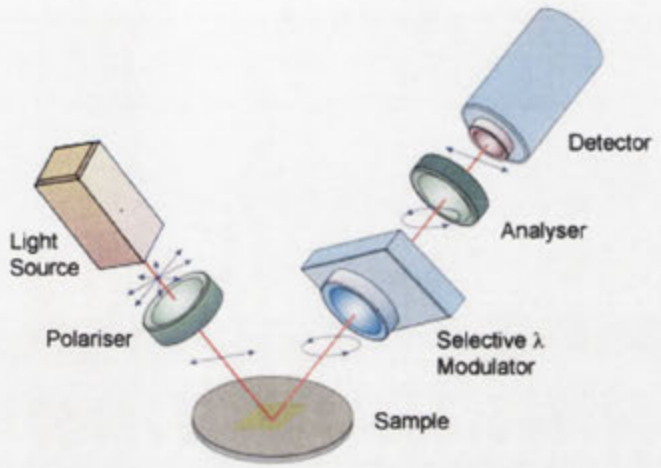

Figure 96: Schematic of spectroscopic ellipsometry setup.

For linearly polarised incident light the result is a reflected light that is elliptically polarised, perpendicular (*s*) and parallel (*p*) to the plane of the incident light. Analysis of the polarisation change allows the thickness of a thin-film layer to be determined. To improve accuracy, samples to be analysed need to be composed of one or two discrete, well-defined, optically homogeneous layers. The concept of ellipsomtery is illustrated in Figure 97a.

As stated. ellipsometry measures the complex dielectric function of reflected light from a given material using the parameters Ψ and Δ as determined by the Fresnel equations for a single wavelength. Following reflection, the amplitudes of the *s* and *p* components are normalised to the incident light are denoted as r_{ab}^{s} and r_{ab}^{p}. The complex reflectance ratio (*p*) is then calculated according to equation (A 14).

$$p = \frac{r_{ab}^{P}}{r_{ab}^{S}} = \tan\Psi . e^{j\Delta} = f\left(n_i, k_i, d_i \cdots\right) \qquad \text{(A 14)}$$

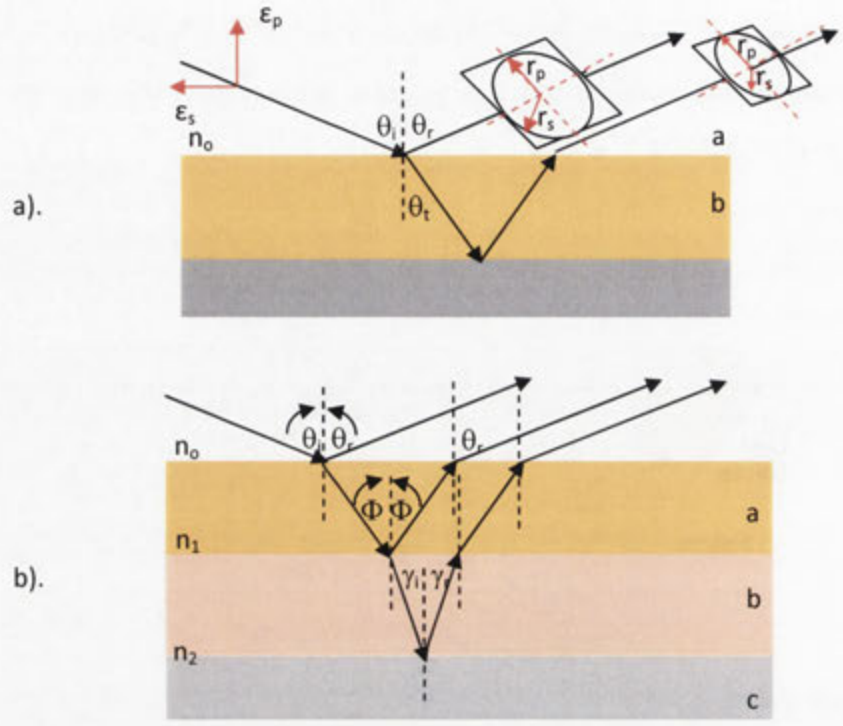

Figure 97: Illustration of ellipsometry technique for incident and reflected light on thin-film layers, a). Incident linearly polarised light and the reflection and refraction elliptically polarised light according to Snell's law and equations (A-15) and (a-16), b). The Fresnel reflection of multiple interfaces.

For multiple layers, the case for calculating the refractive index is more complicated as the relative phase of multiple reflected and refracted beams must be also be addressed (see Figure 97b). The formulation of r^s-polarised and r^p-polarised electric fields for multiple layers is therefore given by equation (A 15) and equation (A 16), respectively.

$$r^S = \frac{r_{ab}^S + r_{bc}^S e^{-j2\beta}}{1 + r_{ab}^S r_{bc}^S e^{-j2\beta}} \quad \text{(A 15)}$$

$$r^P = \frac{r_{ab}^P + r_{bc}^P e^{-j2\beta}}{1 + r_{ab}^P r_{bc}^P e^{-j2\beta}} \quad \text{(A 16)}$$

As the superposition of multiple light beams introduce interference dependent upon the relative phase, Fresnel calculations are necessary to determine the thickness of each layer in terms of pahse according to equation (A 17).

$$\beta = 2\pi\left(\frac{d}{\lambda}\right)(n_b - jk_b)\cos\Phi_b \qquad \text{(A 17)}$$

Ellipsometry measurements are commonly performed using a laser source at a single wavelength (i.e. 623.4nm). However, for a-Si:H layers below 0.2µm deposited onto c-Si surfaces are known to have a large degree of error resulting from the similarity between the thin a-Si:H and the c-Si surfaces at this wavelength; and also the non-isotropic nature of many a-Si:H layers. In the monochromatic case, ellipsometry is restricted to a single set of Ψ and Δ values, and subsequently only one approximation of thickness. To reduce the error in determining the absorption coefficient (α) and the extinction coefficient (k) of the a-Si:H layer, multi-wavelength spectral ellipsometry using a either a broad-band light source or different wavelngth lasers is utlised instead. This provides a series of Ψ and Δ using detector-side angle seletion which can be used to fitting of α and k. The wavelength dependent absorption coefficient is calculated according to equation (A 18).

$$\alpha_{(\lambda)} = \frac{4\pi k}{\lambda} \qquad \text{(A 18)}$$

The IR spectroscopic ellipsometry technique in this thesis utilises the double-modulation method to measure an absorption signal for very thin films [280]. Corrections to the measured IR response for a-Si:H below 1µm in thickness are made according to the model reported by Maley [277].

The refractive index (n) and the thickness of the a-Si:H layer are calculated from the values for α and k according to Tauc-Lorentz adapted from studies by Hazra *et. al.* [281], Chen and Shen [282], and Rao [180]. Using this technique, sub-nanometer thicknesses and refractive index changes as low as 0.01 are detectable.

B.

Appendix B: Wafer doping after annealing

B1. Surface passivation as a function of wafer doping and annealing temperature

An important consideration for evaluating the suitability of a-Si:H(i) layers as a passivating material is their ability to effectively passivated the c-Si wafer surfaces of different doping concentrations. Although, relatively high doping concentrations (≤3Ωcm) are commonly used in silicon solar cell designs, some applications may require wafers with lower concentrations (above 30Ωcm). Therefore, it is prudent to assess the variation in surface passivation quality provided by the a-Si:H(i) layers of different thicknesses deposited in this work on both n- and p-type *FZ* c-Si wafers of different doping concentrations. The results for a-Si:H(i) deposited onto c-Si(n) with doping resistivity's (ρ) between 1.4Ωcm and 100Ωcm (225μm) are presented in Figure 98. All a-Si:H(i) layers are deposited at optimised conditions.

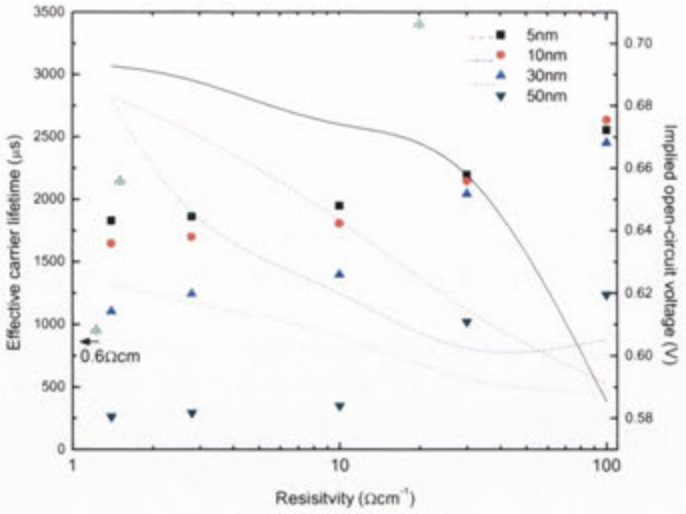

Figure 98: Effective carrier lifetime (symbols) measured at ($\Delta n = 10^{15}cm^{-3}$) and implied open-circuit voltage (lines) for 5nm, 10nm, 30nm, and 50nm a-Si:H(i) are deposited. These may be compared to optimised SiN films reported by Kerr [213].

As shown, a dependence of τ_{eff} on the resistivity of the c-Si wafer does occur. For example, the effective lifetime (measured at $10^{15}cm^{-3}$) obtained with 30nm a-Si:H(i) layers increases from 1ms for p = 1Ωcm to 2.5ms at 100Ωcm. Nevertheless, this dependence on resistivity is relatively weak compared to PECVD SiN reported by Kerr [213]. From this it can be said that for a-Si:H(i), surface passivation is governed more by the thickness of the layer and the presence of a hydrogen-rich interface region, than on the resistivity of the base c-Si wafer.

Further evaluation of the passivation of either 1.4Ωcm n-type or 0.9Ωcm p-type *FZ* c-Si by a-Si:H(i) is provided according to the implied open-circuit voltage (implied-V_{oc}). This valued can be approximated from τ_{eff} measurements at $\Delta n = 10^{16}cm^{-3}$ according to equation (B-1). In this, N_{dop} is N_D for c-Si(n), and N_A for c-Si(p) wafers, and accounts for light absorption, if any, if thicker a-Si:H layers. In both cases, change in neutrality is given by $\Delta n = \Delta p$.

$$V_{oc(implied)} = \left(\frac{kT}{q}\right) Ln\left(\frac{\Delta n\left(\Delta n + N_{dop}\right)}{n_i^2}\right) \qquad \text{(B- 1)}$$

The implied-Voc for a-Si:H(i) on both n- and p-type c-Si wafers given in Figure 98. A clear trend can be seen for each thickness on different doping wafers. Additionally, for both c-Si wafer types, a

maximum implied-Voc of 693mV was achieved. However, the maximum for a-Si:H(i) layers on c-Si(p) appear to be shifted towards higher temperatures. Furthermore, although the implied-V_{oc} remain below 620mV for all a-Si:H(i) thicknesses, results presented as part of this work give support for a further investigation of this relationship. Consistently, for n- and p-type c-Si, thinner intrinsic a-Si:H appear to perform better.

C.

Appendix C: Research level HiT-like devices □

As discussed in the introduction to this thesis, there have been many reported attempts to replicate the Sanyo HiT solar cell. In many cases, different processing conditions have been utilised either by choice or a restriction of the system used to deposit the layers. It would be impractical to list all conditions for the fabrication of these devices, and as such, it is recommended that the following list be used as a guide for the current state of achieved values for these device types. Every attempt has been made to ensure a complete summary is given, however, with the increasing interest in the a-Si:H material and HiT-like devices some more recent reported results may have been overlooked.

Table 7: HIT list for reported cell performances. For many a-Si:H based deigns, a Al-BSF is used at the rear surface instead of the double heterostructure design.

Group	Orientation	Doping (Ωcm)	a-Si:H(i) (nm)	a-Si:H (n or p) layer (nm)	I_{sc} (mA)	V_{oc} (V)	FF (%)	η (%)	Comments
		n-type							
Sakata [205]	(100) Cz (n)	1		DS	36.7	0.719	78.6	20.7	
Taguchi [159]	(100) Cz (n)	1		DS	36.7	0.702	77.9	20.1	
Sawada [29]	(100) Cz(n)	1-2		DS	39.4	0.644	79.0	20.0	
Sawada [29]	(100) Cz(n)	1.35-2.25		SS	31.0	0.600	80.5	14.8	
Sawada [29]	(100) Cz(n)	0.65-0.75			30.0	0.565	72.0	12.3	
Zignani	(?) Cz(n)				34.5	0.573	72.0	14.2	
Muñoz [88]	100) FZ(n)		5nm	50nm μc-Si:H front (n)	28.8	0.525	71	10.7	50nm μc-Si:H rear (p)
Schmidt [283]	(?) FZ(?)		5-10nm	(n)-front / (p)-rear	39.26	0.639	78.9	19.8	
Olibet [284]	(?) (n)		5nm	(p) – front / (n) - rear	32	0.705	78	17.6	
Conrad [285]	(?) FZ(n)		?	(p) – front / (n) - rear	39.26	0.639	78.9	19.8	Textured
Fujiwara [61]	(100) (n)		4nm	5nm (p)-front	33.47	0.591	74.2	14.67	Al-BSF
Maydell [218]	(100) FZ(n)			6nm				17.6	Al-BSF
Schmidt [283]	(?) FZ(?)		5-10nm	(n)-front / (p)-rear	34.9	0.629	79	17.4	
		p-type							
Vetter [220]	(100) FZ(p)	0.4	--	a-SiC_x:H	29.2	0.617	76	13.7	Diffused emitter
Wang [110]	(100?) FZ(p)	0.5	5nm	(n)- front	32.16	0.652	80.5	16.9	Al-BSF
Jagannathan [237]	(100) Cz(p)	1-10			30.0	0.550	64.0	10.6	
Hussein	(100) Cz(p)	1-2			30.2	0.592	79.7	14.2	
De Rosa	(100) Cz(p)	0.7-1.3			33.8	0.612	78.2	16.2	
Fujiwara [61]	(111) (p)		4nm	5nm (p)-front	33.2	0.628	77	16.1	Al-BSF
Wang [110]	(100?) FZ(p)		5nm	(n)- front	33.11	0.645	79.2	16.9	Al-BSF
Muñoz [88]	(100) FZ(p)	1	5nm		28.4	0.617	74.8	13.1	50nm μc-Si:H front (n), rear (p)
Olibet [284]	((?) (p)	0.5	5nm	(n)-front / (p)-rear	32	0.690	74	16.3	
Tucci [286]	(100) Cz(p)	1	5nm	20nm (n) –front	37.1	0.600	76.3	17.1	
Sherff [287]	(100) FZ(p)	0.8-1.2	none	5nm (n) front	30.6	0.606	80.8	14.8	Al-BSF
Janz [219]	(100) FZ(p)	1	a-SiC_x:H(i)	12nm a-SiC_x:H(n)	31.5	0.674	66.7	14.1	Rear (SiO/Al-BSF)
Sherff [288]	(?) Cz(p)	0.8-1	10nm	(n) -front	31.78	0.612	81.73	15.9	Textured, boron diffusion
Conrad [285]	(?) FZ(p)	1-2	?	(n) – front / (p) - rear	34.9	0.629	79	17.4	Textured
Jensen	(100) FZ(p)	0.5	(i)	(n) –front	26.65	0.654	81	14.1	
Maydell [218]	(100) FZ(p)			6nm (n) - front				17.1	Al-BSF

List of Publications

Refereed journal papers

[1]. J. Mitchell, D. Macdonald and A. Cuevas, "Thermal activation energy for the passivation of the n-type crystalline silicon surface by hydrogenated amorphous silicon", Applied Physics Letters 94, 162102 (2009).

Papers presented at international conferences

[1]. J. Mitchell, "Implementation of a Surface Diffusion Hydrogen Passivation for Shallow Acceptors in 3- Dimensional Hybridised Thin Film a-Si:H", presented at *IUMRS – International Conference on Electronics Materials, Yokohama,* Japan (2012)

[2]. J Mitchell, "Surface passivation of multicrystalline silicon by Multi-layer PECVD of hydrogenated amorphous silicon", presented *at IUMRS – International Conference on Electronics Materials,* Yokohama, Japan (2012)

[3]. J. Mitchell, "New insight into the Hydrogen surface passivation mechanism at low temperature", *Proceedings 24th European Photovoltaic Solar Energy Conference, Hamburg, Germany (2009)*

[4]. J. Mitchell, "Surface passivation of multicrystalline silicon by Multi-layer PECVD of hydrogenated amorphous silicon", *Proceedings 24th European Photovoltaic Solar Energy Conference, Hamburg, Germany (2009)*

[5]. J. Mitchell, D. Macdonald and A. Cuevas, "Plasma-Enhanced Chemical Vapour Deposition of a-Si:H to Provide Surface Passivation of c-Si Surfaces at Low Temperature", *Proceedings 22nd European Photovoltaic Solar Energy Conference*, Milan, Italy (2007). pp. 928-931.

[6]. M. Tucci, L. Serenelli, S. De Iuliis, M. Izzi, P. Mangiapane, A. Cuevas and J. Mitchell, "Characterization of SiNx/a-Si:H crystalline silicon surface passivation under UV light exposure", *Proceedings 21st European Photovoltaic Solar Energy Conference*, Dresden, Germany (2006). pp 1404-1407.

[7]. J. Mitchell, D. Macdonald, A. Cuevas and J. Cornish, "Electronic and structural properties of amorphous silicon on crystalline silicon wafers", *Proceedings 20th European Photovoltaic Solar Energy Conference*, Barcelona, Spain (2005). pp. 1004-1007

[8]. J. Mitchell, D. Macdonald and A. Cuevas, "Thermally activated surface passivation of a-Si:H/c-Si interfaces with annealing", *Proceedings 44th Australian and New Zealand Solar Energy Society Conference*, Canberra, Australia (2006).

[9]. J. Mitchell, D. Macdonald, A. Cuevas and P. Jennings, "Surface passivation of n- and p-type crystalline silicon wafers by amorphous silicon films", *Proceedings 42nd Annual Australian and New Zealand Solar Energy Society Conference*, Perth, Australia (2005).

[10]. D. Macdonald, K. McLean, J. Mitchell, P.N.K. Deenapanray, and S. De Wolf, "Alternative scheme for implementing the impurity-photovoltaic effect in crystalline silicon", *Proceedings 20th European Photovoltaic Solar Energy Conference*, Paris, France (2004). pp. 88-91

BIBLIOGRAPHY

1. Tans, P., *Trends in Atmospheric Carbon Dioxide - Mauna Loa*. 2009, National Oceanic & Atmospheric Administration.
2. IEA, *World Energy Outlook: 2008 Executive Summary*. 2008, OECD / International Energy Society: Paris, France.
3. Pacala, S. and Socolow, R., *Stabilization Wedges: Solving the Climate Problem for the Next 50 Years with Current Technologies*. Science, 2004. **305**(5686): p. 968-972.
4. Becquerel, A. E., *Mémoire sur les effets électriques produits sous l'influence des rayons solaires*. Comptes rendus de l'Académie des Sciences, 1839. **9**: p. 561-567.
5. Chapin, D. M., Fuller, C. S., and Pearson, G. L., *A New Silicon p-n Junction Photocell for Converting Solar Radiation into Electrical Power*. Journal of Applied Physics, 1954. **25**(5): p. 676-677.
6. Solarbuzz. *Solarbuzz Reports World Solar Photovoltaic Market Grew to 18.2 Gigawatts in 2010, Up 139% Y/Y*. 2011 14th March 2011 15th March 2011]; Available from: http://solarbuzz.com/our-research/recent-findings/solarbuzz-reports-world-solar-photovoltaic-market-grew-182-gigawatts-20.
7. Zhao, J., Wang, A., and Green, M. A., *19.8% efficient "honeycomb" textured multicrystalline and 24.4% monocrystalline silicon solar cells*. Applied Physics Letters, 1998. **73**(14): p. 1991.
8. Moschner, J. D., Henze, J., Schmidt, J., and Hezel, R., *High-quality surface passivation of silicon solar cells in an industrial-type inline plasma silicon nitride deposition system*. 2004. p. 21-31.
9. Lindmayer, J. *Semi-crystalline solar cells*. in *12th IEEE Photovoltaic Specialists Conference*. 1976. Baton Rouge, LA, United States: IEEE.
10. Schultz, O., Glunz, S., and Willeke, G. P., *SHORT COMMUNICATION: ACCELERATED PUBLICATION: Multicrystalline silicon solar cells exceeding 20% efficiency*. Progress in Photovoltaics: Research and Applications, 2004. **12**(7): p. 553-558.
11. Hirshman, W. P., Photon International, 2009: p. 170.
12. Hangleiter, A. and Häcker, R., *Enhancement of band-to-band Auger recombination by electron-hole correlations*. Physical Review Letters, 1990. **65**(2): p. 215-218.
13. Pierret, R. F., *Advanced Semiconductor Fundamentals, vol. VI: .* 1989: Addison-Wesley.
14. Kerr, M. and Cuevas, A., *Very low bulk and surface recombination in oxidized silicon wafers*. Semiconductor Science and Technology, 2002. **17**: p. 35.
15. Aberle, A. G. and Hezel, R., *Progress in Low-temperature Surface Passivation of Silicon Solar Cells using Remote-plasma Silicon Nitride*. Progress in Photovoltaics: Research and Applications, 1997. **5**(1): p. 29-50.
16. Leguijt, C., Lölgen, P., Eikelboom, J. A., Amesz, P. H., Steeman, R. A., Sinke, W. C., Sarro, P. M., Verhoef, L. A., Michiels, P. P., Chen, Z. H., and Rohatgi, A., *Very low surface recombination velocities on 2.5 Ωcm Si wafers, obtained with low-temperature PECVD of Si-oxide and Si-nitride*. Solar Energy Materials and Solar Cells, 1994. **34**(1-4): p. 177-181.
17. Schmidt, J., Kerr, M., and Cuevas, A., *Surface passivation of silicon solar cells using plasma-enhanced chemical-vapour-deposited SiN films and thin thermal SiO_2/plasma SiN stacks*. Semiconductor Science and Technology, 2001. **16**(3): p. 164.
18. Mehta, V., Sopori, B., Rupnowski, P., Moutinho, H., Shaikh, A., Khadilkar, C., Bennett, M., and Carlson, D., *Progress in Low-Temperature Surface Passivation of Silicon Solar Cells using Remote-Plasma Silicon Nitride*. Material Research Society.
19. Sterling, H. F. and Swann, R. C. G., *Chemical vapour deposition promoted by r.f. discharge*. Solid-State Electronics, 1965. **8**(8): p. 653-654.
20. Chittick, R. C., Alexander, J. H., and Sterling, H. F., *The Preparation and Properties of Amorphous Silicon*. Journal of the Electrochemical Society, 1969. **116**(1): p. 77-81.

21. Spear, W. E. and Le Comber, P. G., *Substitutional doping of amorphous silicon.* Solid State Communications, 1975. **17**(9): p. 1193-1196.
22. Ovadyahu, Z. and Wiesmann, H., *A transparent-conducting coating for a-Si:H based devices.* Journal of Applied Physics, 1981. **52**(9): p. 5865-5866.
23. Daiello, R. V. and Twesme, E. N., *Thin-film module circuit design: Practical and reliability aspects* S.T.F. Division, Editor. 1985, NASA: Newtown, PA. p. 33-46.
24. Walsh, F. and Simon, J., *Silicon Film Formation by MIRPD of Phenylsilane, Phase 2, Final Report.* 1987, Tracer Technologies, Inc.: Somerville, MA. p. 54.
25. Hidenori, M. and Yoshinori, H., *The use of amorphous-crystalline silicon heterojunctions for the application to an imaging device*. 1987, AIP. p. 2575-2580.
26. Staebler, D. L. and Wronski, C. R., *Optically induced conductivity changes in discharge-produced hydrogenated amorphous silicon.* Journal of Applied Physics, 1980. **51**(6): p. 3262-3268.
27. Yang, J. and Guha, S., *High-Efficiency Amorphous Silicon and Nanocrystalline Silicon Based Solar Cells and Modules: Annual Technical Progress Report*. 2007, United Solar Ovonic LLC: Troy, Michigan. p. 56.
28. Wang, W., Povolny, H., Du, W., Liao, X. B., and Deng, X. *Triple-junction a-Si solar cells with heavily doped thin interface layers at the tunnel junctions*. in *Photovoltaic Specialists Conference, 2002. Conference Record of the Twenty-Ninth IEEE*. 2002. New Orleans, USA: IEEE.
29. Sawada, T., Terada, N., Tsuge, S., Baba, T., Takahama, T., Wakisaka, K., Tsuda, S., and Nakano, S. *High-efficiency a-Si/c-Si heterojunction solar cell*. in *IEEE Photovoltaic Specialists Conference: Photovoltaic Energy Conversion*. 1994. Waikoloa, Hawaii.
30. Tanaka, M., Taguchi, M., Matsuyama, T., Sawada, T., Tsuda, S., Nakano, S., Hanafusa, H., and Kuwano, Y., *Development of New a-Si/c-Si Heterojunction Solar Cells: ACJ-HIT (Artificially Constructed Junction-Heterojunction with Intrinsic Thin-Layer).* Japanese Journal of Applied Physics, 1992. **31**: p. 3518-3522.
31. Kawamoto. in *12th International PVSEC*. 2001. Korea.
32. Jensen, N., Hausner, R., Bergmann, R., Werner, J., and Rau, U., *Optimisation and Characteristion of Amorphous/Cyrstalline Silicon Heterojunction Solar Cells.* Progress in Photovoltaics: Research and Applications, 2002. **10**: p. 1-13.
33. Green, M. A., Emery, K., Hishikawa, Y., and Warta, W., *Solar Cell efficiency tables (version 35).* Progress in Photovoltaics: Research and Applications, 2010. **19**: p. 144-150.
34. Maruyama, E., Terakawa, A., Taguchi, M., Yoshimine, Y., Ide, D., Baba, T., Shima, M., Sakata, H., and Tanaka, M. *Sanyo's Challenges to the Development of High-efficiency HIT Solar Cells and the Expansion of HIT Business*. in *IEEE 4th World Conference on Photovoltaic Energy Conversion*. 2006. Hawaii.
35. Tsunomura, Y., Yoshimine, Y., Taguchi, M., Baba, T., Kinoshita, T., Kanno, H., Sakata, H., Maruyama, E., and Tanaka, M., *Twenty-two percent efficiency HIT solar cell.* Solar Energy Materials and Solar Cells, 2009. **93**(6-7): p. 670-673.
36. Dauwe, S., Mittelstädt, L., Metz, A., and Hezel, R., *Experimental evidence of parasitic shunting in silicon nitride rear surface passivated solar cells.* Progress in Photovoltaics: Research and Applications, 2002. **10**(4): p. 271-278.
37. Green, M. A., Emery, K., Hishikawa, Y., and Warta, W., *Solar cell efficiency tables (version 37).* Progress in Photovoltaics: Research and Applications, 2011. **19**(1): p. 84-92.
38. Kushner, M., *A model for the discharge kinetics and plasma chemistry during plasma enhanced chemical vapor deposition of amorphous silicon.* Journal of Applied Physics, 1988. **63**(8): p. 2532-2551.

39. Shirafuji, T., Nakajima, S., Wang, Y. F., Genji, T., and Tachibana, K., *Direct Photochemical Vapour Deposition of Hydrogenated Amorphous Silicon Effects of Excitation Wavelengths and Source Gases.* Japanese Journal of Applied Physics, 1993. **32**: p. 1546-1557.
40. Fujiwara, H. and Kondo, M., *Impact of Epitaxial Growth at the Heterointerfaces of a-Si:H/c-Si Solar Cells.* Applied Physics Letters, 2007. **90**(1): p. 013503.
41. Robertson, J., *Deposition mechanism of hydrogenated amorphous silicon.* Journal of Applied Physics, 2000. **87**(5): p. 2608-2617.
42. Fontcuberta i Morral, A. and Roca i Cabarrocas, P., *Etching and hydrogen diffusion mechanisms during a hydrogen plasma treatment of silicon thin films.* Journal of Non-Crystalline Solids, 2002. **299-302**(Part 1): p. 196-200.
43. Street, R. A., *Hydrogenated Amorphous Silicon*. 1991: Cambridge University Press.
44. Ray, S., Das, C., Mukhopadhyay, S., and Saha, S. C., *Substrate temperature and hydrogen dilution: parameters for amorphous to microcrystalline phase transition in silicon thin films.* Solar Energy Materials and Solar Cells, 2002. **74**(1-4): p. 393-400.
45. Danesh, P., Pantchev, B., Grambole, D., and Schmidt, B., *Effect of film thickness on hydrogenated amorphous silicon grown with hydrogen diluted silane.* Applied Physics Letters, 2002. **80**(14): p. 2463-2465.
46. Jagannathan, B., Anderson, W. A., and Coleman, J., *Amorphous silicon/p-type crystalline silicon heterojunction solar cells.* Solar Energy Materials and Solar Cells, 1997. **46**(4): p. 289-310.
47. Tanino, H., Ganguly, G., and Matsuda, A., *Raman study of ultrathin films of hydrogenated amorphous silicon.* Physical Review B, 1992. **46**(23): p. 15277.
48. von Roedern, B., Ley, L., and Cardona, M., *Photoelectron Spectra of Hydrogenated Amorphous Silicon.* Physical Review Letters, 1977. **39**(Copyright (C) 2010 The American Physical Society): p. 1576.
49. v. Maydell, K., Conrad, E., and Schmidt, M., *Efficient silicon heterojunction solar cells based on p- and n-type substrates processed at temperatures < 220°C.* Progress in Photovoltaics: Research and Applications, 2006. **14**(4): p. 289-295.
50. Pearce, J. M., Podraza, N., Collins, R. W., Al-Jassim, M. M., Jones, K. M., Deng, J., and Wronski, C. R., *Optimization of open circuit voltage in amorphous silicon solar cells with mixed-phase (amorphous + nanocrystalline) p-type contacts of low nanocrystalline content.* Journal of Applied Physics, 2007. **101**(11): p. 114301.
51. Martin, I., Vetter, M., Orpella, A., Puigdollers, J., Cuevas, A., and Alcubilla, R., *Surface passivation of p-type crystalline Si by plasma enhanced chemical vapor deposited amorphous SiC_x:H films.* Applied Physcis Letters, 2001. **79**(14): p. 2199-2201.
52. Tucci, M., Serenelli, L., Salza, E., De Iuliis, S., Geerligs, L. J., Caputo, D., Ceccarelli, M., and de Cesare, G., *Back contacted a-Si:H/c-Si heterostructure solar cells.* Journal of Non-Crystalline Solids, 2008. **354**(19-25): p. 2386-2391.
53. Rinnert, H. and Vergnat, M., *Influence of the substrate temperature on the structure and the optical properties of amorphous Si:H thin films prepared by reactive evaporation.* Thin Solid Films, 2002. **403-404**: p. 153-156.
54. Arendse, C., Knoesen, D., Britton, D., Hempel, A., Hempel, M., Dabrowski, A., and Van der Weg, W. F., *Thermal Stability of Hot-Wire Deposited Amorphous Silicon.* Thin Solid Films, 2005. **501** (1–3): p. 3.
55. Clark, G. J., White, C. W., Allred, D. D., Appleton, B. R., Magee, C. W., and Carlson, D. E., *The use of nuclear reactions and SIMS for quantitative depth profiling of hydrogen in amorphous silicon* Applied Physics Letters, 1977. **31**: p. 582-586.
56. Carlson, D. E. and Magee, C. W., *A SIMS analysis of deuterium diffusion in hydrogenated amorphous silicon.* Applied Physics Letters, 1978. **33**(1): p. 81-83.

57. Santos, P. V., Johnson, N. M., and Street, R. A., *Light-enhanced hydrogen motion in a-Si:H.* Physical Review Letters, 1991. **67**(19): p. 2686.
58. Britton, D. T., Hempel, A., Härting, M., Kögel, G., Sperr, P., Triftshäuser, W., Arendse, C., and Knoesen, D., *Annealing and recrystallization of hydrogenated amorphous silicon.* Physical Review B, 2001. **64**(7): p. 075403.
59. Lien, S.-Y., Wu, B.-R., Liu, J.-C., and Wuu, D.-S., *Fabrication and characteristics of n-Si/c-Si/p-Si heterojunction solar cells using hot-wire CVD.* Thin Solid Films, 2008. **516**(5): p. 747-750.
60. Arce, R., Koropecki, R. R., Cutrera, M., and Buitrago, R., *The thickness dependence of electronic properties of doped a-Si:H alloys.* Journal of Physics: Condensed Matter, 1993. **5**: p. A339--A340.
61. Fujiwara, H. and Kondo, M., *Effects of a-Si:H layer Thicknesses on the Performance of a-Si:H/c-Si Heterojunction Solar Cells.* Journal of Applied Physics, 2007. **101**(5): p. 054516-054516-9
62. Yoshihiro, H., Sadaji, T., Noboru, N., Shinya, T., Shoichi, N., and Yukinori, K., *Effect of substrates and film thickness on the structural, optical, and electrical properties of hydrogenated amorphous silicon films.* 1990, AIP. p. 771-773.
63. Gleason, K. K., Petrich, M. A., and Reimer, J. A., *Hydrogen microstructure in amorphous hydrogenated silicon.* Physical Review B, 1987. **36**(6): p. 3259.
64. De Wolf, S. and Kondo, M., *Abruptness of a-Si:H/c-Si Interface revealed by carrier lifetime measurements.* Applied Physics Letters, 2007. **90**: p. 042111 1-3.
65. Dauwe, S., Schmidt, J., and Hezel, R. *Very low surface recombination velocities on p- and n-type silicon wafers passivated with hydrogenated amorphous silicon.* in *29th IEEE Photovoltaic Specialists Conference*. 2002. New Orleans.
66. Aberle, A., G., *Surface passivation of crystalline silicon solar cells: a review.* Progress in Photovoltaics: Research and Applications, 2000. **8**(5): p. 473-487.
67. Dekkers, H. F. W., De Wolf, S., Agostinelli, G., Duerinckx, F., and Beaucarne, G., *Requirements of PECVD SiNx:H layers for bulk passivation of mc-Si.* Solar Energy Materials and Solar Cells, 2006. **90**(18-19): p. 3244-3250.
68. Dupuis, J., Fourmond, E., Lelièvre, J. F., Ballutaud, D., and Lemiti, M., *Impact of PECVD SiON stoichiometry and post-annealing on the silicon surface passivation.* Thin Solid Films, 2008. **516**(20): p. 6954-6958.
69. Sopori, B. L., Deng, X., Benner, J. P., Rohatgi, A., Sana, P., Estreicher, S. K., Park, Y. K., and Roberson, M. A., *Hydrogen in silicon: A discussion of diffusion and passivation mechanisms.* Solar Energy Materials and Solar Cells, 1996. **41-42**: p. 159-169.
70. Koch, C., Ito, M., and Schubert, M., *Low-temperature deposition of amorphous silicon solar cells.* Solar Energy Materials and Solar Cells, 2001. **68**(2): p. 227-236.
71. De Wolf, S. and Kondo, M., *Surface Passivation Properties of Stacked Doped PECVD a-Si:H Layers for Hetero-structure c-Si Solar Cells*, in *4th WCPEC*. 2006: Waikoloa, Hawaii.
72. Mitchell, J., Macdonald, D., and Cuevas, A., *Plasma-Enhanced Chemical Vapour Deposition of a-Si:H to Provide Surface Passivation of c-Si Surfaces at Low Temperatures*, in *22nd European Photovoltaic Solar Energy Conference*. 2007: Milan, Italy.
73. Pandey, K. C., Sakurai, T., and Hagstrum, H. D., *Si(111): SiH_3- A Simple New Surface Phase.* Physical Review Letters, 1975. **35**(25): p. 1728.
74. Takakuwa, Y., Nogawa, M., Ishida, H., Niwano, M., Kato, H., and Miyamoto, N., *In Situ Observation of Photon-Stimulated Hydrogen Removal on a HF-Passivated Si(111) Surface by Ultraviolet Photoelectron Spectroscopy Using Synchrotron Radiation.* Japanese Journal of Applied Physics, 1997. **36**(1): p. 7699-7705.
75. Appelbaum, J. A., Hamann, D. R., and Tasso, K. H., *Hydrogen Chemisorption on Si: A New Type of Chemisorptive Bond.* Physical Review Letters, 1977. **39**(23): p. 1487.

76. Saint-Cast, P., Hofmann, M., Dimitrova, T., Wagenmann, D., Rentsch, J., and Preu, R., *Firing Stable Passivation with a-Si/SiNx Stack Layer for Crystalline Silicon Solar Cells*, in *24th European Photovoltaic Solar Energy Conference, .* 2009: Hamburg, Germany. p. 1649 - 1653.
77. Powell, M. J. and Deane, S. C., *Defect-pool model and the hydrogen density of states in hydrogenated amorphous silicon.* Physical Review B, 1996. **53**(15): p. 10121.
78. Winer, K., *Chemical-equilibrium model of optimal a-Si:H growth from SiH4.* Physical Review B, 1990. **41**(11): p. 7952.
79. Winer, K., *Chemical-equilibrium description of the gap-state distribution in a-Si:H.* Physical Review Letters, 1989. **63**(14): p. 1487.
80. Andrew, W. B., Aihua, W., Adele, M. M., Jianhua, Z., and Martin, A. G., *22.8% efficient silicon solar cell*. 1989, AIP. p. 1363-1365.
81. Thomas, L., Jens, M., Armin, G. A., and Rudolf, H., *Optimization and characterization of remote plasma-enhanced chemical vapor deposition silicon nitride for the passivation of p-type crystalline silicon surfaces*. 1998, AVS. p. 530-543.
82. Dewarrat, R. and Robertson, J., *Binding and surface diffusion of SiH_3 radicals and the roughness of hydrogenated amorphous silicon.* Applied Physics Letters, 2003. **82**(6): p. 883-885.
83. John, R., *Deposition mechanism of hydrogenated amorphous silicon*. 2000, AIP. p. 2608-2617.
84. Oura, K., Yamane, J., Umezawa, K., Naitoh, M., Shoji, F., and Hanawa, T., *Hydrogen adsorption on Si(100)-2 x 1 surfaces studied by elastic recoil detection analysis.* Physical Review B, 1990. **41**(2): p. 1200.
85. Roca, F., della Sala, D., Di Francia, G., Grillo, P., Fameli, G., Pascarella, P., and Citarella, A. in *Proceedings of the Thirteenth European Phototvol Solar Energy Conference*. 1995. Nice, France.
86. Trucks, G. W., Raghavachari, K., Higashi, G. S., and Chabal, Y. J., *Mechanism of HF etching of silicon surfaces: a theoretical understanding of hydrogen passivation.* Physical Review Letters, 1990. **65**(4): p. 504--507.
87. Martin, I., Munoz, D., Voz, C., Vetter, M., Alcubilla, R., Damon-Lacoste, J., Roca i Cabarrocas, P., Villar, F., Bertomeu, J., and Andreu, J. *Comparison of (n+) a-Si:H /(p) c-Si Heterojunction Emitters using a-Si:H Films Deposited by PECVD or HWCVD.* in *Photovoltaic Energy Conversion, Conference Record of the 2006 IEEE 4th World Conference on*. 2006.
88. Muñoz, D., Voz, C., Fonrodona, M., Garin, M., Orpella, A., Vetter, M., Puigdollers, J., Alcubilla, R., Villar, F., Bertomeu, J., and Andreu, J., *Characterization of bifacial heterojunction silicon solar cells obtained by hot-wire CVD.* Journal of Non-Crystalline Solids, 2006. **352**(9-20): p. 1953-1957.
89. Ferrjeua, F., Stehlea, J. L., Bernouxa, F., and Thomas, O. *Multispectral Spectroscopic Ellipsometry-A New Tool for In Situ Surface Analysis*. in *MRS Fall Meeting*. 1987: MRS.
90. Kempen, L. U., *Multi-Spectral Imaging Ellipsometer for Fast In-Situ Monitoring of Monolayer Film Deposition*. 1998, Physical Optics Corporation Torrance, California 90505. p. 37.
91. Li, Y. M., An, I., Nguyen, H. V., Wronski, C. R., and Collins, R. W., *Thin-film coalescence in hydrogenated amorphous silicon probed by spectroscopic ellipsometry with millisecond-scale resolution.* Physical Review Letters, 1992. **68**(Copyright (C) 2010 The American Physical Society): p. 2814.
92. Fujiwara, H., Kaneko, T., and Kondo, M., *Optimization of interface structures in crystalline silicon heterojunction solar cells.* Solar Energy Materials and Solar Cells, 2009. **93**(6-7): p. 725-728.
93. Drevillon, B., *In situ studies of the growth of hydrogenated amorphous silicon.* Journal of Non-Crystalline Solids, 1989. **114**(Part 1): p. 139-144.

94. Park, Y.-B. and Rhee, S.-W., *Microstructure and initial growth characteristics of the low temperature microcrystalline silicon films on silicon nitride surface.* Journal of Applied Physics, 2001. **90**(1): p. 217-221.
95. Kailer, A., Gogotsi, Y. G., and Nickel, K. G., *Phase transformations of silicon caused by contact loading.* Journal of Applied Physics, 1997. **81**(7): p. 3057-3063.
96. Ricciardi, C., Primiceli, A., Germani, G., Rusconi, A., and Giorgis, F., *Microstructure analysis of a-SiC:H thin films grown by high-growth-rate PECVD.* Journal of Non-Crystalline Solids, 2006. **352**(9-20): p. 1380-1383.
97. Maley, N. and Lannin, J. S., *Influence of hydrogen on vibrational and optical properties of a-Si1-xHx alloys.* Physical Review B, 1987. **36**(Copyright (C) 2010 The American Physical Society): p. 1146.
98. Rella, C. W., van der Voort, M., Akimov, A. V., van der Meer, A. F. G., and Dijkhuis, J. I., *Localization of the Si-H stretch vibration in amorphous silicon.* Applied Physics Letters, 1999. **75**(19): p. 2945--2947.
99. Marinov, M. and Zotov, N., *Model investigation of the Raman spectra of amorphous silicon.* Physical Review B, 1997. **55**(Copyright (C) 2010 The American Physical Society): p. 2938.
100. Jackson, W. B., Tsai, C. C., and Doland, C., *Effect of hydrogen on disorder in amorphous silicon.* Philosophical Magazine Part B, 1991. **64**(5): p. 611 - 622.
101. Furukawa, S., *Vibrational wavenumbers of SiHx bonds in binary Si:H materials.* Journal of Physics: Condensed Matter, 1990. **2**: p. 9209--9213.
102. Beeman, D., Tsu, R., and Thorpe, M. F., *Structural information from the Raman spectrum of amorphous silicon.* Physical Review B, 1985. **32**(2): p. 874.
103. Tsu, R., Paesler, M. A., and Sayers, D., *Phonon linewidth and bond angle deviation in amorphous silicon and germanium.* Journal of Non-Crystalline Solids, 1989. **114**(Part 1): p. 199-201.
104. Smets, A. H. M., Kessels, W. M. M., and van de Sanden, M. C. M., *Vacancies and voids in hydrogenated amorphous silicon.* Applied Physics Letters, 2003. **82**(10): p. 1547--1549.
105. Arendse, C. J., Knoesen, D., and Britton, D. T., *Thermal stability of hot-wire deposited amorphous silicon.* Thin Solid Films, 2006. **501**(1-2): p. 92-94.
106. Acco, S., Williamson, D. L., Stolk, P. A., Saris, F. W., van den Boogaard, M. J., Sinke, W. C., van der Weg, W. F., Roorda, S., and Zalm, P. C., *Hydrogen solubility and network stability in amorphous silicon.* Physical Review B, 1996. **53**(8): p. 4415.
107. Müllerová, J., Jurecka, S., and Sutta, P., *Optical characterization of polysilicon thin films for solar applications.* Solar Energy, 2006. **80**(6): p. 667-674.
108. Toyoshima, Y., Arai, K., Matsuda, A., and Tanaka, K., *In situ characterization of the growing a-Si:H surface by IR spectroscopy.* Journal of Non-Crystalline Solids, 1991. **137-138**(Part 2): p. 765-770.
109. Blayo, N. and Drevillon, B., *In situ study of the growth of hydrogenated amorphous silicon by infrared ellipsometry.* Applied Physics Letters, 1991. **59**: p. 950 - 952.
110. Wang, T. H., Iwaniczko, E., Page, M. R., Levi, D. H., Yan, Y., Yelundur, V., Branz, H. M., Rohatgi, A., and Wang, Q. *Effective Interfaces in Silicon Heterojunction Solar Cells.* in *Conference Record of the Thirty-first IEEE Photovoltaic Specialists Conference*. 2005. Lake Buena Vista: IEEE.
111. Kim, Y. T., Yoon, S. G., Kim, H., Suh, S. J., Jang, G. E., and Yoon, D. H., *Crystallization of a-Si:H and a-SiC:H thin films deposited by PECVD.* Journal of Ceramic Processing Research, 2005. **6**(4): p. 294-297.
112. Street, R. A. and Winer, K., *Defect equilibria in undoped a-Si:H.* Physical Review B, 1989. **40**(9): p. 6236 - 6249.

113. Deenapanray, P., Athukorala, C., Macdonald, D., Everett, V., Weber, K., and Blakers, A., *Influence of Reactive Ion Etching on the Minority Carrier Lifetime in p-type Si*, in *20th EUPVSC Solar Energy Conference*. 2005: Barcelona.
114. Pantchev, B., Danesh, P., Savatinova, I., Liarokapis, E., Schmidt, B., and Grambole, D., *The effect of structural disorder on mechanical stress in a-Si:H films.* Journal of Physics D: Applied Physics, 2001. **34**(17): p. 2589.
115. Bakos, T., Valipa, M. S., and Maroudas, D., *Thermally activated mechanisms of hydrogen abstraction by growth precursors during plasma deposition of silicon thin films.* The Journal of Chemical Physics, 2005. **122**(5): p. 054703-1 to 054703-9.
116. Sriraman, S., Ramalingam, S., Aydil, E. S., and Maroudas, D., *Abstraction of hydrogen by SiH radicals from hydrogenated amorphous silicon surfaces.* Surface Science, 2000. **459**(3): p. L475-L481.
117. Parsons, G. N., *Surface reactions in very low temperature (<150°C) hydrogenated amorphous silicon deposition, and applications to thin film transistors.* Journal of Non-Crystalline Solids, 2000. **266-269, Part 1**(0): p. 23-30.
118. Srinivasan, E. and Parsons, G. N., *Hydrogen abstraction kinetics and crystallization in low temperature plasma deposition of silicon.* Applied Physics Letters, 1998. **72**(4): p. 456-458.
119. Lucovsky, G., *Chemical effects on the frequencies of Si-H vibrations in amorphous solids.* Solid State Communications, 1979. **29**(8): p. 571-576.
120. Langford, A. A., Fleet, M. L., Nelson, B. P., Lanford, W. A., and Maley, N., *Infrared absorption strength and hydrogen content of hydrogenated amorphous silicon.* Physical Review B, 1992. **45**(23): p. 13367.
121. Tsu, D. V., Lucovsky, G., and Davidson, B. N., *Effects of the nearest neighbors and the alloy matrix on SiH stretching vibrations in the amorphous SiOr:H (0<r<2) alloy system.* Physical Review B, 1989. **40**(3): p. 1795.
122. Dutta Gupta, N. and Chaudhuri, P., *Explanation of the structural changes in the Si:H thin films by monohydride cluster formation.* Journal of Physics D: Applied Physics, 2003. **36**: p. 522--528.
123. Flewitt, A. J., Robertson, J., and Milne, W. I., *Growth mechanism of hydrogenated amorphous silicon studied by in situ scanning tunneling microscopy*. 1999, AIP. p. 8032-8039.
124. Myburg, G. and Swanepoel, R., *The influence of substrate temperature on the deposition rate and optical properties of a-Si:H thin films prepared by RF-glow discharge.* Journal of Non-Crystalline Solids, 1987. **89**(1-2): p. 13-23.
125. Kessels, W. M. M., Smets, A. H. M., Marra, D. C., Aydil, E. S., Schram, D. C., and van de Sanden, M. C. M., *On the growth mechanism of a-Si:H.* Thin Solid Films, 2001. **383**(1-2): p. 154-160.
126. Smets, A. H. M., Kessels, W. M. M., and van de Sanden, M. C. M., *Temperature dependence of the surface roughness evolution during hydrogenated amorphous silicon film growth.* Applied Physics Letters, 2003. **82**(6): p. 865--867.
127. von Keudell, A. and Abelson, J. R., *Direct insertion of SiH3 radicals into strained Si-Si surface bonds during plasma deposition of hydrogenated amorphous silicon films.* Physical Review B, 1999. **59**(8): p. 5791.
128. Burrows, M. Z., Das, U. K., Opila, R. L., De Wolf, S., and Birkmire, R. W., *Role of hydrogen bonding environment in a-Si:H films for c-Si surface passivation.* Journal of Vacuum Science and Technology: A, 2008. **26**(4): p. 683-687.
129. Lim, P. K., Tam, W. K., Yeung, L. F., and Lam, F. M. *Effect of hydrogen on danglin bond in a-Si thin film*. in *International Conference on Nanoscience and Technology*. 2006: IOP Publishing, Journal of Physics: Conference Series 61.
130. De Wolf, S. and Kondo, M., *Temperature Dependent c-Si Surface Passivation Properties of Intrinsic PECVD a-Si:H films*, in *16th c-Si NREL workshop*. 2006: Denver, Colorado.

131. Naito, N., Takano, A., Sumiya, M., Kawasaki, M., and Koinuma, H., *In situ optical diagnosis on hydrogenated amorphous silicon grown by vibration superimposed plasma chemical vapor deposition.* Applied Physics Letters, 1995. **66**(9): p. 1071-1073.
132. Fujiwara, H., Toyoshima, Y., Kondo, M., and Matsuda, A., *Interface-layer formation mechanism in a-Si:H thin-film growth studied by real-time spectroscopic ellipsometry and infrared spectroscopy.* Physical Review B, 1999. **60**(19): p. 13598.
133. Pangal, K., Sturm, J., Wagner, S., and Buyuklimanli, T., *Hydrogen plasma enhanced crystallization of hydrogenated amorphous silicon films.* Journal of Applied Physics, 1999. **85**(3): p. 1900-1906.
134. van der Sanden, M., Kessels, W., Smets, A., Korevaar, B., Severens, R., and Schram, D.
135. Jackson, W. B. and Tsai, C. C., *Hydrogen transport in amorphous silicon.* Physical Review B, 1992. **45**(12): p. 6564.
136. Takada, J. and Fritzsche, H., *Drift mobility of doped a-Si:H at high temperatures.* Physical Review B, 1987. **36**(3): p. 1710--1714.
137. Guha, S., Yang, J., Williamson, D. L., Lubianiker, Y., Cohen, J. D., and Mahan, A. H., *Structural, defect, and device behavior of hydrogenated amorphous Si near and above the onset of microcrystallinity.* 1999, AIP. p. 1860-1862.
138. Middya, A., Hamma, S., Hazra, S., Ray, S., and Longeaud, C. *Stability and nanostructure of hetergeneous amorphous silicon thin-film synthesized under high chamber pressures (500 to 2200mTorr) regime of RF PECVD.* in *Material Research Society Symposium Proceedings.* 2001. 2001 MRS Spring Meeting.
139. Ray, S., Hazra, S., Middya, A. R., and Barua, A. K. *Low bandgap a-Si:H film with better stability prepared by RF PECVD method using helium dilution.* in *Photovoltaic Energy Conversion, 1994., Conference Record of the Twenty Fourth. IEEE Photovoltaic Specialists Conference - 1994, 1994 IEEE First World Conference on.* 1994.
140. Brodsky, M. H., Cardona, M., and Cuomo, J. J., *Infrared and Raman spectra of the silicon-hydrogen bonds in amorphous silicon prepared by glow discharge and sputtering.* Physical Review B, 1977. **16**(8): p. 3556.
141. Muñoz, D., Voz, C., Martin, I., Orpella, A., Puigdollers, J., Alcubilla, R., Villar, F., Bertomeu, J., Andreu, J., Damon-Lacoste, J., and Roca i Cabarrocas, P., *Progress in a-Si:H/c-Si heterojunction emitters obtained by Hot-Wire CVD at 200 °C.* Thin Solid Films, 2008. **516**(5): p. 761-764.
142. Lebib, S. and Roca i Cabarrocas, P., *Structure and hydrogen bonding in plasma deposited polymorphous silicon thin films.* The European Physical Journal Applied Physics, 2004. **26**(1): p. 17 to 27.
143. Korte, L., Laades, A., and Schmidt, M., *Electronic states in a-Si:H/c-Si heterostructures.* Journal of Non-Crystalline Solids, 2006. **352**(9-20): p. 1217-1220.
144. Lim, B. C., Choi, Y. L., Choi, J. H., and Jang, J., *Hydrogenated amorphous silicon thin film transistor fabricated on plasma treated silicon nitride.* Electron Devices, IEEE Transactions on, 2000. **47**(2): p. 367-371.
145. Vetter, M., Martín, I., Ferre, R., Garín, M., and Alcubilla, R., *Crystalline silicon surface passivation by amorphous silicon carbide films.* Solar Energy Materials and Solar Cells, 2007. **91**(2-3): p. 174-179.
146. De Wolf, S. and Beaucarne, G., *Surface passivation properties of boron-doped plasma-enhanced chemical vapor deposited hydrogenated amorphous silicon films on p-type crystalline Si substrates.* Applied Physics Letters, 2006. **88**(2): p. 022104-1--022104-3.
147. Prasad, K., Finger, F., Dubail, S., Shah, A., and Schubert, M., *Deposition of phosphorus doped microcrystalline silicon below 70 °C at 70 MHz.* Journal of Non-Crystalline Solids, 1991. **137-138**(Part 2): p. 681-684.

148. Biegelsen, D. K., Johnson, N. M., Stutzmann, M., Poindexter, E. H., and Caplan, P. J., *Native defects at the Si/SiO2 interface-amorphous silicon revisited.* Applications of Surface Science, 1985. **22-23**(Part 2): p. 879-890.
149. Pantelides, S. T., *Mechanisms for peculiar low-temperature phenomena in hydrogenated amorphous silicon.* Physical Review Letters, 1987. **58**(13): p. 1344.
150. Freeman, E. C. and Paul, W., *Optical constants of rf sputtered hydrogenated amorphous Si.* Physical Review B, 1979. **20**(2): p. 716.
151. Nobuo, N., Akihiro, T., Masatomo, S., Masashi, K., and Hideomi, K., *In situ optical diagnosis on hydrogenated amorphous silicon grown by vibration superimposed plasma chemical vapor deposition.* 1995, AIP. p. 1071-1073.
152. Myburg, G. and Swanepoel, R., *The influence of preparation parameters on the deposition rate, density and optical properties of thin hydrogenated amorphous silicon films prepared by r.f. glow discharge.* Thin Solid Films, 1987. **149**(3): p. 331-340.
153. Halindintwali, S., Knoesen, D., Muller, T., Adams, D., Tile, N., Theron, C., and Schropp, R., *Optical characterisation of a-Si:H and nc-Si:H thin films using the transmission spectrum alone.* Journal of Materials Science: Materials in Electronics, 2007. **18**(0): p. 225-229.
154. Schropp, R. E. I. and Zeman, M., *Amorphous and Microcrystalline Silicon Solar Cells: Modelling, Materials and Device technology*, in *Amorphous and Microcrystalline Silicon Solar Cells: Modelling, Materials and Device technology*. 1998, Kluwer Academic Publishers. p. 43.
155. Müllerová, J., Jurecka, S., Sutta, P., and Mikula, M., *Structural and Optical Studies of a-Si:H Thin Films: from Amorphous to Nanocrystalline Silicon.* Acta Physica Slovaca, 2005. **55**(3): p. 351-359.
156. Tuttle, B., Van de Walle, C. G., and Adams, J. B., *Exchange of deeply trapped and interstitial hydrogen in silicon.* Physical Review B, 1999. **59**(8): p. 5493--5497.
157. Jing, Z. and Whitten, J. L., *Pathway of H2 desorption from dihydride Si(100).* Physical Review B, 1993. **48**(23): p. 17296--17300.
158. Bernhard, N. and Bauer, G. H., *Physical properties of a-Si:H based compositional periodic multilayers.* Physical Review B, 1995. **52**(12): p. 8829.
159. Taguchi, M., Kawamoto, K., Tsuge, S., Baba, T., Sakata, H., Morizane, M., Uchihashi, K., Noboru, N., Kiyama, S., and Oota, O., *HIT cells - high-efficiency crystalline Si cells with novel structure.* Progress in Photovoltaics: Research and Applications, 2000. **8**(5): p. 503-513.
160. Taguchi, M., Terakawa, A., Maruyama, E., and Makoto, T., *Obtaining a higher V_{oc} in HIT cells.* Progress in Photovoltaics: Research and Applications, 2005. **13**(6): p. 481-488.
161. Biswas, R., Li, Q., Pan, B. C., and Yoon, Y., *Mechanism for hydrogen diffusion in amorphous silicon.* Physical Review B, 1998. **57**(4): p. 2253.
162. Branz, H. M., Asher, S., Gleskova, H., and Wagner, S., *Light-induced D diffusion measurements in hydrogenated amorphous silicon: Testing H metastability models.* Physical Review B, 1999. **59**(8): p. 5513.
163. Franz, A. J., Mavrikakis, M., and Gland, J. L., *Hydrogen energetics in a-Si:H as determined by a combination of mean-field modeling and experimental evolution data.* Physical Review B, 1998. **57**(7): p. 3927.
164. Street, R. A., Kakalios, J., and Hayes, T. M., *Thermal equilibration in doped amorphous silicon.* Physical Review B, 1986. **34**(4): p. 3030.
165. Zafar, S. and Schiff, E. A., *Hydrogen and defects in amorphous silicon.* Physical Review Letters, 1991. **66**(11): p. 1493.
166. Nakamura, M., Ohno, T., Miyata, K., Konishi, N., and Suzuki, T., *Hydrogenation kinetics and defect termination of post-plasma-treated chemical-vapor-deposited amorphous silicon film.* Journal of Applied Physics, 1989. **65**(8): p. 3061-3068.
167. Van de Walle, C. G., *Energies of various configurations of hydrogen in silicon.* Physical Review B, 1994. **49**(7): p. 4579.

168. Wampler, W. R., Myers, S. M., and Follstaedt, D. M., *Reply to ``Comment on `Surface silicon-deuterium bond energy from gas-phase equilibration'''.* Physical Review B, 1997. **55**(19): p. 13319.
169. Reider, G. A., Hofer, U., and Heinz, T. F., *Desorption kinetics of hydrogen from the Si(111)7 x 7 surface*. 1991, AIP. p. 4080-4083.
170. Branz, H. M., *Dangling bonds in doped amorphous silicon: Equilibrium, relaxation, and transition energies.* Physical Review B, 1989. **39**(8): p. 5107.
171. Kemp, M. and Branz, H. M., *Hydrogen diffusion in a-Si:H: Solution of the tracer equations including capture by exchange.* Physical Review B, 1995. **52**(19): p. 13946.
172. Branz, H. M., *Hydrogen diffusion and mobile hydrogen in amorphous silicon.* Physical Review B, 1999. **60**(11): p. 7725.
173. Carlson, D. E. and Wronski, C. R., *Amorphous silicon solar cell*. 1976, AIP. p. 671-673.
174. Liehr, M., Greenlief, C. M., Offenberg, M., and Kasi, S. R., *Equilibrium surface hydrogen coverage during silicon epitaxy using SiH[sub 4].* Journal of Vacuum Science and Technology A, 1990. **8**(3): p. 2960-2964.
175. Lelièvre, J. F., Fourmond, E., Kaminski, A., Palais, O., Ballutaud, D., and Lemiti, M., *Study of the composition of hydrogenated silicon nitride SiNx:H for efficient surface and bulk passivation of silicon.* Solar Energy Materials and Solar Cells, 2009. **93**(8): p. 1281-1289.
176. Shuran, S., Xianbo, L., Guanglin, K., and Hexiang, H., *Study of microstructure of high stability hydrogenated amorphous silicon films by Raman scattering and infrared absorption spectroscopy*. 1998, AIP. p. 336-338.
177. Marra, D. C., Edelberg, E. A., Naone, R. L., and Aydil, E. S., *Silicon hydride composition of plasma-deposited hydrogenated amorphous and nanocrystalline silicon films and surfaces.* Journal of Vacuum Science and Technology, 1998. **16**(6): p. 3199--3210.
178. Xu, Y., Hu, Z., Diao, H., Cai, Y., Zhang, S., Zeng, X., Hao, H., Liao, X., Fortunato, E., and Martins, R., *Heterojunction solar cells with n-type nanocrystalline silicon emitters on p-type c-Si wafers.* Journal of Non-Crystalline Solids, 2006. **352**(9-20): p. 1972-1975.
179. Das, D., Shirai, H., Hanna, J.-i., and Shimizu , I., *Narrow Band-Gap a-Si:H with Improved Minority Carrier-Transport Prepared by Chemical Annealing.* Japanese Journal of Applied Physics, 1990. **30**: p. L239-L242.
180. Rao, R., *Preparation and properties of a-Si:H thin films deposited on different substrates* Journal of Wuhan University of Technology--Materials Science Edition, 2007. **22**(1): p. 126-128.
181. Gupta, S., Katiyar, R. S., Morell, G., Weisz, S. Z., and Balberg, I., *The effect of hydrogen on the network disorder in hydrogenated amorphous silicon*. 1999, AIP. p. 2803-2805.
182. Kolasinski, K. W., Nessier, W., Bornscheuer, K.-H., and Hasselbrink, E., *Beam investigations of D2 adsorption on Si(100): On the importance of lattive excitation in the reaction dynamics.* Journal of Chemical Physics, 1994. **101**: p. 7082.
183. Kolasinski, K. W., Nessler, W., de Meijere, A., and Hasselbrink, E., *Hydrogen adsorption on and desorption from Si: Considerations on the applicability of detailed balance.* Physical Review Letters, 1994. **72**(9): p. 1356.
184. Brenig, W., Gro$\mathcal{B}$, A., and Russ, R., *Detailed balance and phonon assisted sticking in adsorption and desorption of H2/Si* Zeitschrift für Physik B Condensed Matter, 1994. **96**(2): p. 231-234.
185. Bratu, P. and Höfer, U., *Phonon-Assisted Sticking of Molecular Hydrogen on Si(111)- (7 <rm>x</rm> 7).* Physical Review Letters, 1995. **74**(9): p. 1625.
186. Bratu, P., Kompa, K. L., and Höfer, U., *Optical second-harmonic investigations of H2 and D2 adsorption on Si (100) 2 × 1: the surface temperature dependence of the sticking coefficient.* Chemical Physics Letters, 1996. **251**(1-2): p. 1-7.

187. Shane, S., Kolasinski, K. W., and Zare, R., *A state-specific study of hydrogen desorption from Si(100)-(2x1): comparison of disilane and hydrogen adsorption.* Journal Vacuum Science Technology A, 1992. **10**: p. 1520.
188. Shane, S., Kolasinski, K. W., and Zare, R., *Recombinative desorption of H2 on Si(100)-(2x1) and Si(111)-(7x7): comparison of internal state distributions.* Journal of Chemical Physics, 1992. **97**: p. 1520.
189. Mitchell, J., Macdonald, D., and Cuevas, A., *Thermal activation energy for the passivation of the n-type crystalline silicon surface by hydrogenated amorphous silicon.* Applied Physics Letters, 2009. **94**(16): p. 162102.
190. Tuttle, B. and Adams, J., *Energetics of Hydrogen in Amorphous Silicon: an ab initio study.* Physical Review B, 1998. **57**(20): p. 12589 to 12868.
191. Bratu, P., Brenig, W., Groβ, A., Hartmann, M., Höfer, U., Kratzer, P., and Russ, R., *Reaction dynamics of molecular hydrogen on silicon surfaces.* Physical Review B, 1996. **54**(8): p. 5978.
192. Fedders, P. A., *Some theoretical aspects of hydrogen motion in a-Si:H.* Physical Review B, 2000. **61**(23): p. 15797.
193. Atkins, P. and de Paula, J., *Physical Chemistry*, in *Physical Chemistry*, J. Crowe, J. Fiorillo, and R. Hughes, Editors. 2006, Oxford Universtiy Press, W.H. Freeman and Co: Oxford, New York. p. 1100.
194. Kim, K., Dhungel, S. K., Gangopadhyay, U., Yoo, J., Seok, C. W., and Yi, J., *A novel approach for co-firing optimization in RTP for the fabrication of large area mc-Si solar cell.* Thin Solid Films, 2006. **511-512**: p. 228-234.
195. Buda, F., Chiarotti, G. L., Car, R., and Parrinello, M., *Proton diffusion in crystalline silicon.* Physical Review Letters, 1989. **63**(3): p. 294.
196. Van de Walle, C. G., Denteneer, P. J. H., Bar-Yam, Y., and Pantelides, S. T., *Theory of hydrogen diffusion and reactions in crystalline silicon.* Physical Review B, 1989. **39**(15): p. 10791.
197. Wehrspohn, R. B., Powell, M. J., Deane, S. C., French, I. D., and Roca i Cabarrocas, P., *Dangling-bond defect state creation in microcrystalline silicon thin-film transistors.* Applied Physics Letters, 2000. **77**(5): p. 750 -
198. Pankove, J. I. and Johnson, N. M., *Hydrogen in Semiconductors*. Vol. 34. 1996, New York.
199. Theiss, S. K., *Tunneling Microscopy of Semiconductors*. 1993, AFOSR/PKA: Division of Applied Sciences, Harvard University. p. 3.
200. Wise, M. L., Koehler, B. G., Gupta, P., Coon, P. A., and George, S. M., *Comparison of hydrogen desorption kinetics from Si(111)7 × 7 and Si(100)2 × 1.* Surface Science, 1991. **258**(1-3): p. 166-176.
201. Gupta, P., Colvin, V. L., and George, S. M., *Hydrogen desorption kinetics from monohydride and dihydride species on silicon surfaces.* Physical Review B, 1988. **37**(14): p. 8234.
202. Nachtigall, P., Jordan, K. D., and Janda, K. C., *Calculation of the Si-H bond energies for the monohydride phase of Si(100).* Journal of Chemical Physics, 1991. **95**(11): p. 8652-8654.
203. Wu, C. J., Ionova, I. V., and Carter, E. A., *Ab initio H2 desorption pathways for H/Si(100): the role of SiH2(a).* Surface Science, 1993. **295**(1-2): p. 64-78.
204. Lauinger, T., Moschner, J., G. Aberle, A., and Hezel, R., *Optimization and characterization of remote plasma-enhanced chemical vapor deposition silicon nitride for the passivation of p-type crystalline silicon surfaces.* Journal of Vacuum Science and Technology: A, 1998. **16**(2): p. 530-543.
205. Sakata, H. *20.7% highest efficiency large area (100.5cm^2) HIT cell.* in *29th IEEE PVSC*. 2000. Anchorage: IEEE.
206. Law, J., *adsorption of Hydrogen on Silicon.* Journal of Chemical Physics, 1958. **30**(6): p. 1568.
207. Branz, H. M., Asher, S. E., and Nelson, B. P., *Light-enhanced deep deuterium emission and the diffusion mechanism in amorphous silicon.* Physical Review B, 1993. **47**(12): p. 7061.

208. Kemp, M. and Branz, H. M., *Analytic solution of trap-controlled tracer diffusion in amorphous solids.* Physical Review B, 1993. **47**(12): p. 7067.
209. Nachtigall, P. and Jordan, K., *Barriers for Hydrogen Atom Diffusion on the Si(100)2x1 Surface.* Journal of Chemical Physics, 1995. **102**: p. 8249-8254.
210. Van Wieringen, A. and Warmoltz, N., *On the permeation of hydrogen and helium in single crystal silicon and germanium at elevated temperatures.* Physica, 1956. **22**(6-12): p. 849-865.
211. King, R. R., Sinton, R. A., and Swanson, R. M., *Studies of diffused phosphorus emitters: saturation current, surface recombination velocity, and quantum efficiency.* Electron Devices, IEEE Transactions on, 1990. **37**(2): p. 365-371.
212. Gee, J. M., King, R. R., Reiss, J. H., Mitchell, K. W., and Narayanan, S., *The Effect of Oxidations on Phosphorus-Diffused Crystalline Silicon Substrates*, in *14th European Photovoltaic Solar Energy Conference*. 1997: Barcelona, Spain.
213. Kerr, M., *Surface, Emitter and Bulk Recombination in Silicon and Development of Silicon Nitride passivated Solar Cells*, in *Department of Engineering*. 2002, The Australian National University: Canberra, Australia.
214. Hoex, B., Schmidt, J., Bock, R., Altermatt, P. P., van de Sanden, M. C. M., and Kessels, W. M. M., *Excellent passivation of highly doped p-type Si surfaces by the negative-charge-dielectric Al_2O_3.* Applied Physics Letters, 2007. **91**(11): p. 112107.
215. Benick, J., Hoex, B., Schultz, O., and Glunz, S. W. *Surface passivation of boron diffused emitters for high efficiency solar cells*. in *33rd IEEE Photovoltaic Specialists Conference, 2008.* . 2008: IEEE.
216. Q.Cells, *Design module, flat roof system and world recordsetting cells – Q-Cells presents photovoltaic innovations for higher yields at EU PVSEC 2011*. 2011, Q.Cells: Hamburg.
217. Wang, T. H., Wang, Q., Iwaniczko, E., Page, M. R., Levi, D. H., Yan, Y., Teplin, C. W., Xu, Y., Wu, X. Z., and Branz, H. M. *Heterojunction Silicon Solar Cells with High Open-Circuit Voltages by Interface Optimization*. in *19th European PV Solar Energy Conference*. 2004. Paris.
218. Maydell, K. v., Korte, L., Laades, A., Stangl, R., Conrad, E., Lange, F., and Schmidt, M., *Characterization and optimization of the interface quality in amorphous/crystalline silicon heterojunction solar cells.* Journal of Non-Crystalline Solids, 2006. **352**(9-20): p. 1958-1961.
219. Janz, S., Ziegler, D., Psych, D., Suwito, D., and Glunz, S. W. *Amorphous Silicon Carbide Hetero-Emitters for High Efficiency Silicon Solar Cells*. in *23rd European Photovoltaic Solar Energy Conference and Exhibition*. 2008. Valencia.
220. Vetter, M., Martin, I., Orpella, A., Puigdollers, J., Voz, C., and Alcubilla, R., *Solar Cells with Annealed Amorphous SiC/Si Heterojunction and a-SiC:H Backsurface Passivation*, in *3rd World Conference on Photovoltaic Energy Conversion*. 2003: Osaka, japan.
221. Sanyo (2009) *SANYO Develops HIT Solar Cells with World's Highest Energy Conversion Efficiencyof 23.0%*.
222. Schroder, D., in *Semiconductor Material and Device Characterisation*, K. Chang, Editor, John Wiley & Sons Inc: Arizona. p. 2 of 760.
223. Kane, D. and Swanson, R. *Measurement of the Emitter Saturation Current by Contacless Photoconductivity decay method*. in *18th IEEE Photovoltaic Specialists Conference*. 1985. Las Vegas: IEEE.
224. Aberle, A., *Crystalline Silicon Solar Cells: Advanced Surface Passivation and Analysis*. 1 ed. Vol. 1. 1999: Centre for Photovoltaic Engineering, University of New South Wales. 335.
225. Sinton, R. and Cuevas, A., *Contactless determination of current--voltage characteristics and minority-carrier lifetimes in semiconductors from quasi-steady-state photoconductance data.* Applied Physics Letters, 1996. **69**(17): p. 2510-2512.
226. Bennici, E., Ferrero, S., Giorgis, F., Pirri, C. F., Rizzoli, R., Schina, P., Businaro, L., and Di Fabrizio, E., *a-Si:H based two-dimensional photonic crystals.* Physica E, 2002. **XX**: p. XX.

227. Ferre, R., Martin, I., Ortega, P., Vetter, M., Torres, I., and Alcubilla, R., *n-type emitter surface passivation in c-Si solar cells by means of antireflective amorphous silicon carbide layers.* 2006, AIP. p. 073703.
228. Plagwitz, H., Nerding, M., Ott, N., Strunk, H. P., and Brendel, R., *Low-temperature formation of local Al contacts to a-Si:H-passivated Si wafers.* Progress in Photovoltaics: Research and Applications, 2004. **12**: p. 47--54.
229. Rau, U., Nguyen, V., Matteis, J., Rakhlin, M., and Werner, J. H. *Recombination at a-Si:H Heterointerfaces and in a-Si:H/c-Si Heterojunction Solar Sells.* in *Proceedings of the 3rd World Conference on Photovoltaic Energy Conversion*. 2003. Japan: Arisumi Printin Inc.
230. Garin, M., Rau, U., Brendle, W., Martin, I., and Alcubilla, R., *Characterisation of a-Si:H/c-Si Interfaces by Effective-Lifetime Measurements.* Journal of Applied Physics, 2005. **98**(9a): p. 093711.
231. Kanno, H., Ide, D., Tsunomura, Y., Baba, T., Yoshimine, Y., Taguchi, M., Kinoshita, T., Sakata, H., and Maruyama, E., *Over 22% Efficient Hit Solar Cell,* in *23rd European Photovoltaic Solar Energy Conference*. 2008: Valencia, Spain. p. 1136.
232. Kerr, M., *Surface, Emitter and Bulk Recombination in Silicon and Development of Silicon Nitride Passivated Solar Cells,* in *Engineering*. 2002, The Australian National University: Canberra. p. 242.
233. De Wolf, S. and Kondo, M., *Boron-doped a-Si:H/c-Si interface passivation: Degradation mechanism.* Applied Physics Letters, 2007. **91**(11): p. 112109.
234. Benick, J., Schultz-Wittmann, O., Schön, J., and Glunz, S. W., *Surface passivation schemes for high-efficiency n-type Si solar cells.* 2008. **2**(4): p. 145-147.
235. Einsele, F., Rostan, P., Schubert, M., and Rau, U., *Recombination and resistive losses at ZnO/a-Si:H/c-Si interfaces in heterojunction back contacts for Si solar cells.* Journal of Applied Physics, 2007. **102**(9): p. 094507.
236. Olibet, S., Vallat-Sauvain, E., and Ballif, C., *Model for a-Si:H/c-Si interface recombination based on the amphoteric nature of silicon dangling bonds.* Physical Review B, 2007. **76**(3): p. 035326.
237. Jagnnathan, B. and Andreson, W. A. *a-Si/c-Si solar cells: effect of preparation and processing techniques on the photovoltaic properties.* in *Materials Research Society Symposium Proceedings: Thin Films for Photovoltaic and Related Device Applications*. 1996.
238. Fischer, H. and Pschunder, W. *Low cost solar cells based on large area unconventional silicon.* in *12th IEEE Photovoltaic Specialists Conference*. 1976. Baton Rouge, LA, United States.
239. Chen, F. W., Li, T.-T. A., and Cotter, J. E., *Passivation of boron emitters on n-type silicon by plasma-enhanced chemical vapor deposited silicon nitride.* Applied Physics Letters, 2006. **88**(26): p. 263514.
240. Myers, S. M., Seibt, M., and Schroter, W., *Mechanisms of transition-metal gettering in silicon.* Journal of Applied Physics, 2000. **88**(7): p. 3795 - 3819.
241. Rohatgi, A. and Narasimha, S., *Design, fabrication, and analysis of greater than 18% efficient multicrystalline silicon solar cells.* Solar Energy Materials and Solar Cells, 1997. **48**(1-4): p. 187-197.
242. Shultz, O., Glunz, S. W., Goldschmidt, J. C., Lautenschlager, H., Leimenstoll, A., Scheiderlochner, E., and Willeke, G. P., *Thermal oxidation processes for high-efficiency multicrystalline silicon solar cells,* in *19th European Photovoltaic Solar Energy Conference*. 2004: Paris.
243. Kerr, M. and Cuevas, A. *Comprehensive study of the doping and injection-level dependence of stoichiometric silicon nitride passivation for silicon solar cells.* in *IEEE Photovoltaic Specialists Conference*. 2002. New Orleans, LA, United States.

244. Schmidt, J. and Kerr, M., *Highest-quality surface passivation of low-resistivity p-type silicon using stoichiometric PECVD silicon nitride.* Solar Energy Materials and Solar Cells, 2001. **65**(1-4): p. 585-591.
245. Schneider, A., Gerhards, C., Fath, P., Bucher, E., Young, R. J. S., Raby, J. A., and Carroll, A. F. *Bow reducing factors for thin screenprinted MC-Si solar cells with Al BSF.* in *Photovoltaic Specialists Conference, 2002. Conference Record of the Twenty-Ninth IEEE*. 2002. New Orleans: IEEE.
246. Trupke, T., Bardos, R. A., and Abbott, M. D., *Self-consistent calibration of photoluminescence and photoconductance lifetime measurements.* Applied Physics Letters, 2005. **87**(18): p. 184102.
247. Trupke, T., Bardos, R. A., Schubert, M. C., and Warta, W., *Photoluminescence imaging of silicon wafers.* Applied Physics Letters, 2006. **89**(4): p. 044107.
248. Macdonald, D., Cuevas, A., Kinomura, A., Nakano, Y., and Geerligs, L., *Transition-metal profiles in a multicrystalline silicon ingot*. 2005, AIP. p. 033523.
249. Macdonald, D., *Effect of gettered iron on recombination in diffused regions of crystalline silicon wafers.* Appl. Phys. Lett., 2006. **88**(9): p. 092105.
250. Tan, J., Cuevas, A., Macdonald, D., Bennett, N., Romijn, I., Trupke, T., and Bardos, R., *Optimised Gettering and Hydrogenation of Multi-crystalline Silicon Wafers for use in Solar Cells*, in *22nd European Photovoltaic Solar Energy Conference*. 2007: Milan, Italy.
251. Schmidt, J., Moschner, J. D., Henze, J., Dauwe, S., and Hezel, R. *Recent progress in the surface passivation of silicon solar cells using silicon nitride*. in *19th European Photovolatic Solar Energy Conference*. 2004. Paris, France.
252. Kleekajai, S., *Concentration and penetration depth of H introduced into crystalline Si by hydrogenation methods used to fabricate solar cells.* J. Appl. Phys., 2006. **100**(9): p. 093517.
253. Kleekajai, S., *Infrared study of the concentration of H introduced into Si by the postdeposition annealing of a SiNx coating.* J. Appl. Phys., 2009. **106**(12): p. 123510.
254. Jiang, F., Stavola, M., Rohatgi, A., Kim, D., Holt, J., Atwater, H., and Kalejs, J., *Hydrogenation of Si from SiNx(H) films: Characterization of H introduced into the Si.* Appl. Phys. Lett., 2003. **83**(5): p. 931.
255. Catoir, J., Wolke, W., Griesshammer, M., Preu, R., Trassl, R., and Grambole, D. *Analysis of Hydrogen Passivation by Sputtered Silicon Nitride*. in *23rd European Photovoltaic Solar Energy Conference and Exhibition*. 2008. Valencia, Spain.
256. Lüdemann, R., *Hydrogen passivation of multicrystalline silicon solar cells.* Materials Science and Engineering: B, 1999. **58**(1-2): p. 86-90.
257. Muller, J. C., Quat, V. T., Siffert, P., Amzil, H., Barhdadi, A., and M'Gafad, N., *Temperature parameter in hydrogen passivation of multicrystalline silicon solar cells.* Solar Cells, 1988. **25**(2): p. 109-125.
258. McQuaid, S. A., Binns, M. J., Newman, R. C., Lightowlers, E. C., and Clegg, J. B., *Solubility of hydrogen in silicon at 1300 [degree]C*. 1993, AIP. p. 1612-1614.
259. Binns, M. J., McQuaid, S. A., Newman, R. C., and Lightowlers, E. C., *Hydrogen solubility in silicon and hydrogen defects present after quenching*. 1993. p. 1908.
260. Perkin-Elmer. [Webpage] 3rd November, 2008 [cited 2009 14th January, 2009]; Spectrum One FTIR spectrometer]. Available from: http://las.perkinelmer.com/.
261. Pearton, S. J., Corbett, J. W., and Stavola, M., *Hydrogen in in Crystalline Semiconductors*. 1992, Springer-Verlag: Berlin.
262. in *Hydrogen in Semiconductors II: Semiconductors and Semimetals*, N.H. Nickel, Editor. 1999, Academic Press: New York.
263. Meaudre, R., Meaudre, M., and Roca i Cabarrocas, P., *Thermal quenching and relaxation in doped hydrogenated amorphous silicon deposited by plasma-enhanced chemical vapor deposition from He-diluted silane.* Applied Physics Letters, 1993. **62**(6): p. 594--596.

264. Akhmetov, V. D. and Richter, H., *FTIR spectroscopic system with improved sensitivity*, in *11th International Conference on Defects - Recognition Imaging and Physics in Semiconductors (DRIP-XI): Materials Science in Semiconductor Processing*. 2006: Beijing, China. p. 92-95.
265. Chabal, Y. J. and Raghavachari, K., *New Ordered Structure for the H-Saturated Si(100) Surface: The (3 <rm>x</rm> 1) Phase.* Physical Review Letters, 1985. **54**(Copyright (C) 2010 The American Physical Society): p. 1055.
266. Ouwens, J. D., Schropp, R. E. I., and van der Weg, W. F., *Interpretation of the silicon-hydrogen stretching doublet in a-Si:H hydrogenated amorphous silicon.* Applied Physics Letters, 1994. **65**(2): p. 204--206.
267. Knobloch, J. and Hess, P., *In situ infrared transmission spectroscopy of nucleation and growth of amorphous hydrogenated silicon.* Applied Physics Letters, 1996. **69**(26): p. 4041--4043.
268. Freeman, E. C. and Paul, W., *Infrared vibrational spectra of rf-sputtered hydrogenated amorphous silicon.* Physical Review B, 1978. **18**(8): p. 4288.
269. Agarwal, S., Hoex, B., van de Sanden, M. C. M., Maroudas, D., and Aydil, E. S., *Hydrogen in Si-Si bond center and platelet-like defect configurations in amorphous hydrogenated silicon.* Journal of Applied Physics, 2004. **22**(6): p. 2719--2726.
270. Queeney, K. T., Chabal, Y. J., and Raghavachari, K., *Role of interdimer interactions in NH3 dissociation on Si(100)-(2 x 1).* Physical Review Letters, 2001. **86**(6): p. 1046--1049.
271. Gurevich, A. B., Stefanov, B. B., Weldon, M. K., Chabal, Y. J., and Raghavachari, K., *Heterogeneous nucleation of oxygen on silicon: Hydroxyl-mediated interdimer coupling on Si(100)-(2 <rm>x</rm> 1).* Physical Review B, 1998. **58**(Copyright (C) 2010 The American Physical Society): p. R13434.
272. Pereyra, I., Carreno, M. N. P., Tabacniks, M. H., Prado, R. J., and Fantini, M. C. A., *The influence of ``starving plasma'' regime on carbon content and bonds in a-Si[sub 1 - x]C[sub x]:H thin films.* Journal of Applied Physics, 1998. **84**(5): p. 2371-2379.
273. Romijn, I., Soppe, W. J., Rieffe, H. C., Sinke, W. C., and Weber, A. W., *Passivating Multi-crystalline Si Solar Cells using SiN x: H*, in *15th Workshop on Crystalline Silicon Solar Cells & Modules: Materials and Processes*. 2005: Vail, Colorado, USA.
274. Vink, R. L., Barkema, G. T., and van der Weg, W. F., *Raman spectra and structure of amorphous Si.* Physical Review B. **63**: p. 115210-1 to 115210-6.
275. Sokolov, A. P., Shebanin, A. P., Golikova, O. A., and Mezdrogina, M. M., *Structural order in amorphous silicon and its alloys: Raman spectra and optical gap.* Journal of Non-Crystalline Solids, 1991. **137-138**(Part 1): p. 99-102.
276. Fortner, J. and Lannin, J. S., *Structural relaxation and order in ion-implanted Si and Ge.* Physical Review B, 1988. **37**: p. 10154.
277. Maley, N., *Critical investigation of the infrared-transmission-data analysis of hydrogenated amorphous silicon alloys.* Physical Review B, 1992. **46**(4): p. 2078.
278. Yndurain, F. and Sen, P. N., *Effects of the local configuration on the lattice dynamics of group-IV semiconductors.* Physical Review B, 1976. **14**(2): p. 531.
279. Fung, M. K., Chan, W. C., Lai, K. H., Bello, I., Lee, C. S., Wong, N. B., and Lee, S. T., *Deposition of ultra-thin diamond-like carbon protective coating on magnetic disks by electron cyclotron resonance plasma technique.* Journal of Non-Crystalline Solids, 1999. **254**(1-3): p. 167-173.
280. Heitz, T., Drévillon, B., and Godet, C., *Improvement of sensitivity in the analysis of vibrational properties of thin films by use of in situ ellipsometry:applications to hydrogenated amorphous carbon films.* Journal of the Optical Society of America B, 1999. **16**(7): p. 1044.
281. Hazra, S., Yamanaka, M., Sakata, I., Tsutsumi, T., Maeda, T., and Suzuki, E., *Spectroscopic Ellipsometry Studies on Ultrathin Hydrogenated Amorphous Silicon Films* Japanese Journal of Applied Physics, 2005. **39**(1/11): p. 6196-6201.

282. Chen, H. and Shen, W. Z., *Perspectives in the characteristics and applications of Tauc-Lorentz dielectric function mode.* The European Physical Journal B - Condensed Matter and Complex Systems, 2005. **43**(4): p. 503-507.
283. Schmidt, M., Korte, L., Laades, A., Stangl, R., Schubert, C., Angermann, H., Conrad, E., and Maydell, K. v., *Physical aspects of a-Si:H/c-Si hetero-junction solar cells.* Thin Solid Films, 2007. **515**(19): p. 7475-7480.
284. Olibet, S., Vallat-Sauvain, E., and Ballif, C., *Model for a-Si:H/c-Si Interface recombination based on the amphoteric nature of silicon dangling bonds.* Physical Review B, 2007. **76**.
285. Conrad, E., Maydell, K. v., Angermann, H., Schubert, C., and Schmidt, M. *Optimization of Interface Properties in a-Si:H/c-Si Heterojunction Solar Cells.* in *Conference Record of the 2006 IEEE 4th World Conference on Photovoltaic Energy Conversion*. 2006: IEEE.
286. Tucci, M. and de Cesare, G., *17% efficiency heterostructure solar cell based on p-type crystalline silicon.* Journal of Non-Crystalline Solids, 2004. **338-340**: p. 663-667.
287. Scherff, M. L. D. and Fahrner, W. R., *Dependency of Heterojunction Solar Cell Efficiency on the Indium Tin Oxide Deposition Parameters*, in *20th European Photovoltaic Solar Energy Conference*. 2005: Barcelona.
288. Scherff, M. L. D., Froitzheim, A., and Schmidt, M. in *19th European PV Solar Energy Conference*. 2004. Paris.